

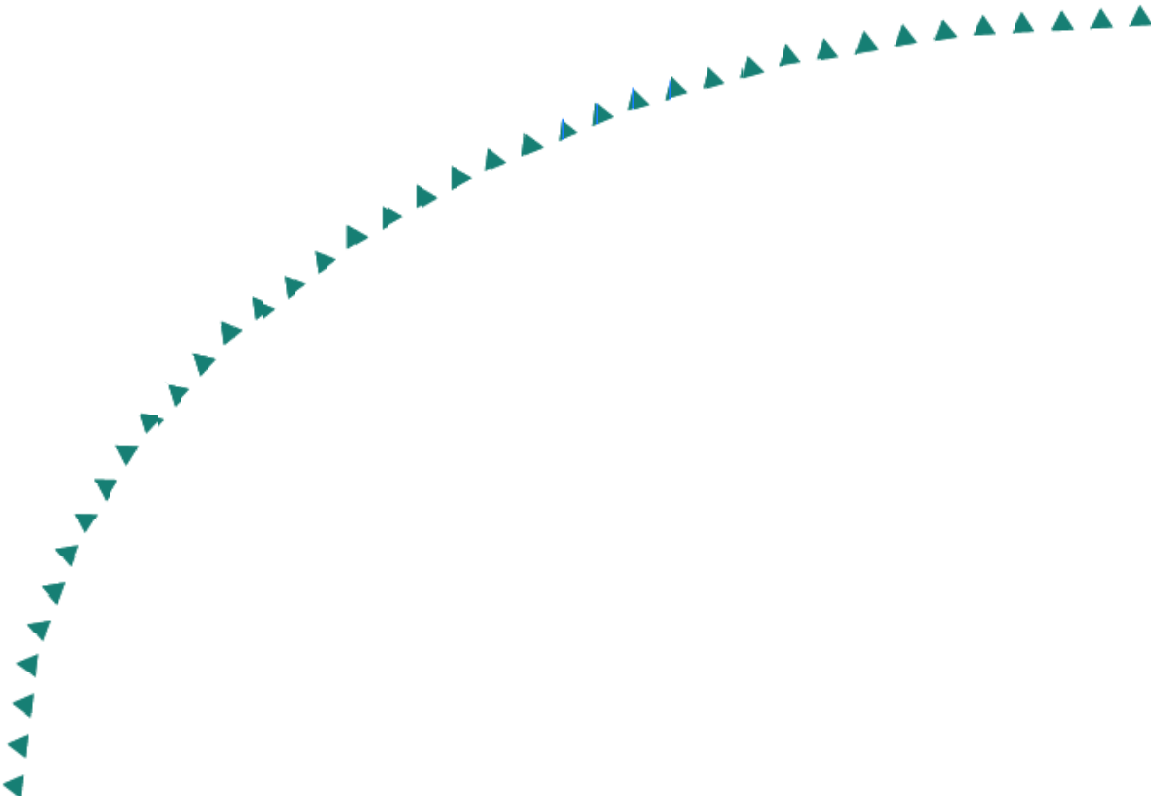
2006-07

Final Report

Fatigue-Resistant Design for Overhead Signs,
Mast-Arm Signal Poles, and Lighting Standards



Research



Technical Report Documentation Page

1. Report No. MN/RC-2006-07	2.	3. Recipients Accession No.	
4. Title and Subtitle Fatigue-Resistant Design for Overhead Signs, Mast-Arm Signal Poles, and Lighting Standards		5. Report Date March 2006	
		6.	
7. Author(s) Justin M. Ocel, Robert J. Dexter, and Jerome F. Hajjar		8. Performing Organization Report No.	
9. Performing Organization Name and Address University of Minnesota Department of Civil Engineering 500 Pillsbury Dr, SE Minneapolis, MN 55455-0116		10. Project/Task/Work Unit No.	
		11. Contract (C) or Grant (G) No. (c) 81655 (wo) 59	
12. Sponsoring Organization Name and Address Minnesota Department of Transportation 395 John Ireland Boulevard Mail Stop 330 St. Paul, Minnesota 55155		13. Type of Report and Period Covered Final Report	
		14. Sponsoring Agency Code	
15. Supplementary Notes http://www.lrrb.org/pdf/200607.pdf			
16. Abstract (Limit: 200 words) Traffic signs and signals are often supported by flexible cantilevered structures that are susceptible to wind-induced vibration and fatigue. The latest version of the design specifications published by the American Association of State Transportation Officials (AASHTO) now considers fatigue as a limit state. However, most of the fatigue classifications for welded details were not based on full-scale testing, and are thought to be overly conservative. This research will address the fatigue resistance of two common mast arm-to-pole connections used in the state of Minnesota. The resistance attained experimentally aligned with current predictions using AASHTO procedures, except for in-plane loading of box connection details. As a consequence of specimen design, a variety of tube-to-transverse plate connections were also tested using multi-sided tube cross-sections with different tube diameters, tube thicknesses, as well as base plate thicknesses. The standard tube-to-transverse plate connection exhibited Category K ₂ resistance, two categories lower than the E' specified by AASHTO. This resistance was enhanced to Category E' through impact treatment or Category E by doubling the base plate thickness. Gusset plates could not prevent cracking of the tube at the base plate, but the tips of the gusset plate exhibited Category E resistance.			
17. Document Analysis/Descriptors Fatigue Socket Connection Traffic Structure		Tubular Box Connection	18. Availability Statement No restrictions. Document available from: National Technical Information Services, Springfield, Virginia 22161
19. Security Class (this report) Unclassified	20. Security Class (this page) Unclassified	21. No. of Pages 190	22. Price

Fatigue-Resistant Design for Overhead Signs, Mast-Arm Signal Poles, and Lighting Standards

Final Report

Prepared by:

Justin M. Ocel
Robert J. Dexter
Department of Civil Engineering
University of Minnesota
500 Pillsbury Drive SE
Minneapolis, MN 55455-0116

Jerome F. Hajjar
Department of Civil and Environmental Engineering
205 North Mathews Avenue
University of Illinois – Urbana/Champaign
Urbana, Illinois 61801-2352

March 2006

Published by:

Minnesota Department of Transportation
Research Services Section
395 John Ireland Boulevard, MS 330
St. Paul, Minnesota 55155-1899

This report represents the results of research conducted by the authors and does not necessarily represent the views or policies of the Minnesota Department of Transportation and/or the Center for Transportation Studies. This report does not contain a standard or specified technique.

The authors and the Minnesota Department of Transportation and/or Center for Transportation Studies do not endorse products or manufacturers. Trade or manufacturers' names appear herein solely because they are considered essential to this report

Acknowledgements

This research was sponsored by the Minnesota Department of Transportation, the Center for Transportation Studies, and the University of Minnesota. In-kind funding was provided by Millerbernd Mfg.

The authors wish to thank Tom Merritt, Erik Wolhowe, and Ben Osenemen of the Minnesota Department of Transportation and Steve Engebretson and Mike Wendolek of Millerbernd Mfg. for their valuable assistance with this research. Special thanks are due to Prof. Robert J. Dexter of the University of Minnesota, the original investigator and lead researcher on this project, who passed away prior to the completion of this project.

Table of Contents

CHAPTER 1 INTRODUCTION	1
CHAPTER 2 FATIGUE IN RELATED STRUCTURES.....	3
2.1 PRESENT DESIGN SPECIFICATIONS.....	10
2.2 BACKGROUND IN FATIGUE	12
2.2.1 <i>Nominal Stress Approach</i>	12
2.2.2 <i>Hot-Spot Stress Approach</i>	14
2.2.3 <i>Fracture Mechanics Approach</i>	15
CHAPTER 3 LITERATURE REVIEW	16
3.1 NCHRP RESEARCH	16
3.1.1 <i>Natural Wind Gust</i>	16
3.1.2 <i>Vortex Shedding</i>	16
3.1.3 <i>Galloping</i>	17
3.1.4 <i>Truck Gusts</i>	17
3.2 ARCHER AND GURNEY (1970)	18
3.3 MIKI ET. AL. (1981)	20
3.4 SOUTH (1994)	21
3.5 SOUTH (1997)	22
3.6 UNIVERSITY OF MINNESOTA (1998)	23
3.7 ALDERSON (1999)	26
3.8 HEEDEN (1999)	28
3.9 KASHAR (1999).....	29
3.10 UNIVERSITY OF WYOMING (1999-2002)	30
3.11 GILANI (2000)	35
3.12 VALMONT FATIGUE TESTING (2001)	36
3.13 UNIVERSITY OF TEXAS – AUSTIN (2002).....	42
3.14 IOWA HIGH MAST FAILURE	46
3.15 RELATED FATIGUE RESEARCH	47
3.15.1 <i>Determination of SCFs by Testing</i>	50
CHAPTER 4 EXPERIMENTAL PROGRAM.....	53
4.1 TYPE I SPECIMENS	53
4.2 TYPE I LONG POLE SPECIMENS	56
4.3 TYPE II SPECIMENS.....	57
4.4 TYPE I LOADING SYSTEMS	60
4.4.1 <i>Frame 1</i>	61
4.4.2 <i>Frame 2</i>	64
4.4.3 <i>Frame 3</i>	65
4.5 TYPE II LOADING SYSTEMS.....	67
CHAPTER 5 EXPERIMENTAL INSTRUMENTATION.....	71
5.1 TYPE I SPECIMEN INSTRUMENTATION PLAN (FRAME 1).....	71
5.1.1 <i>Mast Arm</i>	73
5.1.2 <i>Pole</i>	74
5.1.3 <i>Box Connection</i>	75
5.1.4 <i>Pole Base Plate</i>	76
5.2 TYPE I SPECIMEN INSTRUMENTATION (FRAME 2).....	77
5.3 TYPE I SPECIMEN INSTRUMENTATION (FRAME 3).....	78
5.4 TYPE II SPECIMEN INSTRUMENTATION PLAN	78
5.4.1 <i>Mast Arm/Mast Can Detail</i>	79
5.4.2 <i>Pole</i>	81
CHAPTER 6 STATIC TEST RESULTS.....	84

6.1 TYPE I SPECIMEN (FRAME 1).....	84
6.1.1 Midpoint Strain Gauges (Nominal Strains).....	84
6.1.2 Mast Arm Socket Connection (Frame 1).....	85
6.1.3 Pole Socket Connection (Frame 1).....	86
6.1.4 Box Connection (Frame 1).....	89
6.1.5 Pole Wall.....	90
6.1.6 Pole Base Plate Rosettes.....	93
6.2 THICK BASE PLATE SOCKET CONNECTION (FRAME 2).....	94
6.3 TYPE I MAST ARMS (FRAME 3).....	97
6.4 COMPARISONS OF TYPE I TUBE-TO-TRANSVERSE PLATE CONNECTIONS.....	99
6.5 TYPE II SPECIMENS.....	100
6.5.1 First Static Test.....	100
6.5.2 Second Static Test.....	103
CHAPTER 7 FATIGUE RESULTS.....	108
7.1 TYPE I POLE SOCKET CONNECTIONS.....	108
7.2 TYPE I BOX CONNECTIONS.....	124
7.3 TYPE I MAST ARMS WITH FULL-PENETRATION WELDS.....	134
7.4 TYPE I MAST ARM WITH GUSSET PLATE STIFFENERS.....	137
7.5 TYPE I TRANSFORMER BASE CRACKING.....	143
7.6 TYPE II MAST ARMS.....	147
7.7 TYPE II POLES.....	152
CHAPTER 8 CONCLUSIONS AND RECOMMENDATIONS.....	157
8.1 MULTI-SIDED TUBE-TO-TRANSVERSE PLATE CONNECTIONS.....	157
8.2 TUBE-TO-TUBE CONNECTIONS.....	158
8.3 BOX CONNECTIONS ON MULTI-SIDED TUBES.....	158
8.4 ACCESS HOLES.....	160
8.5 SUGGESTIONS FOR FUTURE RESEARCH.....	161
REFERENCES.....	164
APPENDIX A.....	A-1

List of Figures

Figure 2.1 Three types of horizontally cantilevered structures. Top: Monotube mast arm. Middle: Vierendeel trussed mast arm. Bottom: Four chord trussed mast arm.	5
Figure 2.2 Vertical cantilever used to support light fixtures (high mast tower).....	5
Figure 2.3 Typical bridged-type supports. Top: Four chord truss. Bottom: Monotube.....	6
Figure 2.4 Crack emanating from hand hole detail in high mast tower, Clear Lake, IA.....	7
Figure 2.5 Four chord, space truss, bridged-type support using tube-to-tube connections.	7
Figure 2.6 Picture of a cracked tube-to-tube welded connection.	8
Figure 2.7 AASHTO 2001 Specifications tube-to-transverse plate fatigue classifications.....	9
Figure 2.8 Left: Built-up box connection used to connect the mast arm to the pole. Right: Typical cracks emanating from side plate termination of box connection (29).	10
Figure 2.9 Difference between stresses near a welded detail.....	12
Figure 2.10 Nominal stress S-N curves used in AASHTO, AISC, AWS specifications.....	14
Figure 3.1 Picture of von Karman vortex street.	17
Figure 3.2 Schematic of Archer and Gurney specimens. Top: Type F specimen. Bottom: Type S specimen.	19
Figure 3.3 Test results of Archer and Gurney specimens plotted against AASHTO fatigue curves	20
Figure 3.4 Results of the Lehigh socket connection fatigue data, plotted against AASHTO S-N curves.....	21
Figure 3.5 Fatigue data of 24 mast arm specimens test by South (1997).	23
Figure 3.6 Close-up view of spacer connection between pole and crossarm.....	24
Figure 3.7 Stadium lighting fatigue test set-up	25
Figure 3.8 Plot of original and stiffened connections of lighting structures against AASHTO S-N curves.....	25
Figure 3.9 Close-up view of ring-stiffened connection between pole and crossarm.....	26
Figure 3.10 University of Missouri Columbia “fatigue-resistant” weld detail	27
Figure 3.11 Plot of fatigue data for mast arms tested at University of Missouri-Columbia.	28
Figure 3.12 Typical CMS structure used in California (27).	30
Figure 3.13 Laboratory set-up for Wyoming testing (29).....	32
Figure 3.14 Three different types of box connections, (a) Closed, (b) Open, (c) Ring stiffened (29).....	32
Figure 3.15 Fatigue data of mast arms and box connections conducted at University of Wyoming.	35
Figure 3.16 Plot of the Gilani pole and mast arm data along with relevant AASHTO design curves.....	36
Figure 3.17 Valmont fatigue testing load frame. (a) Elevation view of rotating beam set-up made from two masts arms bolted together. (b) Rotating beam fatigue load frame.	38
Figure 3.18 Valmont Gusset 1 & 2 specimens.	39
Figure 3.19 Valmont Gusset 3 & 4 specimens.	39
Figure 3.20 Valmont Gusset 5 & 6 specimens.	40
Figure 3.21 Plot of the fatigue data of three different types of tube-to-plate connections tested by Valmont.	42
Figure 3.22 UTexas mast arm fatigue setup.....	44
Figure 3.23 UTexas fatigue data for socket connections.	45

Figure 3.24 UTexas fatigue data for gusset stiffened socket connections.	45
Figure 3.25 UTexas fatigue data for miscellaneous socket connections.	46
Figure 3.26 Collapsed I-29 high mast tower in Sioux City, Iowa.	47
Figure 3.27 Definitions of CHS T and Y-joint dimensions.	49
Figure 3.28 Hot-spot S-N curves for CHS joints ($4 \text{ mm} \leq t \leq 50 \text{ mm}$) and RHS joints ($4 \text{ mm} \leq t \leq 16 \text{ mm}$).....	50
Figure 3.29 Picture of extrapolation region.	51
Figure 3.30 Difference between linear and quadratic stress extrapolation.	52
Figure 4.1 Type I pole, mast arm, and transformer base details.....	55
Figure 4.2 Dimensions of Type I long pole specimens	57
Figure 4.3 Mock-up of Type II specimen with cut-away view of mast can detail.	58
Figure 4.4 Schematic of Type II specimens.	59
Figure 4.5 Cap plate welded to Type II mast can.	60
Figure 4.6 Schematic of three loading positions used for Type I specimens in Frame 1.	63
Figure 4.7 Schematic of Frame 2 layout.	65
Figure 4.8 Schematic of Frame 3 loading system.....	66
Figure 4.9 Schematic of Frame 1 for Type II specimens.....	68
Figure 4.10 Type II pole foundation connection.	69
Figure 4.11 Thick plate washer beneath load cell for Type II specimen out-of-plane loading.....	69
Figure 4.12 Load frame used to only test Type II poles.	70
Figure 5.1 Strain gauge layout on Type I specimen.	73
Figure 5.2 Mast arm strain gauge locations and labels.	74
Figure 5.3 Pole strain gauge layout and labeling.....	75
Figure 5.4 Box connection strain gauge layout and labels.....	76
Figure 5.5 Pole base plate strain gauge layout and labels.....	77
Figure 5.6 Frame 2 socket connection strain gauge labeling system.....	78
Figure 5.7 Type II mast arm strain gauge layout.....	80
Figure 5.8 View of Type II mast arm showing how strain gauges are orientated perpendicular to weld toe.	81
Figure 5.9 Type II pole instrumentation	82
Figure 5.10 Access hole instrumentation of Type II pole.	83
Figure 5.11 Strain gauges placed at bottom of access hole.....	83
Figure 6.1 SCFs of gusset-stiffened mast arm socket connection under three different loadings.....	86
Figure 6.2 SCFs of pole socket connection under three different loadings.	88
Figure 6.3 Pictorial example of strain profile at socket connection showing shear lag effect.....	89
Figure 6.4 Strains in box connection side plates. Top: In-plane loading. Bottom: Out-of-plane loading.	91
Figure 6.5 Strains in pole wall at the pole/side plate intersection. Top: In-plane loading. Bottom: Out-of-plane loading.....	92
Figure 6.6 Principle strains from base plate rosettes. Top: Out-of-plane loading. Middle: In-plane loading. Bottom: 45 degree loading.....	93
Figure 6.7 SCFs from two different base plate thickness socket connections tested, each tube having 7.9mm (0.3125 inch) thick tubes.	95
Figure 6.8 SCFs of socket connection with two different tubewall thicknesses, but same thickness base plate.	96
Figure 6.9 Measured strain in pole socket connections with decomposed resultants.	97

Figure 6.10 Type I mast arm SCFs from Frame 3.....	98
Figure 6.11 Measured strains in gusset plate under static moment.	99
Figure 6.12 SCF comparison between various Type I tube-to-transverse plate connections.	100
Figure 6.13 Measured static strains on mast arm/mast can detail. (Middle) Strains in mast arm tube. (Bottom) Strains in mast can tube.	102
Figure 6.14 Type II pole SCFs at full-penetration weld adjoining the pole tube to transformer base.....	103
Figure 6.15 Strains in transformer base with access hole at extreme bending fiber. Top: Section B-B gauges. Bottom: Section A-A gauges.	106
Figure 6.16 Strains in transformer base with access hole near neutral bending access. Top: Section B-B gauges. Bottom: Section A-A gauges.....	107
Figure 7.1 Location of cracks in socket connections.....	111
Figure 7.2 Weld toe cracks in pole socket connections.	112
Figure 7.3 Macro etched cross-section of weld toe crack.....	113
Figure 7.4 Weld root cracks in pole socket connections.....	114
Figure 7.5 Macro etched cross-section of weld root crack.	115
Figure 7.6 S-N plot of untreated socket connections with 31.8 mm (1.25 inch) thick base plates.	118
Figure 7.7 S-N plot of hammer-peen repaired socket connections with 31.75 mm (1.25 inch) thick base plates.	119
Figure 7.8 S-N plot of hammer-peen retrofitted socket connections with 31.75 mm (1.25 inch) thick base plates.	120
Figure 7.9 S-N plot of thick base plate socket connection with 7.94 mm (5/16 inch) pole wall thickness.	122
Figure 7.10 S-N plot of thick base plate socket connection with 4.76 mm (3/16 inch) pole wall thickness.	123
Figure 7.11 Crack surfaces of excavated Pole 2 socket.....	124
Figure 7.12 Crack in box connection from out-of-plane loading (Pole #6).....	127
Figure 7.13 Type I box connection cracking from in-plane loading (T1P2).....	128
Figure 7.14 Cross-section of box connection depicting side plate deformation under in-plane loading.	128
Figure 7.15 Box connection cracks in Type I Pole 1 (T1P1).....	129
Figure 7.16 Box connection cracks in T1P3.....	130
Figure 7.17 2001 Specifications fatigue checks on box connections.	131
Figure 7.18 S-N plot of Type I box connection fatigue data.....	133
Figure 7.19 Typical cracks on Type I full-penetration weld mast arm.....	135
Figure 7.20 Fatigue results of Type I, full-penetration weld mast arm plotted against S-N curves.	137
Figure 7.21 Macro etch of gusset stiffener cross-section.....	140
Figure 7.22 Typical cracks found in gusset plates.....	141
Figure 7.23 Seam weld crack in gusset-stiffened specimen.....	142
Figure 7.24 S-N plot of gusset-stiffened mast arm specimens.	143
Figure 7.25 Crack in first transformer base originating from access hole.....	144
Figure 7.26 Crack in second transformer base.	146
Figure 7.27 In-plane crack for Type II specimen.	148
Figure 7.28 Out-of-plane cracks for Type II specimen.....	149

Figure 7.29 S-N plot of Type II mast arm fatigue results.	151
Figure 7.30 Orientations of Type II pole specimens	153
Figure 7.31 Access hole cracks in Type II poles.	153
Figure 7.32 Cracking in tapered base shell originating from stiffening ring.	154
Figure 7.33 S-N plot of Type II pole specimens.	156
Figure 8.1 Detail recommendations for Type I box connection.	160
Figure 8.2 Access hole detail recommendations.	161

List of Tables

Table 2.1	Reproduction of Table 11-1 from 2001 Specifications.	11
Table 3.1	0.01% Exceedance Stress Ranges from South (1994) Data.	22
Table 3.2	Wyoming Fatigue Data for Mast Arm Connections.	33
Table 3.3	Wyoming Fatigue Data for Box Connections.	34
Table 3.4	Valmont Test Matrix	41
Table 3.5	Boundaries of Extrapolation Region for CHS and RHS Joints	51
Table 5.1	General Strain Gauge Lexicon for Fatigue Testing	72
Table 6.1	Comparisons of Experimental to Predicted Nominal Strains at Mast Arm and Pole Midpoints for the Three Loading Cases.	85
Table 6.2	Select SCFs from Type II Pole Static Tests.	105
Table 7.1	Fatigue Results from Frame 1	116
Table 7.2	Fatigue results from Frame 2.	117
Table 7.3	Fatigue Results of Thick Base plate Pole Specimens.	121
Table 7.4	Fatigue Results for Type I Box Connections.	132
Table 7.5	Fatigue Failure Results for Type I Full-Penetration Weld Mast Arms	136
Table 7.6	Fatigue Results for Gusset-stiffened Mast Arms.	139
Table 7.7	Loading History on First Transformer Base	145
Table 7.8	Load History of Second Transformer Base to Crack	146
Table 7.9	Fatigue Results of Type II Mast Arms	150
Table 7.10	Fatigue Results for Type II Pole Specimens.	155

Executive Summary

There have been increasing problems with wind-induced vibration, fatigue, and structural collapse of cantilevered sign, signal and light supports in many states, although Minnesota has not had any significant problems. The increasing rate of fatigue problems is due in part to inadequate design specifications prior to 2001, when the 4th Edition of the AASHTO Standard Specifications for Structural Supports for Highway Signs, Luminaires and Traffic Signals was introduced. This edition is substantially different than previous editions and contains explicit fatigue design criteria including fatigue loads and categorizes many common details. For structures designed in accordance with the new 2001 Specifications, the choice of connection details is usually governed by the fatigue design provisions and often too is the size and thickness of the members. However, the best details from a fatigue design standpoint are often more expensive and difficult to fabricate.

One of the most fatigue-critical connections is the mast arm-to-pole connection of traffic signal structures. Typically, cracks form in the pole, emanating from the corner of the welded built-up connection used to attach mast arms. Several researchers have conducted analytical studies of these connections, which verify the corner of the built-up connection is a region of high stress concentration and susceptible to fatigue. However, there has only been limited testing of these connections, which was inconclusive.

Another fatigue-critical detail in mast arm-to-pole connections is the tube-to-transverse plate connection which is typically used to facilitate the attachment of the mast arm to the built-up box. This detail is also used for attaching pole bases to concrete foundations. The most common type of tube-to-transverse plate detail is the fillet-welded socket detail. The socket detail uses a plate with a hole cut out slightly larger than the outside diameter of the tube. The tube is partially inserted into the hole and fillet welded inside and out. There have been several test programs involving fatigue of fillet-welded socket connections, establishing that this connection is an AASHTO Category E' detail. All the socket connection tests found in the open literature use round cross-sections. However, in Minnesota, the majority of the traffic signal structures use octahedral cross-sections. Finite element studies of socket connections using octahedral cross-sections show that the bent corners of the multi-sided cross-sections are stress risers, and it has been hypothesized this may affect the fatigue resistance, but this has not been verified experimentally. Full-penetration welds may also be used in tube-to-transverse plate details. Likewise, there has been little testing of these details, with some studies showing a fatigue resistance higher than the standard fillet-welded socket connection, and some showing resistance to be lower. Tube-to-transverse plate connections may also feature triangular stiffeners, which have been tested to some extent, but again, only with round tubes demonstrating a lot of scatter in published results.

This research project focused testing on two different mast arm-to-pole connection styles using octahedral pole sections which reflect typical Minnesota designs. The first used conventional built-up "box connection" styling where a series of plates welded to the pole create a stiffened, flat mating surface on the pole for the mast arm. The base of the pole and the ends of these mast arms utilized tube-to-transverse plate connections with fillet-welded socket, full-penetration welds, or gusset-stiffened fillet-welded socket detailing. The second mast arm-to-pole detail

full-penetration welded the mast arm tube to a stub pole section that slip fit over the top of the actual pole. All mast arm-to-pole connections were fatigue tested in three different directions, corresponding to in-plane behavior (mast arm motion in the plane of the structure), out-of-plane behavior (mast arm motion out of the plane of the structure), and an equal superposition of the two (45 degree loading behavior).

The more commonly used system using the built-up box connection demonstrated a complicated load path making a nominal stress categorization difficult to define. Using current code definitions, the box connections suffered punching shear failures at the corners of the box connection in the out-of-plane and 45 degree loading cases with a lower bound fatigue resistance slightly above Category K_2 . This agreed with current AASHTO predictions. However, for in-plane behavior, the box connection cracked the welds between the flange plate and the pole at Category ET resistance. The in-plane resistance is one category lower than the Category E' currently predicted by AASHTO, indicating future designs should be designed with the lower ET resistance pending future experimental results. All the tube-to-transverse plate connections utilized a 4-bolt pattern, and an eight-sided polygonal tube. The standard, multi-sided, fillet-welded socket connection with 1.25 inch thick base plates demonstrated a Category K_2 resistance. AASHTO currently deems all fillet-welded socket connections to be Category E', but the multi-sided socket resistance was two categories lower. Despite a lower resistance, hammer peen treatments were found to enhance the resistance of this connection to Category E', and doubling the base plate thickness increased the resistance to roughly Category E. Tube-to-transverse plate connections with full-penetration welds exhibited Category E' resistance and the triangular gusset plate were found to have Category E resistance, each agrees with current AASHTO predictions.

The second mast arm-to-pole detail using the slip-fit connection style was in essence a tube-to-tube connection. All these connections cracked in the mast can detail despite the loading condition, indicative of a punching shear failure. Using the punch shear stress ranges, the lower bound fatigue results of this connection were just above Category K_2 resistance, which shows slight conservatism using current AASHTO procedures. The poles that mate with the mast can detailed mast arms use an integrated, tapered transformer base with an access hole detail. The access hole had reentrant corners near the base plate that proved to be very weak in fatigue. Using the net section stress range at the corner of the access door, the lower bound resistance of the detail was less than Category K_2 , where the code currently predicts access door details to range from E' to D resistance depending on the detailing. An improved access door detail is suggested with rounded corners to negate the use of reentrant corners.

Chapter 1

Introduction

Cantilevered mast arm signal structures are commonly used at road intersections to support signs and signals over the roadway. The design of sign and signal structures in the United States is guided by the Standard Specifications for Structural Supports for Highway Signs, Luminaires, and Traffic Signals, published by the American Association of State Transportation Officials (AASHTO). The most current 4th Edition of this code was published in 2001 and will herein be referred to as the 2001 Specifications (1). Prior to the 2001 Specifications, previous versions of the specification were strength based and offered little guidance regarding serviceability limits such as fatigue. Essentially, the 1994 specification stated fatigue design should be based on the fatigue provisions from the AASHTO Standard Specifications for Highway Bridges (2), and only pointed designers to exercise care “at the junction of the base and shaft, connection at the bracket arm and shaft, and especially in welded areas,” leaving design for fatigue rather ambiguous.

These structures are often flexible and lightly damped, which coupled together make the structure susceptible to wind-induced vibrations. These vibrations have historically led to fatigue cracks in the welded details of these structures, sometimes leading to structural failure. In 1990, two cantilevered signal structures collapsed in close succession in Michigan, resulting in property damage, injuries, and one fatality (3). Both collapses were attributed to loss of strength from fatigue cracks in the anchor bolts. As a result of this accident, the Michigan Department of Transportation (DOT) had to pay out a large settlement that in turn disrupted their maintenance schedule for a three-year period.

In response to the Michigan collapses, AASHTO determined that their specifications needed to be completely revised, including more guidance on the design for vibration and fatigue. A research project was begun (National Cooperative Highway Research Project (NCHRP) 10-38) to develop improved specifications for vibration and fatigue, including identifying all types of loading that causes fatigue, identifying fatigue prone details, and developing design methods (4). However, fatigue testing in that work focused on anchor rods, and the majority of the fatigue categories in the specification were based on judgment and extrapolated from other design specifications. Currently, there remains great uncertainty in the fatigue categories (5).

Many states and fabricators believe the fatigue provisions of the 2001 Specification are overly conservative, claiming fatigue designs are impossible and not cost effective. The objective of this project was to categorize the fatigue resistance of commonly used welded details of traffic signal structures built in the State of Minnesota. The fatigue resistance was determined through full-scale structural testing at the University of Minnesota-Twin Cities campus in the Department of Civil Engineering Structures Laboratory. Specimen design targeted two commonly used mast arm-to-pole connections, but as a consequence of specimen design, tube-to-transverse plate connections were also tested. This research was unique in the fact that the tubes were multi-sided, not round as addressed by various previous research projects.

This report begins with a description of fatigue in other related structures and a brief fatigue primer in Chapter 2. A literature review in Chapter 3 outlines the findings of past related projects. Chapter 4 describes the experimental program including specimen and load frame descriptions. A large variety of strain gauges were installed on some of the specimens to

understand how these structures behave which is described in Chapter 5. Chapter 6 then presents the data collected with the strain gauge via static tests. The fatigue results of all the tested specimens are then presented in Chapter 7, with final conclusions and recommendations lastly presented in Chapter 8.

Chapter 2

Fatigue in Related Structures

This document will address types of welded details commonly used in three types of structures. These structures will be referred to as horizontal cantilevered, vertical cantilevered, and bridged-type structures. The horizontal cantilevered structures broadly describe structures with two subelements, namely a pole (vertical element with fixed base) and a mast arm (horizontal element cantilevered off the pole). The cantilever design using one pole minimizes the likelihood of a vehicle hitting the structure versus a bridged-type structure with two poles. Three different horizontally cantilevered structures can be seen in Figure 2.1. Vertically cantilevered structures are typically used to support lights high over a roadway, and are commonly called high mast lighting structures. High mast lighting towers are essentially a vertical tube with a fixed base, supporting a large mass of lights at the tip, as seen in Figure 2.2. The bridged-type support (shown in Figure 2.3) describes a structure with two poles and one horizontal element spanning between the two poles. This structure is ill named because of confusion with it being a structure mounted on a bridge, but the name is meant to imply that the structure “bridges” over the roadway.

As part of NCHRP Report 469, a survey of state DOTs was conducted to determine the problems with traffic structures in regard to fatigue (5). Five main types of cracking were reported at the following details; anchor rods, hand hole details, tube-to-tube connections, tube-to-transverse plate connections, and mast arm-to-pole connections.

Anchor rods are susceptible to fatigue, though they are not welded, because the nature of a threaded rod can be thought of having a continuous spiral notch cut into the rod. However, the fatigue strength of anchor rods has been well classified in previous research (4,6), and will not be a focus of this report.

In the poles of traffic structures, hand holes are commonly provided near the base to allow for access to the electrical wiring inside of the pole, or to facilitate with tightening anchor bolts. Because a portion of the pole is cut away, there is a stress concentration around the hole under load and properly sized stiffening rings are needed to make up for the section loss. However, these details have been known to initiate fatigue cracks as shown in Figure 2.4.

Some two, three, and four chord trusses in cantilevered or bridged-type supports only use round cross sections for both the chords and braces (see Figure 2.5). To be properly fabricated the braces need to be “fish-mouthed”, or cut such that the brace fits tightly to the chord around its whole perimeter. These are referred to as tube-to-tube connections. Because the side of the brace is slightly longer than the top of the brace, the difference in axial stiffness around the brace creates a stress concentration, which makes this detail susceptible to fatigue. Figure 2.6 shows a picture of a cracked tube-to-tube connection.

Tube-to-transverse plate connections are probably the most common type of fatigue prone detail used in the fabrication of traffic signal structures. These types of connections facilitate the connection of poles to concrete foundations, or bolting mast arms to poles. There are three types of tube-to-transverse plate connections, fillet-welded sockets, full-penetration groove welded, and either of the latter stiffened with gusset plates, each is shown in Figure 2.7 along with their

fatigue classifications according to the 2001 Specifications. The most common type of tube-to-transverse plate connection is the double fillet-welded socket connection. The socket connection is created by cutting a hole slightly larger than the outside diameter of the tube into the plate, the tube is partial slid into the plate, and finally two fillet welds are applied around the circumference of the tube on the inside and outside intersection of the tube and plate. For slightly better fatigue performance, a full-penetration weld with a backing ring can be specified, which does not require as much of the base plate to be cut away. Either of these two connections can be further enhanced by welding gusset plates to the plate and tube, and various fatigue performances can be expected based on the detailing of the stiffener.

Mast arm-to-pole connections are required because it is often not feasible to transport a pole with a mast arm preattached in a fabrication shop. To facilitate a bolted connection between a pole and a mast arm it is common to construct a “box-connection” on the pole tube, at the level where the mast arm will be cantilevered from. For round pole cross-sections, the box-connection is made using four plates welded to the pole in the shape of a box (two side plates, a top plate, and bottom plate) and fifth flange plate is then welded to the other four plates of the box connection, thus creating a flat surface for the mast arm to bolt to. A box connection on a round tube is shown in Figure 2.8 along with typical fatigue cracks that initiate at the corners of the box where it intersects the pole.





Figure 2.1 Three types of horizontally cantilevered structures. Top: Monotube mast arm. Middle: Vierendeel trussed mast arm. Bottom: Four chord trussed mast arm.

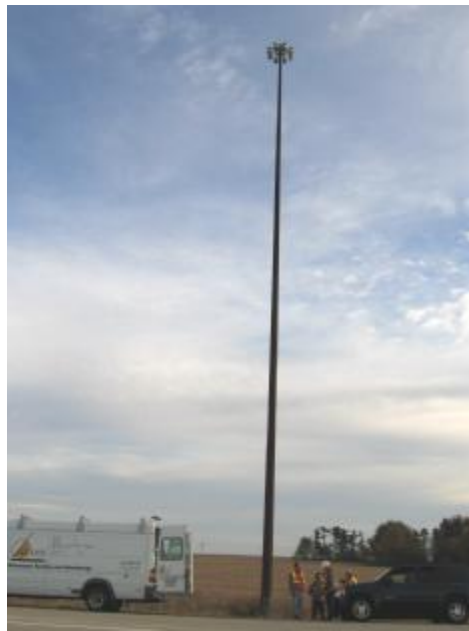


Figure 2.2 Vertical cantilever used to support light fixtures (high mast tower).



Figure 2.3 Typical bridged-type supports. Top: Four chord truss. Bottom: Monotube.

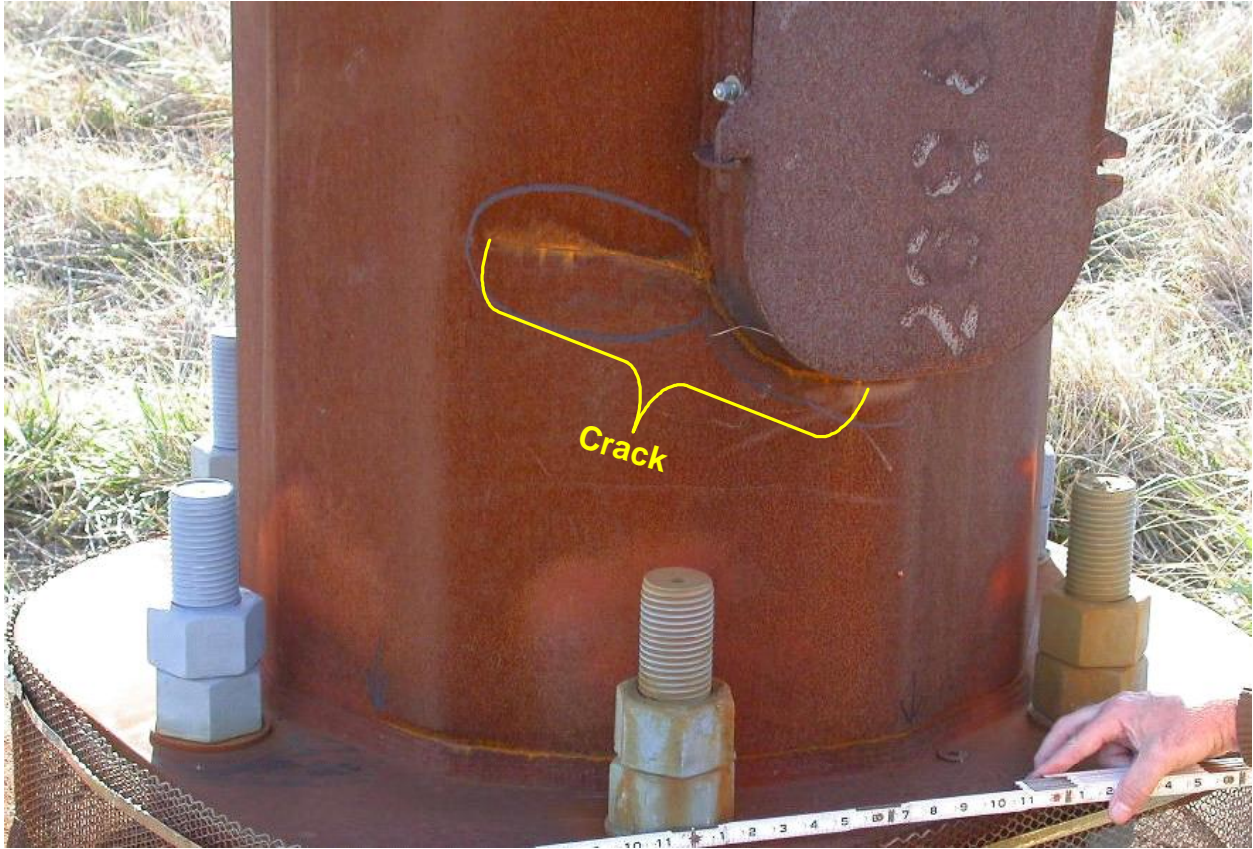


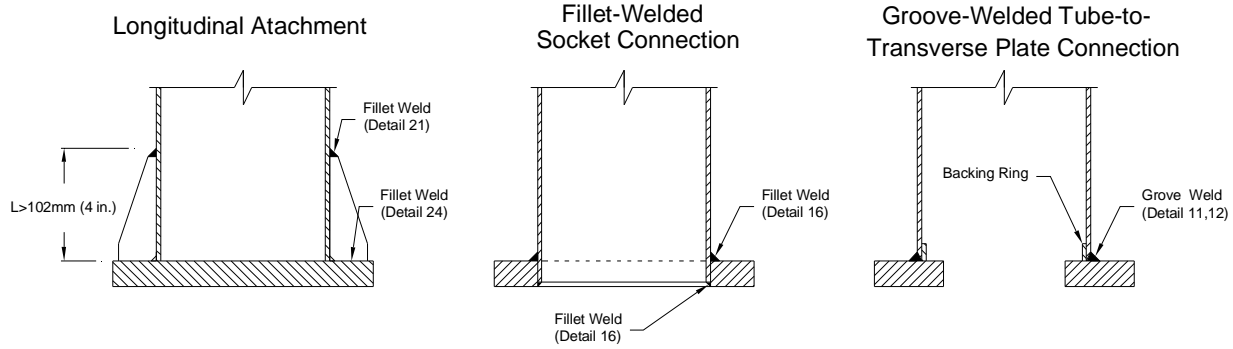
Figure 2.4 Crack emanating from hand hole detail in high mast tower, Clear Lake, IA.



Figure 2.5 Four chord, space truss, bridged-type support using tube-to-tube connections.



Figure 2.6 Picture of a cracked tube-to-tube welded connection.



Construction	Detail	Stress Category
Groove-Welded Connection	11. Full-penetration groove-welded tube-to-transverse plate connections with the backing ring attached to the plate with a full-penetration weld, or with a continuous fillet weld around interior face of backing ring. The thickness of the backing ring shall not exceed 10 mm (0.375 in.) with fillet weld attachment to plate. Full penetration groove-welded tube-to-transverse plate connections welded from both side w/backgouging.	E
	12. Full-penetration groove-welded tube-to-transverse plate connections with the backing ring not attached to the plate with a continuous full-penetration weld, or with a continuous interior fillet weld.	E'
Fillet-Welded Connections	16. Fillet-welded tube-to-transverse plate connections.	E'
Attachments	21. Longitudinal attachments with partial- or full-penetration groove welds, or fillet welds, in which the main member is subjected to longitudinal loading. ¹ L < 51 mm (2 in.) 51 mm (2 in.) < L < 12t and 102 mm (4 in.) L > 12t or 102 mm (4 in.) when t < 25 mm (1 in.)	C D E
	24. Transverse load-bearing fillet-welded attachment where t < 13 mm (0.5 in.) and the main member is subjected to minimal axial and/or flexural loads. [When t < 13 mm (0.5 in.), see note d].	C
¹ Only longitudinal stiffeners with lengths greater than 102 mm (4 in.) are applicable for Detail 21. Caution should be excersized regarding the use of the longitudinal stiffener terminations of Example 12 on some members, such as traffic signal mast arms and traffic signal poles. See commentary for Article 11.5.		

Figure 2.7 AASHTO 2001 Specifications tube-to-transverse plate fatigue classifications.

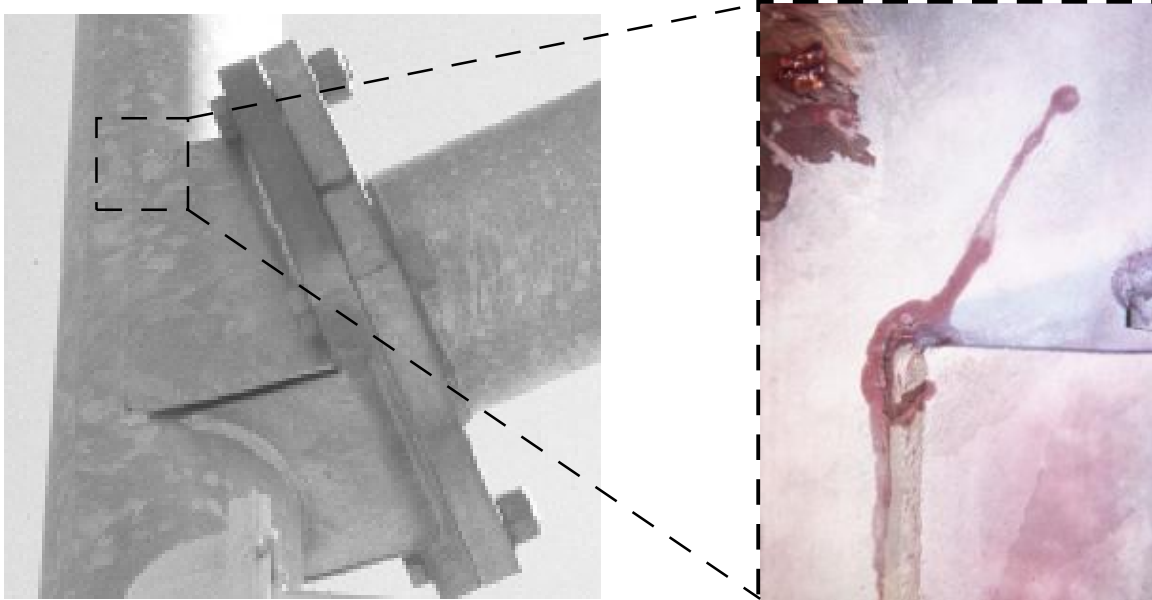


Figure 2.8 Left: Built-up box connection used to connect the mast arm to the pole. Right: Typical cracks emanating from side plate termination of box connection (29).

2.1 Present Design Specifications

The current specification for design of traffic structures is the Standard Specifications for Structural Supports for Highway Signs, Luminaires, and Traffic Signals published by the AASHTO (1). This specification uses a strength based design philosophy and fatigue is considered to be a serviceability check. The fatigue provisions will be the focus of this report. This specification uses the nominal stress approach for evaluating a design for fatigue resistance using equivalent static loads and an “infinite fatigue life” approach using nominal stresses.

The first part of any fatigue design check is to determine the importance of the structure and which loads it will be subjected to. The importance factor (IF) is used to determine the reliability level of the structure. For instance, if a structure will be used on a heavily traveled road, it will have a higher importance factor because of the higher probability of damage induced by a failure. The current problem with the importance factors is their loose definitions, and most transportation departments end up specifying Category I (the most severe category) design just to be conservative. Dexter and Ricker outlined new importance factor definitions, which should reduce the number of incidents of over design (5). The determination of the IF is easily performed using Table 2.1, which is a reproduction of Table 11-1 from the 2001 Specifications. This table also tells the designer which loads are applicable to the structure being designed.

The loads applied to the structure are then determined in sections 11.7.1 – 11.7.4 of the 2001 Specifications for galloping, vortex-shedding, truck-induced gust, and natural wind gusts. The loads determined are equivalent static pressures to be applied to respective projected areas of the structure. When these loads are used in a simple elastic analysis, the loads coming out of the

analysis will represent a load range equivalent to the highly non-linear load ranges from the dynamic interaction of the structure to the different types of aerodynamic and aeroelastic loadings. Once the load ranges are known, they can be converted to nominal stress ranges at particular details using simple equations of mechanics and cross-sectional properties. The calculated stress ranges can then be compared to the respective constant-amplitude fatigue life (CAFL) for the detail being analyzed. The allowable stress range is dependant upon the detail being analyzed, but Figures 11-1 (a) - (f) along with Table 11-2 of the 2001 Specifications allows the designer to categorize the detail being analyzed. Examples of the categorization of fatigue details using the 2001 Specifications can be seen in Figure 2.7.

The fatigue provisions were not in the previous 1994 specification, and are new to the 2001 Specifications. The AASHTO T-12 subcommittee is responsible for the development of the 2001 Specifications. At the annual meeting in Albuquerque, New Mexico (May 2003) presented a questionnaire put forth by the committee to the 50 transportation departments. The results of this questionnaire can be seen in Appendix A. Many states are experiencing difficulty with the fatigue design specifications. If the same detailing is used, large increases in the section sizes seem to be required. However, as demonstrated in the example problems in NCHRP Reports 412 and 469, the way to upgrade the fatigue resistance of a structure, deficient under the new specifications, is to use more fatigue resistant details (4,5). For example, by changing from a Category E' to a Category E detail, the CAFL is increased from 18 MPa to 31 MPa (2.6 ksi to 4.5 ksi), or an increase of 72% in allowable stress.

Table 2.1 Reproduction of Table 11-1 from 2001 Specifications.

Fatigue Category		Importance Factor, IF			
		Galloping	Vortex Shedding	Natural Wind Gusts	Truck-Induced Gusts
I	Sign	1.0	X	1.0	1.0
	Traffic Signal	1.0	X	1.0	1.0
	Lighting	X	1.0	1.0	X
II	Sign	0.65	X	0.75	0.89
	Traffic Signal	0.65	X	0.80	0.84
	Lighting	X	0.65	0.72	X
III	Sign	0.31	X	0.49	0.77
	Traffic Signal	0.30	X	0.59	0.68
	Lighting	X	0.30	0.44	X

Note:
X – Structure is not susceptible to this type of loading

Category Descriptions:
I – Critical cantilevered support structures installed on major highways
II – Other cantilevered support structures installed on major highways and all cantilevered support structures installed on secondary highways
III – Cantilevered support structures installed at all other locations

2.2 Background in Fatigue

Fatigue is the accumulation of damage from repeated cycling in a structure from fluctuating loads or vibration. The damage appears in the form of cracks that can grow and eventually lead to failure by ductile rupture, brittle fracture, or buckling. There are three different approaches for determining fatigue resistance and they are dependent upon the level of analysis one is willing to perform. The difference in level of analysis is illustrated in Figure 2.9, which shows a plate under uniform stress, with a transverse fillet-welded attachment such as a stiffener.

The uniform stress remote from the attachment is the nominal stress that can be calculated using simple mechanics of materials equations. This nominal stress is intensified closer to the attachment from two sources of stress concentration. First there is the effect of global geometry of the connection, which produces an elevated stress referred to as the geometric stress. It is typically possible to reasonably estimate this geometric stress using relatively coarse finite-element analysis. Then there is a further stress concentration due to the local geometry of the weld toe, this is referred to as the local notch stress. This local notch stress concentration is dependent on random parameters such as ripples in the weld toe and typically cannot be accurately characterized through analysis.

For example, if there were a uniform flat plate panel with a butt weld transverse to the nominal stress, there would be a local notch stress concentration at the weld toe but no geometric stress concentration. However, if there were a tee-joint or misalignment of the plates, this would give rise to the geometric stress concentration as well. These three different levels of stress located in the area around a weld give rise to three different types of analysis used to calculate fatigue life. These are, 1) Nominal stress approach, 2) Hot-spot stress approach, and 3) Fracture mechanics.

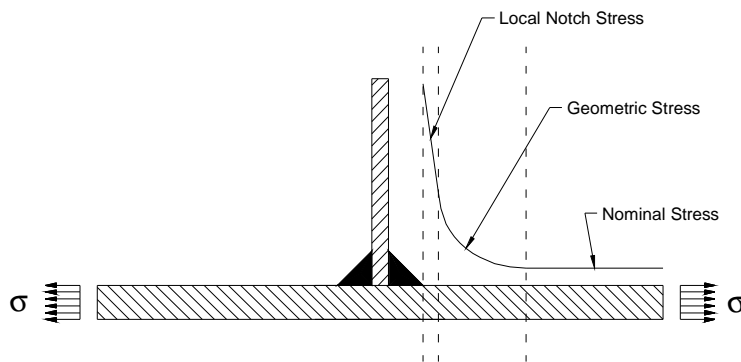


Figure 2.9 Difference between stresses near a welded detail

2.2.1 Nominal Stress Approach

The nominal stress approach is the most simple way to assess the fatigue resistance of a detail and therefore is most suitable for design specifications. This approach determines the fatigue resistance based on a nominal stress near the welded joint, with the stress computed through simple equations of bending and axial loadings. This design procedure relies on full-scale fatigue testing of each unique geometry. Failure is commonly defined as the development of a

through-thickness crack. The test data are presented in stress range (S) vs. number of cycles to failure (N) curves, where the stress range in this case is the nominal stress range. Because weld profiles, residual stresses, and weld discontinuities are highly variable from specimen to specimen, the fatigue data based on nominal stresses has a large amount of scatter, and the S-N curve represents a lower bound of the data. Specifically, the S-N curve is two standard deviations of the logarithm of the cycles to failure below the mean of the data, this is equivalent to a 97.5 percent survival rate. This lower bound approach makes this method very conservative.

Different S-N curves are used to evaluate the fatigue resistance of different details depending on the geometry of the detail. Each S-N curve represents a particular detail category, where details with similar fatigue strength are put in the same category. The test data indicate that the fatigue resistances of details are independent of the type of steel and the welding process used (7,8,9,10). S-N curves are well developed for simple details such as longitudinal welds, transverse butt welds, cover plated beams, etc. Figure 2.10 shows the S-N curves from AASHTO Specifications, as well as American Welding Society (AWS) and American Institute of Steel Construction (AISC) specifications. In the nominal stress approach, the effect of the geometric and local stress concentrations are included in the test data and they do not need to be accounted for by the designer. Variations in the combined stress concentrations are reflected in the different detail categories.

In addition to the S-N curve, each detail category has a constant-amplitude fatigue limit (CAFL). The CAFL is a stress range below which no fatigue failures are expected to occur in tests conducted with constant-amplitude loading. These limits are shown as the horizontal lines on the right side of the S-N curves in Figure 2.1. The CAFL can be used in the “infinite life approach”. This design philosophy ensures that the nominal stress range at a fatigue detail due to the fatigue-limit-state load range is below the CAFL, hence no fatigue cracking would ever be expected. The fatigue-limit-state load range is nominally supposed to be a load range that is only exceeded 0.01% of the time by all load ranges (11). For example, the recommended fatigue loads in the 2001 Specifications are supposed to have approximately this exceedence probability when compared to the real loading spectrum.

If the loading has variable amplitudes, a more complex analysis using Miner's rule can be used to determine an equivalent nominal stress range (12).

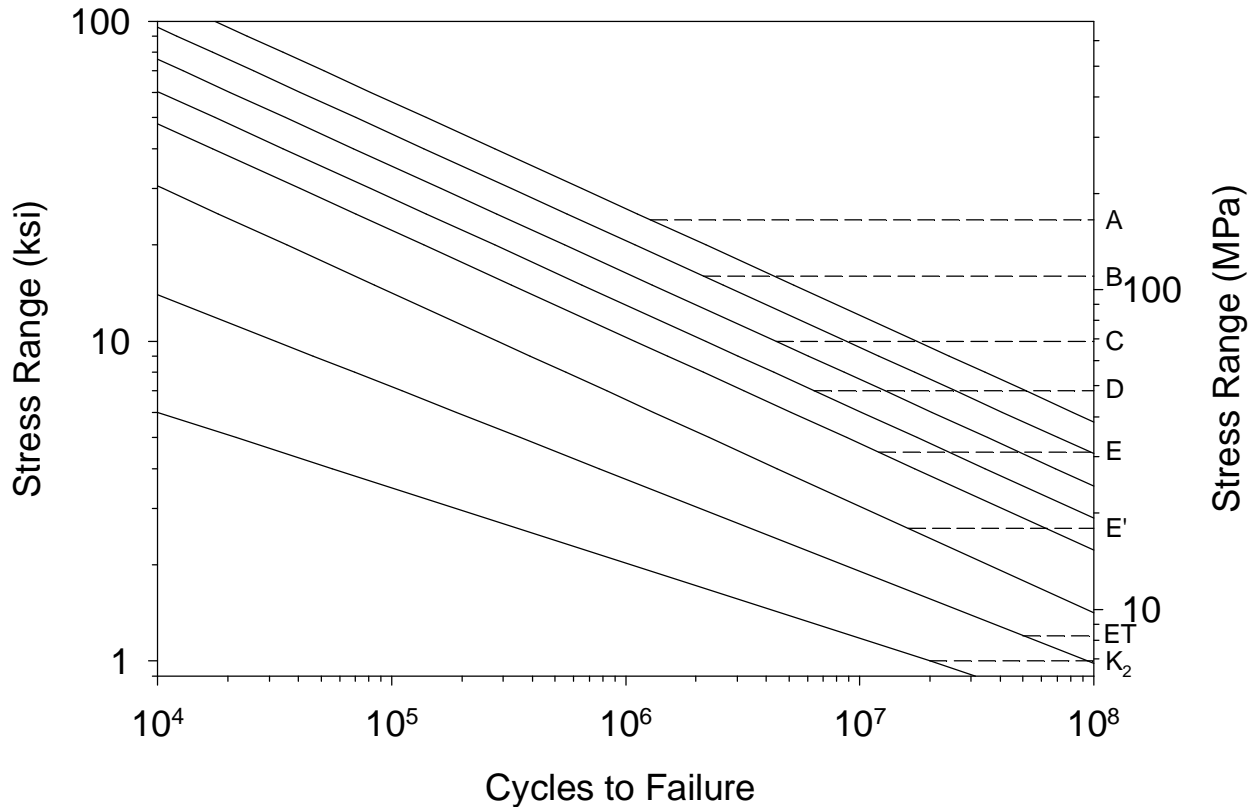


Figure 2.10 Nominal stress S-N curves used in AASHTO, AISC, AWS specifications

2.2.2 Hot-Spot Stress Approach

The hot-spot stress approach is similar to the nominal stress approach, but the S-N curves in this approach are based on the range in the geometric stress, also called the hot-spot stress. Full-scale tests are performed, but it is attempted to measure or calculate the hot-spot stress and plot the results in terms of the hot-spot stress range. In essence, the effect of the geometric stress concentration is taken out of the fatigue resistance and instead is included in the analysis. This has the advantage of collapsing all the S-N curves for different categories into a single baseline S-N curve, but it increases the complexity of the analysis. The test data and the baseline S-N curve still include the effect of the local notch stress concentration, which may be impossible to accurately calculate and therefore must still be treated empirically.

For bridges, there are a limited number of details, and it is possible to perform full-scale tests on all of these and characterize their fatigue resistance with a limited number of categories. Therefore, the nominal stress approach has been satisfactory. However, for tubular structures, including many sign and signal support details, there may be a huge number of detail geometries, and it is not possible to test them all or have a unique S-N curve for each geometry. In these cases, the hot-spot stress approach may be the only practical alternative.

The geometric stress is often in high strain gradient fields, and measurement of the geometric stress involves considerable uncertainty. To address this problem, guidelines have been established to extrapolate a SCF from multiple strain gauge measurements (13). Another simple

approach that was found to work was to define the hot-spot stress as the stress measured with a 3 mm strain gage placed as close as practically possible to the weld toe, i.e., centered about 5 mm from the weld toe. This is essentially the definition used by AWS D1.1 (14). The baseline curve is sensitive to the definition of the hot-spot stress. British Standards (BS) 7608 defines a Category T curve, along with a correction factor based on the plate thickness, and AWS uses the X2 curve (15).

As it turns out, these curves are similar to the AASHTO Category C curve, which is the nominal stress S-N curve associated with butt welds with reinforcement (not ground flush) in a flat uniform plate (16). This makes sense since the stress at the weld toe of this detail would include the local stress concentration but would not include any effect of geometric stress concentration. Therefore the hot-spot stress is equal to the nominal stress in this detail.

In design, the hot-spot stress approach involves the calculation of geometric stress concentration factors (SCF) using parametric equations or finite elements analysis (FEA) (13,17). However, FEA may be highly mesh dependant, since the geometric stress is often in an area of high strain gradients. The disadvantage in this method lies mainly in the variability between different hot-spot stress definitions and varying baseline S-N curves. Another problem involves the CAFL. The hot-spot approach implies that all details will have a CAFL at the same number of cycles, while full-scale fatigue tests show that the CAFL occurs at different orders of magnitude of cycles for different categories. Conservatively, the CAFL is typically ignored for hot-spot stress analysis.

2.2.3 Fracture Mechanics Approach

Fatigue crack growth can be calculated using the Paris Law. The Paris Law relates the number of cycles to the stress intensity parameter through the following relationship:

$$\frac{da}{dN} = C \cdot \Delta K^m$$

where da/dN = the crack growth rate, C = material constant, ΔK = the stress intensity parameter, and m = material constant equal to 3.0 for carbon steels. The differential equation can be solved to uniquely define the crack length for a given number of cycles. The problem with this approach is the calculation of the stress intensity parameter. There are handbook solutions available depending on the loading condition and crack shape, but they all require the initial defect size. This highlights the problem with the fracture mechanics approach because there is no way to measure the defect size in design, and even assuming a size could greatly affect the results from the equation. Previous analytical studies have found that assuming an initial crack depth of 0.25 mm and elliptical crack K solutions have correlated well to test data (18). Another problem is that the local notch stress concentration must also be known, and as stated previously, this is often dependent on highly random parameters.

Chapter 3

Literature Review

The focus of this literature review will be to provide an overview of all knowledge regarding the fatigue design of cantilevered sign and signal support structures, fatigue resistance of mast arm-to-pole connections and pole base connections. The state-of-the-art in the fatigue design of general tubular structures is also summarized.

3.1 NCHRP Research

After the cantilever collapse in Michigan (3), AASHTO mandated the design code for traffic signal structures needed to be revised. Thus, National Cooperative Highway Research Program (NCHRP) initiated project 17-10 to completely revise the 1994 specification, except for fatigue and vibration which were being addressed in the smaller NCHRP 10-38 project. The final report for project 10-38, NCHRP Report 412 (4), included draft specifications, which essentially became adopted into the Chapter 11, Fatigue Design in the 2001 Specifications.

Report 412 researched the wind loadings which create fatigue damage and found equivalent static pressures to represent the complex dynamic loading on actual structures (4). The static pressures could then be used in a static structural analysis to produce a stress at a detail, which is then equal to the dynamic stress range for use in a fatigue analysis. The equivalent stress range can then be compared to standard AASHTO fatigue categories using the nominal stress approach. This offered designers a very simple and quick approach to conduct a fatigue analysis.

Report 412 also identified four different types of loading which can induce vibrations in signs, luminaries, and traffic signal supports. These loadings cause two primary motions of cantilevered traffic structures, in-plane and out-of-plane motion. In-plane motion describes mast arm motion in the vertical plane (normal to the road surface) and out-of-plane loading refers to the motion in the horizontal plane (parallel to the road surface). The four loadings that cause these motions are 1) natural wind gust, 2) vortex shedding, 3) galloping, and 4) truck gust. The following sections will provide a description of these loadings.

3.1.1 Natural Wind Gust

Natural wind gust describes the random variability of the speed, direction, and particularly frequency of which wind blows. The frequencies which wind blows cover a large spectrum that can potentially affect a large number of structures. When any fluctuating air flow is interrupted by a structure, it naturally causes a fluctuating pressure differential across the structure, which imparts a force. Typically, natural wind gust only affect the out-of-plane behavior of cantilevered signal structures.

3.1.2 Vortex Shedding

Unlike natural wind gusts, vortex shedding is a phenomenon that can occur when a bluff body interrupts a uniform, steady airflow. In the wake of the airflow, small vortices alternately form on each side of the body that the airflow passes over, commonly referred as the von Karman vortex street (shown in Figure 3.1). As the vortices spin off on alternating sides of the bluff

body, an area of low pressure is formed after each vortex, or eddy. Therefore, the alternating pressure differential imparts a loading similar to a sinusoidal forcing function normal to the airflow (4). When the frequency of the shedding vortices matches that of one of the vibrational modes of the structure, it is said to be “locked-in” and resonance occurs. Vortex shedding only affects long monolithic bodies, like high mast towers or bridged monotube supports. For cantilevered mast arm structures, attachments such as signal heads and signs disrupt the airflow enough such that vortex shedding does not occur as the air moves around the tube.

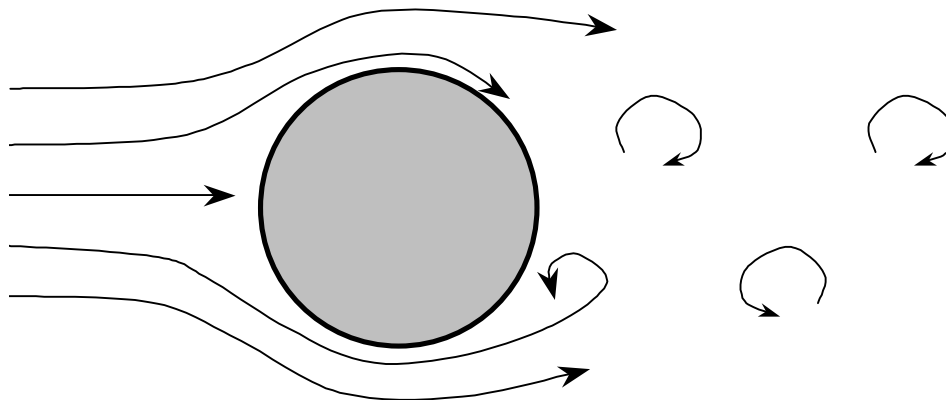


Figure 3.1 Picture of von Karman vortex street.

3.1.3 Galloping

As with vortex shedding, galloping is an across-wind response that occurs in a uniform, steady flow of air. If the structure is vibrating across the flow, the flow itself begins to oscillate, which causes periodic changes in the angle of attack of wind on the structural element. The change in angle of attack of the flow can add a force component in a direction either with or against the structural motion. Galloping occurs when the additional force is aligned with the structural motion, which is analogous to having negative structural damping. This exacerbates the structural motion, hence the name, galloping. Galloping does not affect circular cross-sections, however, the traffic signal heads attached to the mast arms of cantilevered structures make them susceptible to galloping. Susceptibility to galloping is worsened when backplates are attached to the signal head to increase visibility of the traffic signal.

3.1.4 Truck Gusts

When large trucks pass beneath traffic signal structures, they impose both horizontal and vertical gusting forces on the structure. However, the magnitudes of the horizontal gusts are small in comparison to natural wind gust, and are therefore ignored for fatigue calculations. The vertical component of the truck gust force particularly affects the in-plane bending behavior of cantilevered signal structures as the gust hits the projection of the cross-section in the horizontal

plane. Truck gust forces are important for structures with variable message signs (VMS) and overhead bridge supports with exposed walkways.

3.2 Archer and Gurney (1970)

This project was conducted to find the fatigue strength of tube-to-transverse plate fillet welds, and to find the ideal weld size, such that failure occurred by a crack through the weld throat not through the tube at the weld toe (19). A total of 24 specimens were tested using two different designs. One design was meant to represent the modern socket connection (Type S specimen), except only one fillet weld was provided around the outside diameter of the tube, unlike common practice today of using double fillets. The second connection tested (Type F specimen) allowed the tube to bear tightly upon the plate, around a machined spigot surface. A fillet weld was then placed along the outside diameter circumference. For clarity, Figure 3.2 shows a drawing of these two specimen designs. In each design case, the size of the fillet weld was a variable such that the ideal weld size for fatigue could be determined. The tests were run using an out-of-balance rotating mass to induce a rotating bending moment upon the specimen. This meant that the specimens were cycled about zero mean stress, or zero dead load. As seen in Figure 3.2 the specimens were fabricated such that two joints were tested simultaneously.

The results of this testing are plotted in Figure 3.3 in log-log format along with the AASHTO fatigue curves. In regards to the Type F specimens, there is a notable trend that larger welds have higher fatigue strengths. The 7.9 mm (0.3125 inch) fillet data followed the Category E curve quite well, and these welds were noted to always fail by a crack in the tube originating from the weld toe. The 11.1 mm (0.4375 inch) fillet welds plotted along the Category D curve and were found to fail by a combination of both weld toe and weld root failures. Finally, the 17.5 mm (0.6875 inch) fillets only failed through the weld throat, and their data plotted closely with the Category C curve. For the Type S specimens, the weld size trend was not as apparent as in the Type F connections, and the data plotted along the Category D curve. However, the same failure mode trend of the Type F connections was also noted in the Type S connections.

One final observation of these tests was made in regards to the weld profile. All cracking was noticed to occur from weld profiles with a 45° angle. All the welds tested were noticed to have unequal profiles around the circumference of the tube, which was a result of the MIG welding process. When the welder first starts, the weld profile is shallow but as it travels around the tube, the legs of the fillet even out to make the 45° profile. They theorized the shallower angle had a smaller stress concentration and further research should be performed to quantify the dependence of fatigue strength from weld profile.

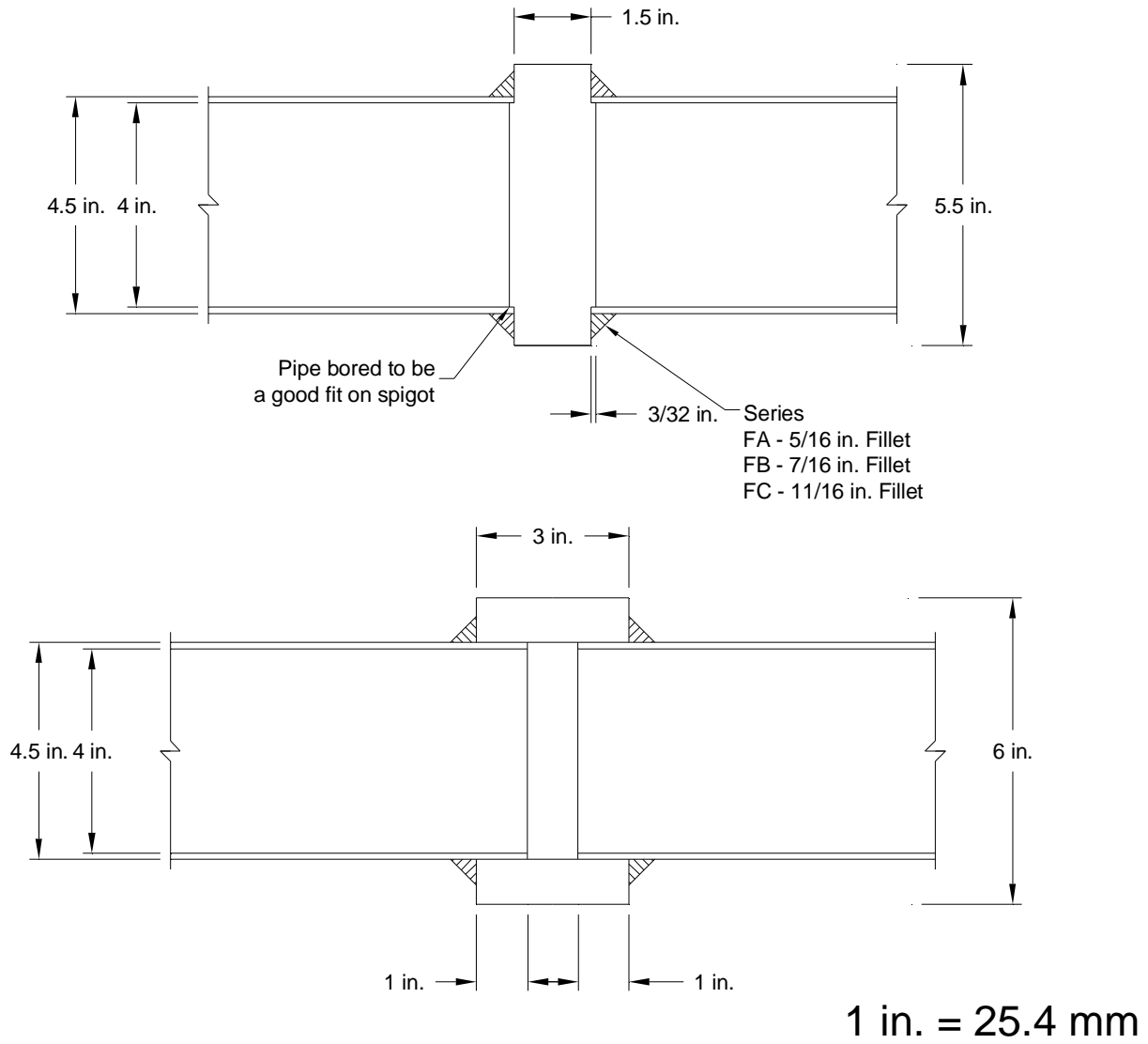


Figure 3.2 Schematic of Archer and Gurney specimens. Top: Type F specimen. Bottom: Type S specimen.

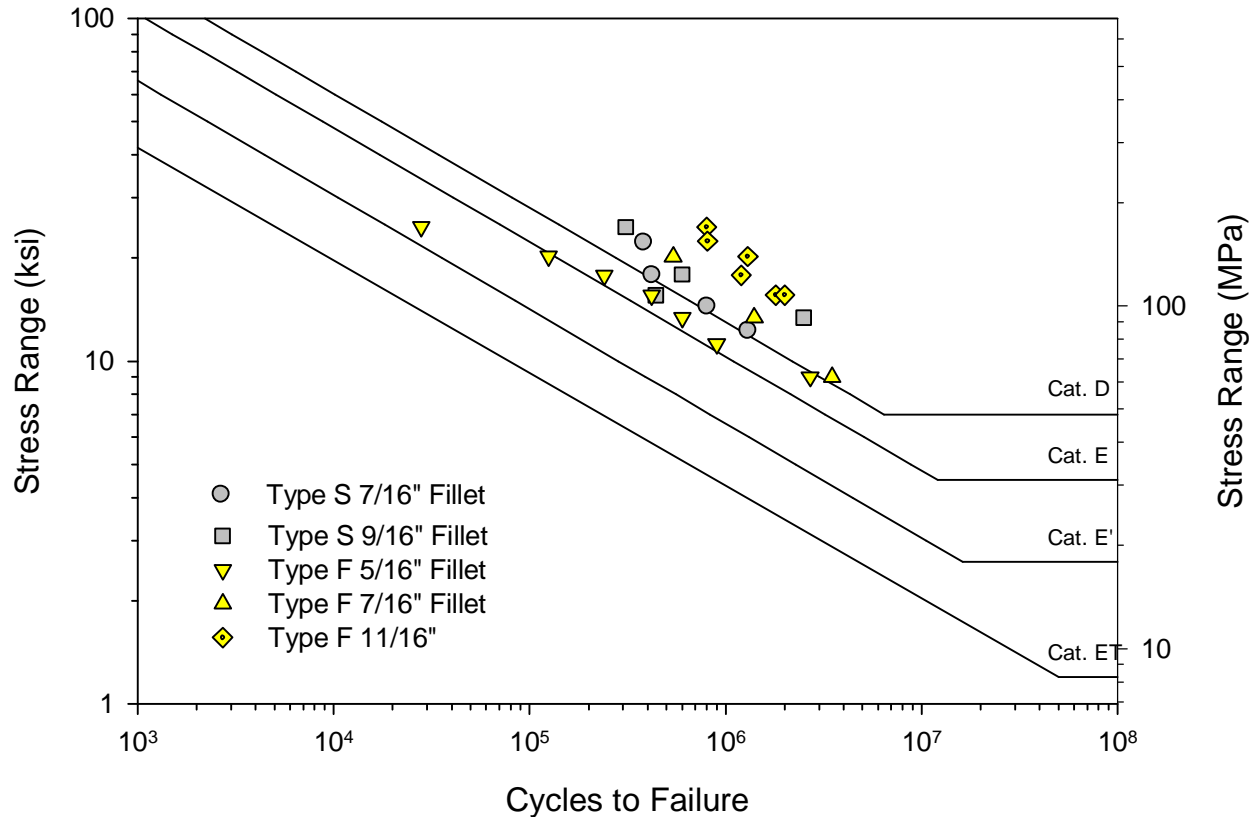


Figure 3.3 Test results of Archer and Gurney specimens plotted against AASHTO fatigue curves

3.3 Miki et. al. (1981)

In 1981, Lehigh University conducted fatigue testing of steel tube-to-transverse plate connections (socket connections) for the California Department of Transportation (20). Six specimens were fabricated from A283 Grade D steel and had equal leg fillet welds (45°). Six more specimens were made from A595 Grade D steel with unequal leg fillet welds ($\sim 34^\circ$), with the longer leg on the tube. The specimens were cycles at a rate of ~ 4.2 Hz under a constant load which created a 34.5 MPa (5 ksi) dead load stress. Figure 3.4 shows a graph of the Lehigh data plotted on a log-log scale along with the relevant AASHTO S-N curves. The unequal leg fillets have a longer leg along the tube than on the plate. After testing was complete, the equal leg fillet welds were found to have a resistance slightly less than Category E', and the unequal leg fillet welds had a fatigue resistance slightly better than Category E'. In response to this finding, two more specimens were fabricated with unequal leg fillet welds to verify the fact unequal leg fillet welds have a higher fatigue resistance, which they did. Coincidentally, this report mentioned nothing of the research performed by Archer and Gurney, which noted increased fatigue resistance with unequal leg fillet welds (19).

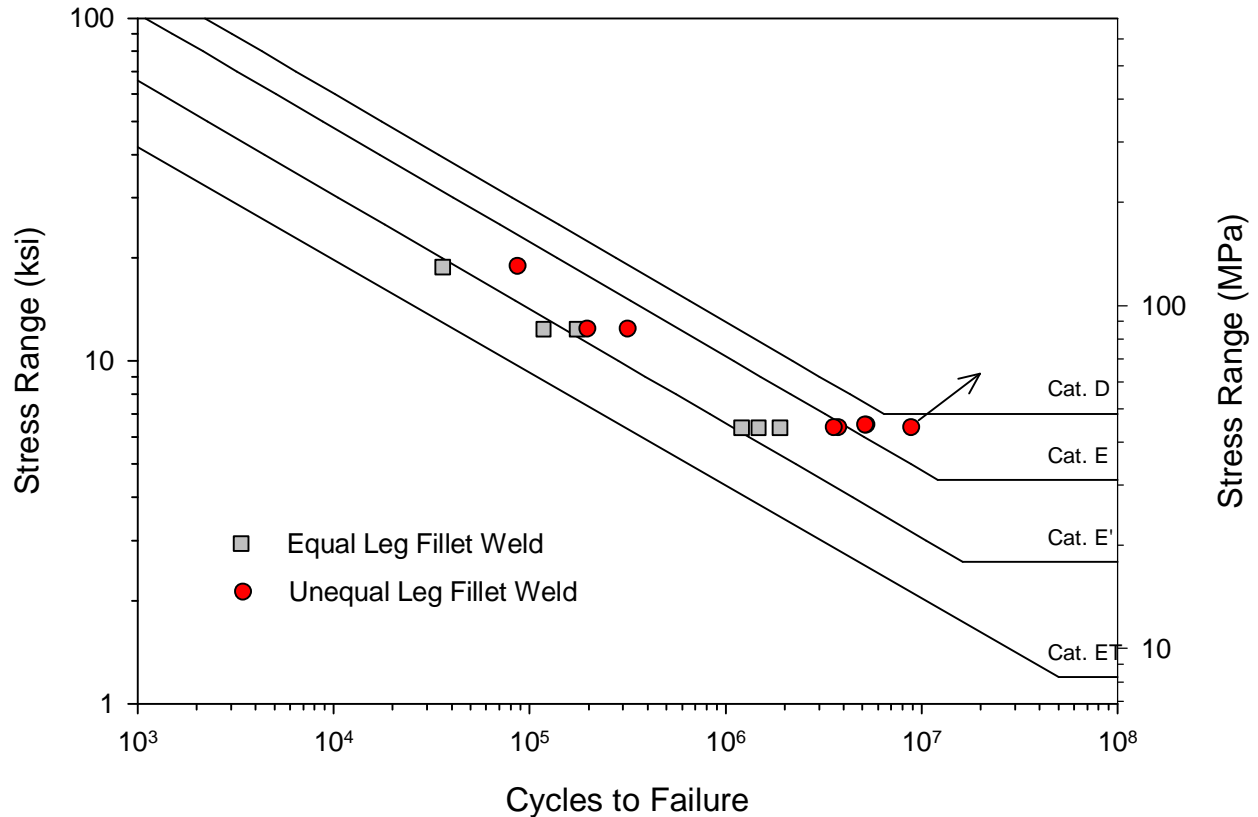


Figure 3.4 Results of the Lehigh socket connection fatigue data, plotted against AASHTO S-N curves.

3.4 South (1994)

This is the first phase of a research project conducted by the Illinois Department of Transportation Physical Research Laboratory. The goal of the first phase is to get a better understanding on the loadings and in-situ stress ranges on cantilevered traffic structures (21). A cantilevered signal structure was instrumented at the Illinois Physical Research Laboratory with strain gauges on the mast arm and on the anchor bolts. During construction of the structure, dead load stresses in the mast arm were measured to be 88.9 MPa (12.9 ksi) with traffic signals installed. Controlled wind speed tests using a blower on the outer most traffic signals showed the following for up to 128 km/hr (80 mph) wind speeds: In-plane stress ranges of the mast arm are a maximum of 23.4 MPa (3.4 ksi) and 60.7 MPa (8.8 ksi) out-of-plane. Rainflow data were then collected over a four-month period from February 1993 to June 1993. The data were not presented statistically within the report, but the raw rainflow data were published. This data was analyzed in a spreadsheet by setting up a cumulative probability distribution and the important conclusion can be seen in Table 3.1, regarding the 0.01% exceedance stress ranges. The infinite life fatigue design using nominal stresses assumes that no fatigue cracks will develop assuming that 99.99% of all loading cycles are less than the CAFL. Mast arm socket connections, as instrumented in this study, are Category E' details with a CAFL of 17.9 MPa (2.6 ksi), and anchor bolts have a CAFL of 48.3 MPa (7 ksi). The two anchor bolts and out-of-plane cycling of the socket connection displayed 0.01% exceedance stress ranges higher than the CAFL, meaning

fatigue cracking is expected. However, the in-plane cycling of the socket connection has a 0.01% exceedance stress less than the CAFL, so fatigue cracking should not be expected from in-plane loading on this structure. This information just shows how long term monitoring maybe used to determine susceptibility of a structure to fatigue by using a few strain gauges.

Table 3.1 0.01% Exceedance Stress Ranges from South (1994) Data.

	Mast Arm (In-Plane Loading)	Mast Arm (Out-of-Plane Loading)	Anchor Bolts (NW Bolt)	Anchor Bolts (SW Bolts)
Stress Range for 0.01% exceedance	13.8 MPa (2.0 ksi)	31.0 MPa (4.5 ksi)	62.1 MPa (9 ksi)	96.5 MPa (14 ksi)

3.5 South (1997)

This was the second phase of the aforementioned project. The second phase of the project targeted the actual fatigue strength of tube-to-plate connections used for mast arms (22). In total, 24 specimens were tested at six different stress ranges. All the specimens used a 76.2 mm (3 inch) outside diameter, 3.2 mm (0.125 inch) thick AISI DOM (drawn over mandrel) steel tubes. Strain gauges were placed 0.79 mm (0.03125 inch) away from the weld toe such that the center of the gauge grid was 1.20 mm (0.04688 inch) from the weld toe. This would allow for a hot-spot stress measurement from which a stress concentration factor (SCF) could be calculated. The nominal stress range was calculated from simplified material mechanics equations because the beam tip was cycled in displacement control, so stress was back calculated from the known displacement. The SCF was measured to have an average of 1.78 with a standard deviation of 0.014. The specimens were cyclically loaded at 3Hz about zero mean stress (complete load reversal). The data is presented in S-N format in Figure 3.5. All the specimens plot above the Category E curve, and 19 of these plot above the Category D curve.

The second part of this report was devoted to improvement techniques, but it only presents previous research, and no testing was performed. It speaks of pros and cons of grinding, weld toe dressing, and peening. Grinding was described to be inexpensive, easy and may be readily conducted, but it maybe detrimental to mast arm structures because the tubes used are very thin, so over grinding the specimen is easy which could be detrimental to fatigue performance. Weld toe dressing is expensive and harder to perform. Peening is inexpensive and may be readily conducted, but South (1997) acknowledges that peening can be over done.

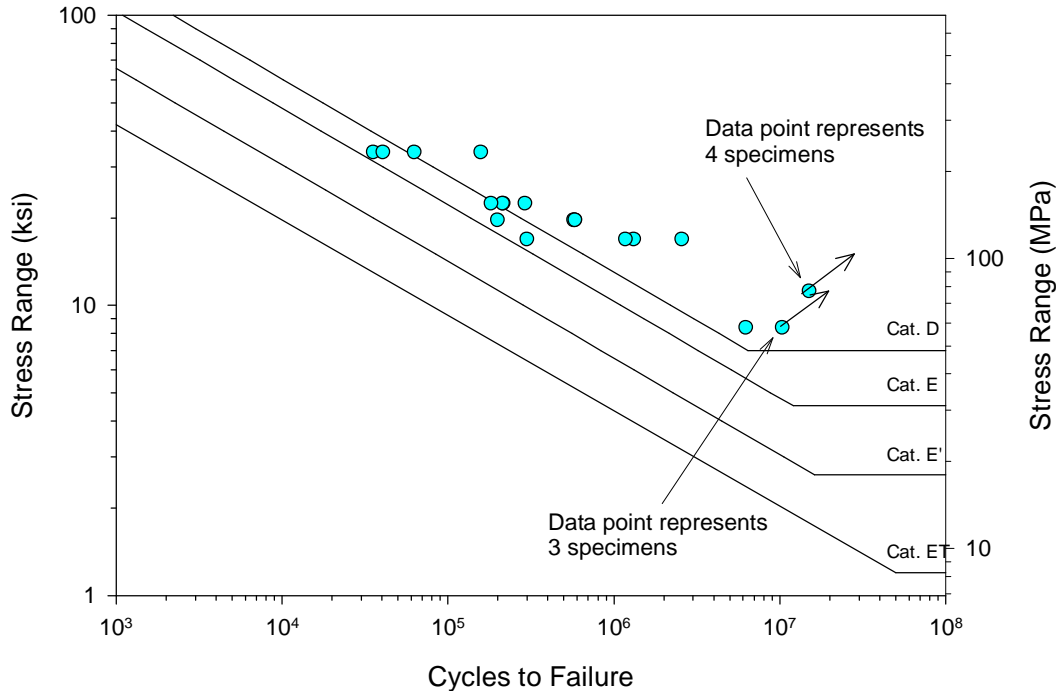


Figure 3.5 Fatigue data of 24 mast arm specimens test by South (1997).

3.6 University of Minnesota (1998)

The University of Minnesota was contracted by a stadium lighting manufacturer to determine the fatigue resistance of the details they use to connect crossarms to poles. The crossarms are used to support lighting fixtures to poles that illuminate stadiums. The testing became necessary, as this particular manufacturer was experiencing fatigue cracking of their structures in the field. The crossarms are welded to the pole through the use of a spacer connection. The spacer is a rectangular tube which has been fish-mouthed to fit against the round pole section, and the spacer is then welded to both the pole and the crossarm, this can be seen in Figure 3.6. The specimens were designed such that the cyclic loads within the connection correspond to unbalanced wind forces striking the centroidal area of the lights attached to the crossarms. The cyclic loads applied to the crossarms would simultaneously cause torsion and bending in the pole section. A picture of the load frame can be seen in Figure 3.7. The original spacer design used a spacer whose width was less than the pole diameter. This detailing was particularly susceptible to fatigue because of “oil-canning”. Oil-canning is the cross-sectional distortion of pole due to loads only being applied to a portion of the pole. This distortion mode then causes high secondary stresses within the pole section which are difficult to account for in design. Oil-canning was an obvious phenomena observed during the cycling of these specimens. Figure 3.8 shows the fatigue data collect during this project against the AASHTO fatigue design categories. It can be seen that the original spacer design performed poorly, as it plotted way below the Category ET curve, in fact, it plots below any published fatigue category by AWS or AASHTO.

Due to the poor performance of the spacer connection, a new proposed connection was recommended and also tested as part of this project. The new connection, referred as the “ring-stiffened” connection utilized a much more robust design using a continuously welded hoop

around the pole (see Figure 3.9). The ring detail was effective in eliminating oil-canning of the pole as it was not observed during cycling. As seen in Figure 3.8, the ring-stiffened connection exhibited a drastic improvement in fatigue performance when compared to the original spacer connection. Most of the data plotted along the Category C curve, with statistical lower bound making this a Category D detail. This represents an improvement in fatigue life of approximately a factor of 500 over the original spacer connection.

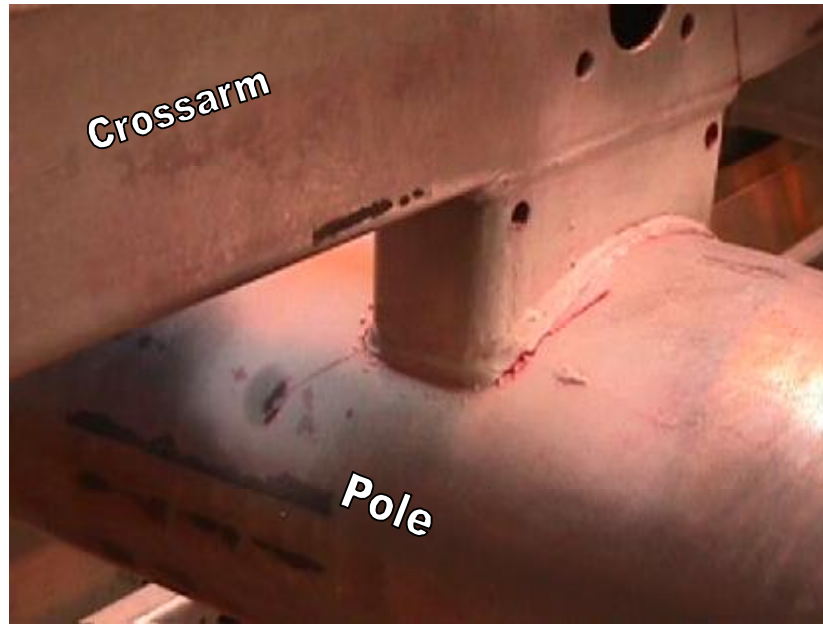


Figure 3.6 Close-up view of spacer connection between pole and crossarm.

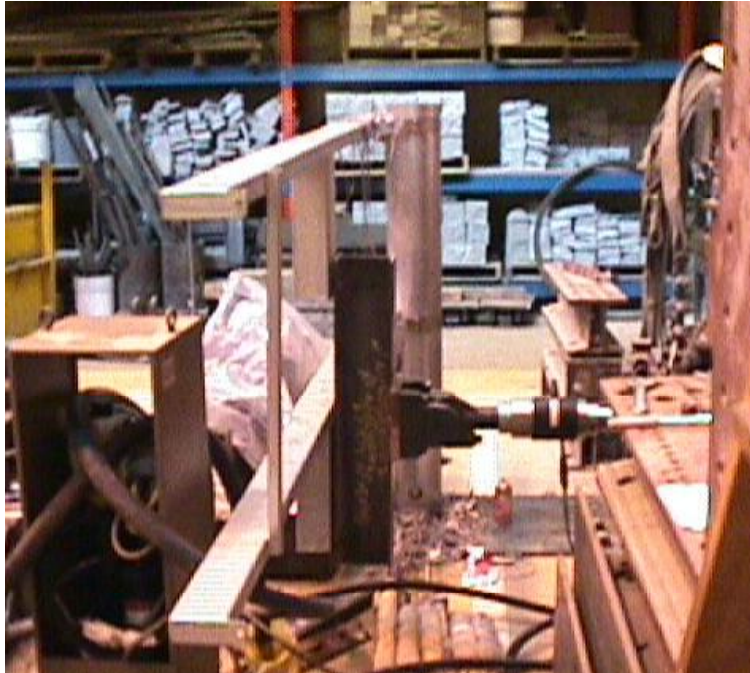


Figure 3.7 Stadium lighting fatigue test set-up

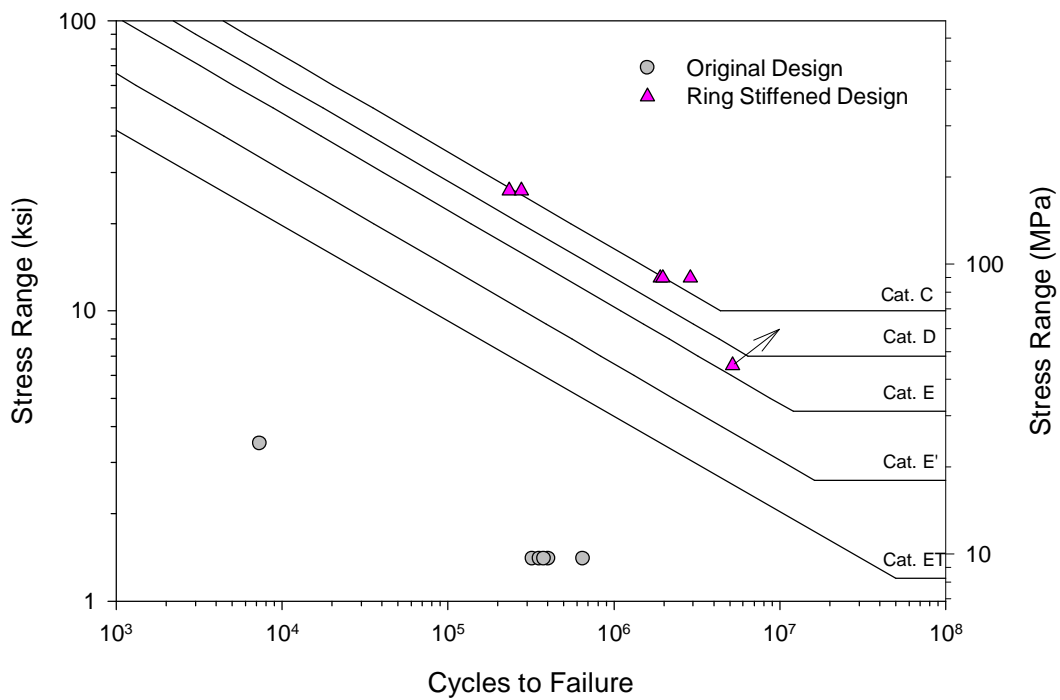


Figure 3.8 Plot of original and stiffened connections of lighting structures against AASHTO S-N curves.

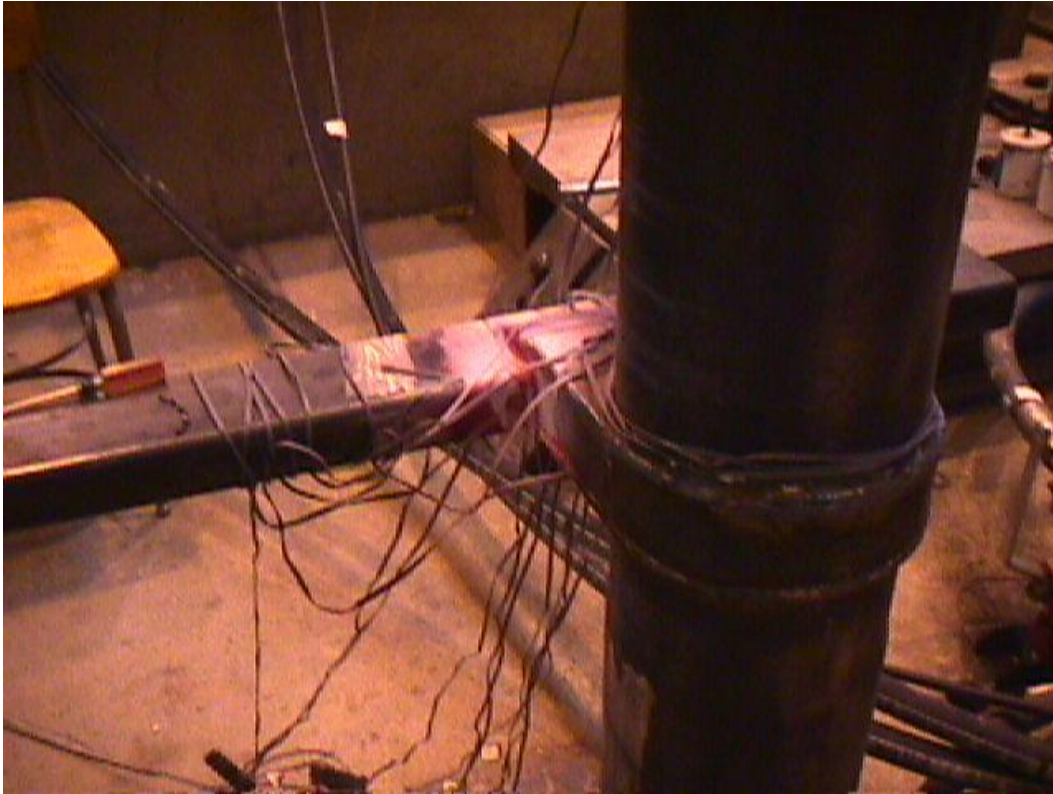


Figure 3.9 Close-up view of ring-stiffened connection between pole and crossarm.

3.7 Alderson (1999)

Missouri had over a dozen traffic signal mast arm failures from 1993 to 1999 (23). Cracks formed in the weld joining the mast arm to the base plate. In response to mast arm cracking, the University of Missouri-Columbia initiated a small research program to investigate the problem. Two existing structures were field instrumented and monitored, also limited laboratory testing of mast arms was conducted (24).

Two cantilevered traffic signal structures were chosen for field monitoring. The first was 16.5m (54 feet) long mast arm with 4 signal heads and 3 signs, spanning two lanes of 80.5 km/hr (50 mph) traffic. This structure was fabricated by Valmont using round tubes. The second structure had a 12.8 m (42 feet) mast arm with 3 signal heads and 2 signs, spanning over two lanes of 64.3 km/hr (40 mph) traffic. The second structure was fabricated by JEM using tubes with an octagonal cross-section. In both structures, the mast arms used typical socket connections which are Category E' detail in regards to fatigue. The structures were not monitored long term, but the following was found on the short term. The maximum truck gust stress range measured was 14.1 MPa (2.04 ksi), which was sporadically measured as trucks drove underneath the structure, which is below the CAFL for Category E' details. The out-of-plane stresses due to wind gust were greater than the in-plane stresses with 35.1% of the out-of-plane stresses exceeding the CAFL, and none of the in-plane stresses exceeded the CAFL. No galloping was ever observed.

Five mast arm specimens were fatigue tested as part of this research using constant amplitude loading. All five specimens were cycled with a 96.5 MPa (14 ksi) mean stress at a stress range of 55.2 MPa (8 ksi). The first three specimens were manufactured by Valmont, one with a standard weld, and two with a “fatigue-resistant” weld. The “fatigue-resistant” weld was a theory that a weld with two unequal leg fillets will have better fatigue resistance than only one unequal leg. Figure 3.10 shows the detail of the “fatigue-resistant” weld. The fourth mast arm was a round tube fabricated by Union Metals. The fifth arm was an octagonal section produced by JEM that was taken out of service. However, this arm cracked prematurely and it was neglected from the data set since it was thought to be cracked prior to testing since it was taken out of service. The cracks that did form on the octagonal section formed in the corners octagon, which previous finite element analyses at University of Missouri-Rolla showed to be a stress concentration (24). The data for the four mast arms is plotted in Figure 3.11 along with the relevant AASHTO fatigue curves. There is not much to infer from four data points, but it appears as if the “fatigue-resistant” weld is not anymore effective than the standard weld since one plotted near the Category E line and the other near the E' line. The four details plotted are Category E' details, but the one specimen plotted slightly below the E' curve, but not enough to cause alarm.

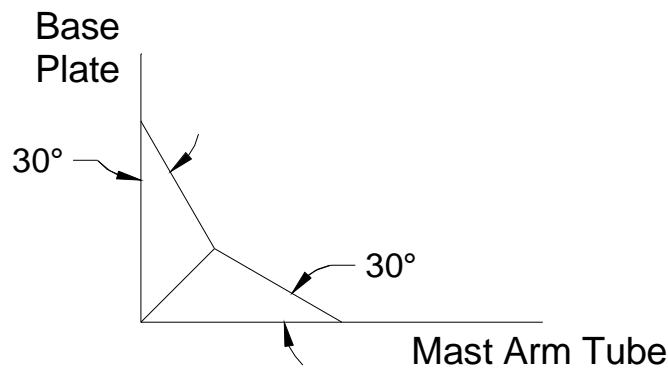


Figure 3.10 University of Missouri Columbia “fatigue-resistant” weld detail

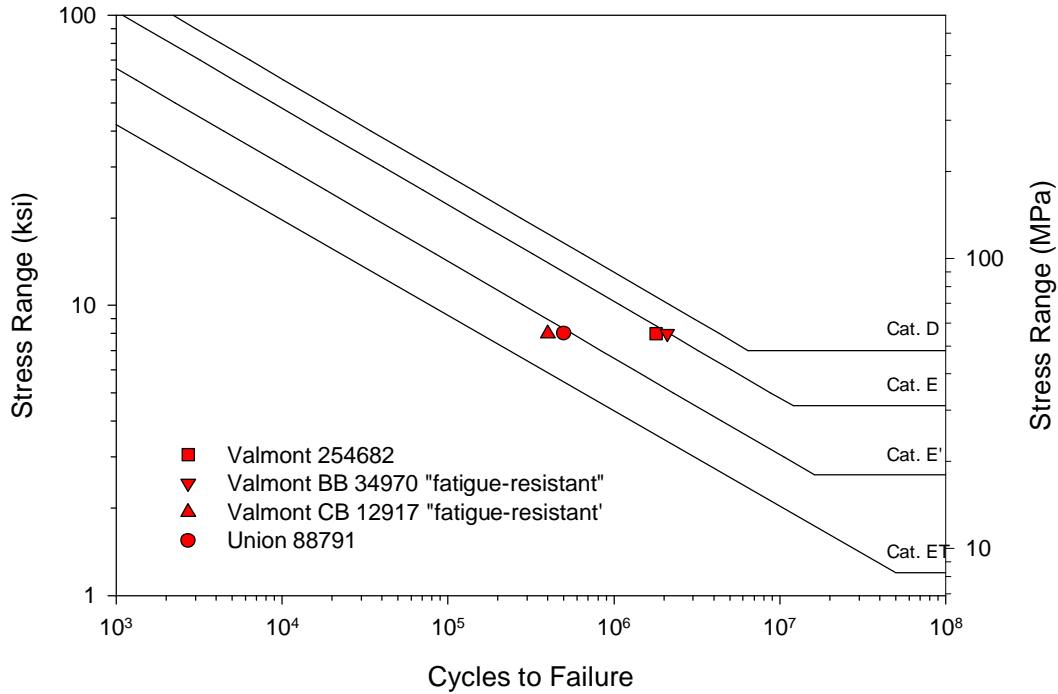


Figure 3.11 Plot of fatigue data for mast arms tested at University of Missouri-Columbia.

3.8 Heeden (1999)

The Kansas DOT has experienced cracking problems with mast arm-to-pole connections (25). Cracks have been observed in the weld toe of the side plate to pole connection, and sometimes in the top and bottom gussets of the box connection. A pure analytical study was done by the University of Kansas to determine the parameters within the connection that affect fatigue. Finite element analysis (FEA) using ANSYS was used to investigate the fatigue performance of the side-side gusset plate connection. The models were of common KDOT structures and used AASHTO specified truck gust pressures as the loading on the models. All models were completely elastic, and inelastic models were going to be run in a second phase of the project.

Since most cracks in the field were noticed at the ends of the weld connecting the side plates to the pole, most comparisons between models were made at this location. Increasing the pole thickness did reduce the stresses at the side plate weld (a reduction of 25-33% could be achieved by using a thickness of 7.94 mm (0.3125 inch), from the standard 6.35 mm (0.25 inch)). The angle at which the side plate frames into the pole was also found to be a factor determining fatigue performance. The lowest stresses were achieved when the side plates framed in perpendicular to the pole. However, when the plate came into the pole at a 34° angle, the stresses at the weld terminations were found to increase by 75%. A slight angle of up to 5° was considered not to cause a noticeable increase in stress. The stress in the side plates can be reduced by increasing the depth of the side plate, the FEA verified this fact, but was not recommended because of increased fabrication cost. The analyses also covered the ring stiffened detail covered in the 2001 Specifications. The analysis shows for the ring stiffened detail, there was up to a 32.3% reduction in stress in the top weld terminations, and a 120% increase in stress at the bottom weld termination. Because of the large increase in stress at the bottom, this detail

was not recommended. However, these were elastic analyses and are not accounting for local yielding hence the large increase in stress, in addition, the testing done at the University of Wyoming did not find this detail to crack in this location. Tensioned U-bolts were also investigated as a retrofit. The U-bolts would be placed around the pole and tensioned to beneficially compress the box connection into the pole. The U-bolts were effective in reducing the top weld stresses significantly, while slightly increasing the lower weld stresses.

3.9 Kashar (1999)

California had fatigue problems with changeable message sign structures (CMS) in the mid 1990's. A picture of a typical CMS structure can be seen in Figure 3.12. On November 27, 1995 a CMS structure collapsed in California, crushing a vehicle passing beneath it (26). The 28 kN (6.3 kip) CMS was 7.74 m (25.4 feet) high and cantilevered 10 m (32.8 feet) from its single column support base. The failed support column was a 457.2 mm (18 inch) diameter and 12.7 mm (0.50 inch) thick galvanized carbon steel pipe. The steel base plate 69.9 mm (2.75 inch) thick, supported by eight 35 mm (1.375 inch) diameter double-nutted anchor bolts. The column/base plate joint was a socket design with 12.7 mm (0.50 inch) fillet welds on both the inside and outside. There is an electrical service access hole in the column above the base. Failure was attributed to high cycle fatigue and then fracture of the tube-to-transverse base fillet weld. In response to this tragedy, a small research initiative was completed using FEA to determine the stresses in this structure. Finite element analysis showed the following:

The SCF of the welded socket was found to range from 4.5 to 6.

The size of the socket weld had little effect on local stresses.

The electrical access hole had negligible effects on stresses in the socket weld.

Socket connections were found to have higher SCF's than full-penetration connection because of increased plate warping in the socket connection.

Gussets were more effective in reducing the stress concentration than using thicker cross-sections for the tubes, but nothing was said of stresses at the end of the gussets.

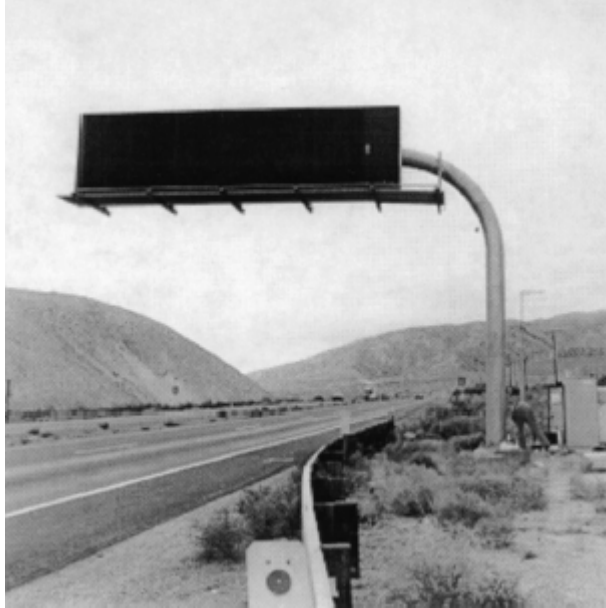


Figure 3.12 Typical CMS structure used in California (27).

3.10 University of Wyoming (1999-2002)

Following the collapse of two cantilevered traffic signal poles in Wyoming, the Wyoming Department of Transportation sponsored a research project through the University of Wyoming (UW) to determine non-destructive methods for crack inspection of these structures (28). Specifically, the cracks that developed in the in-service structures originated from the welds of the built-up box connection on the pole. The researchers at UW focused on using acoustic emissions (AE) to determine if box connections were cracked and to determine the severity of existing cracks. Because the focus of the research was non-destructive evaluation techniques, the fatigue data collected during this project was approximate as compared to typical fatigue data that is collected, for two reasons. First, the majority of specimens tested were in-service structures, in which the previous loadings are unknown and some of the specimens were even cracked prior to testing. Second, most of the specimens were testing under increasingly severe stress ranges, rather than typical constant amplitude loading, but using Miner's Rule, the variable amplitude loading was converted into an equivalent constant amplitude stress range (ECASR). Therefore classification of these welded details is not possible because the specimens were not virgin and cannot be directly compared to previous constant-amplitude fatigue tests. However, the data can at least show trends in resistance between different details.

All testing was conducted in a structures laboratory using a hydraulic actuator to apply the cyclic loads. The actuator was run in displacement control, and because of this, testing was stopped every 250,000 cycles to reevaluate specimen stiffness to adjust the cyclic displacement limits. A specimen was made from one pole and a mast arm bolted to the box connection on the pole. The pole was clamped to the strong floor and the cyclic loads were applied to the mast arm, as seen in Figure 3.13. The cyclic loads were applied to the mast arm at an angle. Field observations of in-service structures showed that mast arms move in-plane and out-of-plane simultaneously, and applying the load at an angle to the mast arm was meant to reproduce this behavior. It was not

specifically outlined in the research whether or not dead load effects were accounted for, but it is interpreted that cycling was done about zero load, or dead load effects were neglected.

The testing matrix involved testing both mast arms and box connections. Two different types of mast arm connections were tested, fillet-welded and full-penetration socket connections. Most of the mast arms used round cross-sections, but a couple specimens used multi-sided tubes. Three different types of box connections were tested, closed, open, and ring-stiffened which can be seen in Figure 3.14. The open box connection meant the top and side plate of the box connection were not welded together, this allows for galvanizing to flow in and out of the box during fabrication, whereas the closed connection does not allow for the galvanizing to enter the box. The ring stiffened connection has the top and bottom plate of the box continuously wrapped around the pole's perimeter. This constrains the deformation of the pole under load to prevent “oil-canning”.

Figure 3.15 shows selected fatigue data for mast arms and box-connections tested in this project. Again, this does not represent all the data collected because many of the specimens were from retired structures, cracked prematurely and were therefore neglected. However, a few of the specimens taken out of service demonstrated a fair amount of fatigue resistance and are reported in this report. The majority of the data presented are those of “run-outs”, or tests that were terminated prior to cracking. Displaying the run-outs can at least demonstrate a minimum amount of fatigue resistance. The selected data has been plotted in Figure 3.15 against the AASHTO S-N curves. Conclusions regarding this data are difficult because the majority of the data points are run-outs. Most of the full-penetration welded mast arms plotted above the Category D line, whereas the fillet welded connections are down by the Category E' line. There also seems to be little difference between the open and closed box connections of the poles, as they all seem to plot well against the Category E' line. The surprising data is that of the ring stiffened box connections because two of these connections (which were virgin) cracked prior to achieving Category ET, but testing on the third was terminated at Category E'. This connection should perform better than the open and closed connections because the rings prevent “oil-canning” which would reduce secondary bending effects in the pole.

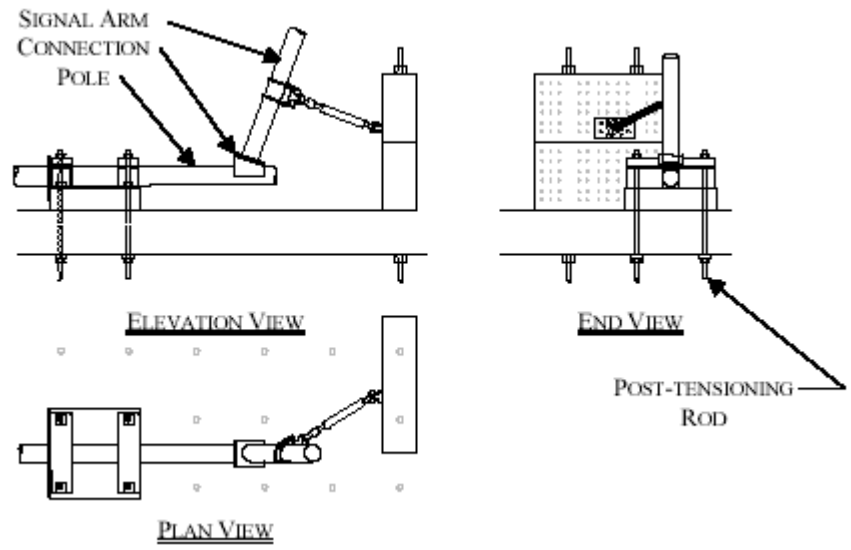


Figure 3.13 Laboratory set-up for Wyoming testing (29).

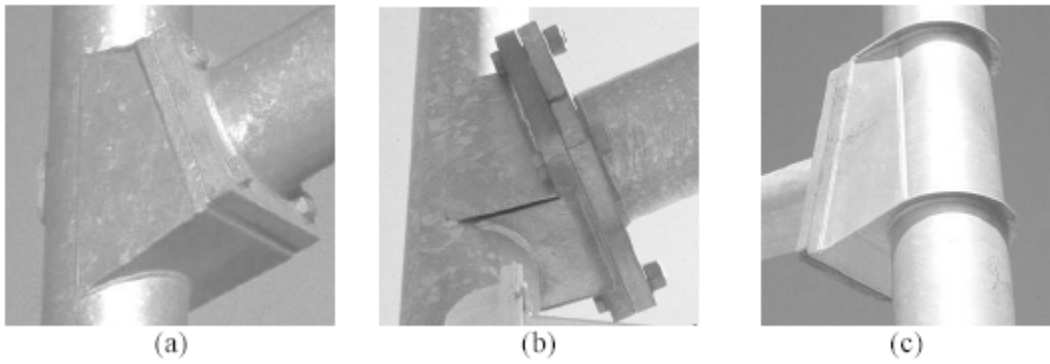


Figure 3.14 Three different types of box connections, (a) Closed, (b) Open, (c) Ring stiffened (29).

Table 3.2 Wyoming Fatigue Data for Mast Arm Connections.

Mast Arm Specimen	Type of Connection	Stress Range or ECASR ⁽¹⁾ MPa (ksi)	Cycles to Cracking
D	Fillet welded	37.99 (5.51)	750,000
G	Full-pen	58.40 (8.47)	6,250,000 ⁽²⁾
K	Fillet welded	35.65 (5.17)	2,750,000 ⁽²⁾
A1 ⁽³⁾	Full-pen	135.00 (19.58)	3,712,687 ⁽²⁾
A2 ⁽³⁾	Full-pen	69 (10)	3,750,000 ⁽²⁾
A3 ⁽³⁾	Full-pen	117 (17)	3,250,000 ⁽²⁾
A4 ⁽³⁾	Full-pen	117.07 (16.98)	3,000,000 ⁽²⁾
A5 ⁽³⁾	Full-pen	57.64 (8.36)	19,500,000 ⁽²⁾
A6 ⁽³⁾	Full-pen	44.06 (6.39)	2,250,000 ⁽²⁾
⁽¹⁾ - Some tests were run using an increasing stress range, so reported stress range is an equivalent constant amplitude stress range (ECASR) computed using Miner's Rule ⁽²⁾ - Run-out data (i.e., test terminated prior to cracking) ⁽³⁾ - Virgin specimens			

Table 3.3 Wyoming Fatigue Data for Box Connections.

Pole Specimen	Type of Connection	Stress Range or ECASR ⁽¹⁾ MPa (ksi)	Cycles to Cracking
#2	Closed	39.02 (5.66)	1,388,820
M	Open	32.27 (4.68)	2,250,000 ⁽²⁾
R	Closed	26.41 (3.83)	4,000,000 ⁽²⁾
A	Closed	59.09 (8.57)	5,000,000 ⁽²⁾
D	Open	42.26 (6.13)	1,000,000 ⁽²⁾
G	Closed (multi-sided)	33.85 (4.91)	1,750,000
K	Closed	36.20 (5.25)	2,750,000 ⁽²⁾
N	Closed (multi-sided)	53.92 (7.82)	1,750,000
P1 ⁽³⁾	Ring Stiffened	31.78 (4.61)	61,997
P2 ⁽³⁾	Ring Stiffened	39.96 (5.65)	306,463
P3 ⁽³⁾	Ring Stiffened	31.03 (4.50)	23,000,000 ⁽²⁾
<p>⁽¹⁾ - Some tests were run using an increasing stress range, so reported stress range is an equivalent computed using Miner's Rule ⁽²⁾ - Run-out data (i.e., test terminated prior to cracking) ⁽³⁾ - Virgin specimens ** it was not specifically outlined, but it is assumed that the stress range reported is that in the side plates of the box connection **</p>			

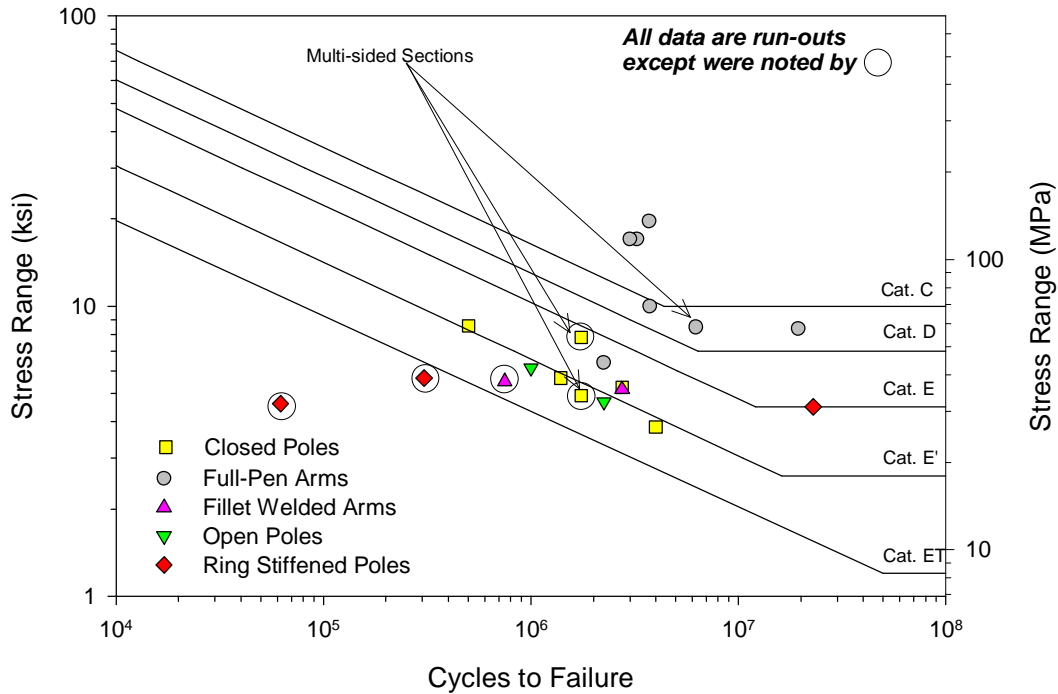


Figure 3.15 Fatigue data of mast arms and box connections conducted at University of Wyoming.

3.11 Gilani (2000)

In response to the same sign collapse in California described previously, a separate analytical and experimental program was carried out at the University of Berkeley. The first part of the research field instrumented other similar structures (27). They verified through pull-back tests that the first two fundamental frequencies involved the pure horizontal and vertical motion of the mast arm. The frequency of vibration for these two modes is ~ 1.1 Hz with about 0.5% critical damping. The structures were observed to gallop and stress ranges were measured as high as 138 MPa (20 ksi), and equivalent stress ranges using Miners rule was calculated to be 82 MPa (11.8 ksi), much higher than the allowable 18 MPa (2.6 ksi) for the Category E' fatigue detail.

Finite element analyses were run on models representing the failed structure. The modeling found that the critical section for high stresses was not at the socket connection (as described in (26)), but rather just below the electrical access hole. The SCF just below the access hole was found to be 3, whereas it was only 1.6 at the socket connection. The shape of the hole was found not to influence these stress concentration factors. Gussets were effective in reducing the stresses in the socket connection and at the access hole, the stresses at the tip of the stiffeners were on the same order of those at the access hole (i.e., $SCF=3$).

The second part of the research experimentally verified the fatigue resistance of the CMS post and mast arm details (30). There were four specimens, one pole section and three mast arms. A concrete pedestal with anchor bolts was used to support the specimens and to represent correct boundary conditions. However, the mast arms use a round, 26-bolt pattern which cannot be bolted directly to the concrete pedestal, so an extension piece was constructed from the same

tube sections and welded details as the failed structure to serve as a transition from the eight-bolt anchor rod pattern to the 26-bolt pattern of the mast arms. The pole specimen was cycled about zero mean stress, but the mast arms and extension piece were cycled about a mean stress of 62.1 MPa (9 ksi). Figure 3.16 shows the results of this experimental testing plotted on a log-log scale. The pole specimen plotted above the Category D curve, while the mast arms showed better than Category E performance, but the extension piece plotted directly on the Category E. All specimens were found to crack at access holes, not in the weld of the connection, however, access hole reinforcement was not used to account for the reduction in cross-section which would explain this premature failure mode.

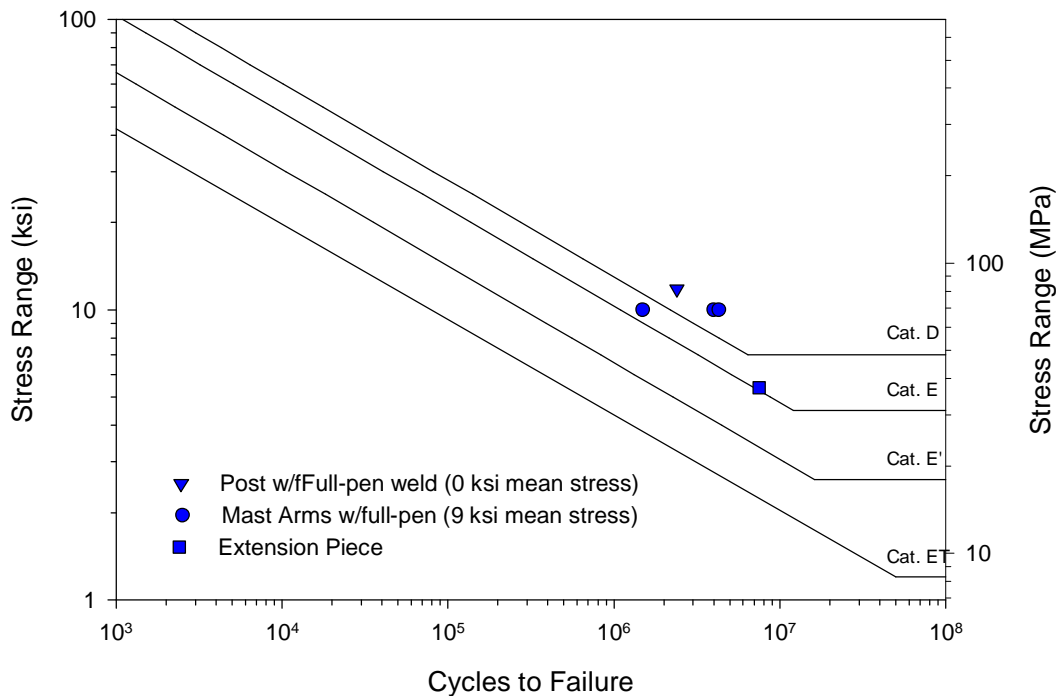


Figure 3.16 Plot of the Gilani pole and mast arm data along with relevant AASHTO design curves.

3.12 Valmont Fatigue Testing (2001)

Valmont is a large manufacturer of traffic signal structures, street lighting, and high mast lighting poles, with two large facilities in Nebraska and Texas. After the release of the 2001 AASHTO specifications, they conducted fatigue testing on their details to proof-test their designs because current designs were not in compliance to the 2001 Specifications. They specifically tested tube-to-transverse plate connections, using three different details, fillet-welded sockets, fillet-welded sockets reinforced with gusset plates, and full-penetration welds. The testing was done at an outdoor facility using a revolving beam set-up with two mast arms bolted back-to-back to form the revolving beam. The stress range for each test was altered by varying the amount of weight suspended at the center of the beam since one 360° rotation of the beam would induce one complete load cycle in the tube-to-transverse plate connection. A picture of this rotating beam fatigue load frame can be found in Figure 3.17.

In total, 20 specimens were tested, but only 16 of these will be reported here, three of the remaining four details used an experimental ultrasonic impact treatment (UIT) treatment and the final specimen tested a collar detail not specifically covered in the AASHTO specification. Table 3.4 outlines the testing results and descriptions of the 16 specimens tested by Valmont, using 6 different details. The first detail tested was a fillet-welded socket connection using unequal leg fillet welds. This detail is identical to the Detail 16 in the 2001 Specifications (see Figure 2.7). The second type of connection was identical to Detail 12 (see Figure 2.7) which is a full-penetration groove weld with a backing bar, attaching the tube to the plate. The backing ring was first welded to the tube with a continuous fillet weld, then the groove weld was completed, which makes this a Category E' detail because an unfused notch still exist between the backing bar and the plate. If the backing bar were attached to the plate with a continuous fillet weld, then this notch would be buried, and the detail would be improved to Category E.

The remaining details were variations on fillet-welded sockets utilizing gusset stiffeners. The first two gusseted specimens (Gussets 1 & 2) were designed to be in accordance with Detail 21 of the 2001 Specifications (see Figure 2.7), using 8 gussets fillet welded to the pole. The gussets used only had a length of 82.6 mm (3.25 inch), meaning this does not fulfill all the requirements of Detail 21 which specifies gussets can be no shorter than 102 mm (4 inch), so the best this detail could be is Category E. A picture of this detail can be seen in Figure 3.18. The next two gusseted specimens (Gusset 3 & 4) were made to validate Detail 22 in the 2001 Specifications. The gussets were 152.4 mm (6 inch) tall and made with a 152.4 mm (6 inch) radius. The eight gussets were attached to the tube with full-penetration welds, and ground smooth to the tube at the gusset terminations. According to the 2001 Specifications, this detail should be Category C. Figure 3.19 shows this detail after testing was complete. Gussets 5 & 6 used eight gussets that were 138.2 mm (5.44 inch) long were fillet welded to the pole. However, the fillet welds were not wrapped around the stiffener, and were rather stopped short, this detail is not exclusively covered in the 2001 Specifications. Figure 3.20 shows a picture of this detail along with a schematic drawing. For all the socket connections with gusset stiffeners, cracks always formed at the tips of the gusset details and not in the socket weld.

The data presented in Table 3.4 is plotted in log-log format in Figure 3.21. The fillet-welded socket connections are defined by the 2001 Specification to be Category E' details, but the Valmont data is showing them to test much higher than this. Even taking into account the scatter in the data, the fillet-welded sockets tested are better than Category E. Firm conclusions cannot be made regarding the fatigue strength of the full-penetration detail because only two specimens were tested. However, the lower bound data point plotted greater than Category D whereas the 2001 Specification define this detail as Category E. Gussets #1, 2, 5, and 6 plotted above the Category E curve, whereas Gussets #1 and 2 were expected to be Category E according to AASHTO. Gussets #3 and 4 were expected to be Category C by the 2001 Specifications because of the use of full-penetration welds along with smoothly ground transitions, but the data shows a resistance of about Category D.

The Valmont testing has shown that the fatigue resistance all details tested, except for Detail 21, is conservative as described by the 2001 Specifications. The discrepancy that exists between the Valmont fatigue load frame and loading in real structures is the Valmont fatigue frame cannot account for the presence of a dead load. The present categorization of socket connection in AASHTO was based on the data of Miki, present earlier in this chapter, which did include the

effects of dead load. The revolving beam setup cycles specimens at a load ratio of -1, hence the fatigue results maybe artificially high.

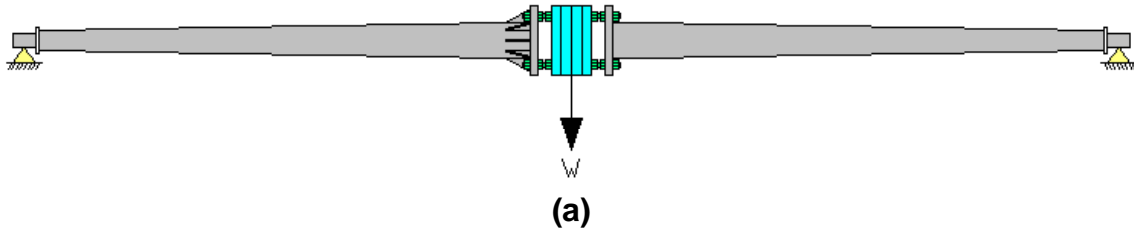


Figure 3.17 Valmont fatigue testing load frame. (a) Elevation view of rotating beam set-up made from two masts arms bolted together. (b) Rotating beam fatigue load frame.



Figure 3.18 Valmont Gusset 1 & 2 specimens.

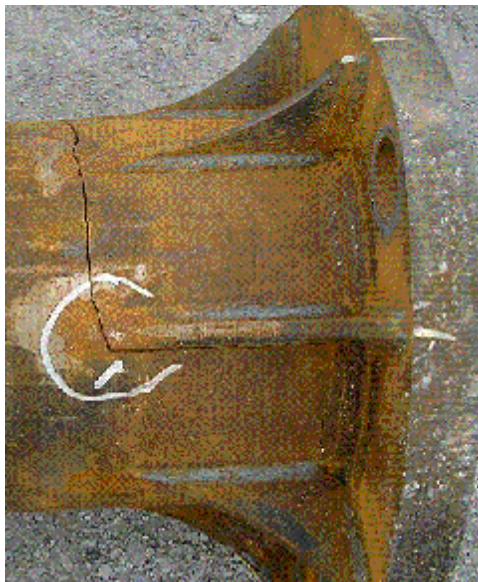


Figure 3.19 Valmont Gusset 3 & 4 specimens.

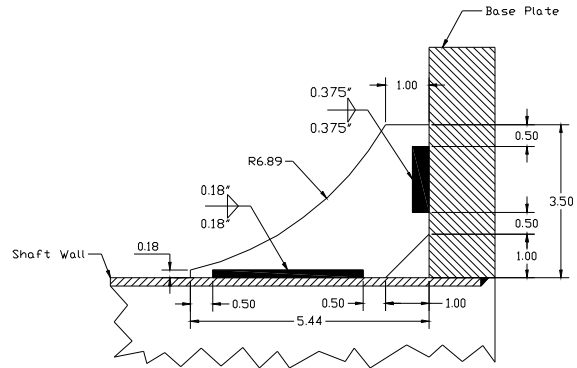


Figure 3.20 Valmont Gusset 5 & 6 specimens.

Table 3.4 Valmont Test Matrix

Specimen	Stress Range MPa (ksi)	Description	Number of Cycles to Initialize Crack
Socket 1	92.4 (13.4)	Unequal Leg Fillet Weld (0.25" x 0.44", Long Leg on Shaft)	Test Suspended at 4,808,700
Socket 2	121.3 (17.6)	Unequal Leg Fillet Weld (0.25" x 0.44", Long Leg on Shaft)	1,240,200
Socket 3	121.3 (17.6)	Unequal Leg Fillet Weld (0.25" x 0.44", Long Leg on Shaft)	Test Suspended at 5,321,160
Socket 4	121.3 (17.6)	Unequal Leg Fillet Weld (0.25" x 0.44", Long Leg on Shaft)	Test Suspended at 1,932,743
Socket 5	166.2 (24.1)	Unequal Leg Fillet Weld (0.25" x 0.44", Long Leg on Shaft)	Disregarded, crack formed at dent in midspan of tube
Socket 6	166.2 (24.1)	Unequal Leg Fillet Weld (0.25" x 0.44", Long Leg on Shaft)	148,281
Socket 7	166.2 (24.1)	Unequal Leg Fillet Weld (0.25" x 0.44", Long Leg on Shaft)	303,118
Socket 8	166.2 (24.1)	Unequal Leg Fillet Weld (0.25" x 0.44", Long Leg on Shaft)	110,688
Gusset 1	92.4 (13.4)	8 – 45 Degree Gussets 3.23" tall x 3.23" wide x 5/16" Fillet welded to Pole	802,620*
Gusset 2	92.4 (13.4)	8 – 45 Degree Gussets 3.25" tall x 3.25" wide x 5/16" Fillet welded to Pole	376,740
Gusset 3	92.4 (13.4)	8 – 15 Degree, Tangent Contour Gussets (R=10") 6.00" tall x 3.25" wide x 5/16" Full Penetration Weld to Pole	950,040
Gusset 4	121.3 (17.6)	8 – 15 Degree, Tangent Contour Gussets (R=6") 6.00" tall x 3.25" wide x 5/16" Full Penetration Weld to Pole	657,540
Gusset 5	121.3 (17.6)	8- Tangent Contour Gussets 5.83" tall x 3.25" wide x 5/16" Fillet Welded to Pole, Weld Stopped ½" from ends of Gusset	514,085
Gusset 6	121.3 (17.6)	8- Tangent Contour Gussets 5.83" tall x 3.25" wide x 5/16" Fillet Welded to Pole, Weld Stopped ½" from ends of Gusset	673,989
Full Pen 1	121.3 (17.6)	Full Penetration Weld with Backup Ring	498,960
Full Pen 2	121.3 (17.6)	Full Penetration Weld with Backup Ring	4,504,500
* Believe initial crack occurred between 500,000 to 650,000 cycles first observed at 802,620			

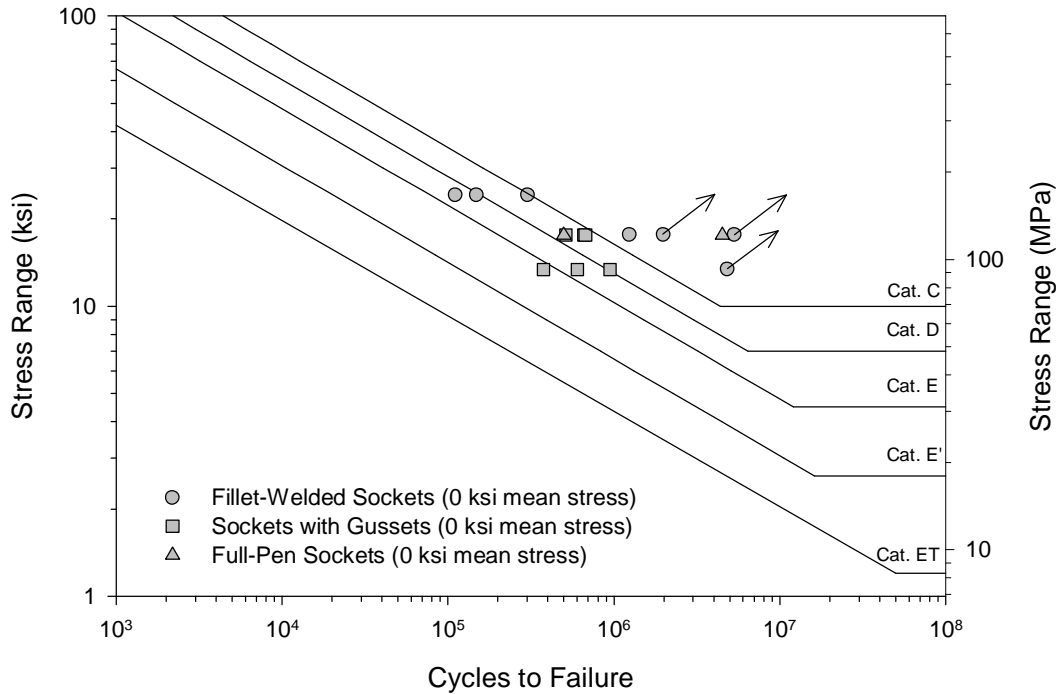


Figure 3.21 Plot of the fatigue data of three different types of tube-to-plate connections tested by Valmont.

3.13 University of Texas – Austin (2002)

After the introduction of the 2001 AASHTO specifications, the Texas Department of Transportation (TxDOT) wanted to investigate whether the mast arm socket connections should be categorized as E' details for fatigue (31). To verify this classification, they contracted the University of Texas-Austin (UTexas) to test a series of socket connections. In all, 59 specimens were tested, most were socket connections and a few miscellaneous details were also tested.

The UTexas load frame is shown in Figure 3.22. The setup was simple and efficient, with two mast arm bolted back-to-back via a loading box. An actuator applied vertical loads to the loading box. The advantages of this loading setup are:

- two specimens could be tested simultaneously
- dead load could be applied with the actuator then cycled about the dead load
- when run in displacement control, high cycling rates could be attained (between 3-5 Hz)

All the specimens utilized a 38.1 mm (1.5 inch) thick base plate, 482.6 mm (19 inch) square, with a 269.2 mm (10.6 inch) bolt circle for four 31.8 mm (1.25 inch) diameter bolts. The mast arm was tapered but the diameter at the base plate was 254 mm (10 inch). Two pole wall thicknesses were investigated, 6.1 mm (0.239 inch) and 4.5 mm (0.179 inch). All mast arms used unequal leg fillet welds. Some of the mast arms were galvanized and others were not.

Triangular gusset stiffeners were also investigated as part of this research, with each stiffened socket connection utilizing four individual stiffeners. Three stiffener sizes were investigated, 76.2 mm x 6.4 mm (3 x 0.25 inch), 76.2 mm x 9.5 mm (3 x 0.375 inch), and 152.4 mm x 9.5 mm (6 x 0.375 inch). These stiffeners were orientated in the “strong” direction with two of stiffeners aligned on the neutral axis, and the other two on the extreme bending fibers. However, since the mast arms use a 4-bolt pattern, this stiffener orientation does not align bolt patterns, which does not give the a direct load path from the stiffener to the bolt. Four stiffened socket connections used a four stiffeners, but they were offset by 45 degrees such that the stiffeners where aligned with the bolts. Four specimens looked at internal and exterior collar details. These details add an additional ring at the socket connection to locally increase the section modulus to reduce stress ranges. The remaining specimens investigated the performance of ultrasonic impact treatment (UIT) on mast arm socket connections. UIT is a treatment that can be applied to weld toes to introduce favorable compression residual stress. The benefits of the treatment are similar to hammer peening. The UIT was investigated being applied before adding dead load, with dead load present, and after galvanizing.

The data from the 59 specimens is broken down into three figures, to help disseminate all of it. Figure 3.23 shows an S-N plot of plain socket connections along with two socket connections with 50.8 mm (2 inch) thick base plates and two specimens using a full-penetration weld. The original pool of data from Lehigh (20) used to categorize socket connections found them to be category E' details when using unequal leg fillet welds. The circles in Figure 3.23 represent the pool of socket connections that were either galvanized or not, and using both pole wall thicknesses. As seen in the figure, the UTexas data agrees that the socket connection are indeed Category E' details, despite pole wall thickness and whether or not it galvanized. Also shown in this figure are two data points for full-penetration weld details. The 2001 Specifications classify this detail as Category E if the backing ring is fillet welded to both the base plate and tube. Both data points plotted on the Category D curve, indicating that the current code maybe conservative. The last two data points (triangles) in Figure 3.23 represent socket connections with a 50.8 mm (2 inch) thick base plate. AASHTO does not have provisions to alter the fatigue strength based on base plate thickness, but one data point plots on the Category D curve, while the other went over Category C. This implies a two category fatigue life improvement just by adding an extra 12.7 mm (0.5 inch) thickness to the base plate, which is a dramatic improvement for very little extra fabrication cost.

Figure 3.24 show an S-N plot of the data for socket connections stiffened with triangular gussets. The AASHTO code does not allow for gussets less than 101.6 mm (4 inch) but the lowest fatigue rating a gusset has is Category E. The code also allows for higher fatigue resistance if the groove welds or a radiused transition into the tube are used. Half of the specimens tested at UTexas do not even pass code requirements, but the data of all the sizes and thickness gussets generally plot around the Category E line, which does fit the lower bound resistance published in the 2001 Specifications.

Figure 3.25 displays the fatigue results from the four collar details and the specimens that received UIT treatment. The internal collar details displayed the same fatigue resistance as a bare socket connection, however, the external collar detail demonstrated fatigue resistance around Category C, which is a four category fatigue improvement over a bare socket connection. The UIT treatment was found to show dramatic fatigue life improvement under certain

conditions. The square data points represent specimens that received UIT treatment, then galvanized and their performance was no better than a bare socket connection. This indicates the temperature cycling involved in galvanizing erases the benefits provided by the UIT. The diamond shaped data point represents a mast arm that was fabricated, galvanized, loaded to a representative dead load stress, subjected to UIT treatment, then unloaded and put aside to wait for fatigue cycling. The data plots between Category E and D, which is at least a category fatigue improvement over a bare socket connection. The best performance was noted by the specimens that were galvanized, placed in the load frame under dead load, and immediately fatigue cycled. These specimens are meant to represent a UIT retrofit that can be done in the field of an existing structure. The data for these specimens plots above the Category C line which is a three category fatigue life improvement. Obviously the true benefits of UIT are recognized when is applied under dead load after galvanizing. However, the treatment process slightly machines the surface, removing the zinc coating meaning cold galvanized treatment must be applied post-UIT.



Figure 3.22 UTexas mast arm fatigue setup.

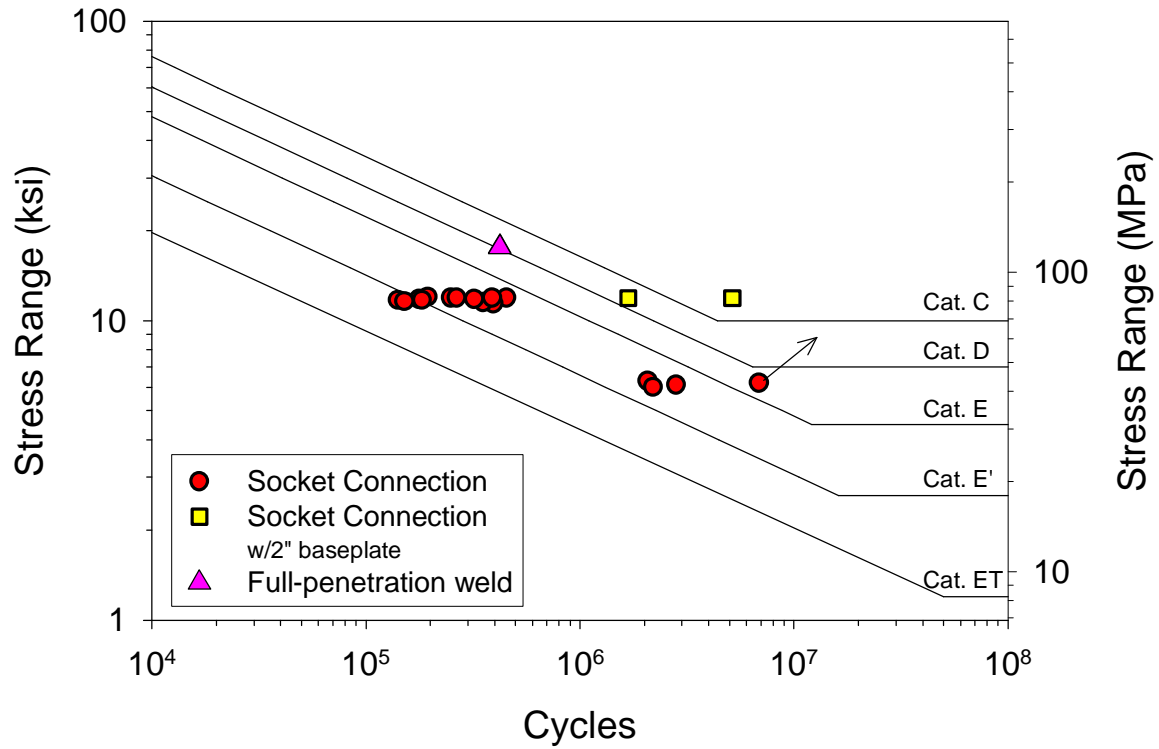


Figure 3.23 UTexas fatigue data for socket connections.

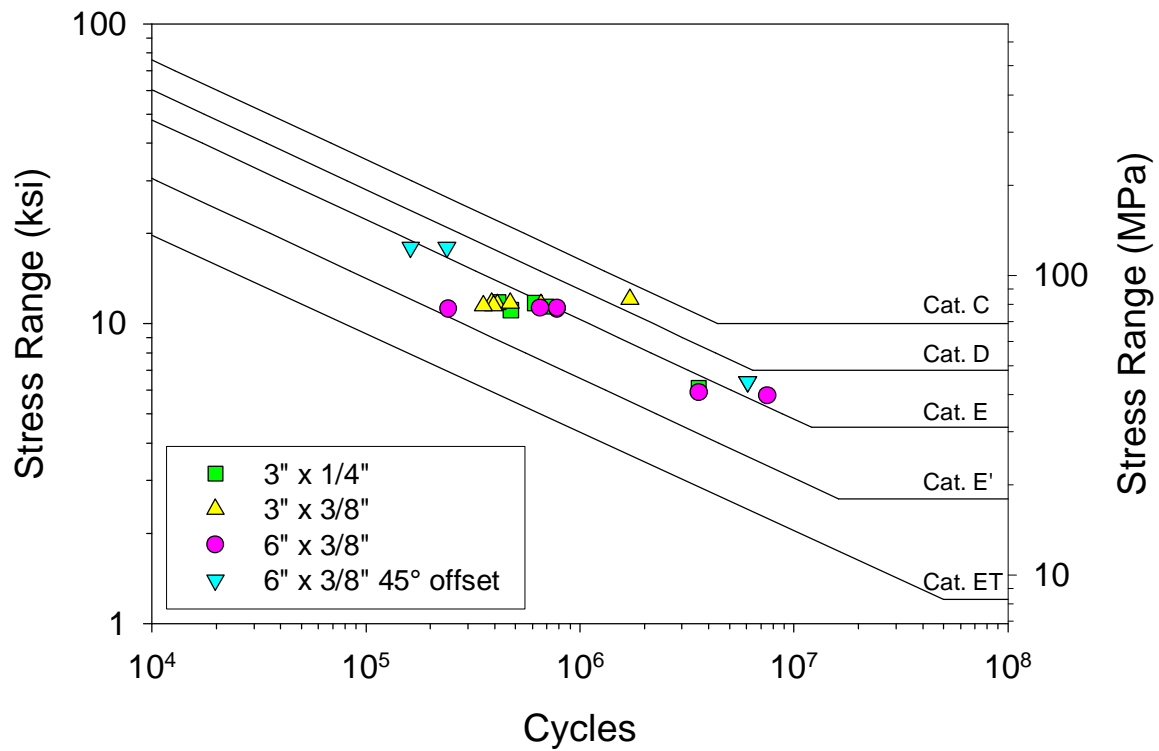


Figure 3.24 UTexas fatigue data for gusset stiffened socket connections.

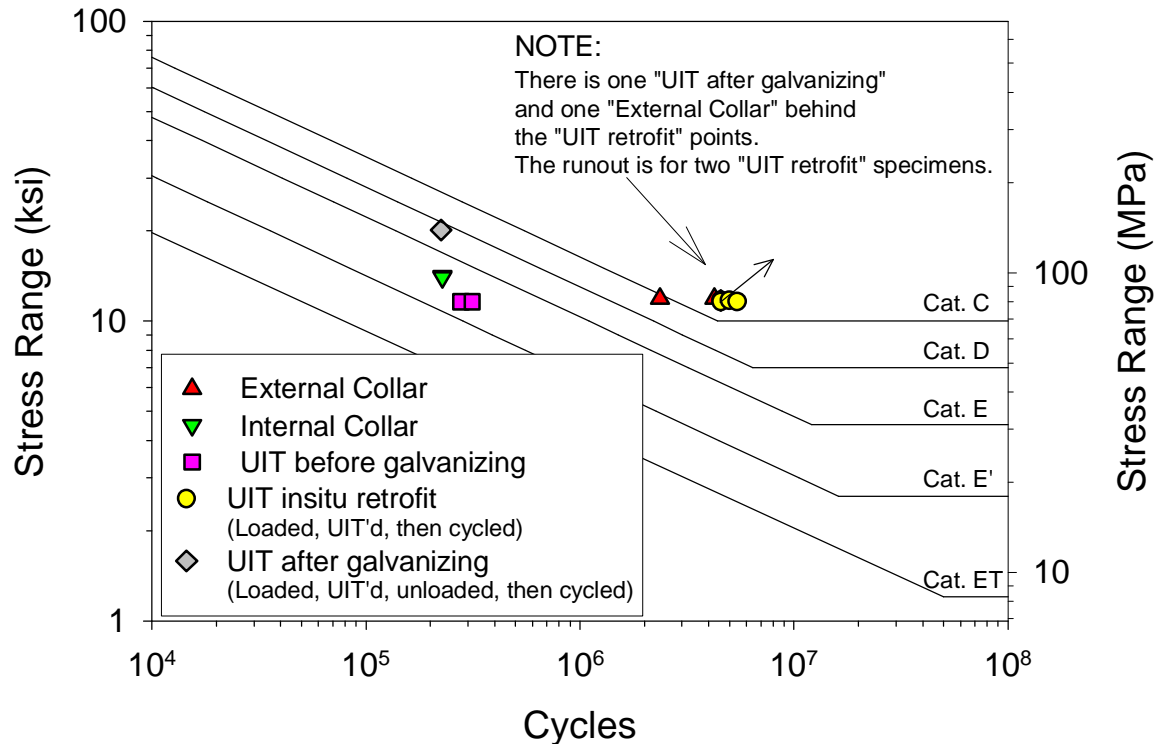


Figure 3.25 UTexas fatigue data for miscellaneous socket connections.

3.14 Iowa High mast Failure

On 12 November 2003, a 42.7 m (140 feet), galvanized, high-mast lighting tower along I-29 near Sioux City, Iowa collapsed. At the time of collapse, the winds were reported to be from the northwest at 16.5 m/s (37 mph) and had reached a peak of 25.0 m/s (56 mph) earlier that day. The tower was fabricated from an extremely slender (tube radius/tube thickness = 132) base tube section using a socket connection design. Typically, fabricators use a full-penetration weld detail in this location, over a socket connection design, for higher reliability. Failure analysis found that the tower design did not meet the fatigue provisions in the 2001 Specifications, though it was not required by design. Cracks formed at all the bend corners of the tube, and eventually coalesced into one large crack that eventually cause the collapse. There was no evidence that cracks were pre-existing from fabrication, but the fact that all the corners were cracked insisted that natural wind gusts were the cause of the fatigue cracking. This tower collapse prompted state-wide inspections of the remaining 232 high mast towers in Iowa's inventory. Inspections found 21 more towers with fatigue cracks, and were immediately removed from service.

Inspection found cracks at base tube-to-plate welds, and at hand hole details. Cracks at the tube-to-base connections seemed to initiate at the bend corners of the tube, an indication that this location is a stress riser. Cracks were either found on all the bend corners (indicating fatigue loading was random in direction such as caused by natural wind gust) or on the corners of opposing sides of the tube (indicative of across-wind motions caused by vortex shedding.)

Finite element analysis was used to analyze the failed pole to determine how the load flows from the pole, into the base plate, and out through the anchor rods. The models showed how the corners of the multi-sided poles were stress risers, explaining why the cracks initiated at the corners. More interestingly, the models showed how the pole walls were subjected to high through-thickness bending components at the base plate and that this extra stress can be mitigated by thickening the base plate. As the base plate becomes thicker, its stiffness increases and the pole tube is subjected to a more “fixed” boundary condition. Plots of tube wall stress versus base plate thickness found that increasing the base plate thickness beyond 76.2 mm (3 inches) did not reduce the tube wall stress and was recommended as an ideal base plate thickness for future designs.

An AASHTO fatigue analysis was conducted on the failed poles as well of those still in-service. The analysis used AASHTO recommended fatigue loads and detail categorizations. However, the vortex shedding provisions were known to be incorrect, and a more detailed steady-state dynamic analysis was used to predict the stress ranges for vortex shedding loading. However, assumed values of correlation length and damping ratio had to be assumed to conduct this analysis. Most of the in-service poles were found to fail the AASHTO fatigue analysis, though many of them failed from higher mode vortex shedding vibration. It was unclear what mode the poles would truly vibrate in under vortex shedding and an extensive long-term, field monitoring project is on going to determine the loads and vibration properties of high mast poles. Recommendations were made to thicken all pole bases in future designs to reduce the stress ranges from vibration to enhance fatigue life.



Figure 3.26 Collapsed I-29 high mast tower in Sioux City, Iowa.

3.15 Related Fatigue Research

As discussed previously, in most cases there were insufficient data to properly characterize the fatigue resistance of details in the 2001 Specifications, therefore other international specifications were used to extrapolate the fatigue strengths of many common details. Since these structures are tubular, there is some similarity to the fatigue design of offshore tubular structures. The offshore oil industry has been researching fatigue of tubular joints for over forty years. In the early years, fatigue design was done with the nominal stress approach, but it was

realized later that the hot-spot stress approach provided more accurate results, and has since been adopted in that industry (32).

There have been numerous publications regarding the fatigue strength of rectangular and circular hollow sections, but it is best summarized in Van Wingerde et al. (33). The majority of this work has taken place in Europe under the advisement of the European Coal and Steel Community (ECCS), British Department of Energy (DEn), now called the Health and Safety Executive, and the Comité International pour le Développement et l'Etude de la Construction Tubulaire (CIDECT) (34). This research has updated parametric equations used for SCF calculations, unified the definition of hot-spot stress, along with recognition of the thickness effect in the definition of the hot-spot S-N curves. These design recommendations have been adopted by the International Institute of Welding (IIW Document XIII-1804-99 and XV-1035-99), and CIDECT Design Guide #8, and have been proposed for inclusion into AWS D1.1, and Eurocode 3 (EC3) (13, 34, 35, 36). The remainder of this section will be devoted to the description of this design philosophy for the fatigue assessment of hollow structural sections (HSS) using the CIDECT Design Guide #8 guidelines.

There are two different types of connections covered by this design guideline. Connections can either involve the use of circular hollow sections (CHS) or rectangular hollow sections (RHS). The design guidelines outline both the nominal stress approach and the hot-spot stress method, but only the latter will be discussed further. The first step in the hot-spot fatigue design of hollow section connections would be the calculation of stress concentration factors (SCFs). The guidelines contain various parametric equations that can be used to calculate SCFs based on using four different non-dimensional parameters. Though the equations may predict a small SCF, a minimum SCF of 2.0 is recommended. The four dimensionless variables used for SCF calculations, for CHS T- and Y-joints are as follows:

$$\begin{aligned} b &= \frac{d_1}{d_o} & g &= \frac{d_o}{2t_o} \\ t &= \frac{t_1}{t_o} & a &= \frac{2L}{d_o} \end{aligned}$$

where β is the brace to chord diameter ratio, γ is the brace diameter to thickness ratio, τ is the brace to chord thickness ratio, and α is the chord length to diameter ratio, and Figure 3.27 can be used as reference for these dimensions. The same variables are used for different connection geometries and RHS joints, but the CHS example is just for demonstration purposes. A simple structural analysis can be used to attain the axial and bending forces entering a joint, from which nominal stresses can be calculated. The total hot-spot stress at a weld is determined from a superposition of all SCFs multiplied by the appropriate nominal stress as in the following equations:

$$\begin{aligned}
S_{rhs-chord} &= SCF_{axial-force-in-brace} S_{no\ min\ al-axial-force-in-brace} + SCF_{ipb-in-brace} S_{no\ min\ al-ipb-in-brace} \\
&+ SCF_{opb-in-brace} S_{no\ min\ al-opb-in-brace} + SCF_{axial-force-in-chord} S_{no\ min\ al-axial-force-in-chord} \\
&+ SCF_{ipb-in-chord} S_{no\ min\ al-ipb-in-chord}
\end{aligned}$$

$$\begin{aligned}
S_{rhs-brace} &= SCF_{axial-force-in-brace} S_{no\ min\ al-axial-force-in-brace} + SCF_{ipb-in-brace} S_{no\ min\ al-ipb-in-brace} \\
&+ SCF_{opb-in-brace} S_{no\ min\ al-opb-in-brace}
\end{aligned}$$

The hot-spot stress needs to be calculated at both the crown and saddle locations of the weld, and the fatigue design is governed by the maximum hot-spot stress. The highest hot-spot stress can then be compared to hot-spot S-N curves (see Figure 3.28) to determine the number of cycles to cracking, or be compared to the CAFL for infinite life design. The hot-spot S-N curves use the DEn T' curve (equivalent to the EC3 class 114 curve) as a baseline for use with 16 mm thick sections. In hollow structural joints, there is a pronounced thickness effect, with thinner sections having higher fatigue lives, which can again be seen in Figure 3.28.

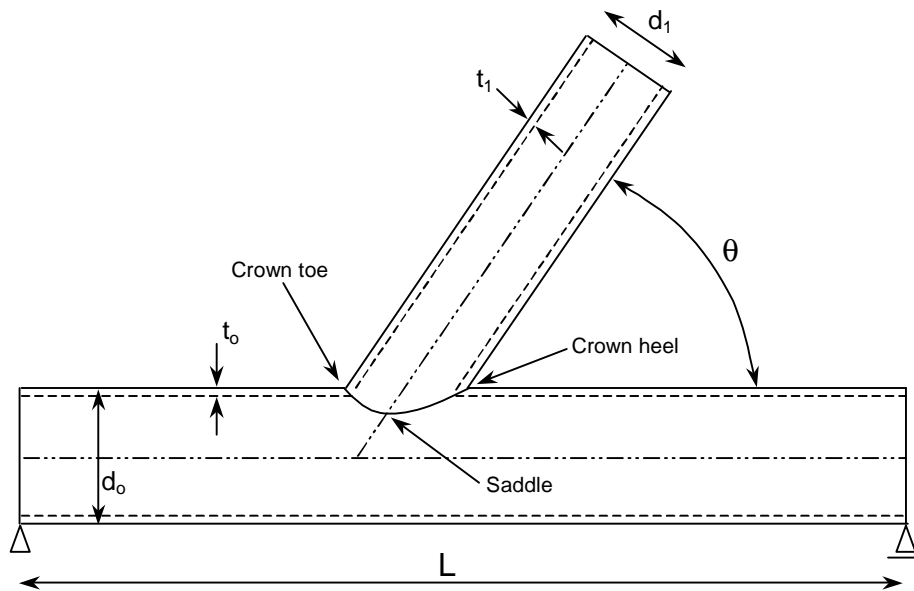


Figure 3.27 Definitions of CHS T and Y-joint dimensions.

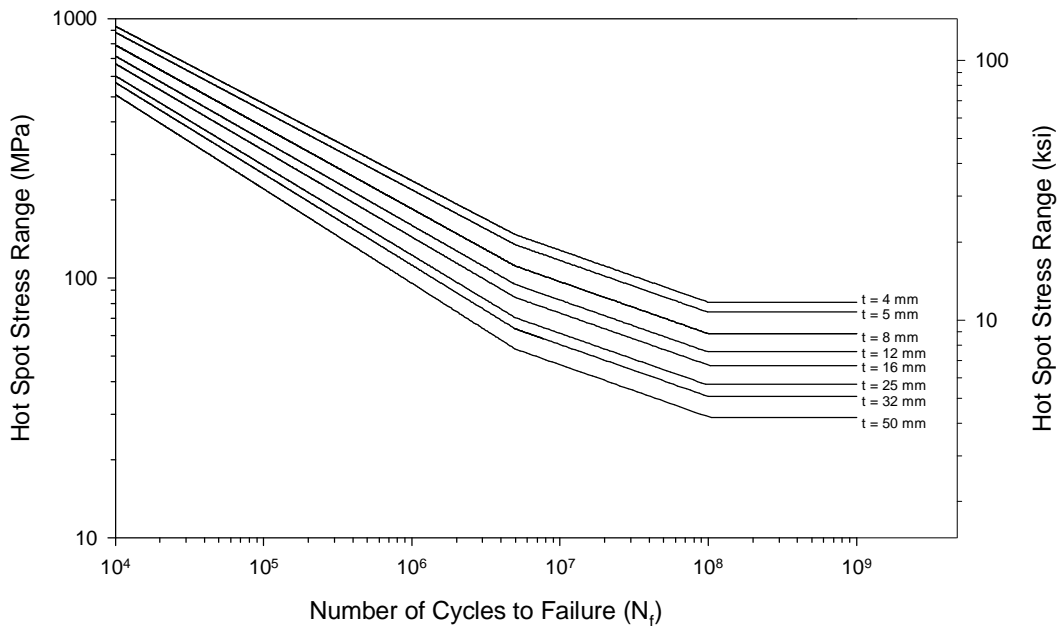


Figure 3.28 Hot-spot S-N curves for CHS joints ($4 \text{ mm} \leq t \leq 50 \text{ mm}$) and RHS joints ($4 \text{ mm} \leq t \leq 16 \text{ mm}$).

3.15.1 Determination of SCFs by Testing

The parametric equations used to calculate SCFs were determined from many full-scale experiments, as well as finite element analysis. In calibration of the parametric equations to experimental data, it was realized there were a wide variety of hot-spot stress definitions. One of the advantages of this guideline is the firm definition of what the hot-spot stress is and how it should be determined.

One of the early challenges using this method was how to measure the hot-spot stress. In experimental testing, strain gauges are used to measure the hot-spot stresses, but what is really being measured is the hot-spot strain. Some would argue that the principal strains need to be used in the hot-spot stress definition, but there are two reasons against this idea. One, there is a complex state of stress in the vicinity of a weld toe, and the principal stress is probably aligned at some angle to the weld. However, all observed cracks in tubular joints have been observed to grow parallel to the weld toes, which would indicate the principal stress, after accounting for residual stresses is perpendicular to the weld toe. Second, the measurement of principal strains would require the use of multiple strain gauges or rosettes, increasing the cost of testing and the amount of data to reduce. For ease of measurement, what was finally recommended is to use single axis strain gauges aligned perpendicular to the weld toe. However, it is not possible to place a strain gauge directly on the weld toe so the true hot-spot stress at the weld toe needs to be extrapolated from multiple strain readings. There are two recommendations for different ways to extrapolate the hot spot strain using linear or quadratic extrapolations. First, the extrapolation region where the strain gauges should be applied needs to be defined and this can be done through the use of Table 3.5 and Figure 3.29 for circular hollow sections (CHS) and rectangular

hollow sections (RHS). Figure 3.30 shows for linear extrapolation only two strain gauges are needed, but four gauges are needed for quadratic extrapolation. Experimentation has shown the stress gradients for CHS is linear, and only the linear extrapolation is needed, but RHS connections have extremely non-linear behavior and quadratic extrapolation is required.

Table 3.5 Boundaries of Extrapolation Region for CHS and RHS Joints

Distances from weld toe		Chord		Brace	
		Saddle	Crown	Saddle	Crown
CHS	$L_{r,min}^{(1)}$	$0.4 * t_o$		$0.4 * t_1$	
	$L_{r,max}^{(2)}$	$0.9 * r_o$	$0.4\sqrt{r_o t_o r_1 t_1}$	$0.65\sqrt{r_1 t_1}$	
RHS	$L_{r,min}^{(1)}$	$0.4 * t_o$		$0.4 * t_1$	
	$L_{r,max}$	$L_{r,min} + t_o$		$L_{r,max} + t_1$	

(1) – Minimum value for $L_{r,min}$ is 4 mm
(2) – Minimum value for $L_{r,max}$ is $L_{r,min} + 0.6 * t_1$

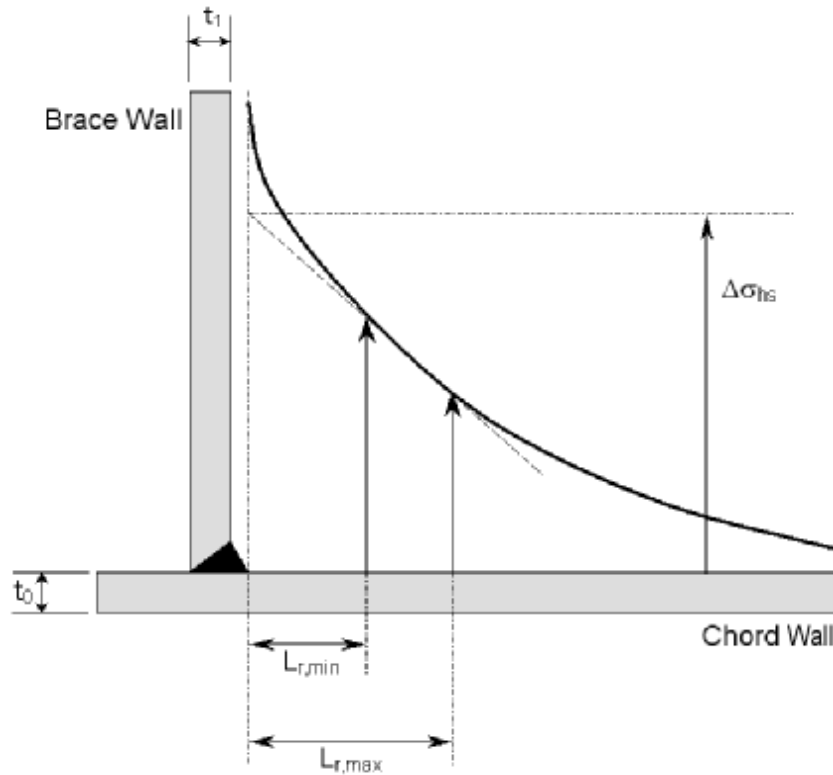


Figure 3.29 Picture of extrapolation region.

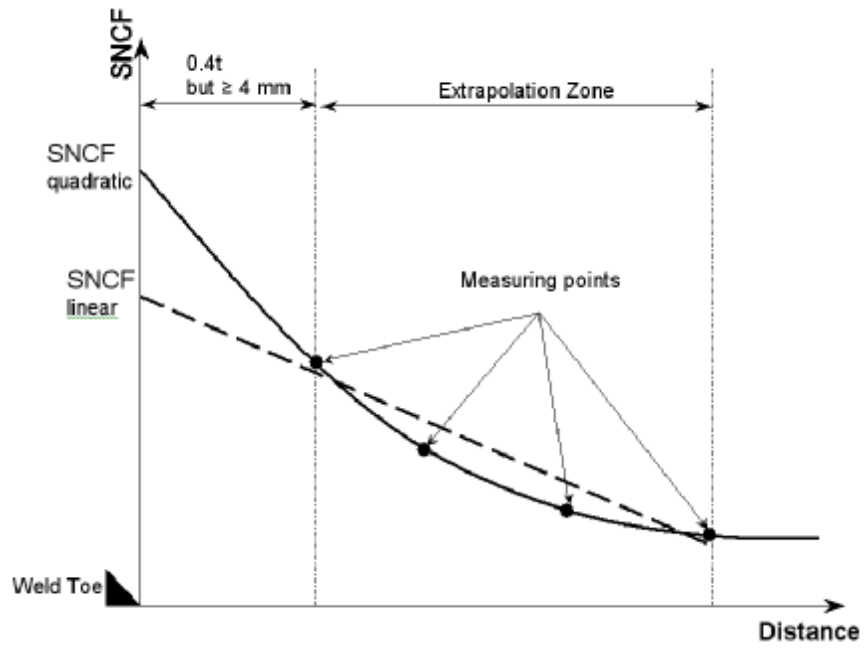


Figure 3.30 Difference between linear and quadratic stress extrapolation.

Chapter 4

Experimental Program

The core of this research project was to fatigue test common details used by Minnesota in the fabrication of traffic signal structures. At the time the experimental specimens were being designed, there seemed to be scant and ambiguous fatigue data from built-up box connections of traffic signal poles (presented in the University of Wyoming research summary of Chapter 3). Because of this, fatigue testing of Minnesota style box connections became the focus of this research project. Minnesota utilizes two standard types of mast arm-to-pole connections. Both types of mast arm-to-pole connections use 8-sided polygonal tubes for the poles and mast arms. The following sections describe the two types of specimens tested which will be referred to as Type I and Type II specimens. The loading systems for each specimen type are also described.

For all specimens, the multi-sided tubes were bent from steel sheet stock using either A588, A606, or A572 steel. The A588 and A606 are formed of weathering steel and the A572 is a non-weathering steel, but the use of certain steel grades depended upon availability at the time of fabrication and the thicknesses needed. All steel used had a minimum specified yield strength of 345 MPa (50 ksi). Any miscellaneous plate material used in the specimens (i.e., base plates, gusset plate, etc.) was specified to be A36 (minimum yield resistance of 248 MPa (36ksi)). All tubes were brake pressed into shape and welded closed with a longitudinal submerged arc welded (SAW) seam weld using E70 filler material. All other welds on the specimens were performed by hand using a gas metal arc welding (GMAW) process and E70 filler material.

4.1 Type I Specimens

In this report, a Type I specimen describes the first kind of Mn/DOT standardized mast arm-to-pole connection. The Type I mast arm-to-pole connection is truly a box connection, however detailed differently from previously described round tube box connections because the pole is an 8-sided polygonal tube. The pole is always tapered with the box connection located ~5.5m (18feet) off the ground. The box connection is built-up from three plates, one flange plate, and two side plates. The flange plate is thick and bears directly on one of the tube flats and is continuously fillet-welded everywhere the flange plate touches the pole tube. The outstanding portions of the flange plate are further reinforced with two side plates welded to the flange plate and further back near the midpoint the pole tube. The flange plate has four predrilled holes with nuts welded to the backside of the flange plate so the mast arm can bolt directly to the box connection. Specimens utilizing this box connection detail will herein be referred to as Type I specimens. It should be noted that the three plate box connection is the main difference between Mn/DOT box connections and other states details that use round tubes. In a round tube box connection it is not feasible for the flange plate to bear directly on the tube and top, bottom, and side plates are used to offset the flange plate away from the pole, and these four plates transfer all load from the mast arm into the pole. Contrast this with the Mn/DOT design where there is a direct load path between the mast arm and pole because the flange plate bears directly on the pole tube.

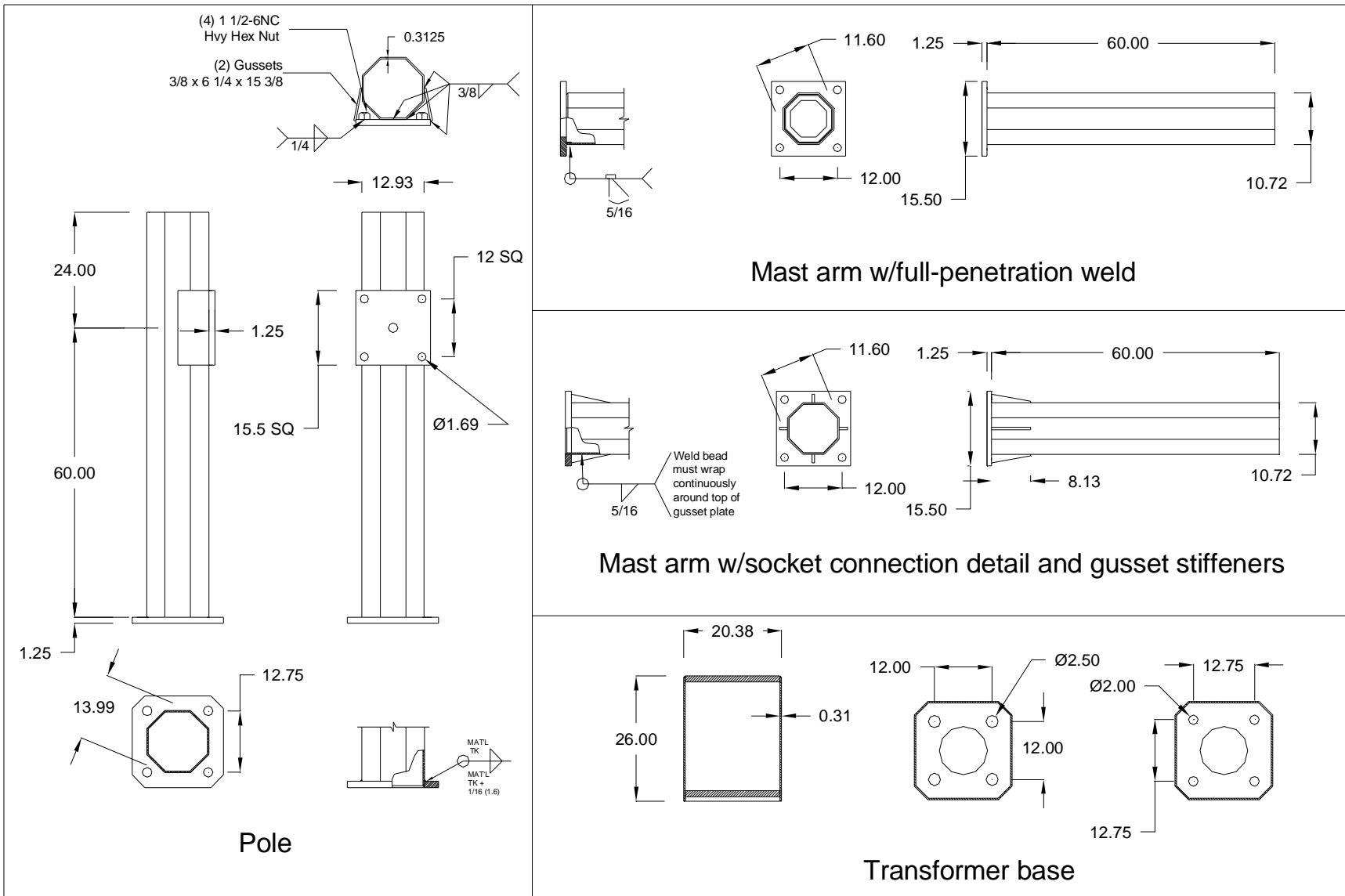
There were a total of eight Type I specimens, where each specimen encompassed one mast arm and one pole. The goal of the research was to initiate and grow a fatigue cracks originating from the box connection, from three different loading conditions. However, to fully represent the

boundary conditions of an in-situ box connection, the testing system had to use a pole (with a box connection) and a mast arm to apply loads through the box connection. In the initial design phase, the 2001 Specifications were used to predict fatigue strength, but there was an ambiguity as to how much load transfer occurred through the flange plate of the box connection, therefore it was assumed only the side plates transferred all load from the mast arm to the pole. Then the tubewall thicknesses were sized such that the code predicted fatigue failure in the box connection prior to the socket connections on the pole and mast arm. This was absolutely necessary because if the socket connection on the pole cracked prior to the box connection, cycling could not continue to fail the box because the pole could no longer resist the base moment because of the cracked section. As will be presented in Chapter 7, this was violated for three of the specimens.

All eight Type I pole specimens were identical. They were constructed from 8-sided, non-tapered tubes. Each tube was bent up from 7.94 mm (0.3125 inch) A588 sheet steel such that the corner-to-corner dimension was 355.6 mm (14.00 inch), and had a 31.75 mm (1.25 inch) thick base plate, fillet-welded socket connection at the base. The box connection was centered 1524 mm (5 ft.) from the socket connection at the base of the pole. The flange plate was 31.75 mm (1.25 inch) thick and was further reinforced with two side plates. Each side plate had a dimension of 393.7 mm x 203.2 mm x 9.53 mm (15.5 inch x 8 inch x 0.375 inch). In the field, the top of each pole is capped in some fashion, either with another pole to hold a luminaire, or a decorative cap. This cap would help to constrain the shape of the tube under deformation, therefore, prior to each pole being tested, a 6.35 mm (0.25 inch) thick plate was stitch welded around the circumference of the pole top to more accurately represent the boundary conditions on the box connection.

For each Type I pole specimen, there was to be a mating mast arm. However, two different socket connection types were fabricated for the mast arms, four had a fillet-welded socket connections with four triangular gusset plates, and the remaining four used a full-penetration tube-to-transverse plate welds. All eight of the Type I mast arms were also 8-sided polygonal tubes with 7.94 mm (0.3125 inch) wall thickness, but the corner-to-corner dimensions were reduced to 294.6 mm (11.6 inch). The mast arms tubes were also constructed from A588 steel

All detailing of the Type I specimens can be found in Figure 4.1. In addition to the eight mast arms and poles, Mn/DOT also specifies the use of a transformer base with these kinds of poles. Historically, these boxes placed between the foundation and the pole base actually housed electrical transformers, which are no longer needed with modern electrical systems, however their use still exist in Minnesota. All Type I specimens were tested with a transformer base present to accurately represent the boundary conditions in the pole socket connection.



Not to scale, units = inches, 1 inch = 25.4 mm

Figure 4.1 Type I pole, mast arm, and transformer base details.

4.2 Type I Long Pole Specimens

After the fatigue testing of the first eight Type I pole socket connection was complete, four more additional pole specimens were tested. The original eight, 31.8 mm (1.25 inch) thick base plate specimens demonstrate a lower fatigue resistance than anticipated, therefore the additional four pole specimens were fabricated to explore the effect of making the base plate thicker. The additional specimens were longer and only targeted testing the socket connection using the standard pole cross-sectional dimensions, but with thicker base plates. All four poles were 3657 mm (12 feet) long measured from the top of the base plate, and the base plates were 63.5 mm (2.5 inches) thick, twice the base plate thickness of the original eight Type I pole specimens. The steel used to construct these four tube was A606. The poles were fabricated longer to reduce the bending-to-shear ratio in the pole tube, because as presented in the Literature Review, the thicker base plate should increase fatigue resistance. In order to crack these specimens in a reasonable time period, higher moment ranges would be needed and increasing the moment arm distance reduces the shear being carried by the pole tube. Two of the long poles used a 7.9 mm (0.3125 inch) thick tube wall, while the remaining two had 4.7 mm (0.1875 inch) thick tube walls. A schematic of the long pole specimens can be seen in Figure 4.2.

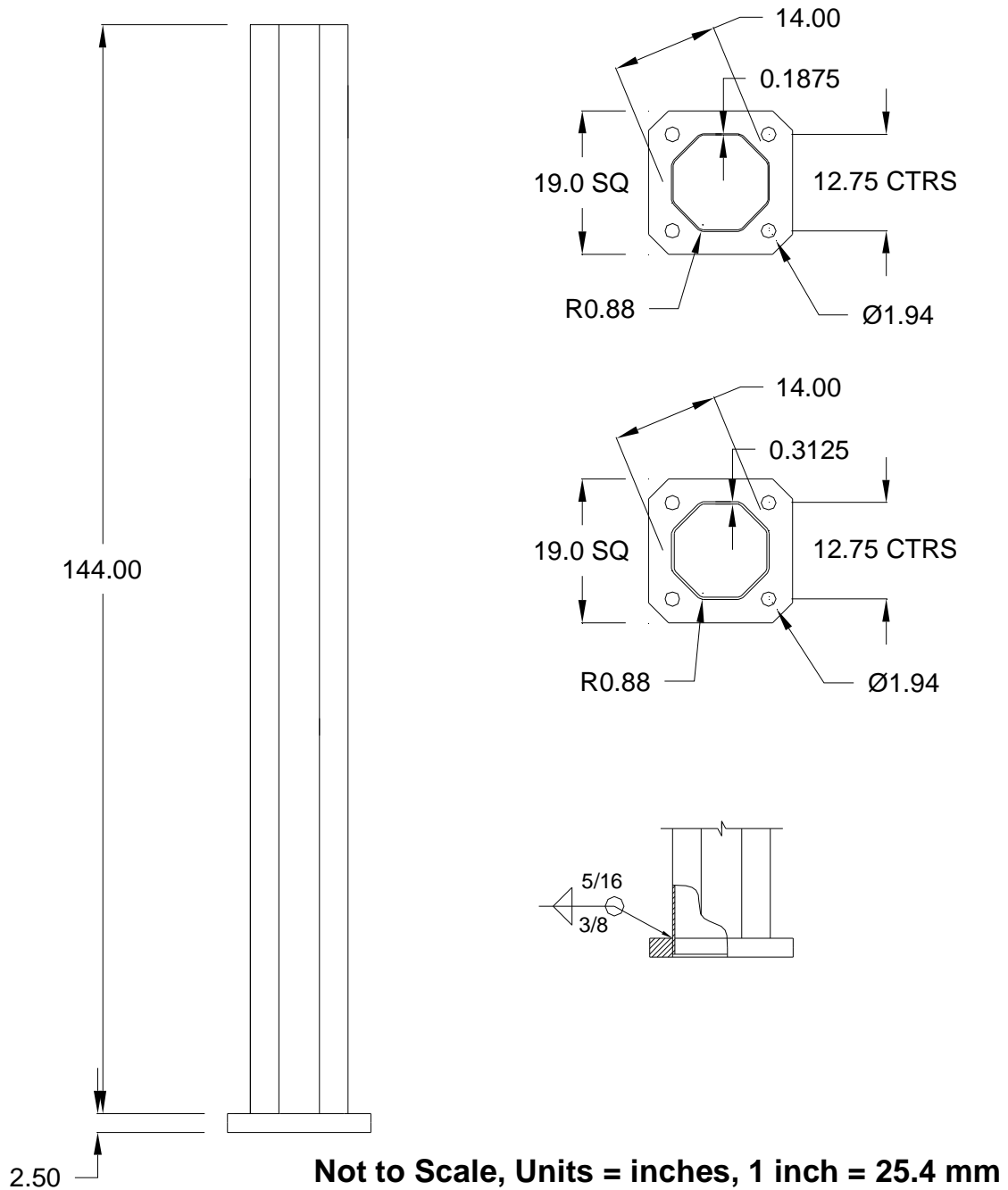


Figure 4.2 Dimensions of Type I long pole specimens

4.3 Type II Specimens

The Type II specimens use a completely different detailing of the mast arm-to-pole connection than the Type I specimens. First, the pole sections utilize an integrated tapered transformer base, instead of using two separate elements as in the Type I specimens. Second, the mast arm is full-penetration welded to a stub section of pole, referred to as a mast can. The key to the system is

the mast can has a slightly larger inside diameter than the outside diameter of the pole, at the location where the mast arm is cantilevered. The mast can with a welded mast arm can then be slipped down upon the top of the pole and resists in-plane moment through bearing of the mast can on the pole tube, and out-of-plane moments via an interlocking mechanism of a small octagon placed within a larger octagon. Figure 4.3 shows a cut-away view of a mast can detail showing how this slip-fit connection transfers load.

The tube section for the mast arm used the same dimensions as the Type I mast arms, except the mast arm was welded into the mast can at a 15 degree angle. This represents typical construction in Minnesota because this system design uses a monotube mast arm which must be pitched up to cancel out the dead load deflection of the mast arm. The pole section was bent-up from thicker 9.5 mm (0.375 inch) A572 sheet steel than the Type I poles. A more formal drawing showing dimensioning of the Type II pole and mast arm can be seen in Figure 4.4

As-built structures using the Type II design do not leave the top of the mast can open to the environment, and instead a cap is used to keep the elements out. The test pole used the same taper as real poles, but since a shorter pole was used for testing, the mast cans tested had a larger diameter than would normally be found on typical Minnesota structures. Therefore, the caps commonly produced by the fabricator would not fit atop the mast can of the mast arm specimens. However, these caps do prevent ovalization of the mast can as the mast arm induces moments on the mast can. To replicate the effect of this cap, a 6.35 mm (0.25 inch) steel plate was welded to the top of the mast can with intermittent fillet welds. The welds were ~76.2 mm (3.0 inches) long on each flat of the mast can. Particularly for in-plane loading, the weld attaching the cap plate to the front of mast can (flat of mast can nearest to top of mast arm) would fatigue crack itself, and an alternative design using an angle section in bearing was used for all the fatigue testing. A picture of this cap plate and angle can be seen in Figure 4.5.

In total, there were eight identical Type II mast arms and eight identical pole specimens.

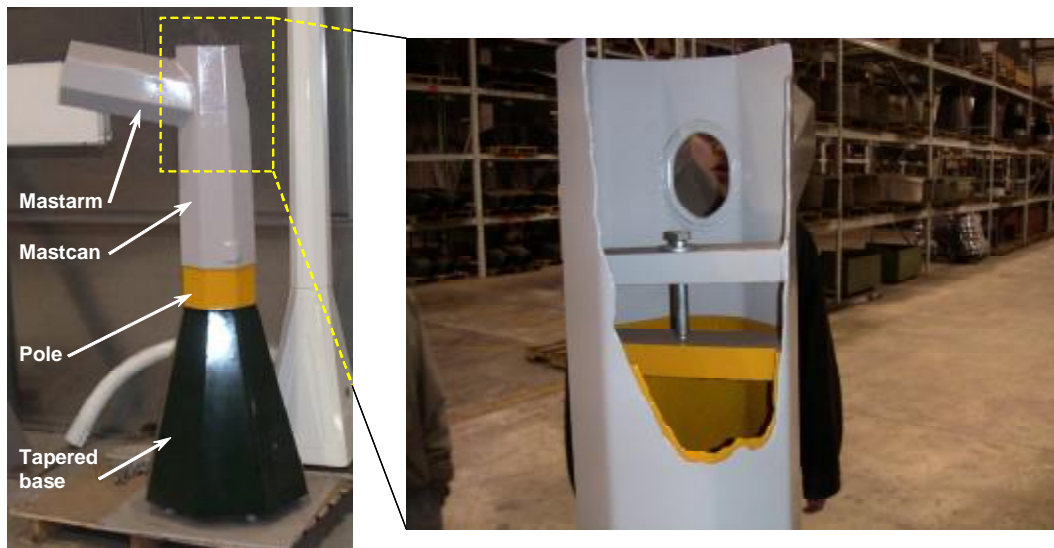
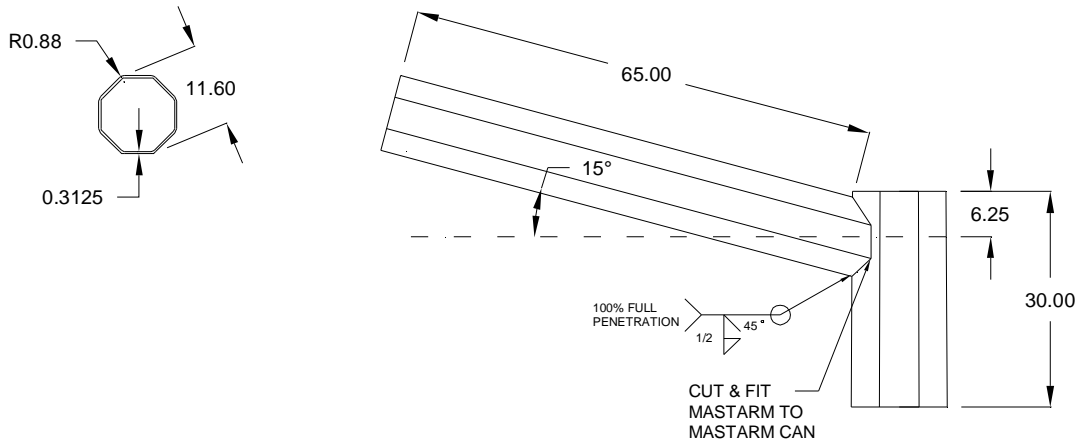
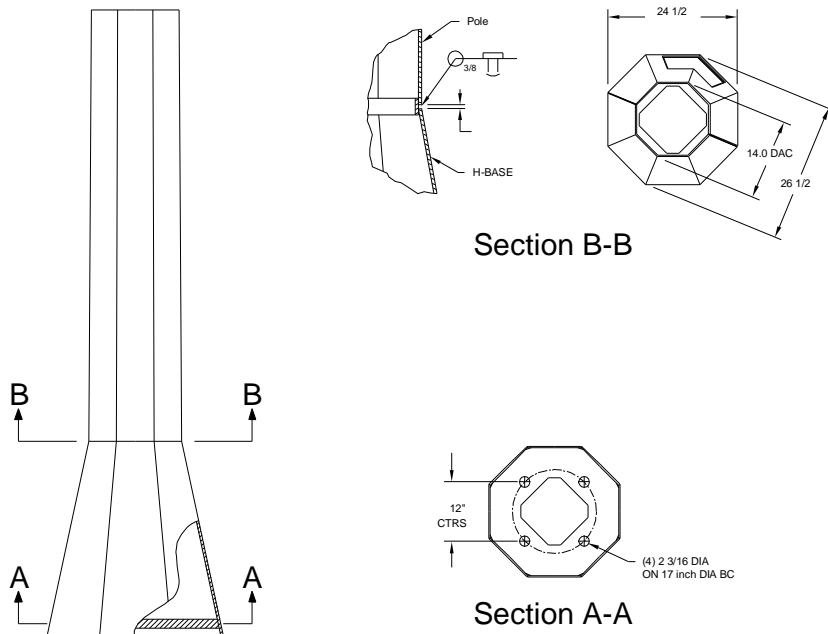


Figure 4.3 Mock-up of Type II specimen with cut-away view of mast can detail.



Mast Arm



Pole

Not to scale
units = inches
1 inch = 25.4 mm

Figure 4.4 Schematic of Type II specimens.

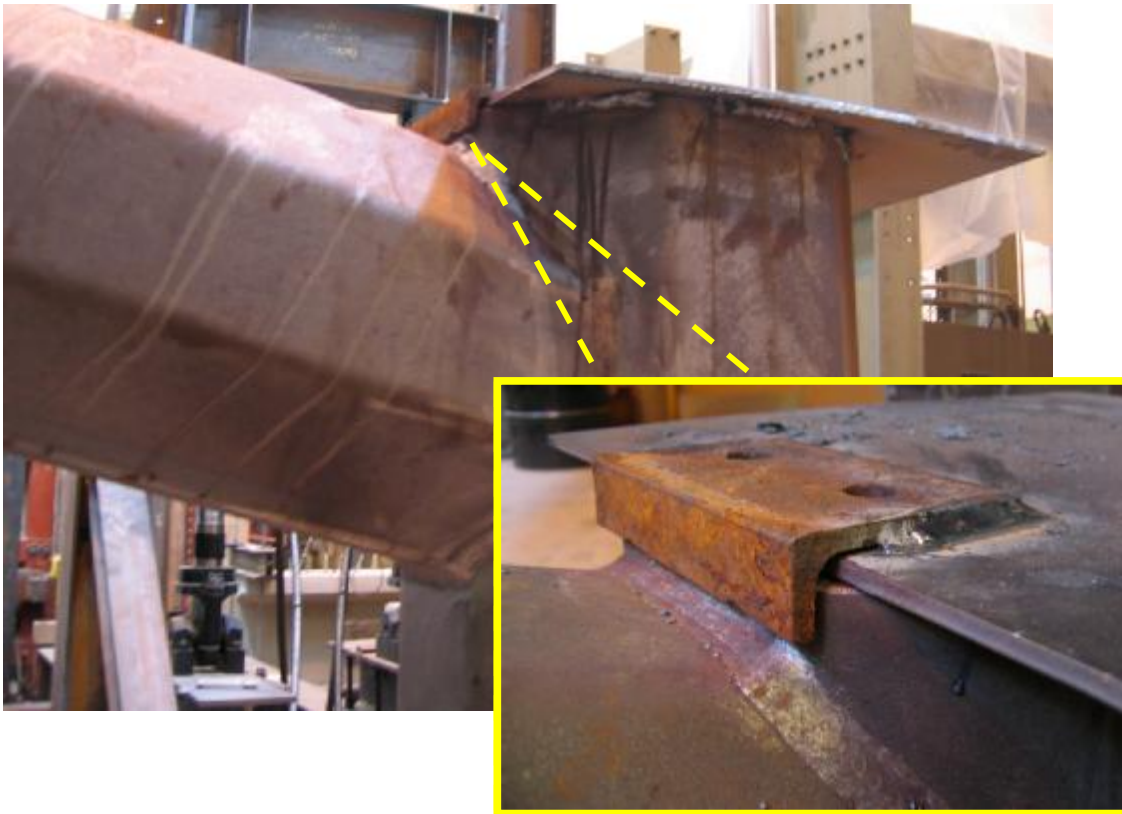


Figure 4.5 Cap plate welded to Type II mast can.

4.4 Type I Loading Systems

The Type I box connections were statically and fatigue tested in three different directions. These will be referred to as in-plane loading which represents mast arm tip motion perpendicular to the roadway; out-of-plane loading which refers to mast arm tip motions parallel to the road; and finally there was a 45 degree loading case which is a simultaneous, equal magnitude, in- and out-of-plane loading condition.

Each Type I pole sat upon a transformer base. Transformer bases (T-base) are used in the field as a transition piece between the concrete foundation and the pole. There is no structural purpose for having a T-base. Historically, T-bases were needed to house voltage transformers that are not needed in modern electrical systems, but the T-base is still used as part of the structure. For this research project, the T-base was integrated into the load frame to accurately represent boundary conditions in the pole socket connection. The key to the loading systems was affixing the T-base to the laboratory strong floor to resist the applied loads. As described in earlier sections, the goal of the Type I specimens was to cycle until the box connection cracked, then in a separate load frame, independently fatigue the pole and mast arm socket connections. Particularly, this did not occur with the three in-plane specimens. The following three sections will discuss the primary load frame (Frame #1), the frame to fatigue the socket connections

(Frame 2), and the third frame (Frame 3) to independently fatigue the three, in-plane box connections that did not crack in Frame 1.

4.4.1 Frame 1

Frame 1 was meant to be the primary load frame for this project. This frame was configured to apply load from one of three directions to each specimen. The specimens used in this load frame were composed of one pole specimen and one mast arm specimen bolted together, and the T-base was reused for all 8 specimens. Loads were applied to the tip of the mast arm by a 156 kN (35 kip) MTS 244 series actuator in a closed-loop servo-valve hydraulic system. The actuator was controlled via a MTS 407 or FlexTest IIm controller depending on the needs elsewhere in the laboratory.

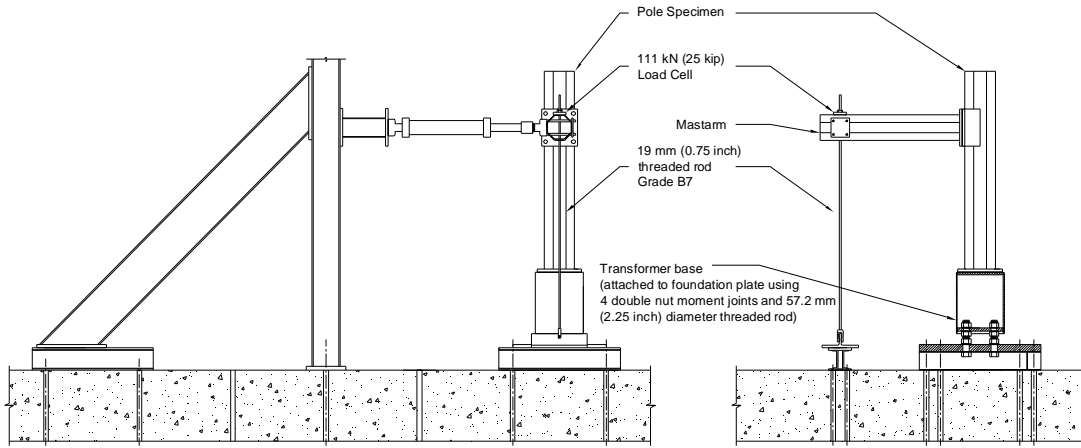
Figure 4.6 depicts a drawing of the three actuator positions in Frame 1 along with different elements of the loading system, which will aid in the following element descriptions. A 76.2 mm (3 inch) thick steel foundation plate, 1168 mm x 1320 mm (46 inch x 52 inch) in plan was first bolted to the strong floor with eight, 38.1 mm (1.5 inch) diameter threaded rods. The foundation plate had W8x13 sections welded to it, whose only purpose was to elevate the foundation plate off the strong floor to allow for access to the nuts for the double-nut moment joints used to bolt the T-base to the foundation plate. Four 57.2 mm (2.5 inch) diameter holes layed out on a 431.8 mm (17 inch) bolt circle were drilled into the center of the foundation plate. Each of these holes were occupied with a 57.2 mm (2.25 inch) diameter threaded rod in a double-nut moment joint configuration. Leveling nuts were turned onto the 57.2 mm (2.25 inch) threaded rod that then protruded from the foundation plate so there was a clear distance of threaded rod of ~25.4 mm (1 inch). The T-base then sat upon the leveling nuts and a final nut was put on to complete the second double-nut moment joint to the bottom of the T-base. However, there was no way to properly tighten the 57.2 mm (2.25 inch) nuts and particularly in the out-of-plane loading condition, the nuts would vibrate loose and fatigue the threaded rod. The fatigue of the threaded rods became a nuisance and the double nut moment joints were eliminated and the T-base was directly post-tensioned down to the foundation plate with four 38.1 mm (1.5 inch) diameter threaded rods and a 63.5 mm (2.5 inch) spacer plate between the T-base and the foundation plate. The ladder of these two connections does not accurately represent typical field practice as certainly the boundary condition at the bottom of the T-base is different. However, the transformer base was not being tested as part of this research project, and strain gauge readings at the pole socket connection showed no difference depending on how the T-base was bolted to the foundation plate so it was felt that this type of connection was suitable. The pole bolted to the top of the T-base with four 44.5 mm (1.75 inch) diameter A354BD bolts torque tensioned to 2576 N-m (1900 ft-lbs). The mast arm bolted to the box connection on the pole with four 38.1 mm (1.5 inch) diameter A325 bolts which were torque tensioned to 1200 ft-lbs. The actuator bolted to the mast arm via four 15.9 mm (0.625 inch) diameter class B7 threaded rods. The rods passed through the mast arm through flame cut holes and 12.7 mm (0.5 inch) thick backing plate on the opposite side of the arm. This connection clamped the actuator to the mast arm, but to prevent the mast arm tube from crushing, spacers were inserted to prevent the mast arm cross-section from distorting.

In the out-of-plane loading case, the actuator reacted off a W12x65 column braced with the W18x35 section. The other unique aspect of this loading case was a 19.1 mm (0.75 inch)

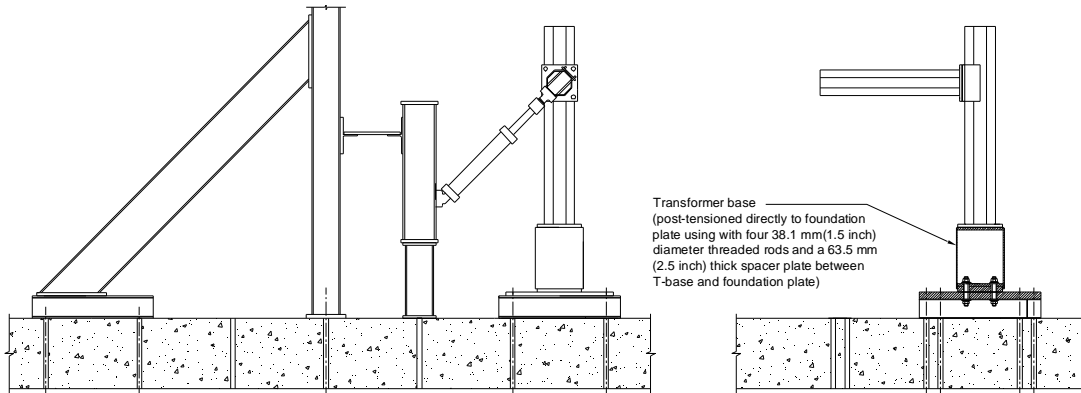
diameter threaded rod used to apply dead loads to the tip of the mast arm. The load from this threaded rod was meant to accurately represent the dead load stress from structural self-weight and signal heads in real structures, all while the mast arm was cycled in the out-of-plane direction. The rod had to be tensioned to 40.5 kN (9.1 kip) (measured with a loadcell) in order to get a dead load stress of 103.4 MPa (15 ksi) at the mast arm socket connection. The threaded rod was fixed to a pivot point on the strong floor so the rod would tip back and fourth as the actuator cycled. There was a concern that as the rod tipped back and fourth there would be a large fluctuation in the dead load force because the rod would be forced to elongate. This load fluctuation was monitored during static load tests and at peak loads, the force in the rod only varied by ± 4.4 kN (100lbs) which is only a 1% difference when compared to the dead load being applied.

In the 45 degree loading case the actuator reacted off a scrap column section. The disadvantage of this loading direction was a true in-plane dead load could not be simultaneously present. Two actuators could be used to cycle the mast arm tip in a 45 degree plane, however experience has found that two actuators fight each other and this idea was not used. Instead, a mean load was applied with the actuator and cycling occurred about this mean load. The mean load was chosen so the strains would not go inelastic during fatigue cycling, however this meant there was only about 50% of the true in-plane dead load present.

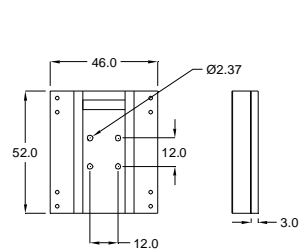
In the in-plane loading case, the actuator reacted off a built-up floor beam section commonly used in the laboratory. In this direction of loading, the actuator could directly apply the dead load force, then cycle about it to fatigue the specimen.



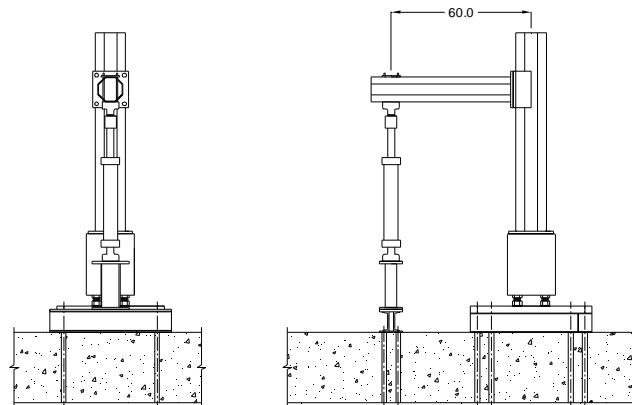
Out-of-plane loading system



45 degree loading system



Foundation plate



In-plane loading system

Not to Scale, Units = inches, 1 inch = 25.4mm

Figure 4.6 Schematic of three loading positions used for Type I specimens in Frame 1.

4.4.2 Frame 2

Frame 2 was constructed to fatigue the Type I pole socket connections. However, in this frame, the actuator bolted directly to the pole and pushed on the pole to creating a linear moment diagram within the pole. In Frame 1, the region of the socket connection beneath the box connection was subjected to compressive stresses because of the applied dead load moment on the mast arm. In Frame 2, the applied moment then subjected this region of the socket connection to tensile stresses. The cyclic loads applied in Frame 2 were done about a dead load that gave an equivalent dead load stress in the pole section as was present with the dead load in Frame 1.

The loads were applied to the pole via a 156 kN (35 kip) MTS 205 series servo-valve hydraulic actuator controlled with a MTS 407 controller. The same system of a foundation plate, T-base, and pole specimen used was identical to that in Frame 1, with the T-base post-tensioned directly to the foundation plate. The actuator reacted off the laboratory strong wall and attached to the pole at the box connection. A 38.1 mm (1.5 inch) thick adapter plate was fabricated with tapped holes to accept the actuator clevis and four mating holes which 38.1 mm (1.5 inch) diameter bolts can pass through to bolt into the box connection on the pole.

Frame 2 was also used to cycle the long pole specimens, with two minor modifications. One, the actuator was moved to a new height to accommodate the longer specimen. Second, since the long poles did not have box connections, a different method of attaching the actuator to the pole was devised. The actuator on the first long pole specimen was bolted to the pole by passing threaded rods through the tube and the actuator clevis was post-tensioned to the pole tube with a backing plate on the opposite side of the tube. This is the same method the actuator was connected to the mast arms in Frame 1. Strain gauges verified the correct loading was getting into the pole with this connection, however, the threaded rods tended to rub on the sides of the tube creating a loud rubbing noise. A new connection was used on the remaining three long pole specimens, where a 9.5 mm (0.375 inch) thick plate was welded to the top of the pole. A small W-section with end plates was then welded to the top of this plate, creating a connection that transferred load into the pole via shear, not bearing. The new connection eliminated the rubbing noise and also increased the moment arm distance such that a higher gain range could be utilized in the actuator controlling system. These two types of connections are shown in Figure 4.7.

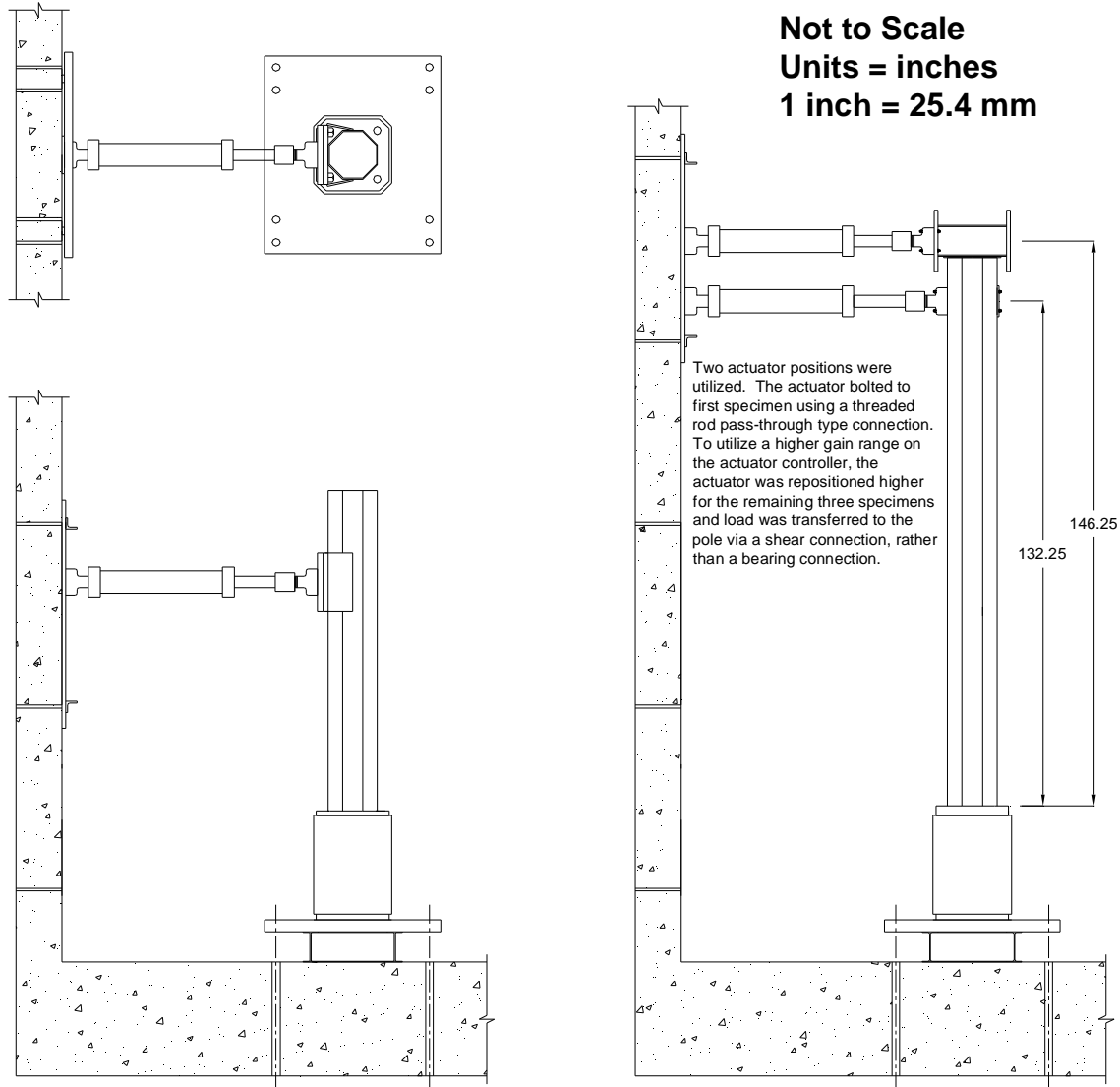


Figure 4.7 Schematic of Frame 2 layout.

4.4.3 Frame 3

Frame 3 was solely built to complete the fatigue cycling of the three, in-plane box connections that did not crack while loading in Frame 1. A completely new loading system had to be devised because by the time the pole specimen got to Frame 3, there were multiple fatigue cracks in the pole socket connection from fatigue cycling at Frames 1 and 2. Therefore a system had to be devised that limited the amount of moment transferred by the pole socket connection, though it was assumed the cracked socket connection could still carry shear.

The T-base was not used in Frame 3, instead a stiffened, stub W14x159 section was bolted to the strong floor and the pole bolted directly to stub W-section. A four column load frame for the actuator to react off of was erected around the pole and mast arm specimen. The actuator applied loads to the tip of the mast arm, creating a linear moment gradient within the mast arm. Moment flowed into the pole and was constant until the point where the pole beared upon a 203.2 mm x

203.2 mm x 28.6 mm (8 x 8 x 1.125 inch) angle. This angle section was further reinforced with two like angles which helped carry the force back into the load frame columns. The system of heavy angles and stub W14x159 resisted the applied moment via a force couple, and this caused the moment at the pole socket connection to be near zero as it lied in the middle of the heavy angles and the strong floor. The interior of the pole tube was also filled with concrete to prevent the tube from crushing under the applied moment.

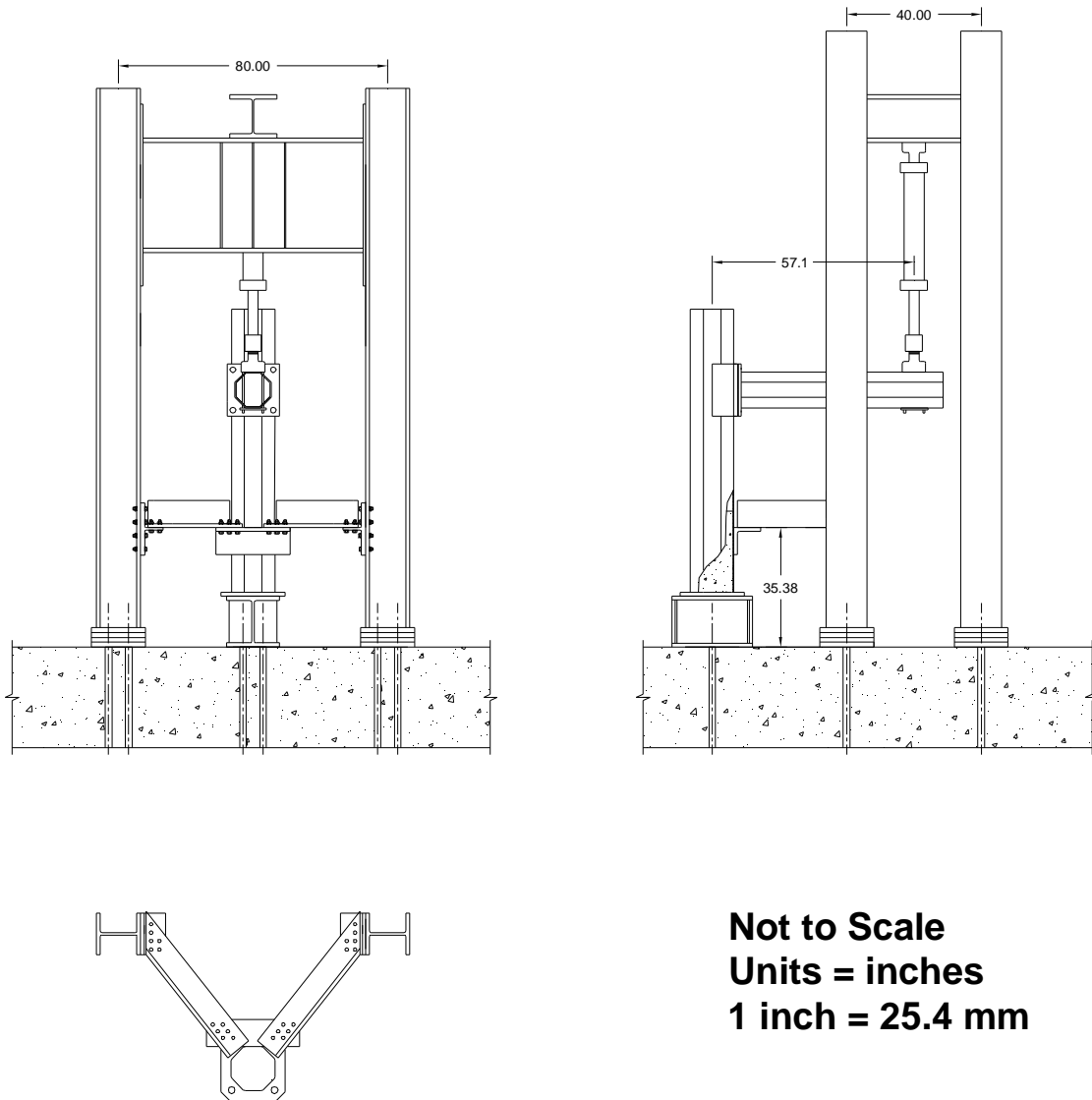


Figure 4.8 Schematic of Frame 3 loading system.

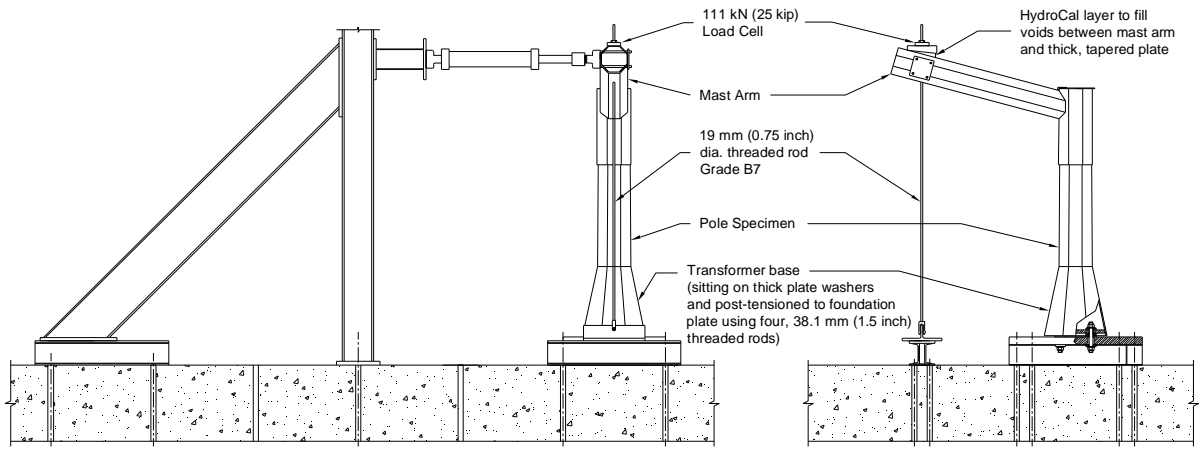
4.5 Type II Loading Systems

The Type II specimens were all loading in Frame 1. The entire system was able to be reused from the testing of the Type I specimens. However, actuator positions had to change because the angled mast arm was at a higher elevation than the Type I mast arm. Detailed drawings of the three loading systems for the Type II specimens are depicted in Figure 4.9.

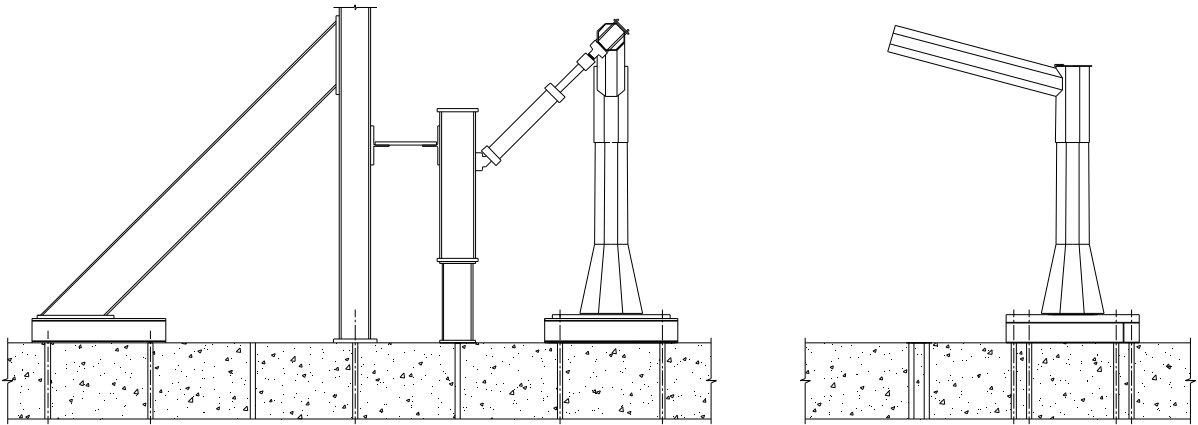
Like the Type I transformer base, the Type II poles are usually connected to concrete foundations via double-nut moment joints. Since there was difficulty with the anchor rods cracking in the double-nut moment joints during testing of the Type I specimens, that joint was not used on the Type II specimens. Instead, the Type II poles were directly post-tensioned to the foundation plate using the connection shown in Figure 4.10. The pole base was post-tensioned to the foundation plate with four, 38.1 mm (1.50 inch) diameter threaded rods. The threaded rods passed through the pole base plate, then two 101.6 mm x 101.6 mm x 19 mm (4 inch x 4 inch x 0.75 inch) thick plate washers with a 38.1 mm (1.50 inch) F436 washer sandwiched between them, and finally through the foundation plate. The thick plate washers were needed to increase the standoff distance of the pole and to cover the 60.3 mm (2.375 inch) holes in the foundation plate because much smaller diameter threaded rods were being used. Since a double-nut moment joint possesses some rotational flexibility, the F436 washer served the purpose to create a smaller bearing area between the thick plate washer to release the rotational rigidity that would exist if the two thick plate washers beared upon each other. This was the best solution to accurately represent the boundary conditions of a double-nut moment joint.

Because the mast arm was angled at 15 degrees, the load cell used to measure load in the threaded rod for out-of-plane loading could not bear directly on the mast arm. An available plate with a 20% (11.3 degree) taper was set upon the mast arm to attain a level surface for the load cell to bear upon. However, with the mast arm being angled at 15 degrees, there was still a small gap between the mast arm and the tapered plate. This void was filled with Hydrocal (registered product of the United States Gypsum Company), which is a high-strength, fast-setting gypsum cement. A picture of an installed tapered plate and load cell can be seen in Figure 4.11.

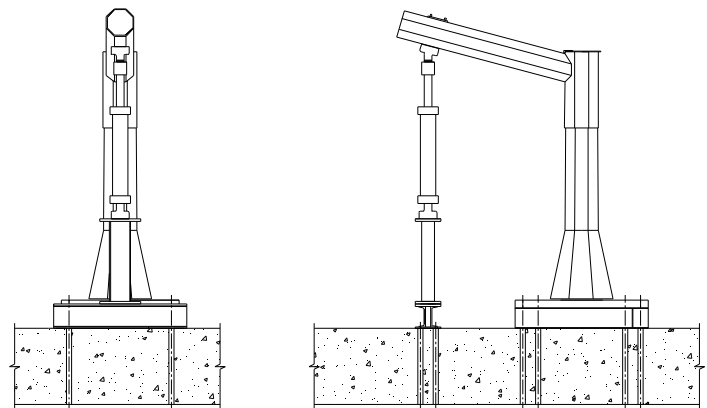
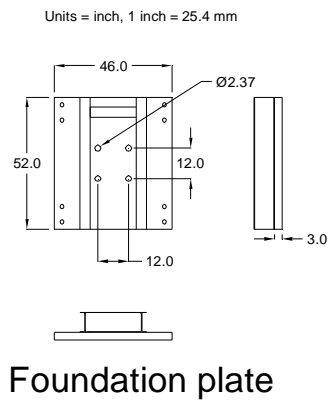
All eight mast arms were able to be cycled using the same pole. Therefore, Frame 1 had to be modified again so the actuator could be repositioned to cycle just the remaining pole specimens. A schematic of this modified load frame is shown in Figure 4.12. The frame was modified by shifting the foundation plate over one hole set on the laboratory strong floor, and adding a second braced column for the actuator to react off. This frame allowed for the actuator to pull the top of the pole specimen, inducing a linear moment diagram in the pole to fatigue the welded details used in the pole base.



Out-of-plane loading system



45 degree loading system



In-plane loading system

Figure 4.9 Schematic of Frame 1 for Type II specimens.

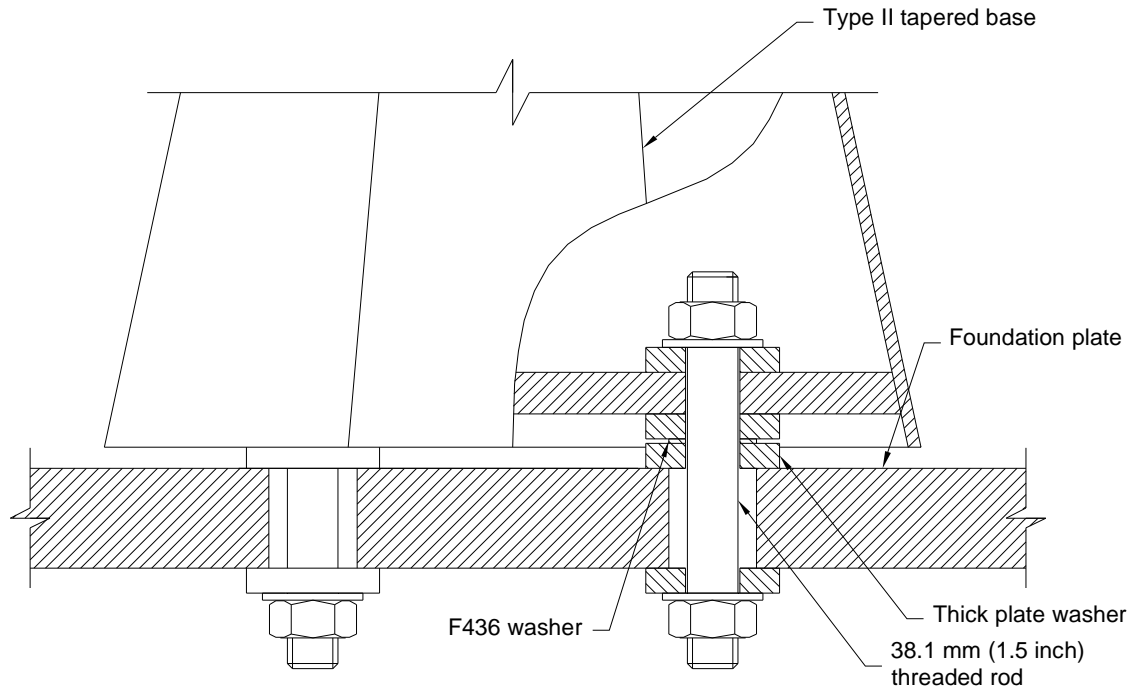


Figure 4.10 Type II pole foundation connection.

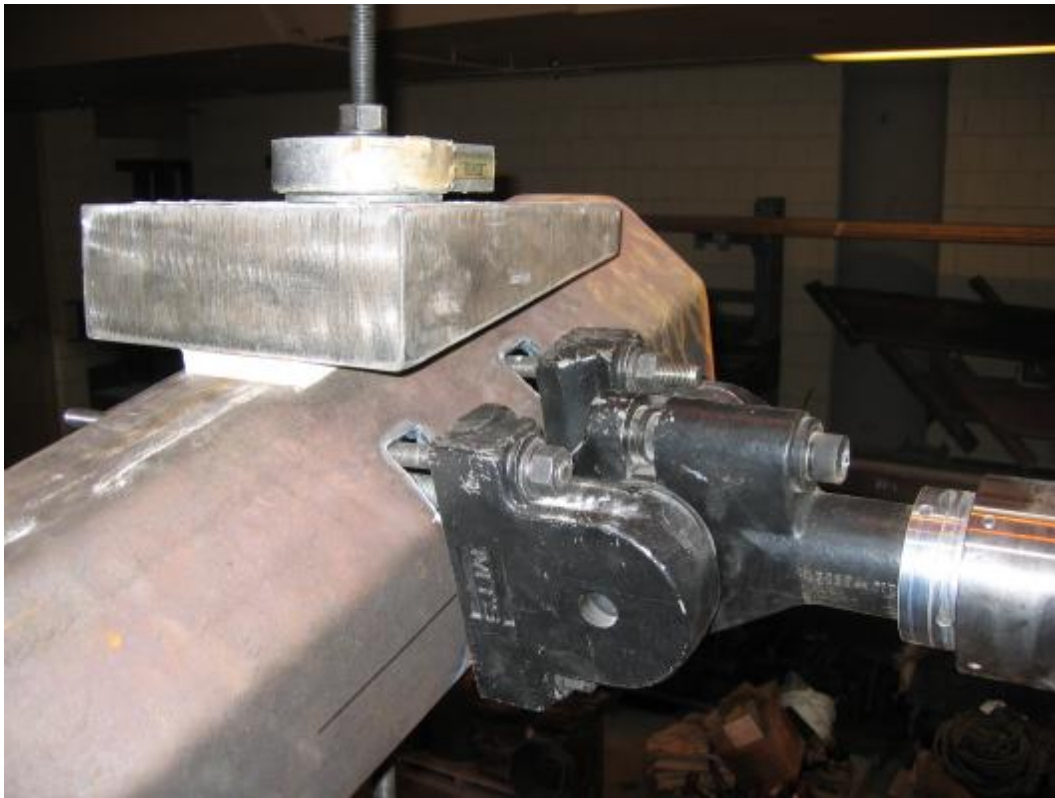


Figure 4.11 Thick plate washer beneath load cell for Type II specimen out-of-plane loading.

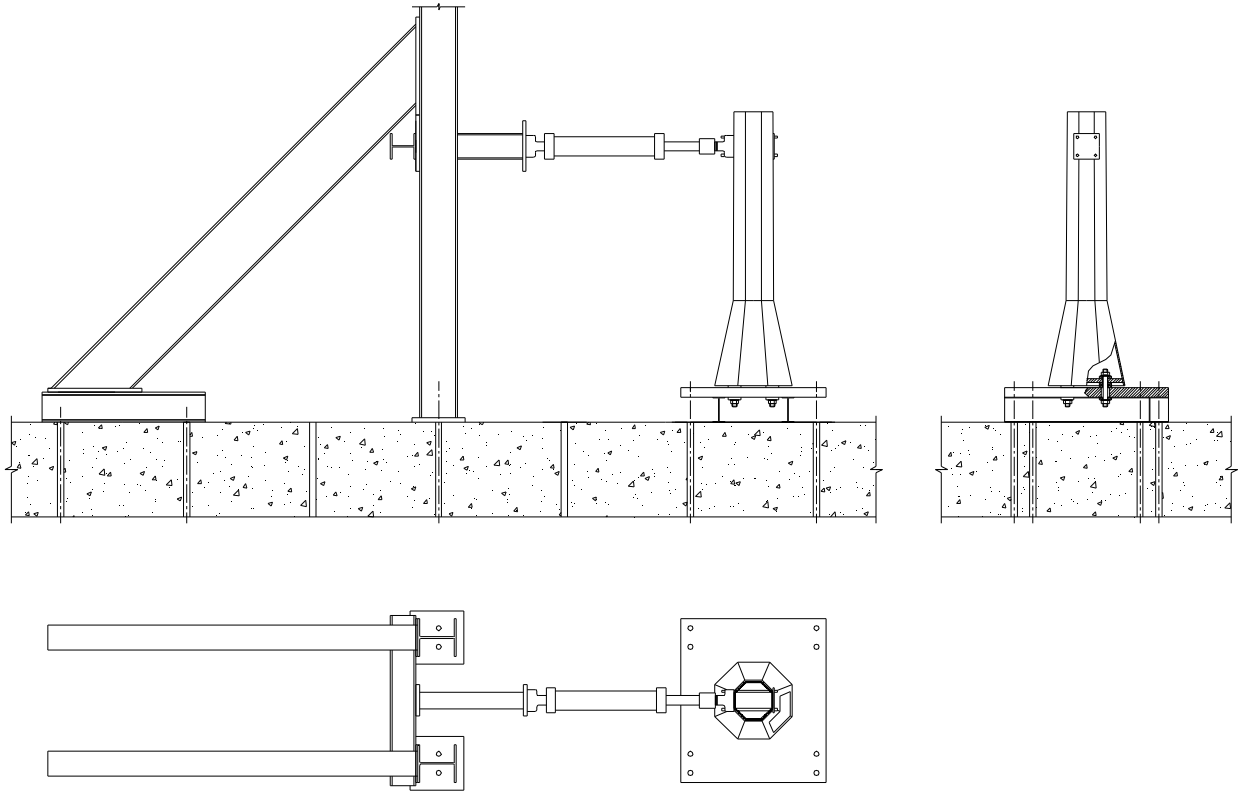


Figure 4.12 Load frame used to only test Type II poles.

Chapter 5

Experimental Instrumentation

In this research, 20 full-scale specimens (poles and mast arms) were tested experimentally to determine load paths through subelements and ultimately to find the fatigue resistance of the details used in Mn/DOT traffic signal structures. Two types of instrumentation plans were used, one for each type of specimen tested. The following sections will describe the instrumentation used for each type of specimen.

5.1 Type I Specimen Instrumentation Plan (Frame 1)

There were eight Type I specimens, where the specimen is defined to be a mast arm and a pole bolted together. The first of these specimens was heavily instrumented and tested statically in the three loading directions to examine the static behavior of the specimen to better understand the load paths and determine the strain concentration factors (SCF) at the critical details. This first specimen utilized 89 strain gauges in total, one linear variable differential transducer (LVDT), and two load cells.

The information presented in the Chapter 3 showed there were potentially three locations of cracking for each specimen; the intersection of the box connection side plates and the pole wall (from in-situ cracking in Wyoming), and the mast arm and pole socket connections, particularly at the bends of the tubes (24,37). The instrumentation plan was formulated to address these three critical details.

Five types of strain gauges were utilized:

- Measurements Group, EA-06-250BG-120 which is a uniaxial strain gauge with 6.35 mm (0.25 in.) grid length.
- Tokyo Sokki Kenkyujo Co., FLA-1-11 which is a uniaxial strain gauge with a 1 mm (0.04 in.) grid length.
- Tokyo Sokki Kenkyujo Co., FRA-3-11 which is a 45°/90° 3-element rosette gauge with a grid length of 3 mm (0.12 in.).
- Tokyo Sokki Kenkyujo Co., FXV-1-11-002LE which a strip gauge with five uniaxial strain gauges placed in a row with a 2 mm (0.08 in.) pitch. Each gauge in the strip had a grid length of 1 mm (0.04 in.).
- Tokyo Sokki Kenkyujo Co., FLA-3-11 which is a uniaxial strain gauge with a 3 mm (0.12 in.) grid length.

The labeling system employed identifies where a gauge is affixed on the specimen and is outlined in Table 5.1 and shown pictorially in Figure 5.1. In certain locations, multiple strain gauges were used to define the SCF at the weld toe via CIDECT extrapolation procedures (35). For tube elements (e.g., mast arm and pole tubes), the labeling procedure was based on a polar coordinate system, whereby gauge locations were given an alphanumeric code. The letter would distinguish the element (i.e., P for pole) and the number represents the number of degrees counterclockwise from the zero axis a gauge was glued to on the tube perimeter. The zero axis was defined by

looking longitudinally down the tube, toward the base plate, and defining the right side of the tube at the neutral bending axis to be the zero degree axis.

Table 5.1 General Strain Gauge Lexicon for Fatigue Testing

	Location	Description
Mast arm		
MA_Mid_XXX ^(a)	Mast arm Midpoint	Gauges used to verify nominal stresses
MA_S_XXX_Y ^{(a), (b)}	Stiffener at mast arm base plate	Used to measure SCF at stiffener terminations
MA_P_XXX_Y ^{(a), (b)}	Socket weld toe	Used to measure SCF at socket connection weld toe
Pole		
P_Mid_XXX	Midheight of pole	Used to verify nominal stresses in pole
P_XXX_Y ^{(a), (b)}	Pole socket weld toe	Used to measure SCF at pole socket connection weld
Box Connection		
Box_(E,W)_(Top,Mid, Bot) E – East side W – West side Top – Top of side plate Mid – Middle of side plate Bot – Bottom of side plate	Side plates of box connection	Used to determine load path through box connection
PBox_(E,W)_(Top, Bot)_(Hor,Ver)_Y ^(b) E – East side W – West side Top – Top of box connection Bot – Bottom of box connection Hor – Gauge orientated horizontally Ver – Gauge orientated vertically	On pole tube near wrap around weld of side plate/pole connection	Used to determine SCF at pole tube were side plates are welded on
^(a) - _XXX denotes number of degrees from away from in-plane bending axis with counterclockwise being positive ^(b) - _Y represents a number from 1-5 denoting position of strain gauges relative to weld toe, 1 represents closest gauge to weld toe and 5 the farthest		

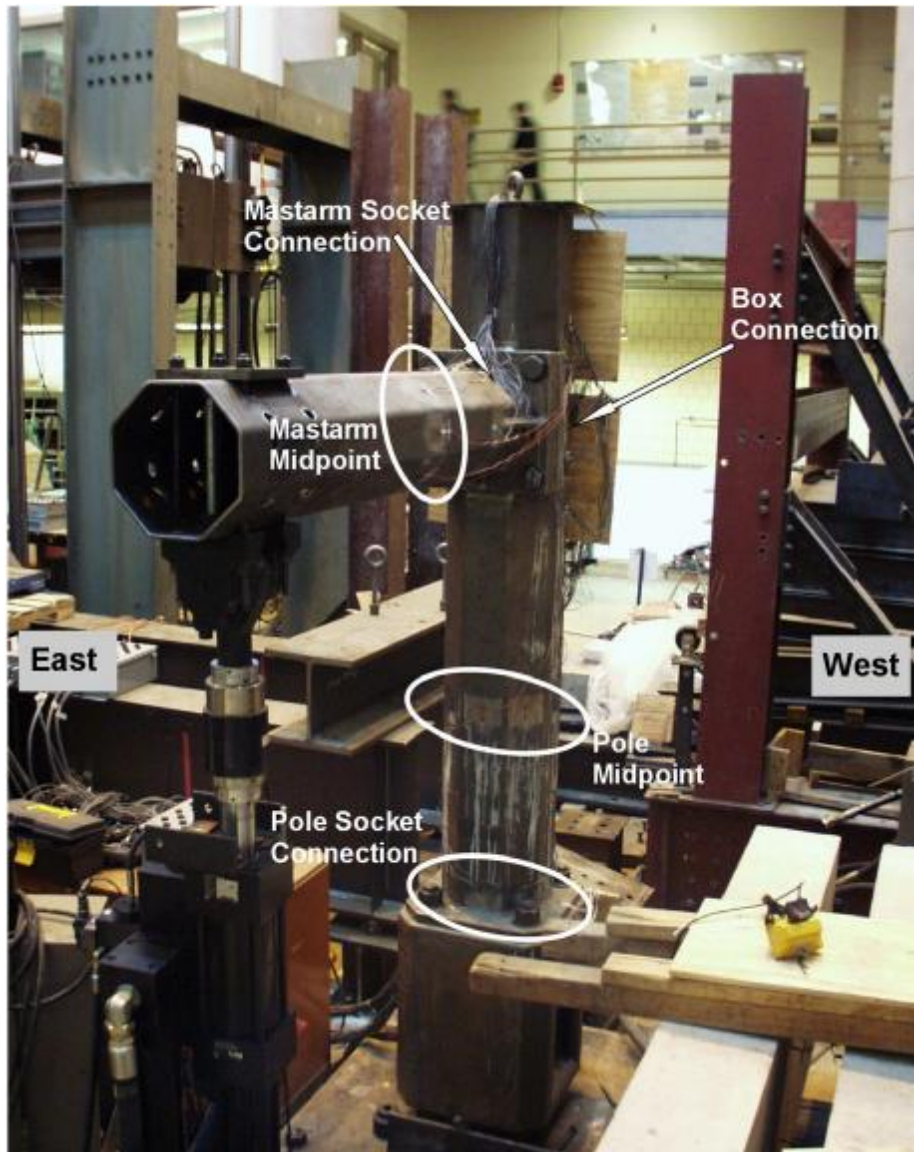


Figure 5.1 Strain gauge layout on Type I specimen.

5.1.1 Mast Arm

Eight strain gauges were affixed to the middle of each flat on the tube, at the midpoint of the mast arm (halfway between the socket weld, and the actuator centerline). The EA-06-250BG gauges were used at this location because the larger grid would give better results for measuring nominal strains.

The remaining gauges on the mast arm were concentrated at the tube-to-transverse plate connection since this was a likely location for cracking. Since the loading on the mast arm always resulted in a linear moment diagram for the three directions of loading, it did not make sense to place strain gauges on all the flats and corners at the socket connection, and only 180 degrees of the socket was strain gauged as shown in Figure 5.2.

In the literature review, it was presented that gusset stiffeners were stress risers and have been shown to have fatigue resistance equal to or worse than a bare socket connection. For this reason, one of the gussets on the mast arm had a strip gauge placed 5 mm (0.20 inch) away from the gusset weld toe. The strip gauge has five strain gauges in a row so this would allow for an accurate extrapolation of strain at the weld toe. As verification, two of the other gussets were only given one, 1 mm, uniaxial strain gauge located 5 mm (0.20 inch) from their weld terminations to verify the extrapolation accuracy of the strip gauge. Each flat and corner in the upper 180 degrees of the mast arm was given one or two 1 mm (0.04 inch), uniaxial strain gauges to determine the SCF at the weld toe. Ideally, two gauges should be used at each location such that linear interpolation could be used to extrapolate the strain at the weld toe, however, limitations on the number channels available on the data collection system dictated that only one gauge could be used at some locations. If a location could only use one gauge, it was attempted to make sure a symmetric point would have two gauges to verify the strain extrapolation.

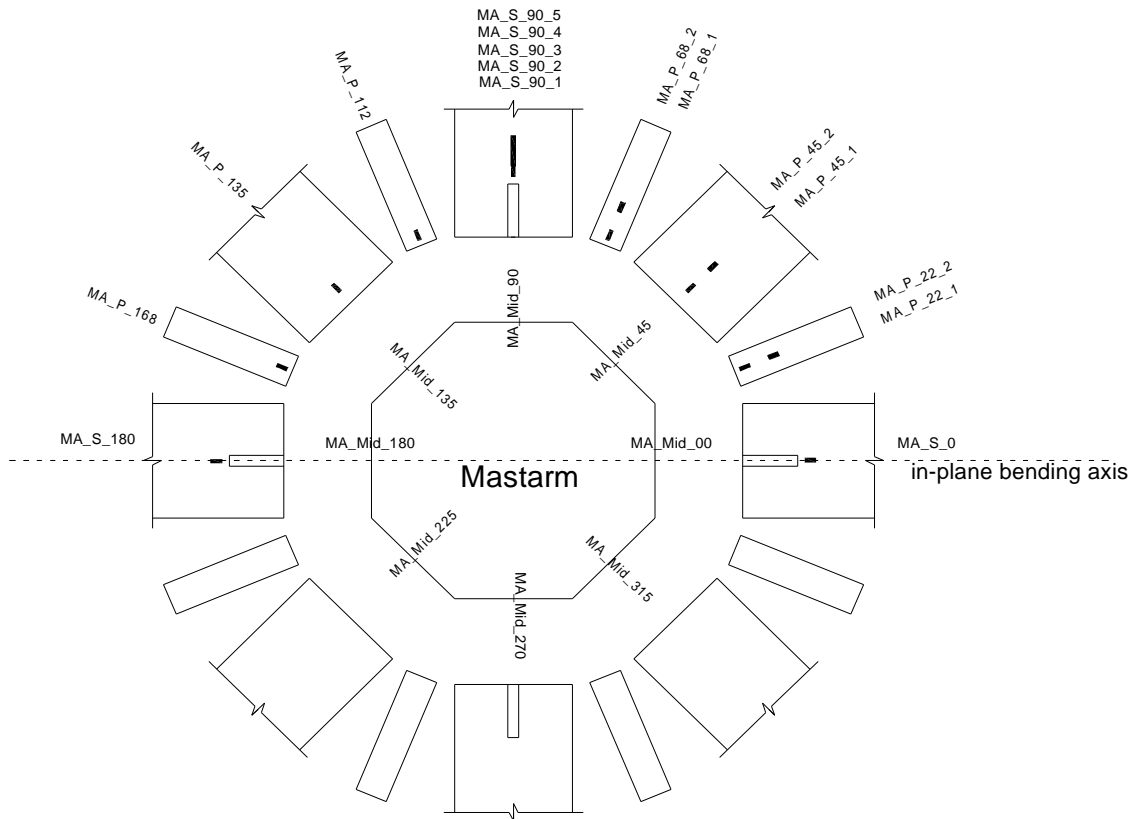


Figure 5.2 Mast arm strain gauge locations and labels.

5.1.2 Pole

The pole was instrumented with a similar philosophy as the mast arm. Eight 6.35 mm (0.25 inch), uniaxial strain gauges were placed at the midheight of the pole, 647.7 mm (25.5 inch) up from the top of the pole base plate. These gauges were meant to measure the nominal stresses in

the pole section. Unlike the mast arm, the pole section will be subjected not only to bending moments and shears, but axial loads and a torque depending on the loading, therefore more strain gauges were placed around a 270 degree arc around the pole perimeter, at the weld toe of the fillet-welded socket connection. Some locations used two strain gauges for stain extrapolation at the weld toe. The strain gauge locations on the pole are shown in Figure 5.3.

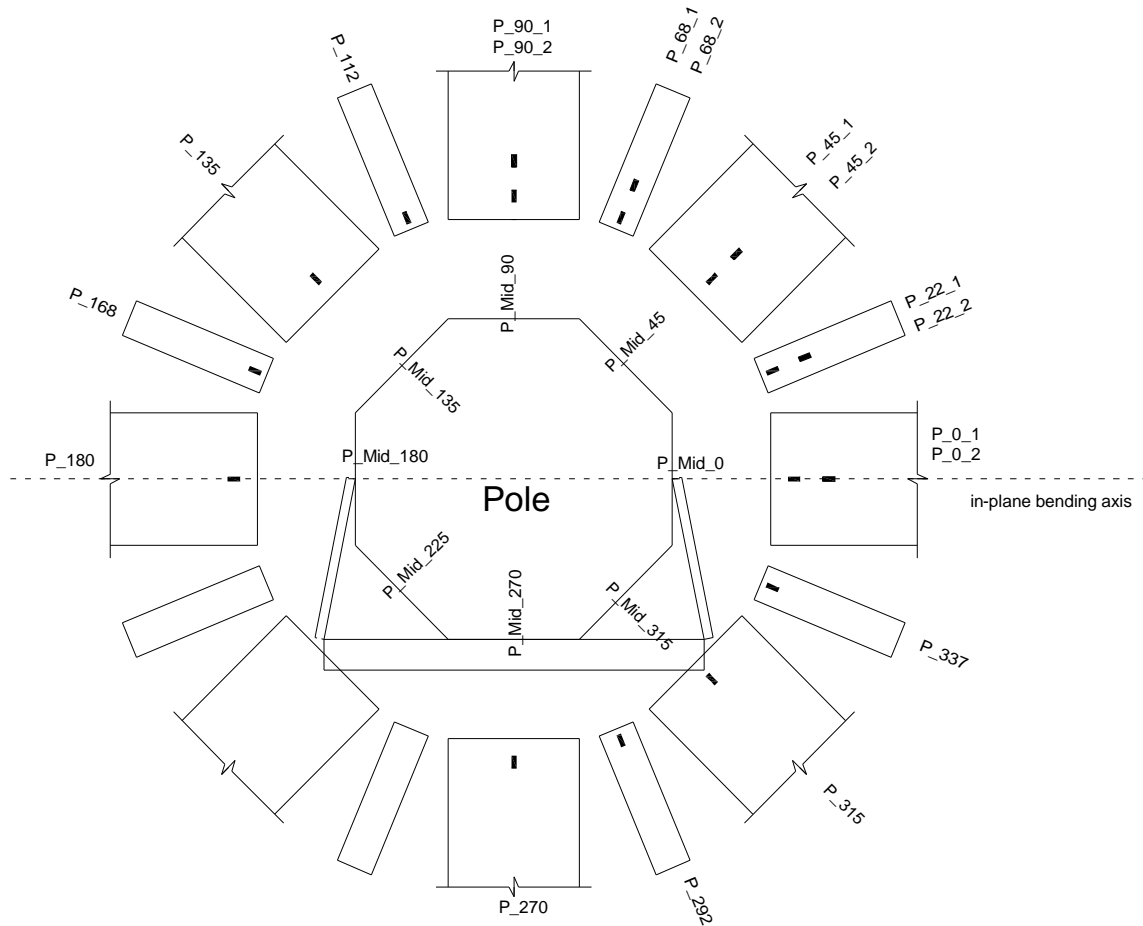


Figure 5.3 Pole strain gauge layout and labeling.

5.1.3 Box Connection

As the main focus of this research, the box connection was given a lot of attention in terms of strain gauges, in lieu of the box connection failure in Wyoming. Fatigue testing of box connections at the University of Wyoming found that cracking occurred at the corners of the box, and the instrumentation scheme targeted this. The box connection utilized by Mn/DOT is different than those tested in Wyoming because their designs use octagonal tubes, and this negates the use of top and bottom box connection plates because the flange plate can bear directly on a flat of the tube. This type of detailing makes it hard to determine the load path through the box connection because there is a direct load transfer mechanism between the flange plate and tube wall. To better understand the load being transferred through the side plates,

three, 6.35 mm (0.25 inch) uniaxial strain gauges were placed on the top, middle, and bottom of the two side plates, in between the flange plate and the pole. Since previous box connection failures formed cracks in the pole tube at the corner of the box, many more smaller gauges were used to understand the strain concentration at this point on the test specimen. On the East side of the box connection, two strain gauges were used for strain extrapolations at the top and bottom corners of the box connection, in two orthogonal directions. This is shown in Figure 5.4 that at each corner, two gauge clusters can extrapolate the horizontal and vertical strain at the corner of the box. The strain gauges were aligned longitudinally with the weld toe on the pole tube, offset 5 mm (0.20 inch) away from the weld toe. On the West side of the tube, strip gauges were used instead of two independent strain gauges. The first gauge in the strip was aligned as in the East side, with the first gauge centered 5 mm (0.20 inch) away from the weld toe on the tube.

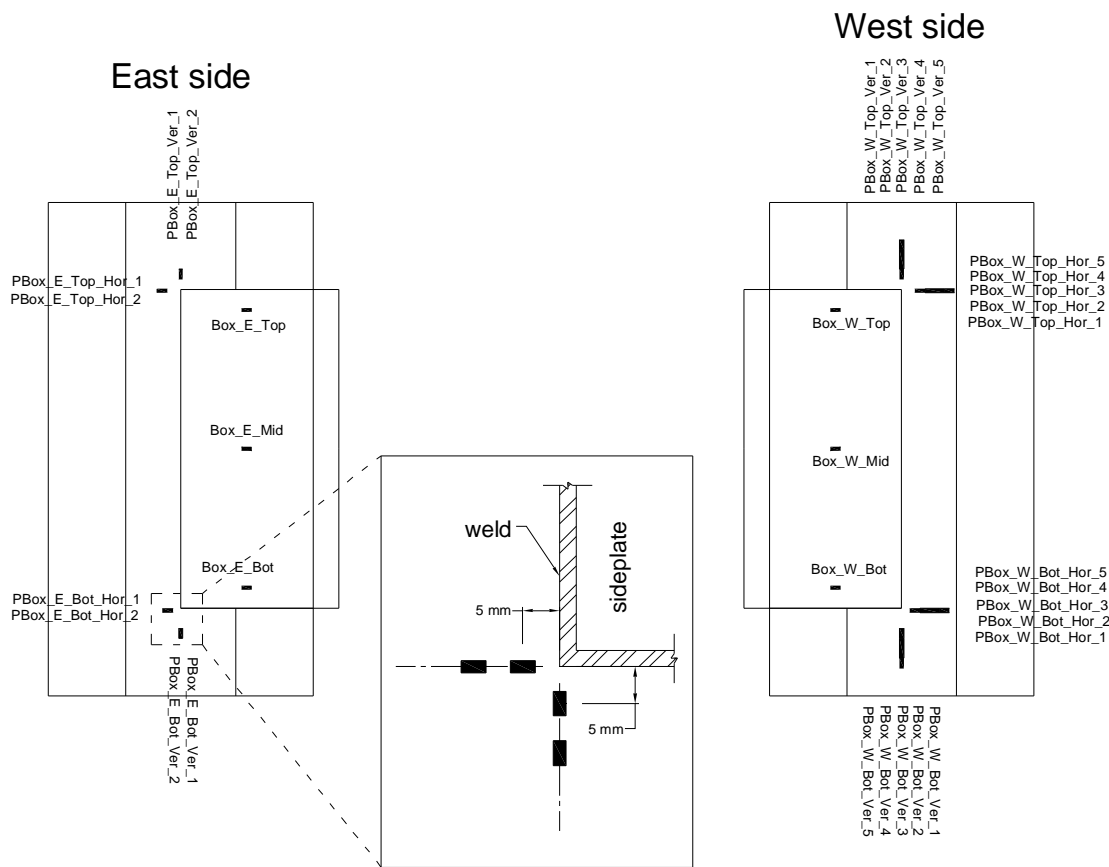


Figure 5.4 Box connection strain gauge layout and labels.

5.1.4 Pole Base Plate

The last set of instrumentation was placed on the base plate of the pole socket connection. Two, 3-element strain rosettes were placed on the base plate at the 0 and 90 degree positions. The rosettes were centered in-between the weld toe and the free edge of the plate. These rosettes would be able to capture the complete state of stress at these two points to better understand the base plate deformations.

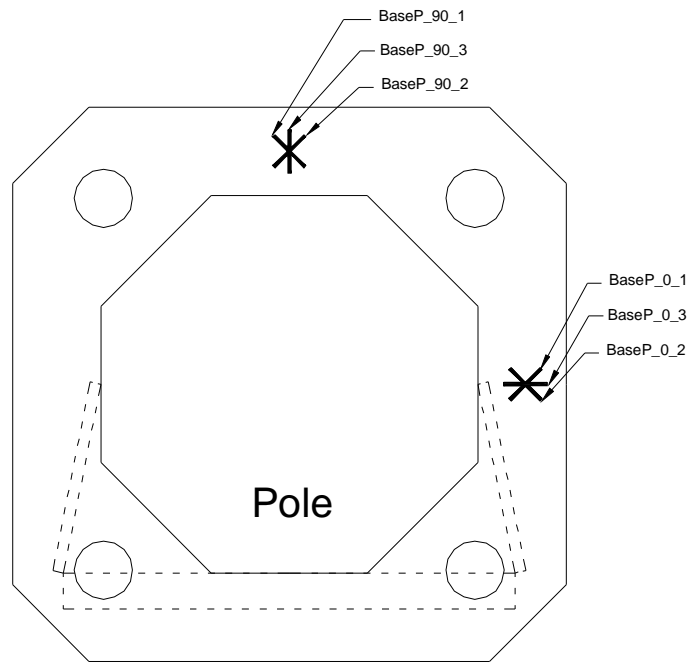


Figure 5.5 Pole base plate strain gauge layout and labels.

5.2 Type I Specimen Instrumentation (Frame 2)

Some of the socket connections tested in Frame 2 were instrumented to correlate back to measurements taken in Frame 1 and to gain additional information not attained in Frame 1. The Frame 2 instrumentation plan only addressed static tests to attain strain concentration factors. The Frame 2 instrumentation only placed one, 1 mm (0.04 inch) strain gauges, centered 5 mm (0.20 inch) above the socket weld toe, negating the use of extrapolation techniques. The gauges were placed in the middle of the tube flats and on the bent corners of the 180 degree arc of the socket connection subjected to tensile bending stresses. Two additional measurements were taken with this instrumentation scheme. First, strain gauges were placed on the inside of the tube, coincident with the strain gauges placed 5 mm (0.02 inch) above the weld toe on the outside of the tube. These gauges could then be used to decompose the strain through the thickness of the tube into membrane and bending components. Second, the specimen was rotated 180 degree so strains on the compression side of the pole could be attained, as the instrumentation in Frame 1 did not fully address this. The labeling system employed in this instrumentation scheme is shown in Figure 5.6 and will be referred to many times in other chapters.

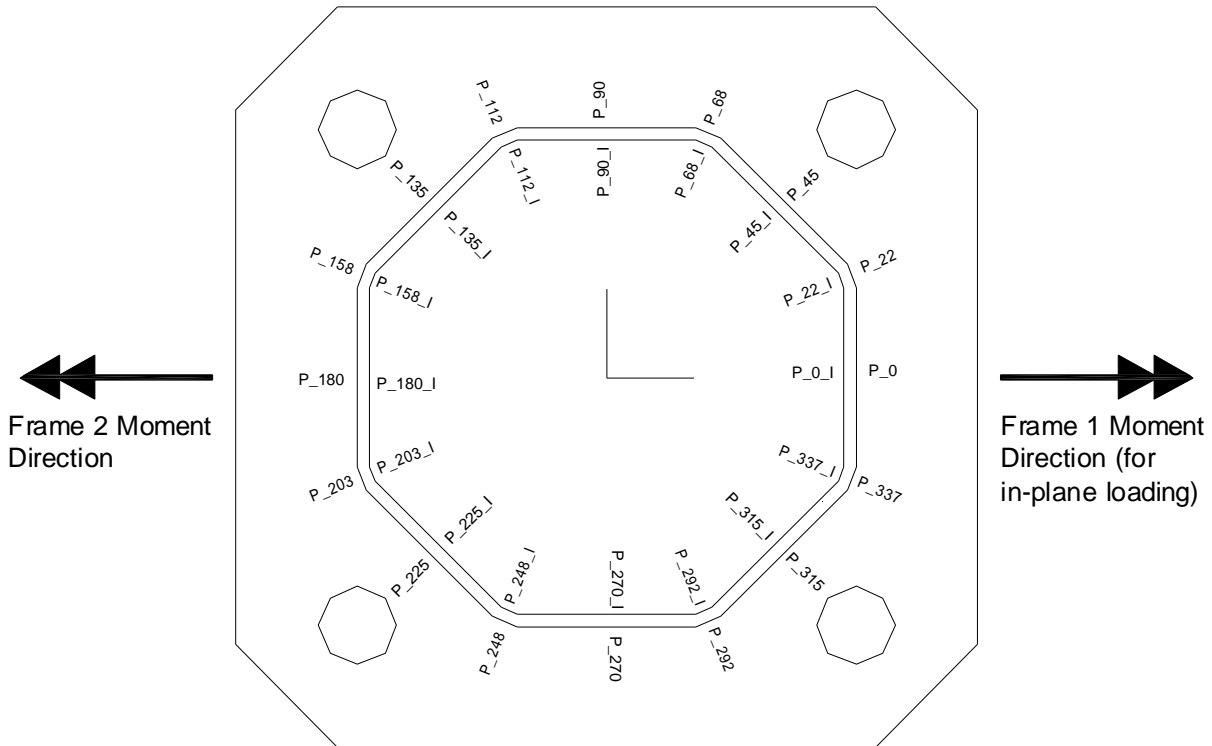


Figure 5.6 Frame 2 socket connection strain gauge labeling system.

5.3 Type I Specimen Instrumentation (Frame 3)

The mast arm using full-penetration welds were instrumented and statically tested in Frame 3 to attain the strain concentration factors for this particular detail. The gauges were placed in the 180 degree arc of the mast arm tube subjected to tensile stresses, and the same pattern of 1 mm (0.04 inch) gauges center 5 mm (0.20 inch) away from the weld toe was used. Strain gauges were not placed in the inside of the mast arm tube because the backing ring interfered with this gauge placement.

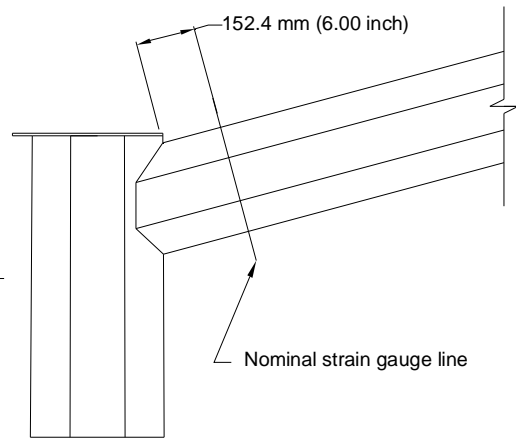
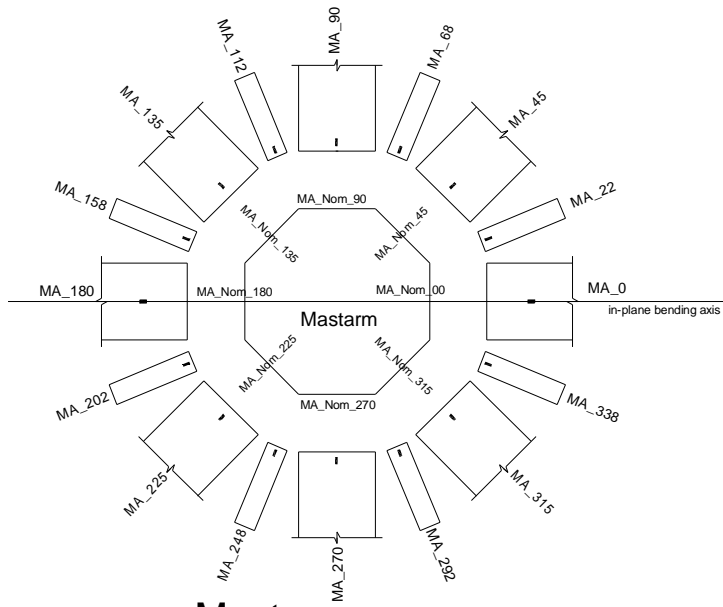
A gusset-stiffened mast arm specimen was also instrumented in Frame 3 and statically tested. This instrumentation was repeated since a gusset-stiffened mast arm was instrumented in Frame 1, however additional gauges were placed in the stiffener itself to ensure that the stiffeners were being activated.

5.4 Type II Specimen Instrumentation Plan

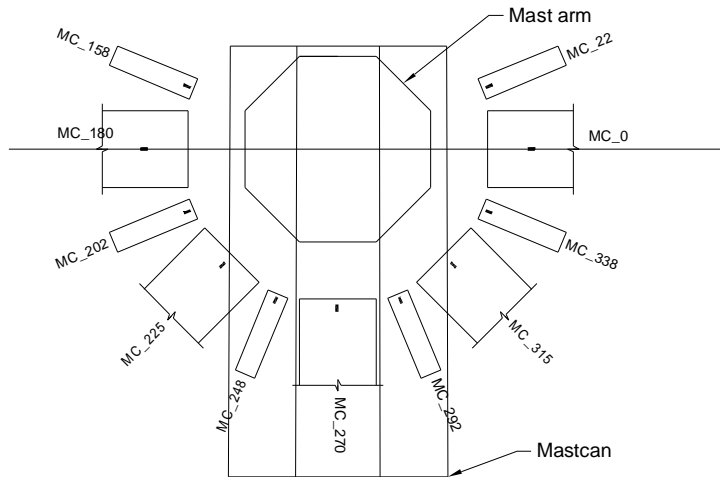
Like the Type I specimen instrumentation, the first Type II specimen consisting of a mast arm and pole was heavily instrumented and tested statically in the three primary load directions prior to fatigue testing. Recall, the focus of this type of specimen was the full-penetration weld between the mast arm and the mast can, as well as the full-penetration weld adjoining the pole tube to the tapered transformer base.

5.4.1 Mast Arm/Mast Can Detail

The Type II mast arm was instrumented in the same fashion as the Type I mast arm. One, FLA-1-11 strain gauge was placed at each bent corner and in the middle of each tube flat around the entire circumference of the mast arm tube. Each of these strain gauges was centered 5 mm (0.20 inch) away, on the mast arm tube, from the toe of the full-penetration weld attaching the mast arm to the mast can. Similarly, the same types of gauges were placed on the mast can at the same position. However, no gauges were placed on the mast can between the 45 and 135 degree positions because there physically was not enough room to glue on a gauge in those regions. At the same time, these positions would be highly influential to the presence of the cap welded atop the mast can, therefore the results would be variable from one specimen to the next. Only one strain gauge was used at each location to attain comparable results between all the gauges as to placing two strain gauges for extrapolation reasons at select points. Eight EA-06-250BG-120 strain gauges were placed in the middle of the tube flats, centered 152.4 mm (6.00 inch) away from the weld toe on the top tube flat. These gauges read the nominal strains in the tube. All these gauge layouts are shown pictorially in Figure 5.7 and the labeling convention follows the format outlined in Table 5.1. To further complicate the instrumentation of the Type II specimen, the mast arm tube is a smaller diameter than the mast can in addition to the two intersecting at a 15 degree angle. Therefore, as one travels around the circumference of the mast arm tube, the weld line is not always perpendicular to the longitudinal axis of the mast arm. Since cracks usually initiate and grow along weld toes because of residual stresses, it is prudent to measure strains that are perpendicular to the weld toe. In doing so, many of the strain gauges are placed at angles not coincident with the longitudinal axis of the mast arm tube as shown in Figure 5.8.



Mast arm gauges



Mastcan gauges

as observer is looking down longitudinal axis of mast arm

Figure 5.7 Type II mast arm strain gauge layout.

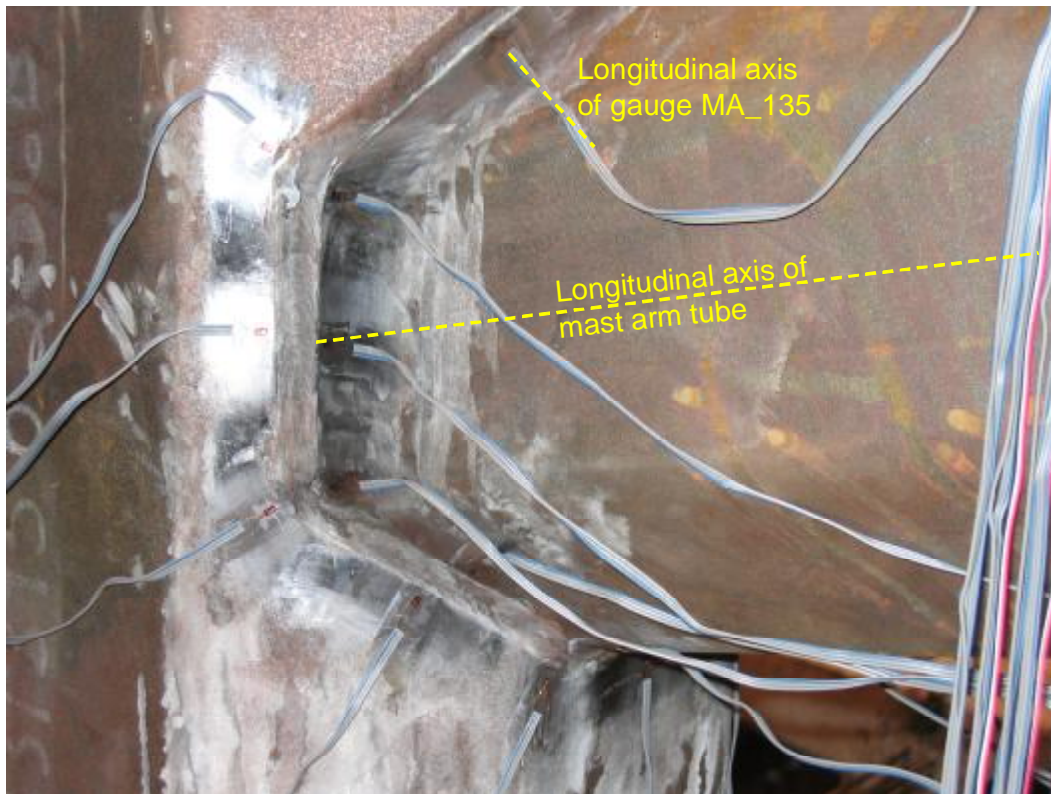


Figure 5.8 View of Type II mast arm showing how strain gauges are orientated perpendicular to weld toe.

5.4.2 Pole

The pole that was mated with the first instrumented mast can only instrumented the pole-side, full-penetration weld toe between the pole tube and the integrated tapered transformer base. Nine FLA-1-11 strain gauges were glued on the pole tube, 5 mm (0.20 inch) above the weld toe at the positions shown in Figure 5.9. These gauges were used to measure the stress concentration at the weld toe of the full-penetration weld adjoining the pole tube to the tapered transformer base. No efforts were made to instrument near the access hole near the base of the pole.

However, when the pole finally developed fatigue cracks, it was at the access hole detail in the base and not in the butt-weld between the pole tube and transformer base. Therefore, after Frame 1 had been modified to individually cycle the Type II pole specimens (this frame is shown in Figure 4.12) the last pole specimen was heavily instrumented to better understand the load path through the transformer base with the presence of an access hole. This pole was tested in two different directions, varying the location of the access hole for each test. Because the base

plate in the pole only uses a 4-bolt anchor rod pattern, there were really only two unique positions for the access hole to be tested in, the first had the access hole at roughly the bending neutral axis and the second placed it at the extreme bending fiber. The strain gauges applied to the last pole specimen are shown in Figure 5.10 and this figure will be referred to in the following descriptions. First there were two lines of EA-06-250BG-120 strain gauges applied to the pole in the middle of the tube flat, and each line was on orthogonal tube flats. The purpose of these gauges was to verify the nominal stresses in the pole according to simple bending theory. The next line of gauges is on Section B-B which again, used EA-06-250BG-120 strain gauges glued to the middle of tube flats on the transformer base, on a 180 degree region of the perimeter over the access hole, which were also meant to verify the nominal stresses in the transformer base. At Section A-A, the middle of every tube flat and bent corner were instrumented with a FLA-3-11 strain gauge. This line of gauges was meant to capture the how the stresses change because of the access hole, as this gauge line was placed at the mid-height of the access hole. Not shown in Figure 5.10 were two additional FLA-1-11 gauges that were placed at the two bottom corners of the access hole. These two gauges were meant to directly measure the hot spot strain at the corner of the hole were this detail ultimately cracked. A picture of one of these gauges is shown in Figure 5.11.

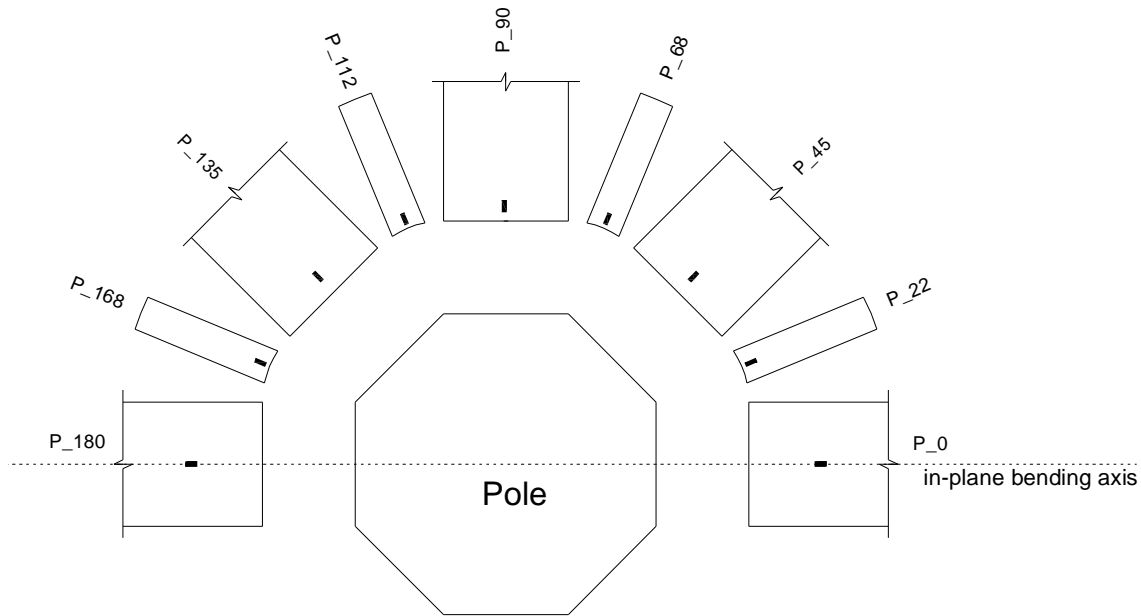


Figure 5.9 Type II pole instrumentation

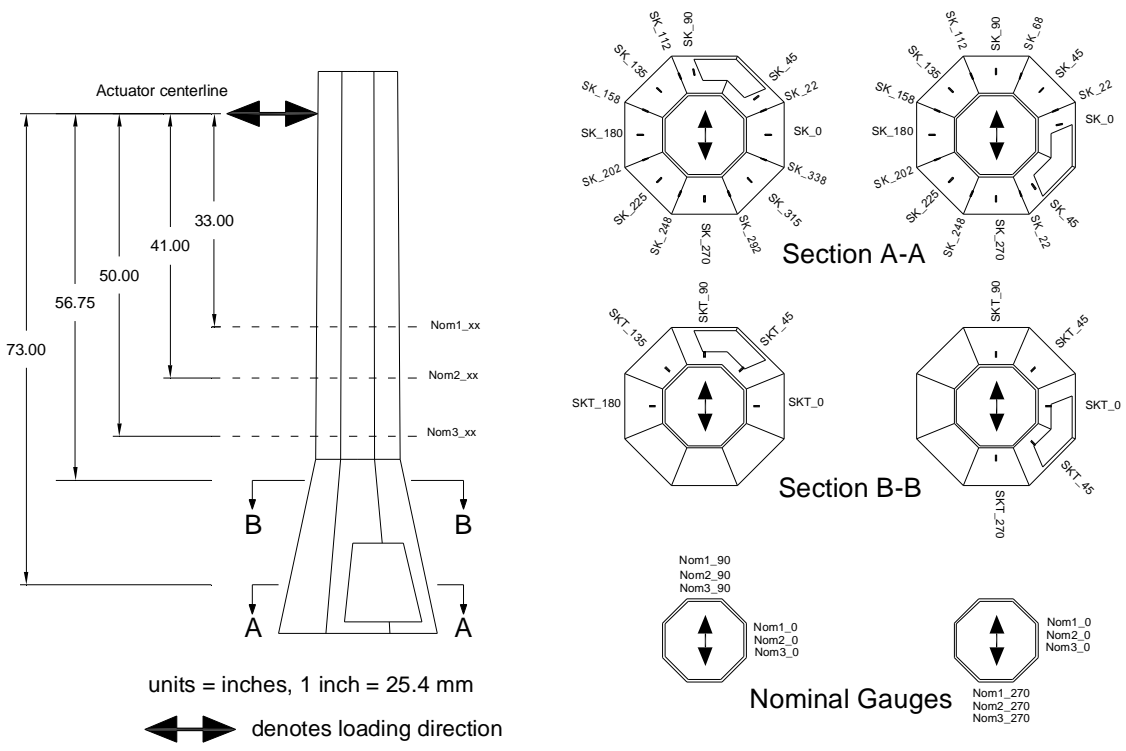


Figure 5.10 Access hole instrumentation of Type II pole.



Figure 5.11 Strain gauges placed at bottom of access hole.

Chapter 6

Static Test Results

The first specimens of each specimen type were heavily instrumented with strain gauges to develop a full understanding of load paths through the system of a mast arm connected to a pole. This was done because all eight specimens of each type were essentially the same and a complete understanding of one, gave an understanding of the rest of the specimens, and relatively few strain gauges needed to be used on the remaining seven specimens. This instrumentation also gave relevant information regarding strain concentration factors (SCF) at different locations on the poles and mast arms. Typically, high strain concentrations lead to the development of fatigue cracks under cyclic loading conditions. The remainder of this chapter outlines the result of static testing conducted on select specimens from the testing matrix.

6.1 Type I Specimen (Frame 1)

This section describes the results of three static tests conducted on a Type I pole with a mast arm bolted to it. The mast arm utilized a socket weld connection, but was stiffened with gusset plates. Three static tests were conducted, two in the primary load directions, in-plane (mast arm motion perpendicular to the road) and out-of-plane (mast arm motion parallel to the road). The third test will be referred to as the 45 degree case which is mast arm motions at a 45 degree angle to the road, halfway in-between in and out-of-plane motion.

For the case of in-plane loading, the actuator was set in a position to apply loads to the mast arm in the vertical plane. First a dead load of 40.0 kN (9 kip) was placed on the mast arm, then five cycles of approximately ± 13.3 kN (3 kip) were conducted while recording data from all the strain gauges. All the results presented below represent the average at the five peak loads. This was done for two reasons;

The actuator was run in displacement control, so each peak load did not hit the exact same values for each cycle.
Averaging would also wash out the hysteresis effects in the strain gauges.

For the out-of-plane case, the actuator was set in the horizontal plane while dead load was applied to the mast arm via a threaded rod in the vertical plane. The threaded rod was first stressed to a load of 32.5 kN (7.3 kip) to represent a dead load. After the dead load was applied, five cycles of ± 8.9 kN (2 kip) were cycled in the horizontal plane (out-of-plane direction). As with the in-plane loading case, the data presented in this section represents the average at the five load peaks in the out-of-plane direction, which in this case was 32.0 kN (7.2 kip) in-plane and 8.6 kN (1.9 kip) out-of-plane.

6.1.1 Midpoint Strain Gauges (Nominal Strains)

The first results to be presented are the nominal strains at the midpoints of the mast arm and pole. These strain gauges should yield measurements close to those predicted through elastic theory because away from boundaries and concentrated loads, plane sections should remain plane and normal. Shown in Table 6.1 are side-by-side comparisons of the measured and

predicted nominal strain values for the three loading cases. Presented along with the strains is the strain concentration factor (SCF), which is the ratio of the measured strain divided by the predicted strain. Ideally, the SCF should be 1.0 representing perfect agreement of measured strains to what is anticipated. The majority of the SCFs in Table 6.1 fall around the regime of 1.0, however there were some anomalies of SCFs much greater or less than 1.0, but these occur in areas where little strain is expected. This decreases the numerical stability in the SCF calculation because the measured strain is being divided by a smaller number. Since the majority of the SCFs were ~1.0, it was felt that the loads were flowing through the specimen as anticipated.

Table 6.1 Comparisons of Experimental to Predicted Nominal Strains at Mast Arm and Pole Midpoints for the Three Loading Cases.

Gauge Location	In-Plane Loading			Out-of-Plane Loading			45 Degree Loading		
	Predicted Strain ($\mu\epsilon$)	Measured Strain ($\mu\epsilon$)	SCF	Predicted Strain ($\mu\epsilon$)	Measured Strain ($\mu\epsilon$)	SCF	Predicted Strain ($\mu\epsilon$)	Measured Strain ($\mu\epsilon$)	SCF
MA_Mid_0	0.0	-4.3	-	57.7	58.0	1.01	60.6	53.3	0.88
MA_Mid_45	250.6	223.6	0.89	188.9	194.0	1.03	90.4	79.9	0.88
MA_Mid_90	354.4	328.6	0.93	207.2	216.3	1.04	67.3	61.8	0.92
MA_Mid_135	250.6	229.2	0.91	112.2	112.0	1.00	4.7	2.7	0.58
MA_Mid_180	0.0	2.9	-	-50.3	-58.0	1.15	-60.6	-49.9	0.82
MA_Mid_225	-250.6	-239.3	0.95	-178.7	-194.0	1.09	-90.4	-79.5	0.88
MA_Mid_270	-354.4	-341.0	0.96	-205.5	-216.3	1.05	-67.3	-52.1	0.77
MA_Mid_315	-250.6	-232.7	0.93	-110.2	-112.0	1.02	-4.7	0.50	-0.11
P_Mid_0	-13.1	-31.1	2.37	40.4	32.5	0.80	47.9	46.6	0.97
P_Mid_45	336.6	370.7	1.10	269.9	262.7	0.97	108.4	107.4	0.99
P_Mid_90	510.0	537.1	1.05	310.4	327.9	1.06	102.0	109.6	1.07
P_Mid_135	351.0	370.7	1.06	176.9	189.9	1.07	32.3	18.6	0.58
P_Mid_180	4.7	-31.1	-6.62	-44.6	-70.5	1.58	-59.8	-44.0	0.74
P_Mid_225	-410.4	-433.0	1.06	-281.8	-300.7	1.07	-120.3	-97.3	0.81
P_Mid_270	-575.6	-599.4	1.04	-354.9	-365.9	1.03	-113.8	-104.6	0.92
P_Mid_315	-403.0	-433.0	1.07	-237.2	-227.9	0.96	-44.1	-44.0	1.00

6.1.2 Mast Arm Socket Connection (Frame 1)

When stress flows down the mast arm tube and into the base plate, there is a global change in geometry and stress must alter its path in order to flow through the base plate and into the bolts. It is anticipated because of this phenomena, that stress will concentrate in certain areas on the weld toe where the tube intersects the base plate. Shown in Figure 6.1 is the SCF of the strains,

at discrete points around the tube circumference, in the tube wall at the intersection of the base plate. Since two strain gauges were used at each location, the measured strains used in the SCF calculation were found using CIDECT (35) extrapolation procedures. In some cases, zero strain is predicted (e.g., at the neutral axis for in-plane loading) and the SCF cannot be defined because of a divide by zero discontinuity and is instead reported as zero. The three plots shown in Figure 6.1 do not show drastic changes in the SCF, and at the heaviest loaded portions of the tube vary between 1.5 and 3.5. It should be noted at the 90 degree location, the strain gauges were placed at the tip of the gusset plate stiffener, not at the toe of the tube/base plate weld. Though not apparent at this point, the next section will discuss the same type of plot, but for the pole socket connection, and the definition of “relative” will become more important.

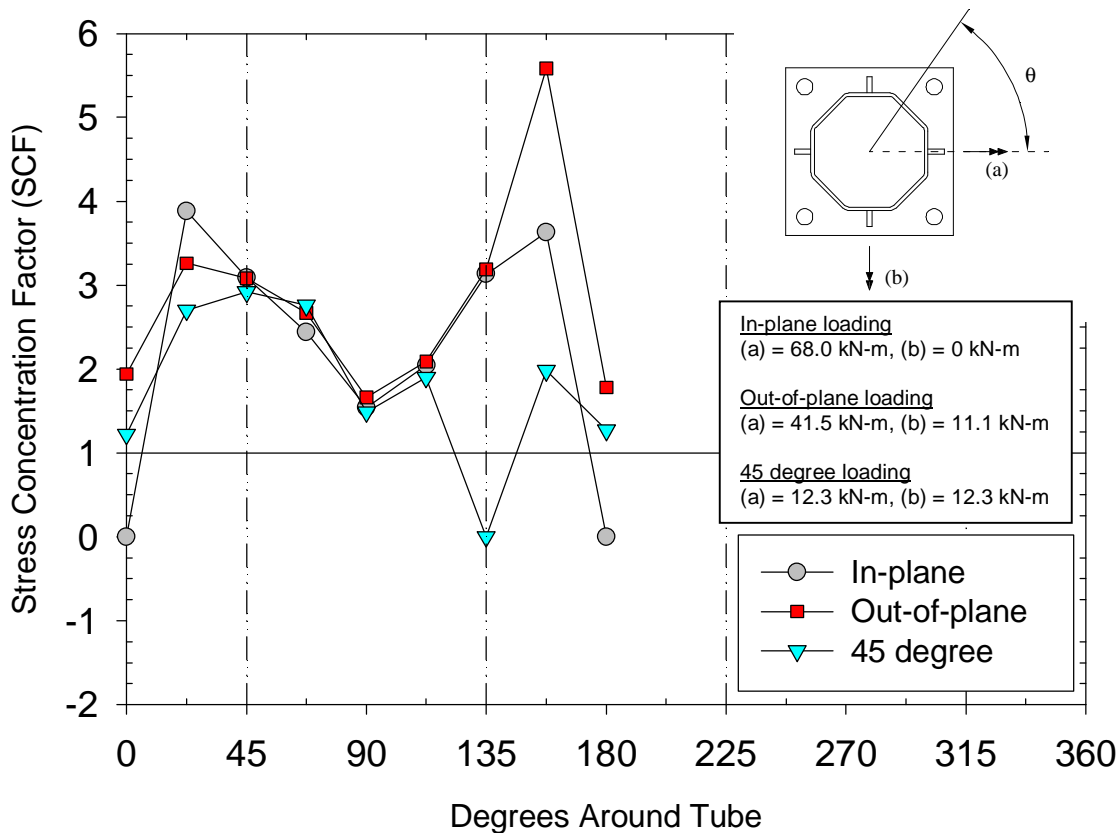


Figure 6.1 SCFs of gusset-stiffened mast arm socket connection under three different loadings.

6.1.3 Pole Socket Connection (Frame 1)

As with the mast arm socket connection, a strain concentration factor is expected at the tube/base plate weld on the pole socket connection. The SCFs are plotted at discrete points on the pole tube circumference in Figure 6.2. In locations where two strain gauges were used, the measured strain used in all calculations was attained through extrapolation. Notice how the SCFs vary much more in the pole socket than in the mast arm socket.

The area of interest of the pole socket occurs in the upper hemisphere of the tube, or 0 to 180 degrees. Particularly for in-plane loading, this hemisphere is always in tension, but note that all three of the loadings plot similarly in this region as shown in Figure 6.2. Looking at the plot for in-plane loadings, notice how the top tube flat (between 67.5 and 112.5 degrees) is the extreme tension bending fiber according to simple mechanics of material assumptions. However, at the 90 degree location, the SCF is less than 1.0 meaning this location is transferring less strain than anticipated. Also, the two points at the end of this tube flat (67.5 and 112.5 degrees) have the highest SCF. Coupling both of these facts together it becomes apparent there is a shear lag effect in the longitudinal strain as it flows down the tube and into the base plate, thus forcing more stress to be transferred through the corners of the tube. An example of what the stresses may look like at the weld toe are shown in Figure 6.3 demonstrating what is meant by the shear lag effect. The shear lag effect can be attributed to base plate flexibility. Since all load eventually has to get to the bolt holes, the stress in the tube flat in extreme bending wants to pry the base plate away from the transformer base, and the compliance of the base plate cause the stress to redistribute in the tube (shear lag). In theory, an infinitely rigid base plate should give uniform stress concentration factors around the tube circumference.

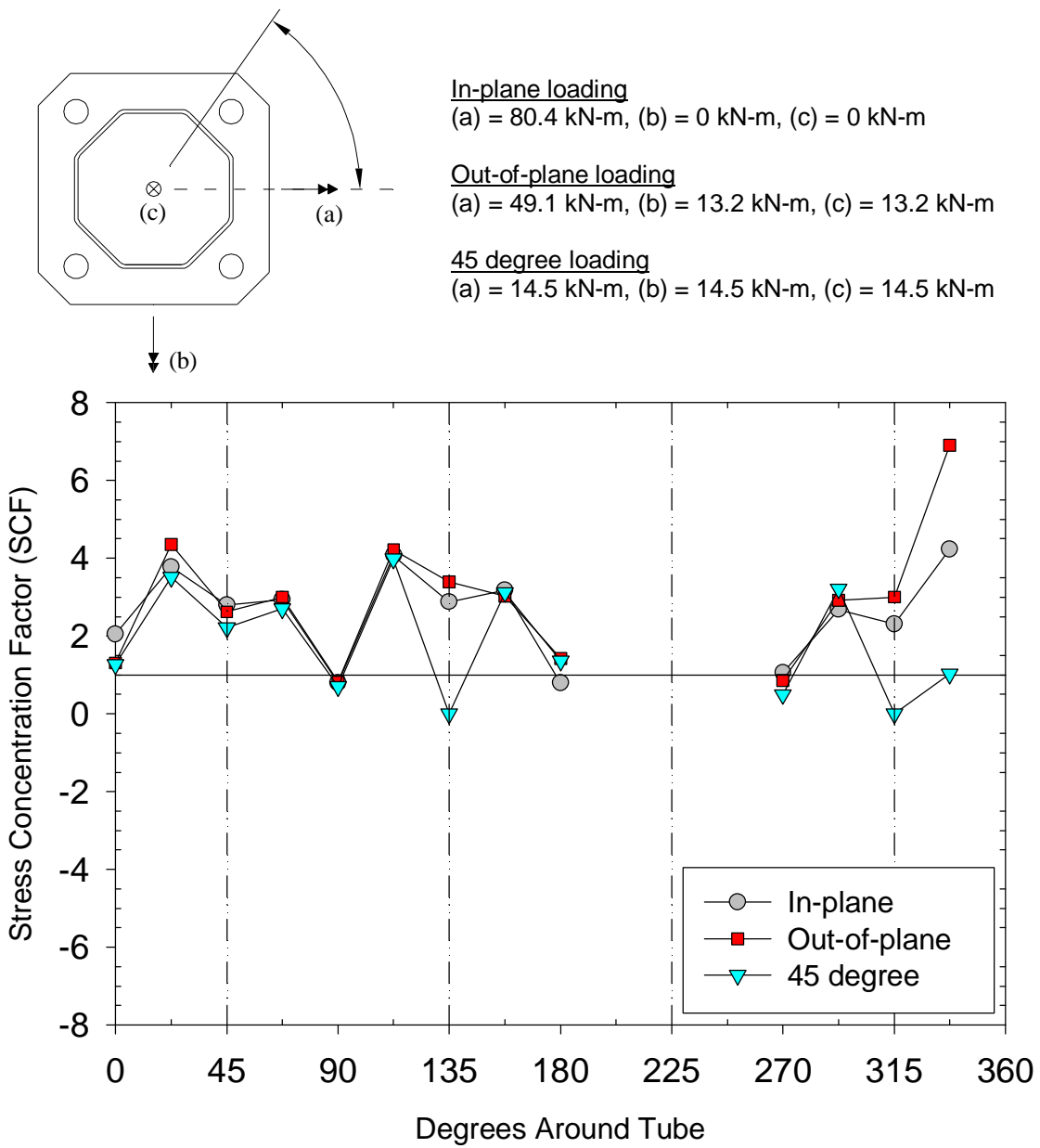


Figure 6.2 SCFs of pole socket connection under three different loadings.

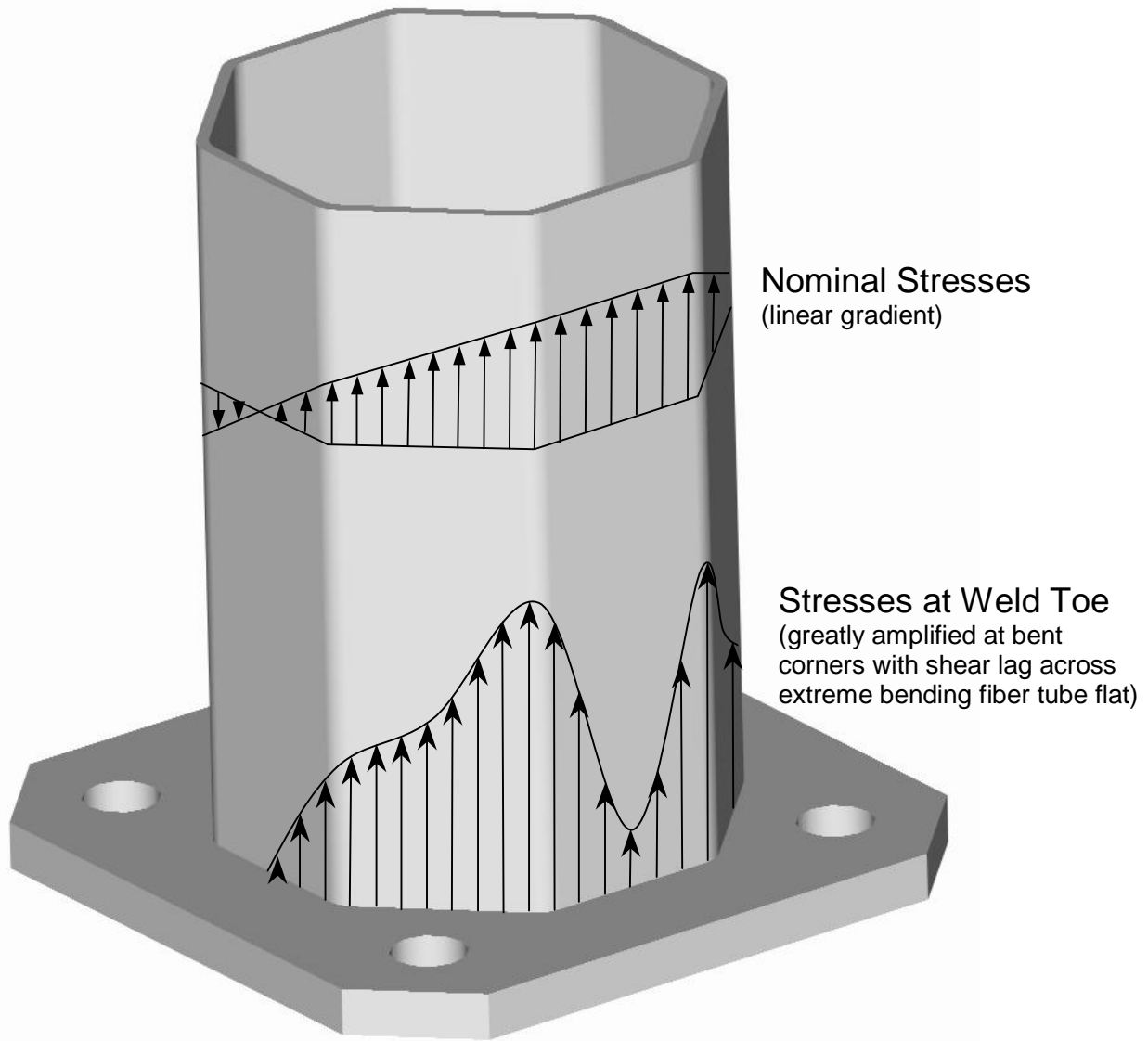


Figure 6.3 Pictorial example of strain profile at socket connection showing shear lag effect.

6.1.4 Box Connection (Frame 1)

Figure 6.4 shows strain profile plots from the six strain gauges affixed to the side plates of the box connection, for in-plane and out-of-plane loading. The 45 degree case was not plotted because it is a superposition of in-plane and out-of-plane loading. However, in the static case, out-of-plane load is too a superposition of in- and out-of-plane loading as both loads are statically present, just at different peak values of load. These plots become critical in deducing the load transfer through the box connection. If the strain in the side plates was considered uniform through the thickness, then the strain diagrams can be integrated and further manipulation can calculate the moment transfer of the side plates alone. Using this assumption, the side plates only transfer 6.2% of the moment for in-plane loading, meaning the bearing

between the flange plate and the pole tube transfers the majority of the moment through the connection. For out-of-plane loading, the side plates are calculated to transfer 154% of the applied moment. Since this cannot happen, the constant strain assumption through the thickness of the side plate must be wrong and the side plates must have a bending component through their thick for out-of-plane loading. However, the strain assumption at least shows how little side plate participation is for in-plane moment transfer, and how nearly fully engaged it is for out-of-plane moment transfer.

For in-plane loading, the strain diagram would be assumed to be linear through the depth of the side plate. However, the three discrete measurement points would more likely fall on a higher order cubic function. The highest strains in the side plates for in-plane loading correlate to the east-top and bottom-west of the box connection showing the bolts at these location are transferring the majority of the moment. This may prove there is an uneven bearing condition between the mast arm and flange plate of the box connection.

For out-of-plane loading, a constant strain diagram through the side plate depth was expected. However, it too seems to follow a higher order polynomial function. It also shows a shear lag effect through the depth of the side plates as the middle portion is not as heavily strained as the top and bottom where the bolts are located.

6.1.5 Pole Wall

Figure 6.5 shows the strains measured in the pole tube, at the corners of the box connection. Multiple strain gauges were used at these locations and the strains reported were derived from extrapolation techniques. It becomes hard to derive conclusions from these measured strain values because there is no way to make simple assumptions to calculate what the strain should be at these locations. The one trend that can be seen is the highest measured strains are always the horizontal component of strain at each side plate corner. The “NF” shown in the figure refers to a strip gauge that was not functioning because of large hysteresis in the measurements indicating a poorly adhered gauge.

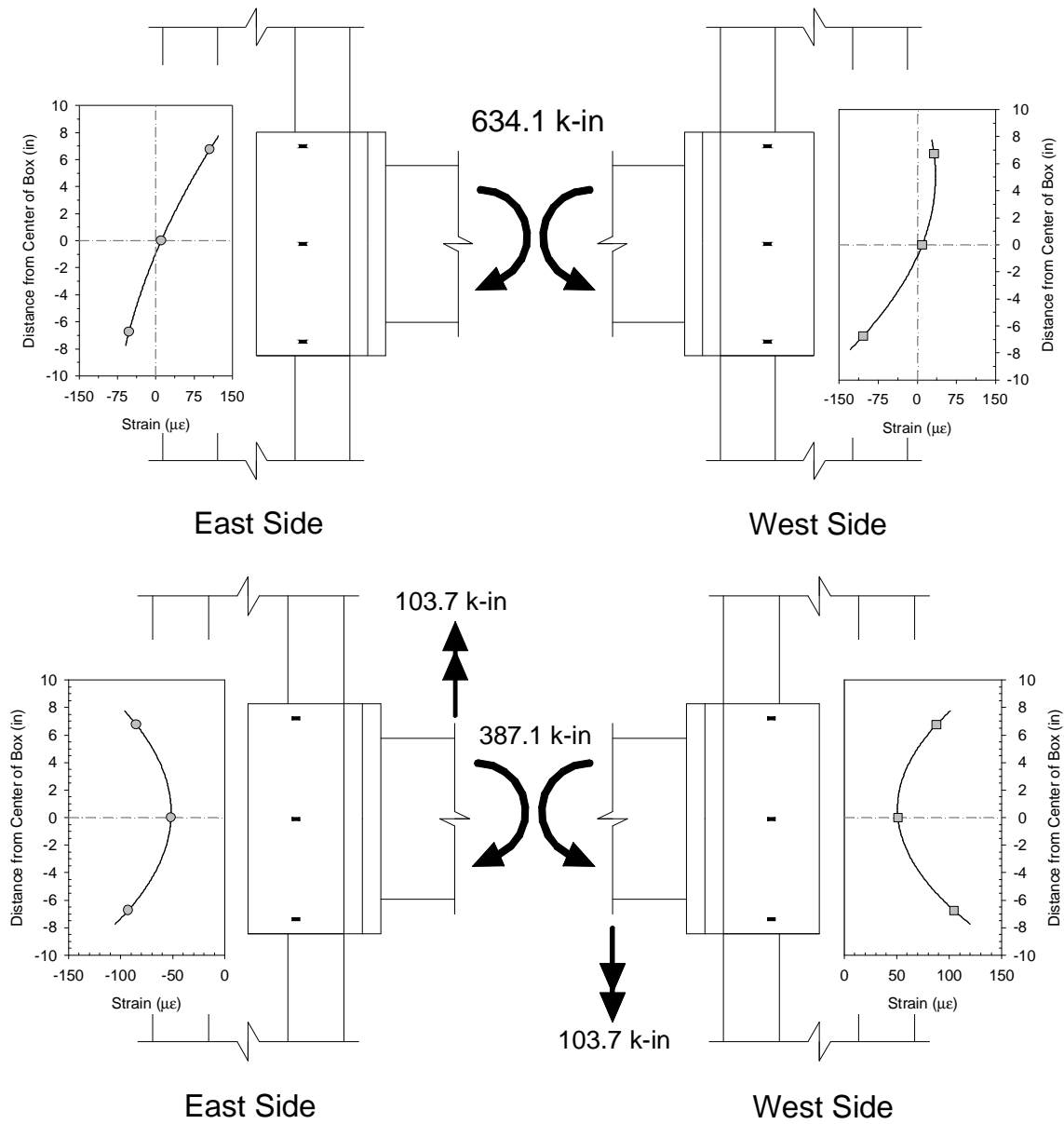


Figure 6.4 Strains in box connection side plates. Top: In-plane loading. Bottom: Out-of-plane loading.

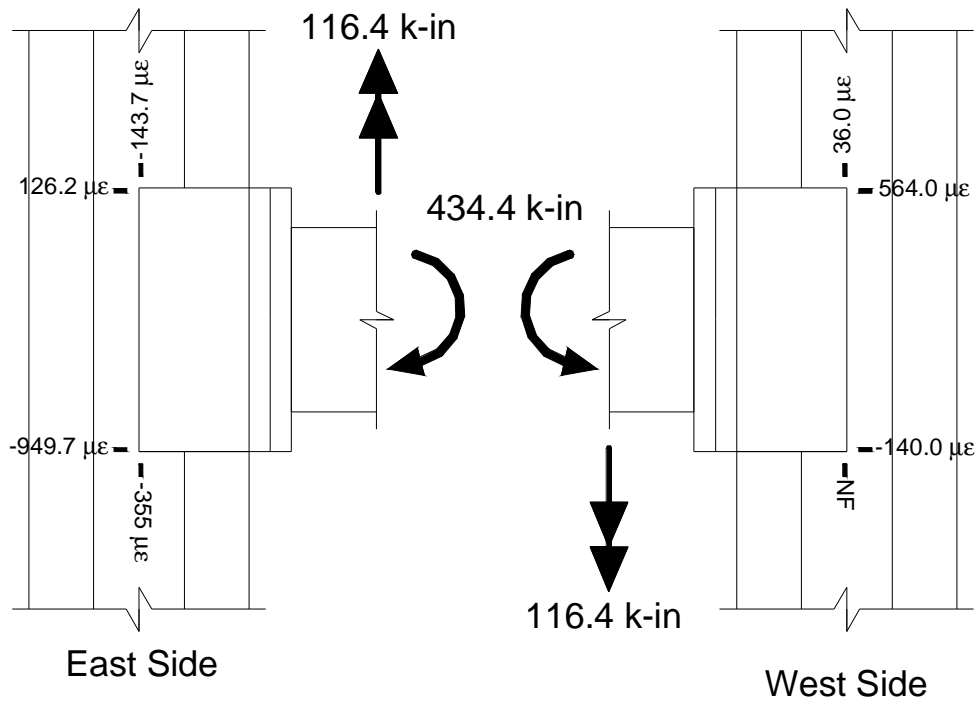
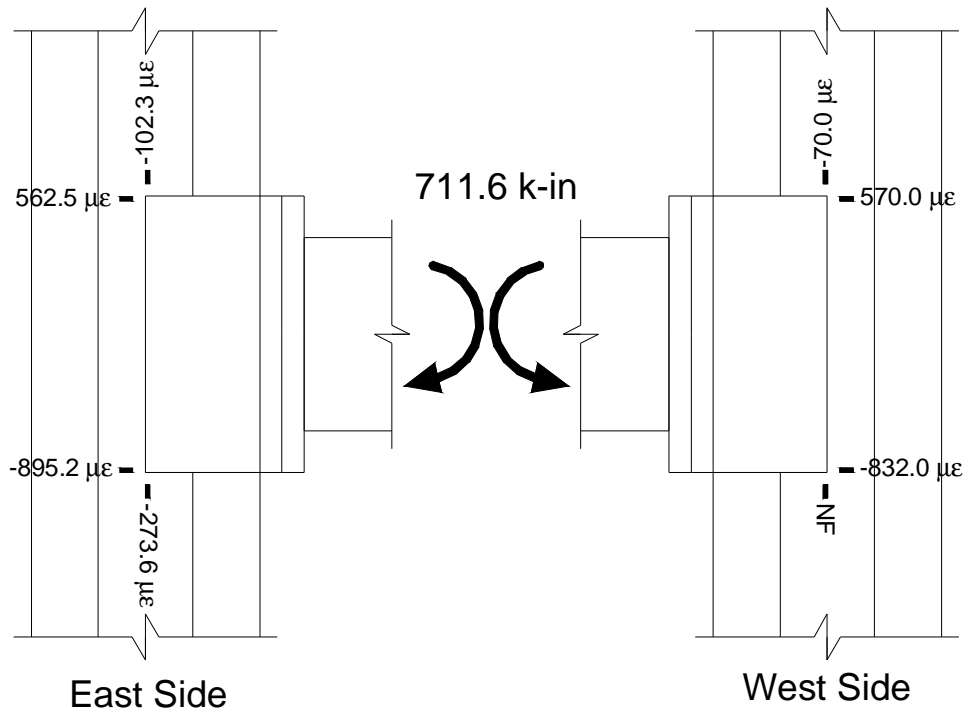
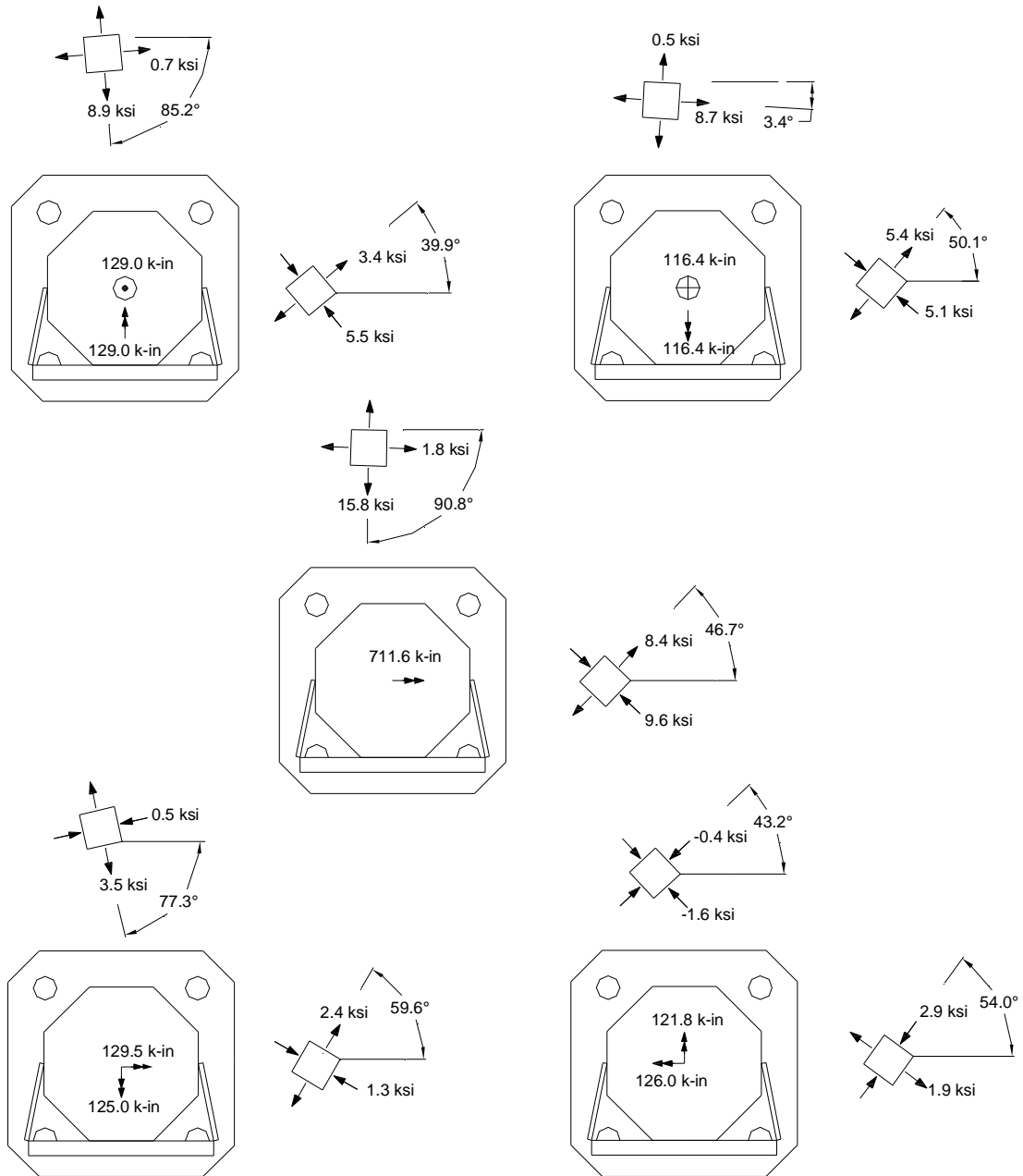


Figure 6.5 Strains in pole wall at the pole/side plate intersection. Top: In-plane loading. Bottom: Out-of-plane loading.

6.1.6 Pole Base Plate Rosettes

Figure 6.6 show the results from the two rosettes that were glued to the base plate of the pole socket connection. The results are presented in terms of rotated elements showing the principle stresses at the two points where the rosettes were placed.



$$1 \text{ kip-in} = 0.11298 \text{ kN-m}$$

Figure 6.6 Principle strains from base plate rosettes. Top: Out-of-plane loading. Middle: In-plane loading. Bottom: 45 degree loading.

6.2 Thick Base Plate Socket Connection (Frame 2)

Three Type I pole specimens were further instrumented and monotonically tested in Frame 2. Two poles had a wall thickness of 7.9 mm (0.3125 inch), but one had a 31.75 mm (1.25 inch) thick base plate, while the other had a thicker 63.5 mm (2.5 inch) base plate. The third pole had a thinner 4.8 mm (0.1875 inch) thick pole wall with a 63.5 mm (2.5 inch) base plate. Strain gauges were placed on the tube wall just above the socket weld toe, similarly to those in Frame 1 except; 1) Only one strain gauge was used at each location placed 5 mm (0.20 inch) from the weld toe. 2) Strain gauges on the outside of the tube were mirrored with a second strain gauge on the inside of the tube to capture through-thickness bending effects.

Figure 6.7 shows a plot of the SCFs around the circumference of the two pole socket connections with 7.9 mm (0.3125 inch) thick tube walls. The solid line with squares should plot similarly to the in-plane result shown in Figure 6.2, since the geometry and loading are the same. Two facts are apparent from analysis of Figure 6.7. One, the strains on the inside of the pole tube have negative SCFs, meaning the measured strain is opposite of what is anticipated. Therefore, the pole wall has a bending component through its thickness. Two, as the base plate gets thicker, the SCFs tend to converge upon 1.0, and the shear lag effect at the 90 degree point is reduced.

Figure 6.8 shows a plot of the SCFs for two socket connections with 63.5 mm (2.5 inch) thick base plates, but two different wall thicknesses. Notice that the SCFs on the outside of the tube change very little with a thinner tube wall, which should indicate tube thickness does not influence this parameter much. However, there is an appreciable change in the SCFs on the inside of the tube between the two tube thicknesses. Specifically, for the thinner wall thickness, the SCFs move into the positive regime, proving that the thinner tubes are not as susceptible to through-thickness bending components and instead are dominated by membrane action predicted by mechanics of material equations.

As an alternative to presenting SCFs, Figure 6.9 shows the strain diagrams for these three instrumented pole socket connections. The strains shown are the average between measurements taken at each bent corner nearest the extreme fibers on the inside and outside of the pole tube. A linear strain diagram through the tube thickness was assumed and was decomposed into membrane and bending components, which are also plotted. Since all three specimens demonstrated linear behavior, all strains were scaled from the static results such that all three sockets have the same predicted strains. The middle and right parts of Figure 6.9 are for the same diameter and thickness pole tube, but different base plate thicknesses. The trend seen between these two parts of the figure are a more pronounced through-thickness bending component in the socket with the thinner base plate and a higher membrane strain resultant with the thicker base plate. The left and middle parts of Figure 6.9 are for sockets with equal diameter pole tubes and base plate thicknesses, but different pole wall thicknesses. The figure shows that as the pole wall thickness decreases, the membrane resultant continues to increase forcing the bending resultant to decrease. Therefore, the compliance of the four-bolt base plate can directly affect the strain concentration factor in socket connections, and decreasing pole wall thickness and increasing base plate thickness causes strains to converge upon design assumptions of pure membrane behavior.

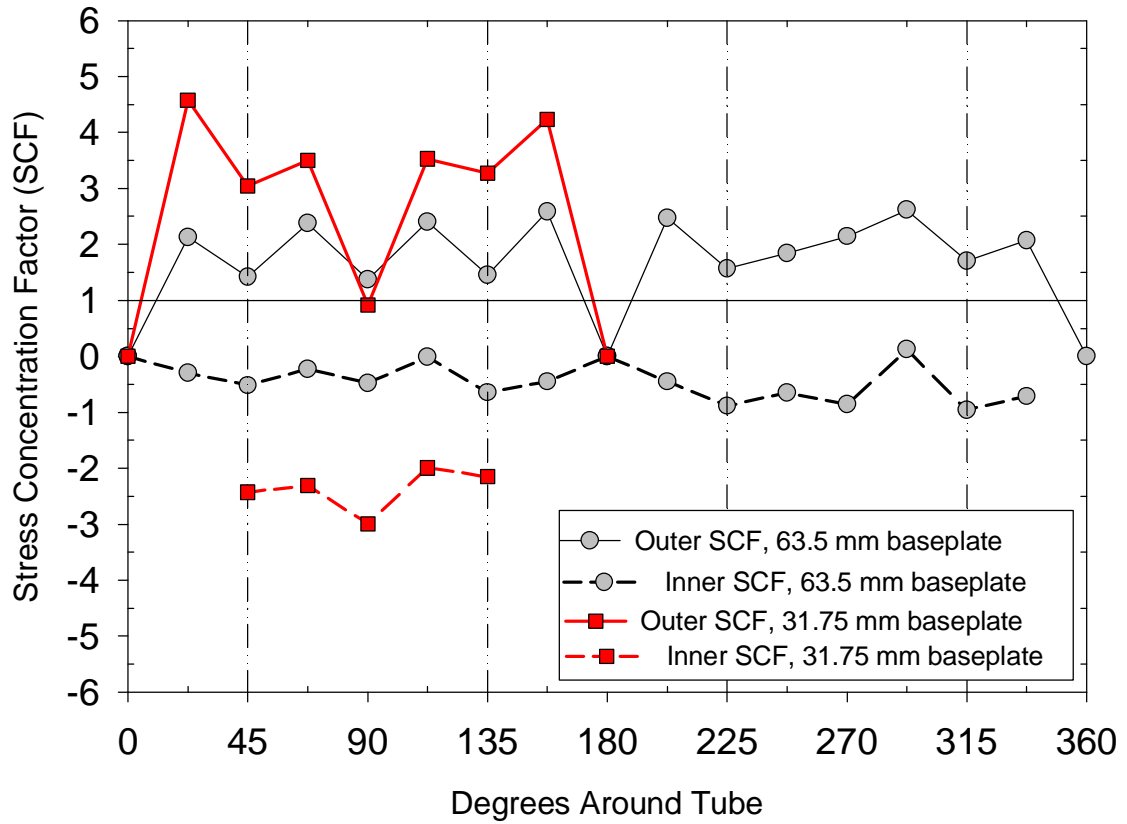


Figure 6.7 SCFs from two different base plate thickness socket connections tested, each tube having 7.9mm (0.3125 inch) thick tubes.

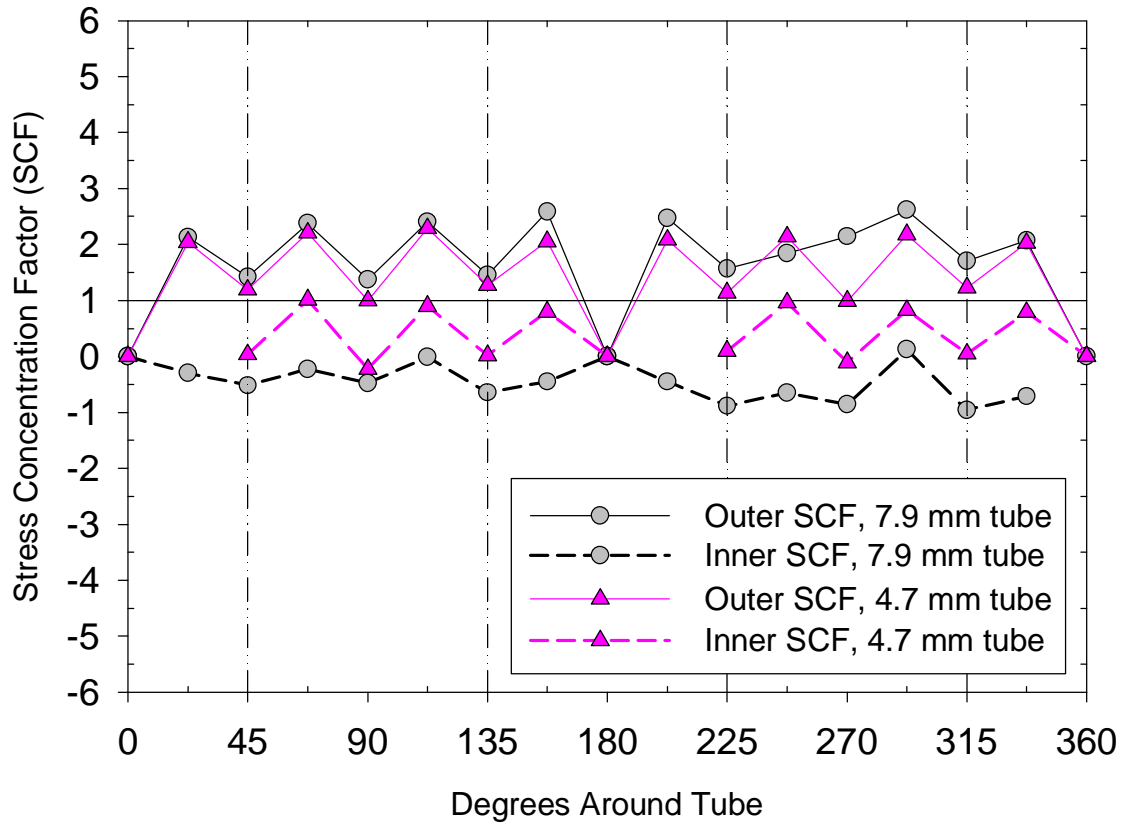


Figure 6.8 SCFs of socket connection with two different tube wall thicknesses, but same thickness base plate.

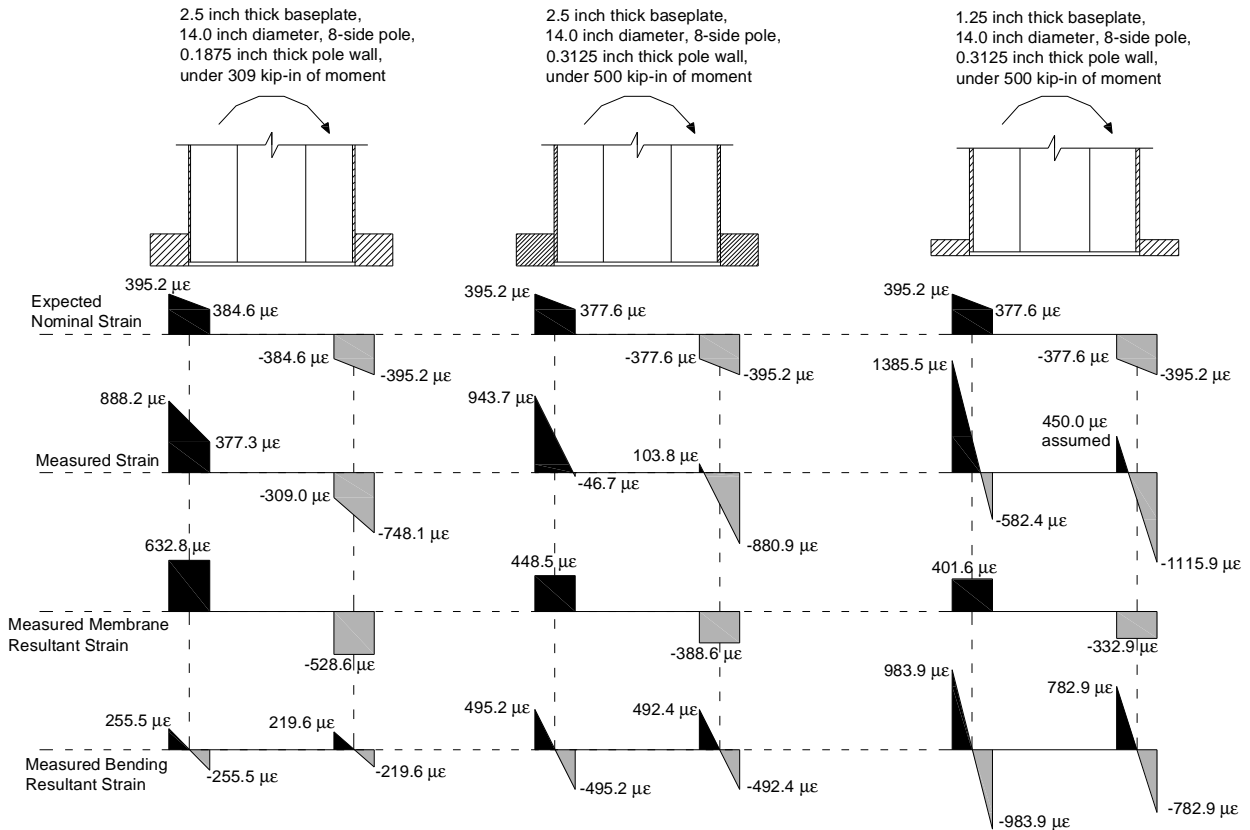


Figure 6.9 Measured strain in pole socket connections with decomposed resultants.

6.3 Type I Mast Arms (Frame 3)

Two Type I mast arm specimens, one socket connection with gusset stiffeners and one with a full-penetration weld were instrumented and statically tested in Frame 3. The instrumentation scheme placed strain gauges in a similar fashion as was done in Frame 1. In the gusset plate specimen, more strain gauges were placed closer to the gusset plate in extreme tension to better understand the load distribution around the stiffener. A SCF plot around both of these mast arm tubes can be found in Figure 6.10. For the gusset plate stiffened mast arm, the SCFs are approximately 2.0 in the heavier loaded area, except in the vicinity of the stiffener. The region of the mast arm tube near the stiffener displays a SCF less than 1.0 meaning there is less stress being transferred in that area than expected. This would indicate that stress is mainly being transferred via the stiffener, which is further verified by a SCF of 1.96 at the 90 degree position. Also note, the SCF in the mast arm tube at the tip of the gusset plate is 1.86, nearly the same SCF at the base of the gusset where it is welded to the base plate. Shown in Figure 6.11 are the measured strains in the gusset plate at three locations, showing the high strain in the mast arm tube near the tip of the gusset, but a much lower strain in the gusset plate itself. The strains in the gusset plate seem to ramp up approaching the base plate, indicating there is a transfer length for the stiffener to fully engage.

The SCFs on the mast arm with the full-penetration are lower than those from the mast arm with gusset stiffeners, hence a longer fatigue life would be expected. However, like other specimens previously presented (Type I poles with 31.8 mm and 63.5 mm thick base plates), the full-penetration weld detail is still susceptible to the shear lag effect at the 90 degree position as the SCF drops below 1.0. On the compression side of the tube, the SCF pattern is no longer symmetric. The compression data was attained after the mast arm cracked on its first side and was then rotated to continue cycling. Therefore, the compression data was attained on a cracked section, but load/displacement plots did not indicate bilinear behavior which would indicate crack closure was occurring to sway the SCF calculation. Compression data was not attained in the gusset stiffened mast arm because the gauges were damaged during hammer peening operations before the mast arm could be flipped over to test the compression side.

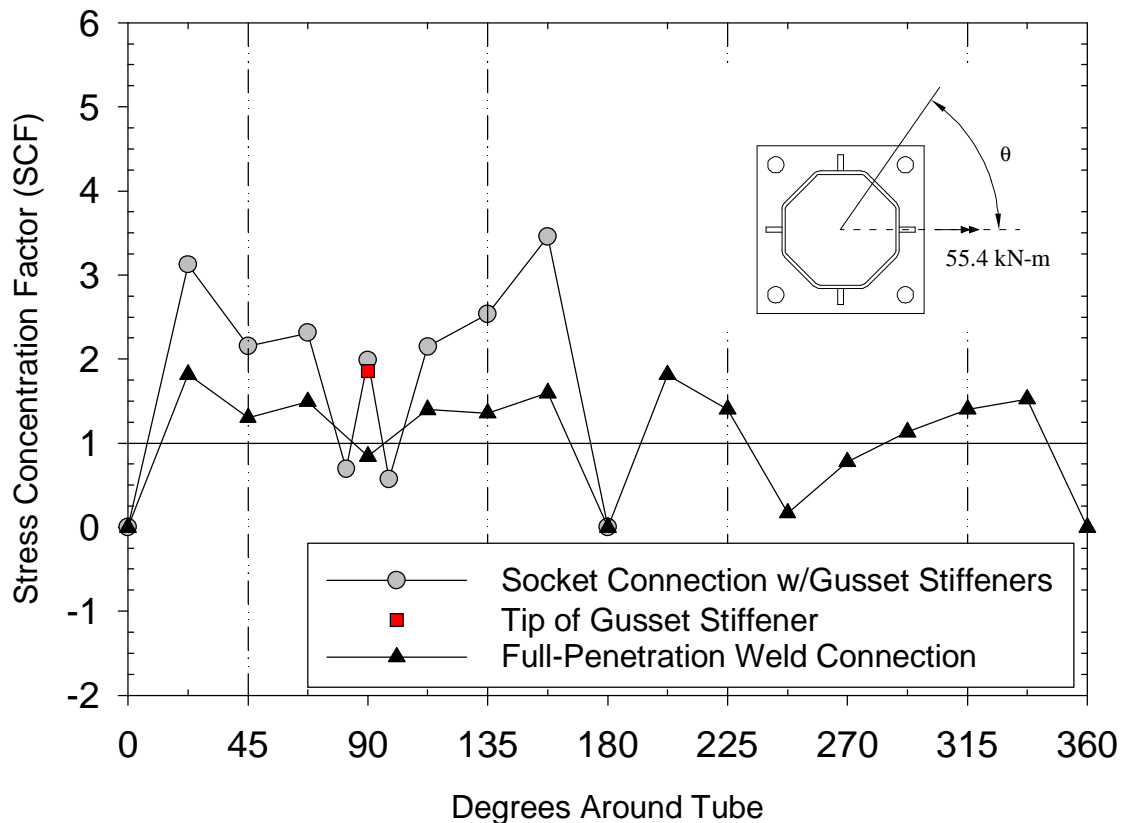


Figure 6.10 Type I mast arm SCFs from Frame 3.

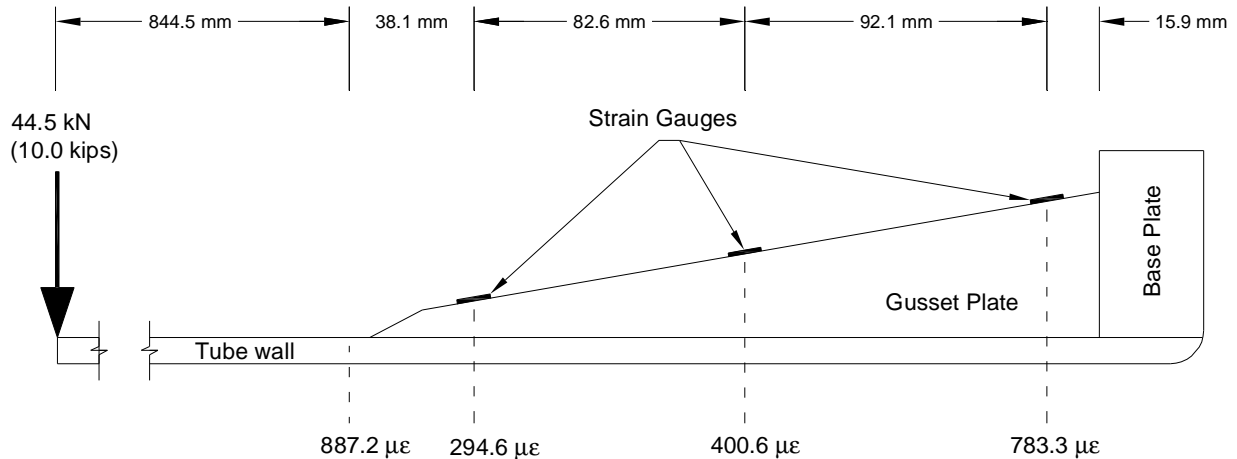


Figure 6.11 Measured strains in gusset plate under static moment.

6.4 Comparisons of Type I Tube-to-Transverse Plate Connections

The static results presented in Sections 5.1-5.3 offer some interesting conclusions in regards to differences in SCF's. First, all the tube-to-transverse plate connections demonstrated some form of shear lag across the tube flat subjected to extreme fiber bending tensile stresses. The theory predicts this tube flat should be uniformly stressed, however the strain gauge readings proved the true strain to be non-uniform across this tube flat, sometimes even lower than expected. With the presence of a shear lag effect, the ends of this tube flat (or the bent corners of the entire cross-section) must transfer more stress and a very high SCF was measured in this location. For instance, shown in Figure 6.12 are SCFs measured at one corner of four different Type I tube-to-transverse plate connections. The thin base plate pole socket connections had an SCF of 3.51, but steadily got smaller as the base plate thickness increased and tube thickness decreased. Contrast this with the full-penetration welded mast arm specimen that only had a SCF of 1.49. The only difference between the thin base plate pole specimen and mast arm specimen shown in Figure 6.12 is the diameter of the tube, and the relative positioning of the bolts. Dotted lines are shown in this picture noting a "bounding box" between the centers of the four bolt holes. Note on the pole socket connection, how the tube actually intersects this bounding box whereas the tube is within the box for the mast arm. The bounding box offers one possible explanation for the high SCF associated with the pole socket connection because stress ultimately must get from the tube into the bolts. In the pole socket, since the tube flat subject to extreme tension stress is outside the box, there is no direct path for stress to flow through the base plate to get to the bolts, therefore more load is shed off to the tube flat nearest the bolt, and hence the SCF in that bent corner is high. For the mast arm specimen, there is a feasible path for stress to flow from the base plate into the bolt because the tube lies completely within the bounding box. This is just one possible reason for the marked difference in SCF between these two tube-to-transverse plate connections. Other possible causes for the difference in SCFs are the difference in tube diameters and the fact that the mast arm specimen had more base plate material left in place to accommodate the full-penetration weld detailing.

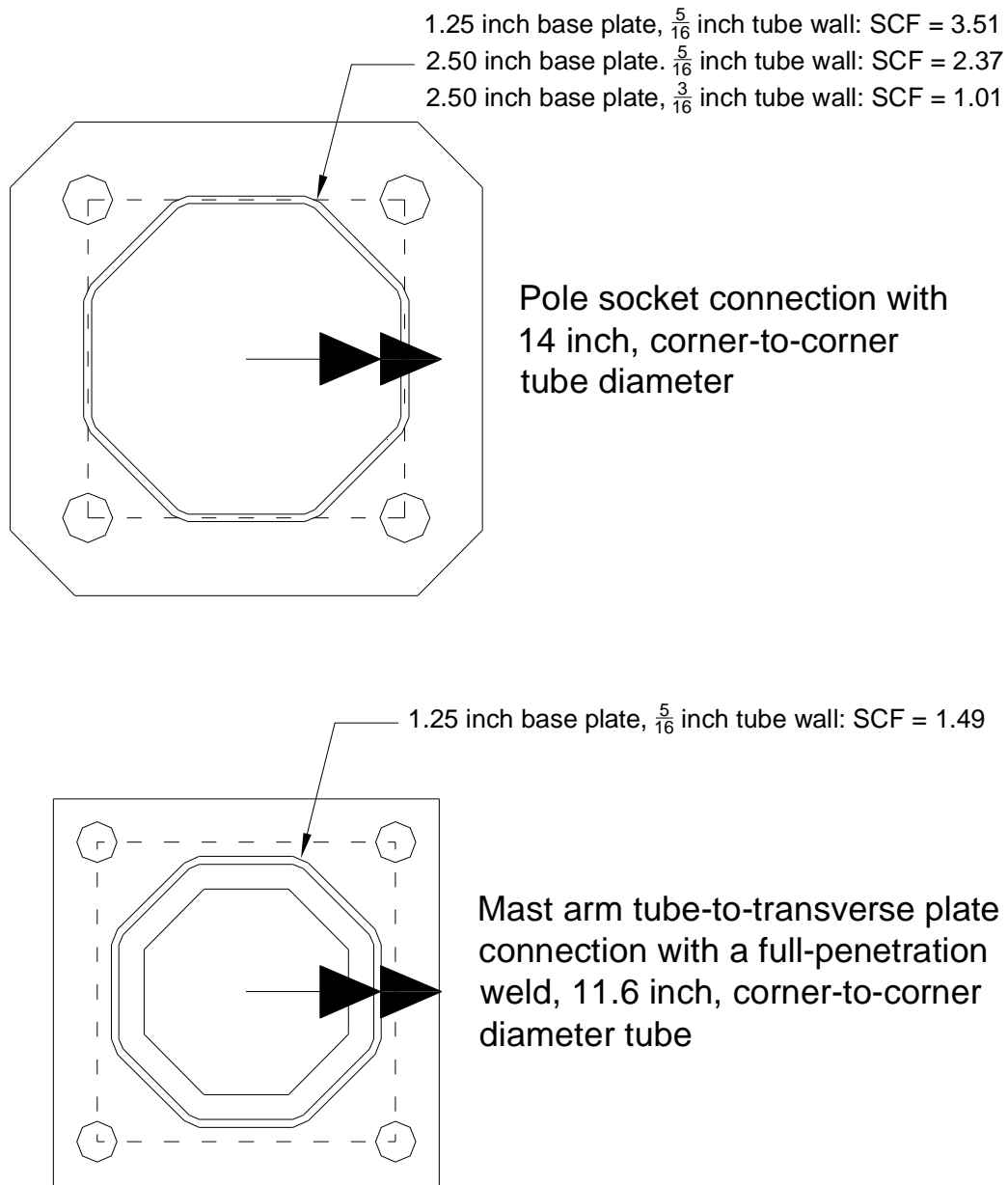


Figure 6.12 SCF comparison between various Type I tube-to-transverse plate connections.

6.5 Type II Specimens

6.5.1 First Static Test

The first static test conducted on the Type II specimens mainly focused on the mast can detail and was tested with three different actuator positions. The instrumentation used to gather the results was described in Section 5.4.1.

The first Type II specimen had a heavily instrumented mast arm and nine gauges on the pole. This specimen was tested in the three primary load directions to attain the hot spot strains at the gauged locations. The results to be presented are not as clean as previously presented for the Type I specimens. As described in Section 5.4.1 the strain gauges applied to the mast arm were glued perpendicular to the weld toe line, and in most cases this orientation did not align with the longitudinal axis of the mast arm tube. Therefore, SCF plots cannot be presented because the predicted strains correlate to the longitudinal axis of the tube and directly comparing that with the measured strains is nonsensical. The graphs to be presented for the mast arm and mast can detail will only plot the measured strain, not SCFs.

Figure 6.13 shows two plots of the measured strain in the mast arm and mast can detail, respectively, under applied static loading. Because strain gauges could not be applied in the MC_45 to MC_135 region on the mast can, the results may seem incomplete, but some conclusions can be made. First, for in-plane loading, the peak tensile strains (i.e., most important for predicting fatigue life) occur at MA_68 and MA_112, which are the bent corners of the mast arm tube in extreme tension from bending. Most likely, this is where the peak tensile strains occurred on the mast can too. Since the only notable difference between the in-plane and out-of-plane loading case is the applied out-of-plane load (i.e., the in-plane dead load moments are virtually the same between each loading case), the difference in measured strains between in-plane and out-of-plane loading would represent the highest strain ranges during cycling, hence the highest likelihood of fatigue crack formation. Looking at the difference between in-plane and out-of-plane loading strains, it can be seen that highest strain ranges occur in the regions on the mast arm and mast can tubes where the out-of-plane bending strains are expected to be the highest (i.e., between degrees 338 and 22, and 158 and 202 on the mast arm and mast can).

Since the gauges on the pole at the full-penetration weld adjoining the pole tube to the transformer base were aligned with the longitudinal axis of the pole tube, SCFs could be calculated at this point. A plot of the SCFs is shown in Figure 6.14 which are on the pole side of the butt weld between the pole and transformer base. Like other specimens, the peak SCFs occur in the bent corner of the tube, particularly at location P_68 and P_112. There is also evidence of the shear lag effect across the extreme tension tube flat from bending as the SCF at P_90 dips below those at P_68 and P_90.

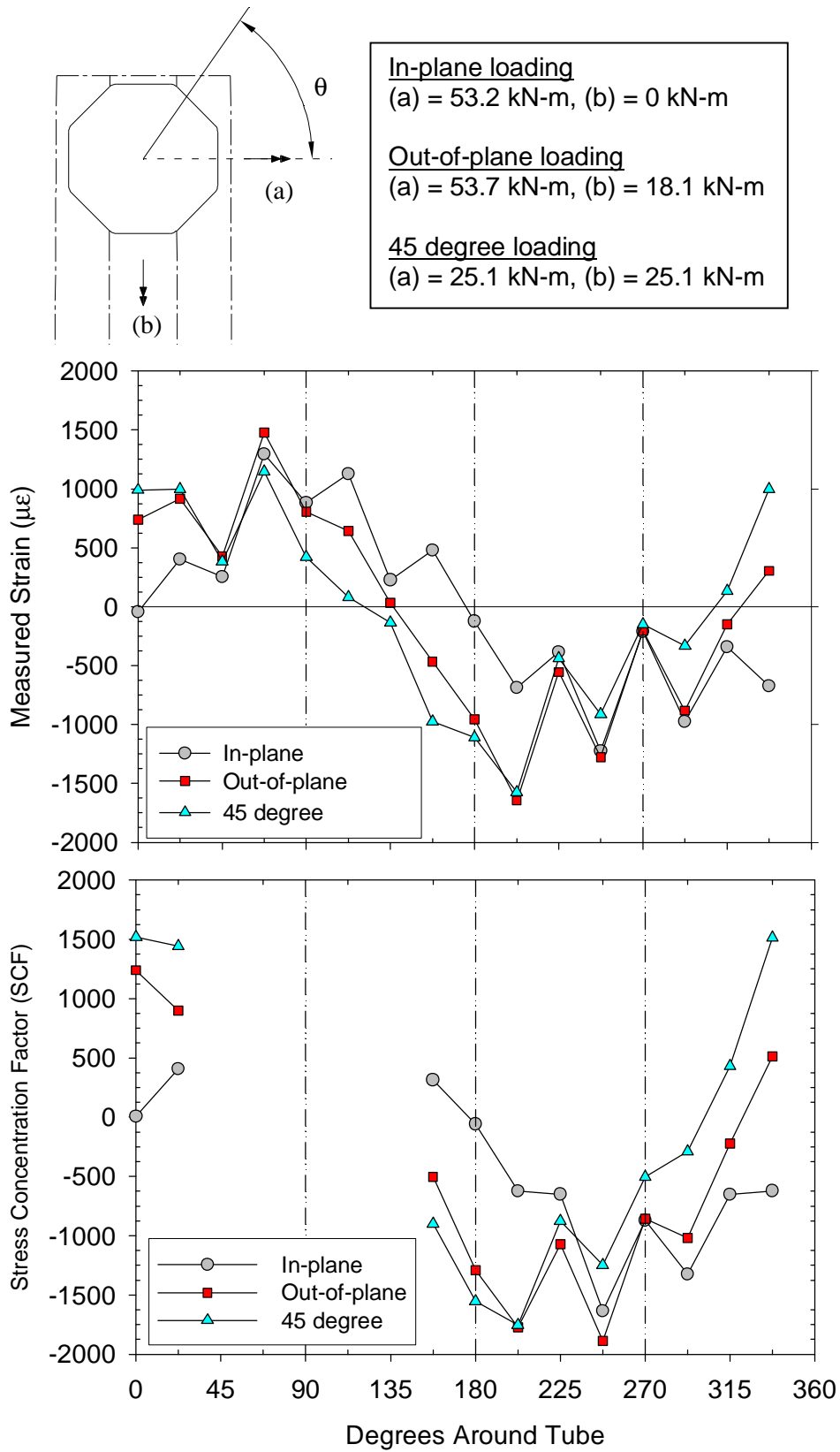


Figure 6.13 Measured static strains on mast arm/mast can detail. (Middle) Strains in mast arm tube. (Bottom) Strains in mast can tube.

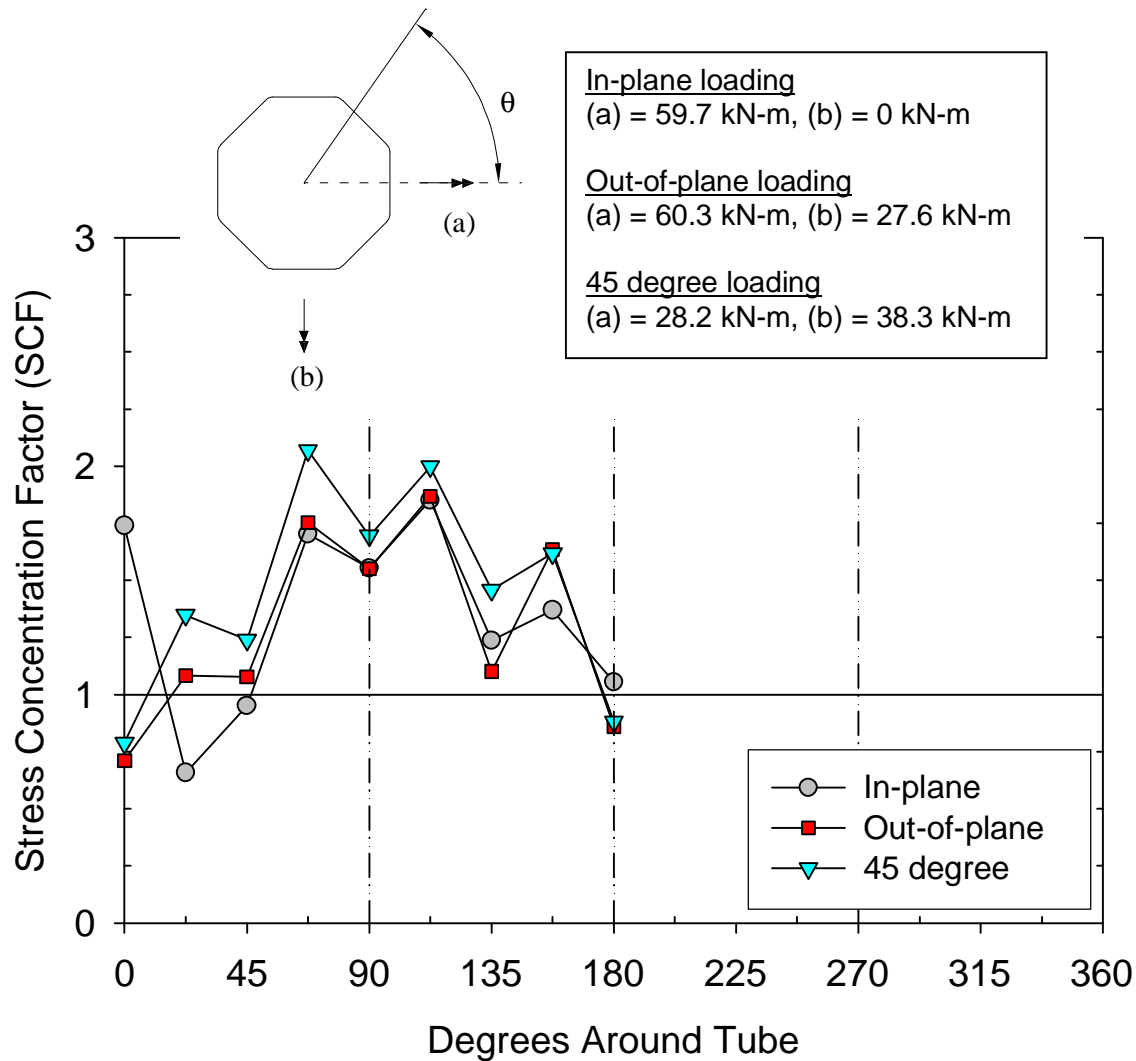


Figure 6.14 Type II pole SCFs at full-penetration weld adjoining the pole tube to transformer base.

6.5.2 Second Static Test

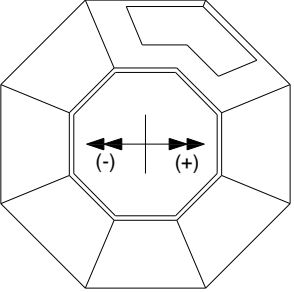
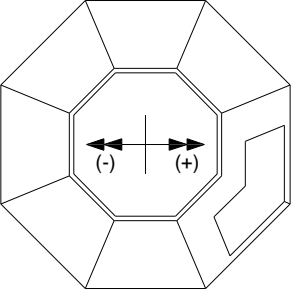
The second static test conducted on the Type II specimens focused on the access hole in the integrated tapered transformer base and was performed with two different orientations of the pole. The instrumentation for the results presented in the following paragraphs was described in Section 5.4.2.

The pole specimen was bolted to the foundation plate such that the access hole was approximately orientated at the neutral bending axis. Because of the 4-bolt anchor rod pattern in the base plate, there were only four positions the access hole could be placed, however two of them are repeated. The static testing included three cycles between 35.6 kN (8 kips and -35.6 kN (-8 kip) and the result presented are three peak strains averaged together. The first results are SCFs presented in Table 6.2. The nominal strain gauges affixed to the pole tube were used to verify the loads follow those calculated using simple beam theory. The SCFs closest to the

actuator are the most accurate being they are closest to 1.0. Recall, the SCF is calculated by dividing the measured strain by the predicted strain, and a SCF of 1.0 means there is a perfect correlation between measured and predicted strains. One would expect the SCF to approach 1.0 the further away from the load point because of the boundary effects from the concentrated load point. However, in this case, the further away from the load point is also closer to the transition of the tube into the transformer base. The SCFs do decrease closer to this transition showing how simple beam theory breaks down at this transition, probably because of a bending component in the thickness of the plates. Also shown in this table are the SCFs at the two bottom corners of the access hole where all cracks were observed, with the peak SCFs ranging from 3.0 to 5.0.

Figure 6.15 and Figure 6.16 depict the rest of the strain measurements taken from the two static tests. The top of each of these figures represent the five, SKT_XX strain gauges shown in Section B-B of Figure 5.10. These gauges were meant to record the nominal strain in the transformer base, above the access hole. The behavior was repeatable whether under negative or positive moments, but there is a pronounced behavior that the predicted strains are larger than those measured. This indicates the influence of the hole in the base and how the stress above the hole begins to redistribute due to its presence. The lower part of each of the mentioned figures represents strain measurements taken from the SK_XX gauges at Section A-A of Figure 5.10. As with the SKT gauges, the behavior is also repeatable under both positive and negative moments. However, what can be seen in these two plots is the observed behavior follows the trend of the predicted behavior, except near the hole. Particularly when the access hole is orientated in the extreme bending fiber, the strain near the hole is larger than predicted, but the next gauge over is less than predicted indicating there is a shear lag effect near the hole. This instrumentation scheme cannot indicate completely whether the differences between predicted and observed behavior is purely from the presence of the access hole. There certainly remains the possibility that there is a bending component through the thickness of the shell which is subtracting away strain from the surface measurements. It is recommended to verify the behavior with finite element analysis.

Table 6.2 Select SCFs from Type II Pole Static Tests.

Specimen Orientation ^a	Gauge ^{b,c}	SCF at 35.6 kN (8 kips) of actuator force	SCF at -35.6 kN (-8 kips) of actuator force
	Nom1_270	0.92	0.92
	Nom2_270	0.91	0.91
	Nom3_270	0.83	0.84
	Door_37.5	3.64	5.37
	Door_97.5	1.67	1.77
	Nom1_0	0.95	0.98
	Nom2_0	0.96	0.98
	Nom3_0	0.85	0.83
	Door_307.5	3.04	1.73
	Door_7.5	-4.96	-0.95
<p>^a- positive actuator loads correspond to positive moment directions. ^b- NomX-XX gauge locations are shown in Figure 5.10. ^c- Door_XX gauges are defined by XX being the angle measured with the positive moment axis as the zero degree axis and the angle direction measured positive counter-clockwise.</p>			

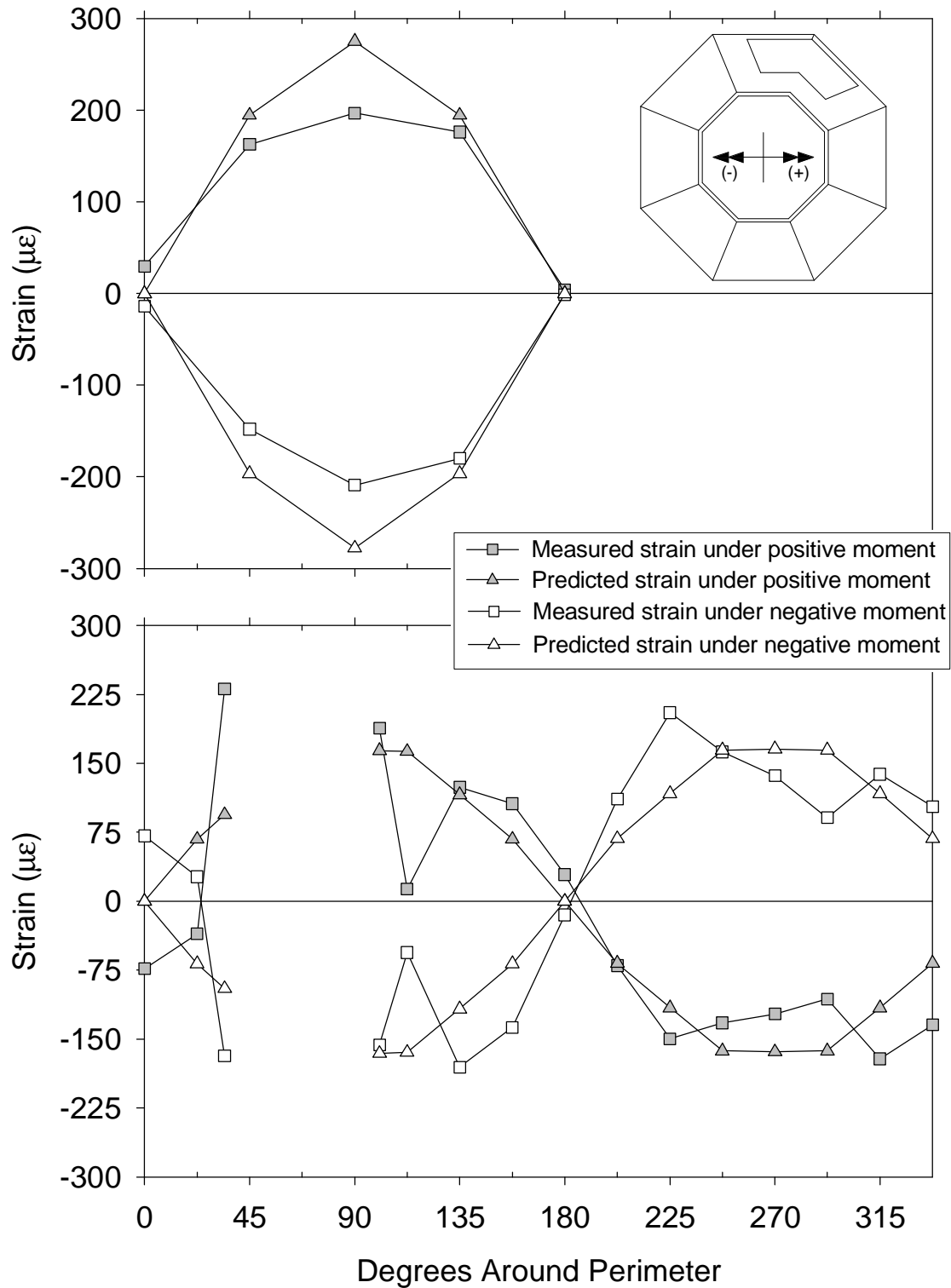


Figure 6.15 Strains in transformer base with access hole at extreme bending fiber. Top: Section B-B gauges. Bottom: Section A-A gauges.

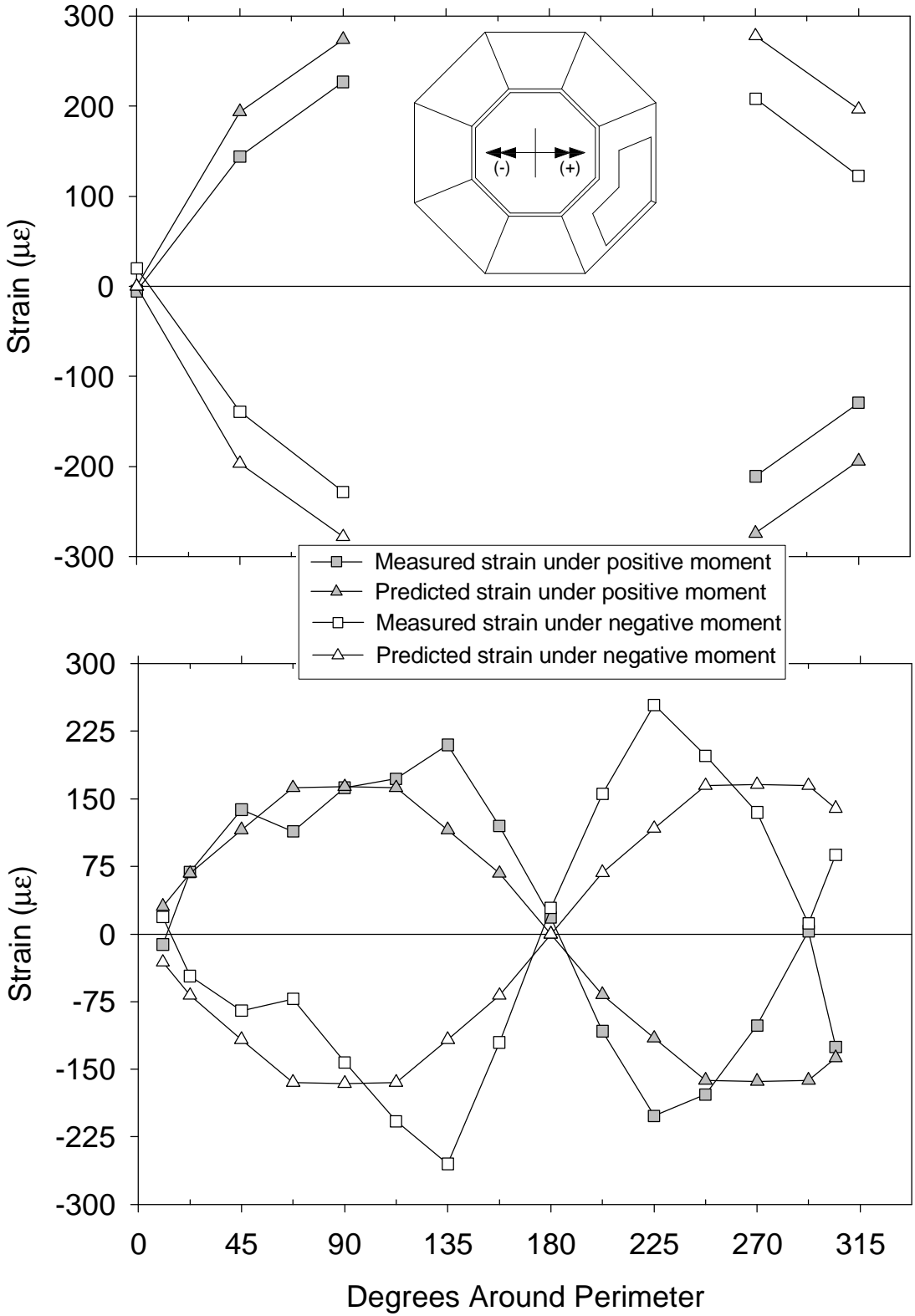


Figure 6.16 Strains in transformer base with access hole near neutral bending access. Top: Section B-B gauges. Bottom: Section A-A gauges.

Chapter 7

Fatigue Results

This chapter discusses the fatigue results from all the specimens tested. All results presented in this report are based on the nominal stress approach, where the nominal stress is calculated using the real loads and nominal section properties. Results are plotted against the AASHTO S-N curves, which are defined in the AASHTO Bridge Code (16). However, the ET and K_2 designations were adopted into the 2001 Specifications directly from AWS D1.1 (1,36). AASHTO fatigue curves A-E' were standardized to have a slope of -3, but the ET and K_2 designations were defined from dated offshore oil industry research of welded tube-to-tube connections. Since AASHTO never standardized the slope of the ET and K_2 curves, these curves were interpreted from those printed in AWS D1.1, thus have a slightly different slope. Regression analysis was performed for details that had more than three specimens to determine the lower bound curve for which 97.5% of all specimens will survive (i.e., the design curve for which only 2.5% of structures would be expected to fail). Since some of the AASHTO fatigue curves were not normalized to have a slope of -3 (i.e., ET and K_2), all the regression analysis presented assumes a slope of -3.

Failure was defined as a 25.4 mm (1 inch) crack that was detected only on the surface. This failure criterion was chosen because it should represent the smallest, paint breaking defect detectable during field inspection, as Minnesota's traffic signal structures are painted.

7.1 Type I Pole Socket Connections

This section will be devoted to the describing the fatigue results of the eight socket connections of the pole specimens shown in Figure 4.1 (those with 31.8 mm (1.25 inch) thick base plates). However, because the detailing is virtually the same, the results from the four, long pole socket connections shown in Figure 4.2 will also be presented (those with 63.5 mm (2.5 inch) base plates).

Cracks in these socket connections always formed at the socket weld in one or both bent corners nearest the extreme bending fiber as shown in Figure 7.1. The socket connections were anticipated to crack at the socket weld toe where it intersected the tube, and then grow through the tube thickness, as this was the case in other research studies. However, for the multi-sided socket connection, cracks were observed to form in two locations in the weld. First, the majority of the cracks did form in the tube side weld toe and grew into the tube as shown in Figure 7.2. Also shown in this figure is the crack surface depicting elliptical crack growth through the tube thickness, originating at the bent corner of the tube. Then shown in Figure 7.3 is a macro etched slice of the tube, weld, and base plate clearly showing how the crack originates at the tube side weld toe and grows into the tube. The second type of cracking observed where those that originated at the socket weld root. These types of cracks were seen to almost come out of the base plate side weld toe as depicted in Figure 7.4. However, a macro etch of the tube, weld, and base plate is shown in Figure 7.5 clearly shows how these cracks originate at the socket weld root from the gap left between the base plate and the tube needed for fabrication fit-up, then grew outward through the weld. It should also be noted that the longitudinal seam weld used to the close-up the octagon tube cross-section was always placed in a bent corner. At times, the seam

weld was orientated such that it was in one of bent corners closest to the extreme bending fiber, and it could be anticipated to have lower fatigue resistance because of the intersecting weld condition (longitudinal seam weld directly crossing the outer socket fillet weld). However, the fatigue strength of corners with seam welds was virtually no different than those with plain base metal. Therefore, the location of the seam weld will not be reported in the following results.

Recall the methodology of testing was to cycle the mast arm and pole specimens together in Frame 1 until the box connection cracked, then the pole could be moved to Frame 2 to complete the fatiguing of the socket connection. However, this was not always the case, and five of the eight, thin base plate socket connections cracked in Frame 1 prior to the box connection cracking. Therefore, most the eight, thin base plate specimens were tested multiple times, depending on the order of crack appearance. When the socket connections were tested in Frame 2, the connection was rotated such that the side cycled under compressive stresses in Frame 1, was then imposed by tensile stresses in Frame 2. There was worry that the previous compressive stress cycling may bias the fatigue strength attained in Frame 2, however no bias was found in the results attained in Frames 1 and 2, thus allowing two data points from each specimen.

After some of these socket connections cracked, the crack was hammer peened repaired (HPR) to investigate retrofit techniques for cracked pole socket connections. Hammer peening is a mechanical weld toe treatment where by means of plastic deformation induced by a pneumatic chisel (or chipping hammer), imposes favorable compressive residual stresses at the weld toe. The compressive residual stress shifts the fatigue stress range either fully or partially into the compression regime to enhance fatigue strength. Hammer peening has been shown to be an effective retrofit for surface cracks (38). In these tests, the retrofit peening process was performed with the dead load present because peening processes were found to be ineffective when not performed under dead load (31). HPR was particularly important for testing in Frame 1 where the box connection was anticipated to crack first. However, as will be described later, the pole socket connections cracked prior to the box connection for in-plane loading. Therefore, hammer peening the cracked socket connections allowed for continued cycling on the box connection. Other socket connections were hammer peened (HP), under dead load, prior to cycling in order to test the validity of weld improvement after fabrication, but prior to structure erection.

The fatigue results for the eight, thin base plate, pole socket connections can be found in Table 7.1 and Table 7.2 from cyclic testing in Frames 1 and 2, respectively. The fatigue results of plain socket connections, with no weld toe improvement are plotted in Figure 7.6. This plot shows that the majority of the data agrees with the ET curve, though it should be noted there were some runouts (i.e., no cracking) near the E' curve. However the three runouts were from the out-of-plane and 45 degree loading case in Frame 1 where the socket connection was in cyclic bending and torsion. The stress ranges presented are from the bending portion only, neglecting mixed mode loading. Neglecting the mixed mode loading could account for the outlying data points, however two other out-of-plane loading fatigue points fall along the ET line, so the effect is attributed to scatter. Also shown in this figure is a solid black line representing the 97.5% survivability curve which falls between ET and K_2 (run outs were neglected in the regression analysis), so it would be appropriate to categorize the untreated, multi-sided, 31.8 mm (1.25 inch) thick base plate socket connections as Category K_2 . Figure 7.7 plots the data for socket connections which cracked, were hammer peened under dead load, and then cycled further after

the cycle counter was returned to zero. There are six data points on this curve, three of which are runouts (i.e., did not crack), but the three points which represent connections that re-cracked plot slightly above the E' line. However, the regression analysis shows for 97.5% survivability, the hammer peen repaired socket connections are Category ET. This is a one category fatigue life improvement from the as-built design, even with a known buried defect. The final set of fatigue data is presented in Figure 7.8 for the socket connections hammer peened under dead load prior to initial cycling. Of the five data points plotted, four of them plotted near the Category E curve. There is no firm explanation for the premature cracking of the stray data point to the far left of the plot, but it could have been misapplication of the hammer peening (for instance the air pressure could have been too low) or that the applied stress range was high enough to completely overcome the compressive residual stress from the peening. The regression shows the 97.5% survivability curve plots between E and E'. Therefore, initially hammer-peened, multi-sided socket connections would be best classified as Category E' details, which is a two category fatigue life improvement over the untreated socket connection.

The fatigue results for the four, thick base plate specimens are summarized in Table 7.3. There were only two specimens of each tube wall thickness, but each specimen was tested twice in Frame 2. The specimen was first cracked, then unbolted from the transformer base and rotated 180 degrees to be tested in the opposite direction. This was done because the first eight pole specimens (those with 31.8 mm thick base plates) did not display bias between the fatigue strength of opposite sides from the same specimen. Therefore, it was thought the thick base plate specimens would demonstrate the same behavior, but this was not the case. First looking at Figure 7.9 which is an S-N plot for the sockets with 7.94 mm (0.3125 inch) thick pole walls, not only does the data show a lot of scatter, but there is a noticeable bias between the fatigue strength of the first and second sides of the same test pole. Because there were not many data points, a regression analysis was not performed for these specimens and no solid comparisons can be made to the thin base plate socket connections. The first side of Pole 1 made it the Category C CAFL, then the stress range was increased to fail the specimen sooner. This data point is represented by the upside down triangle which failed from a weld root crack. However, the first side of Pole 2 had a much lower fatigue resistance, plotting just below Category D. For the specimens with 4.76 mm (0.1875 inch) thick pole walls, there is less scatter in the data, and the bias between the first and second sides is reduced as shown in Figure 7.10. All four of these data points fall in-between the Category E' and E curves, with the data from the first side testing being higher.

There still remains a marked difference between the fatigue strength of the first and second tested sides of each of the four, thick base plate specimens. There is no explanation for this behavior, but for all four specimens, when cycling began on the second side, inspections could not see any preexisting cracks from initial compression side cycling. Interestingly, Figure 7.11 shows a picture of the crack surfaces from a first and second side crack of Pole 2. The crack from the first side was only a shallow surface crack, however the crack on the second side extended almost through the entire pole wall thickness, and much wider than the crack from the first side. This is counterintuitive because more cycles were accumulated on the first side, yet the crack is not nearly as large as the one from the second side. This same cracking behavior was also observed on Pole 3, which had 4.76 mm (0.1875 inch) thick pole wall. Therefore, it is recommended that all the second side data be neglected in future decision making processes,

barring future findings in other related research. The second side data was presented in this report only as a means of record, not to draw conclusions from.

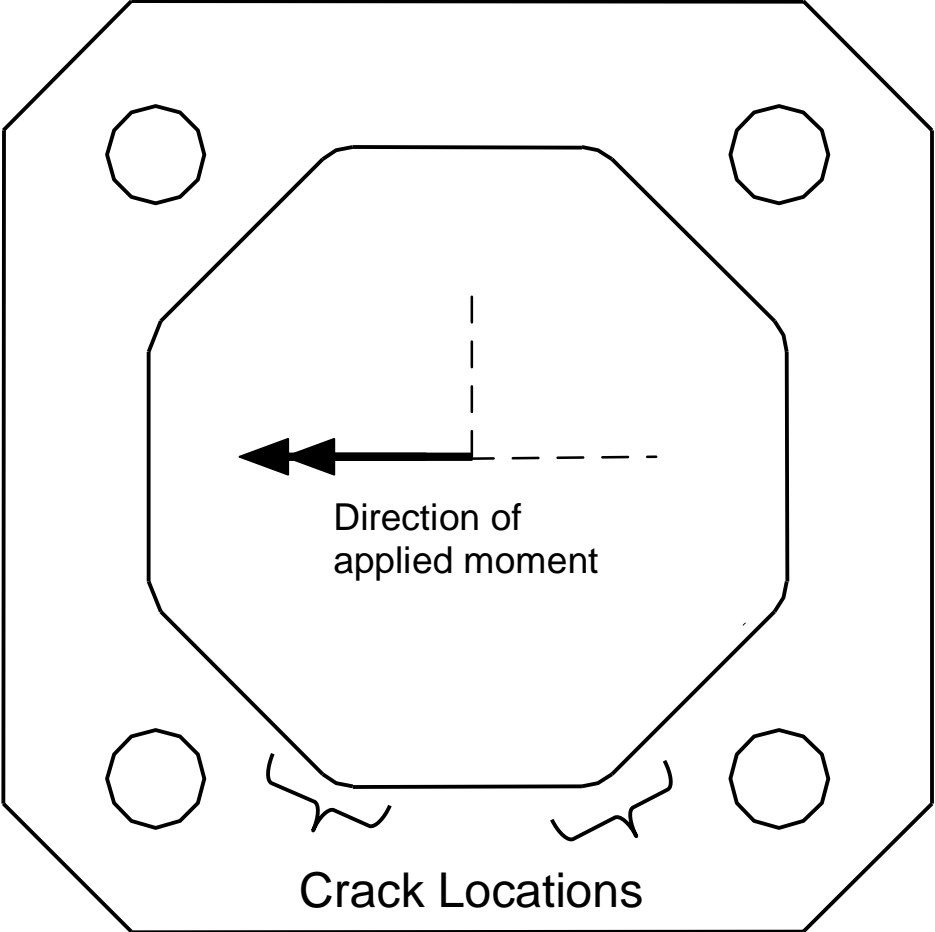


Figure 7.1 Location of cracks in socket connections.

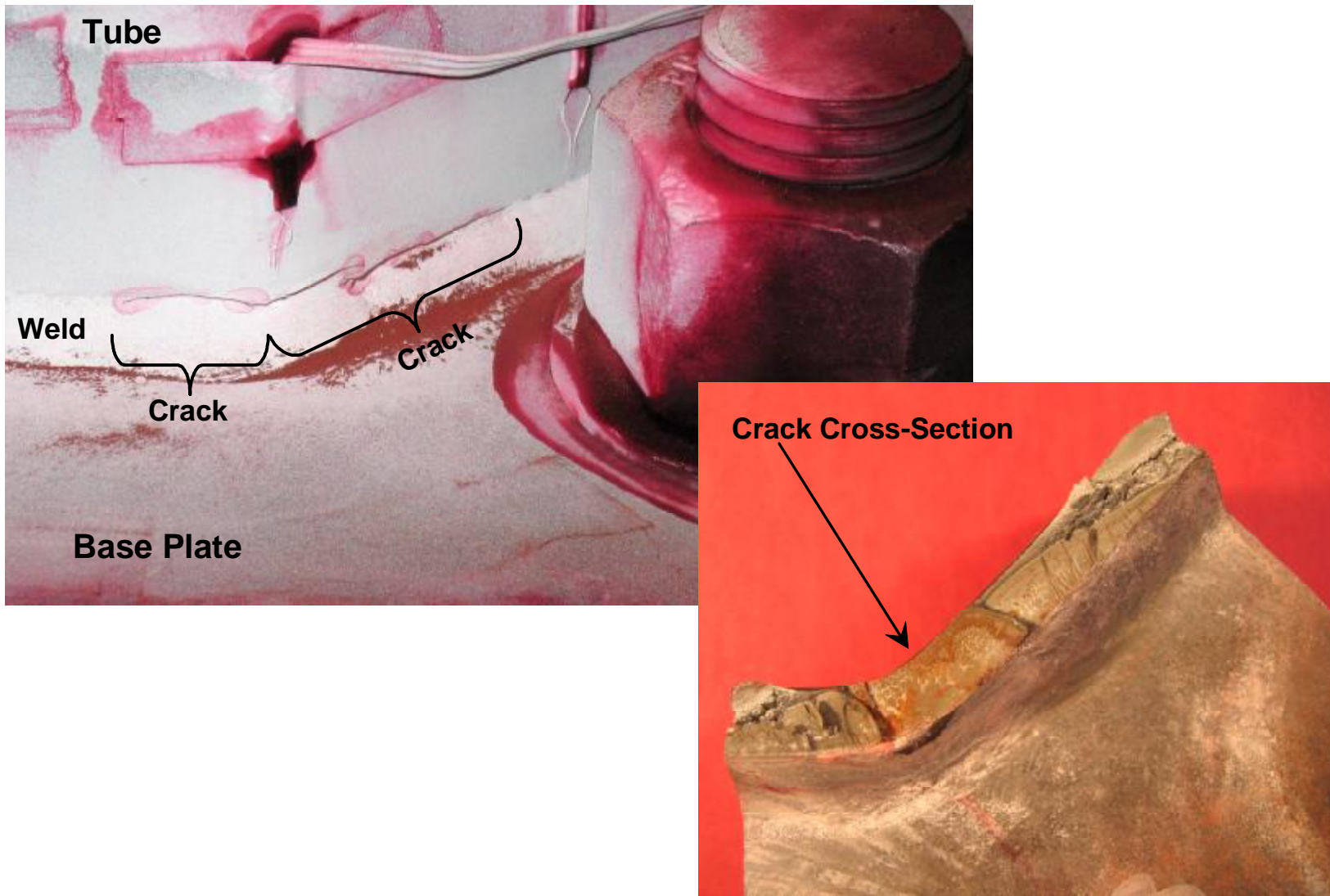


Figure 7.2 Weld toe cracks in pole socket connections.

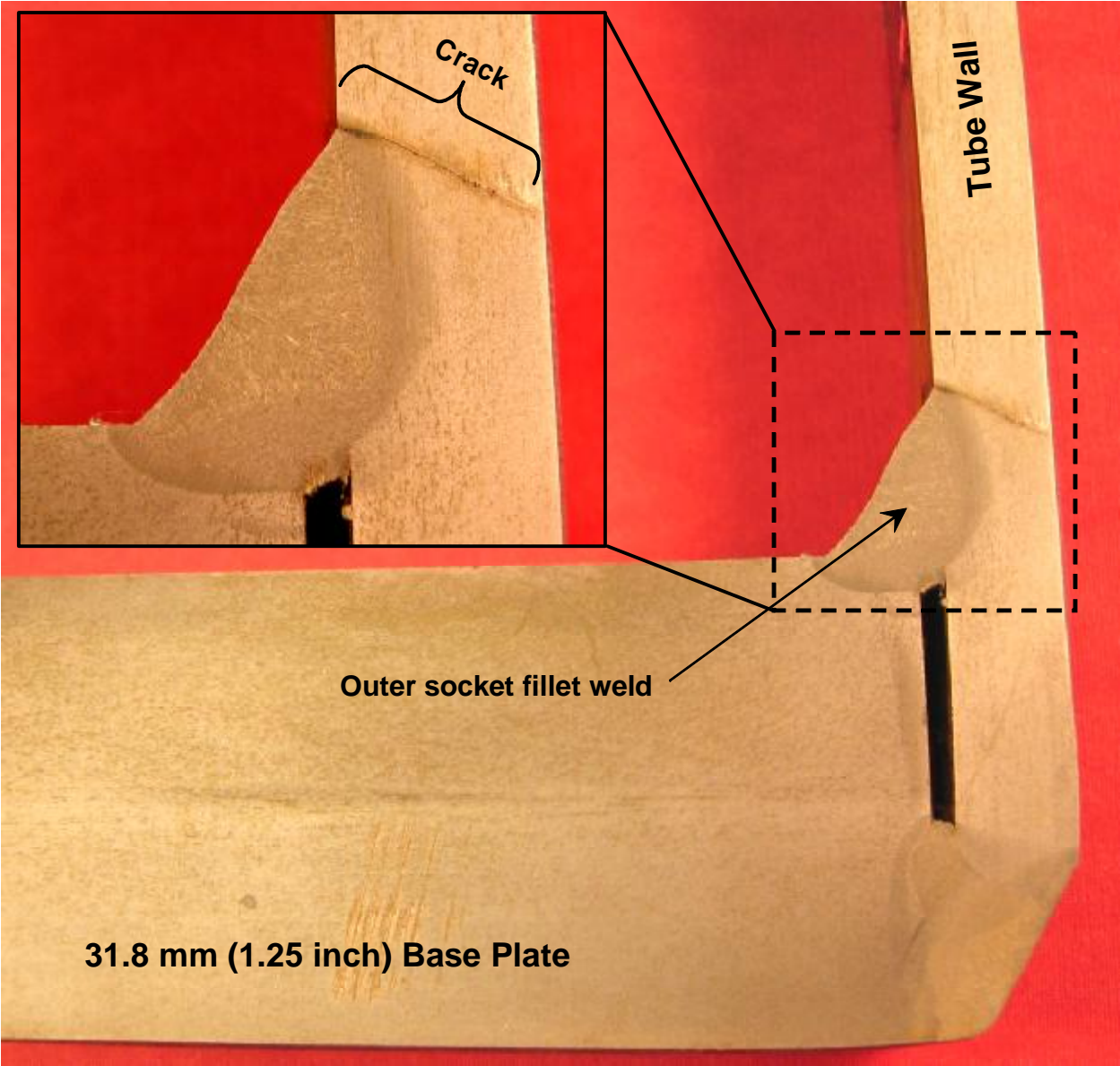


Figure 7.3 Macro etched cross-section of weld toe crack.

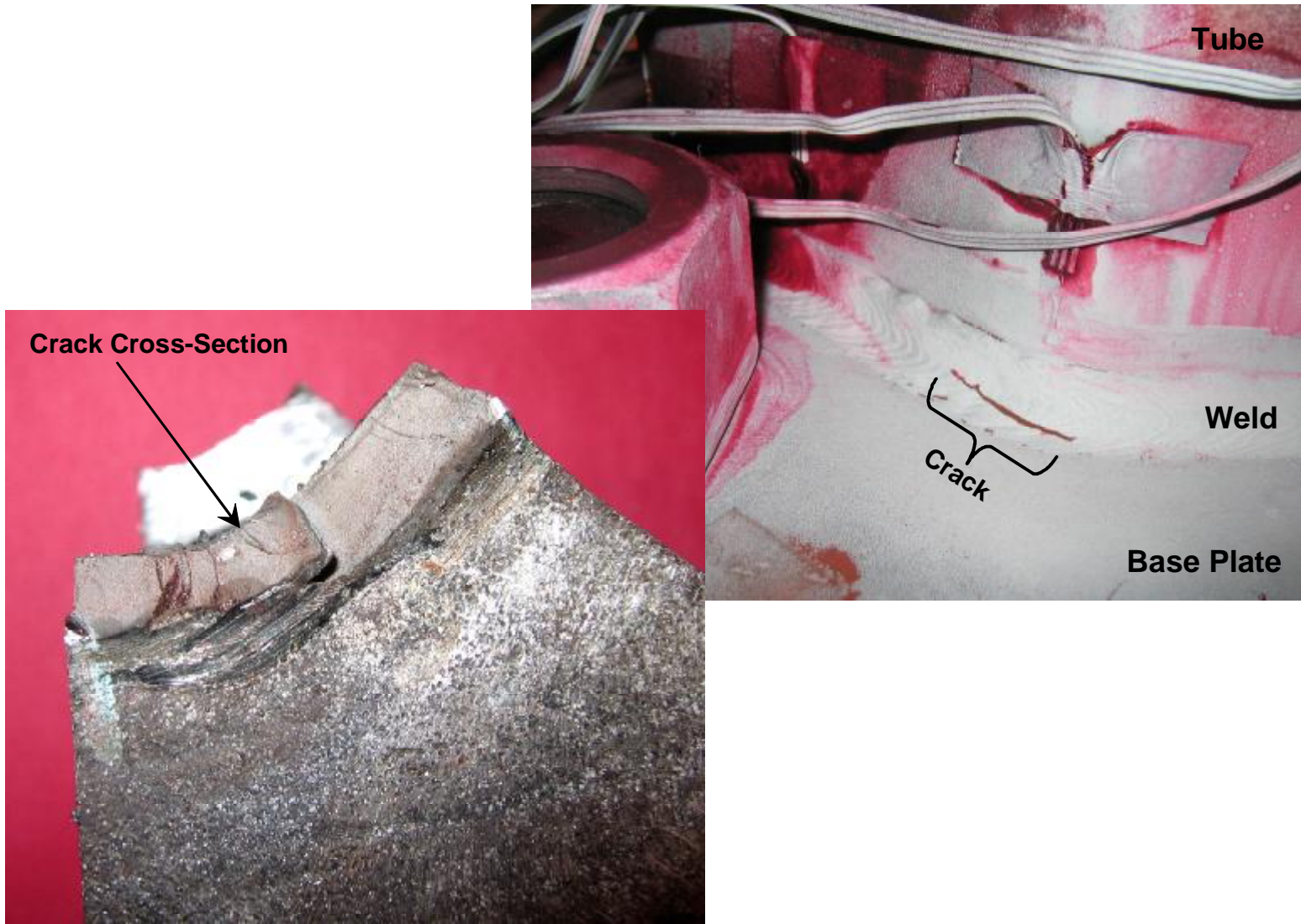


Figure 7.4 Weld root cracks in pole socket connections.

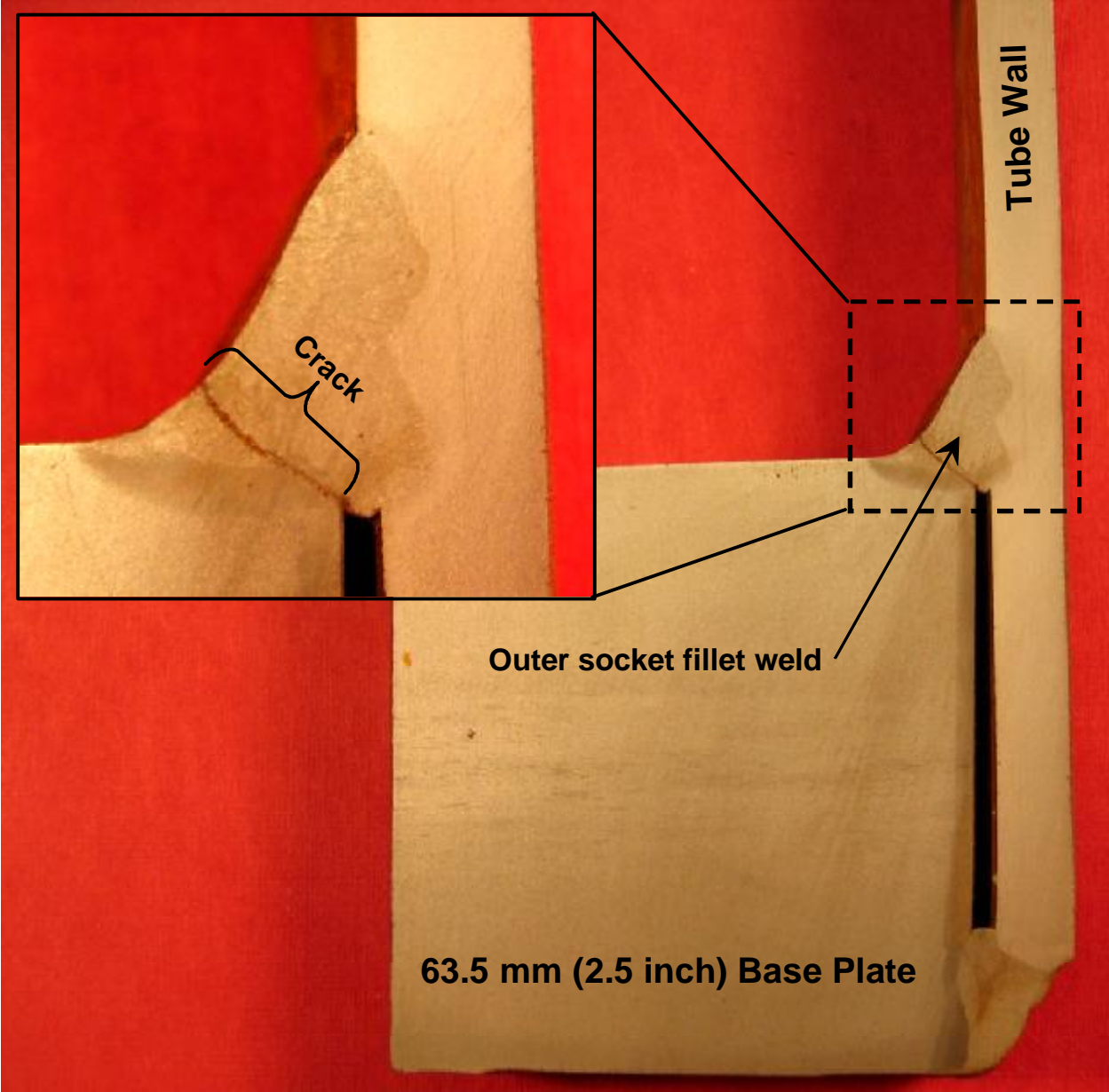


Figure 7.5 Macro etched cross-section of weld root crack.

Table 7.1 Fatigue Results from Frame 1

Pole # and condition ^a	Load Direction ^b	Actuator Min/Max Loads kN (kip)	Failure Location (see Figure 5.6)	Stress Range MPa (ksi)	Cycles to Failure
1A	IP	27.13 / 53.82 (6.1 / 12.1)	P_112	56.89 (8.25)	83806
2A	IP	46.26 / 34.70 (10.4 / 7.8)	P_112	23.65 (3.43)	981490
3A	IP	46.71 / 34.25 (10.5 / 7.7)	P_112	26.18 (3.80)	610124
3HPR	IP	^d	P_68	31.37 (4.55)	4126888
4A	OP	6.67 / -6.67 (1.5 / -1.5)	No Crack	28.21 (4.09)	5038549 ^c
5A	OP	8.90 / -8.90 (2.0 / -2.0)	P_22	37.3 (5.41)	170606
6A	OP	8.90 / -8.90 (2.0 / -2.0)	No Crack	37.3 (5.41)	1292565 ^c
7A	OP	8.90 / -8.90 (2.0 / -2.0)	P_22	37.3 (5.41)	301484
7A	OP	8.90 / -8.90 (2.0 / -2.0)	P_168 ^e	37.3 (5.41)	2293739
8A	45	35.59 / 22.24 (8.0 / 5.0)	No Crack	28.21 (4.09)	4175643 ^c
^a - A (as fabricated), HPR (hammer peened under dead load with crack present) ^b - IP (in-plane), OP (out-of-plane), 45 (45 degree loading) ^c - runout ^d - increasing load ranges were used and an equivalent stress range calculated using Miner's rule is reported (Miner, 1945) ^e - indicates a weld root crack					

Table 7.2 Fatigue results from Frame 2.

Pole # and condition ^a	Actuator Min/Max Loads, kN (kip)	Failure Location (see Figure 5.6)	Stress Range, MPa (ksi)	Cycles to Failure
1A	-33.8 / -47.8 (-7.6 / -10.75)	P_292 and P_248	29.37 (4.26)	591696
1HPR	-29.4 / -52.5 (-6.6 / -11.8)	P_292	48.19 (6.99)	1106830
2HP	^b	P_248	40.13 (5.82)	8501877
3A	-35.1 / -47.2 (-7.9 / -10.6)	P_292	25.18 (3.65)	868266
4HP	-29.4 / -52.5 (-6.6/-11.8)	P_248 ^c and P_292 ^c	48.95 (7.10)	2558528
5HP	-24.5 / -57.4 (-5.5/-12.9)	P_248	68.95 (10.00)	124147
6HP	-31.1 / -50.7 (-7.0 /-11.4)	P_248 ^c	41.37 (6.00)	5571296
7A	-34.3 / -47.6 (-7.7/-10.7)	P_248	28.27 (4.10)	1658906
7HPR	-28.0 / -53.8 (-6.3/-12.1)	P_248	54.54 (7.91)	1131798
8HP	-28.0 / -53.8 (-6.3/-12.1)	P_248	54.54 (7.91)	5366869
^a - A (as fabricated), HP (hammer peened under dead load), HPR (hammer peened under dead load with crack present) ^b – an increasing load range was used to expedite testing, stress range reported is an equivalent stress range calculated using Miner's rule (Miner, 1945) ^c – indicates a weld root crack				

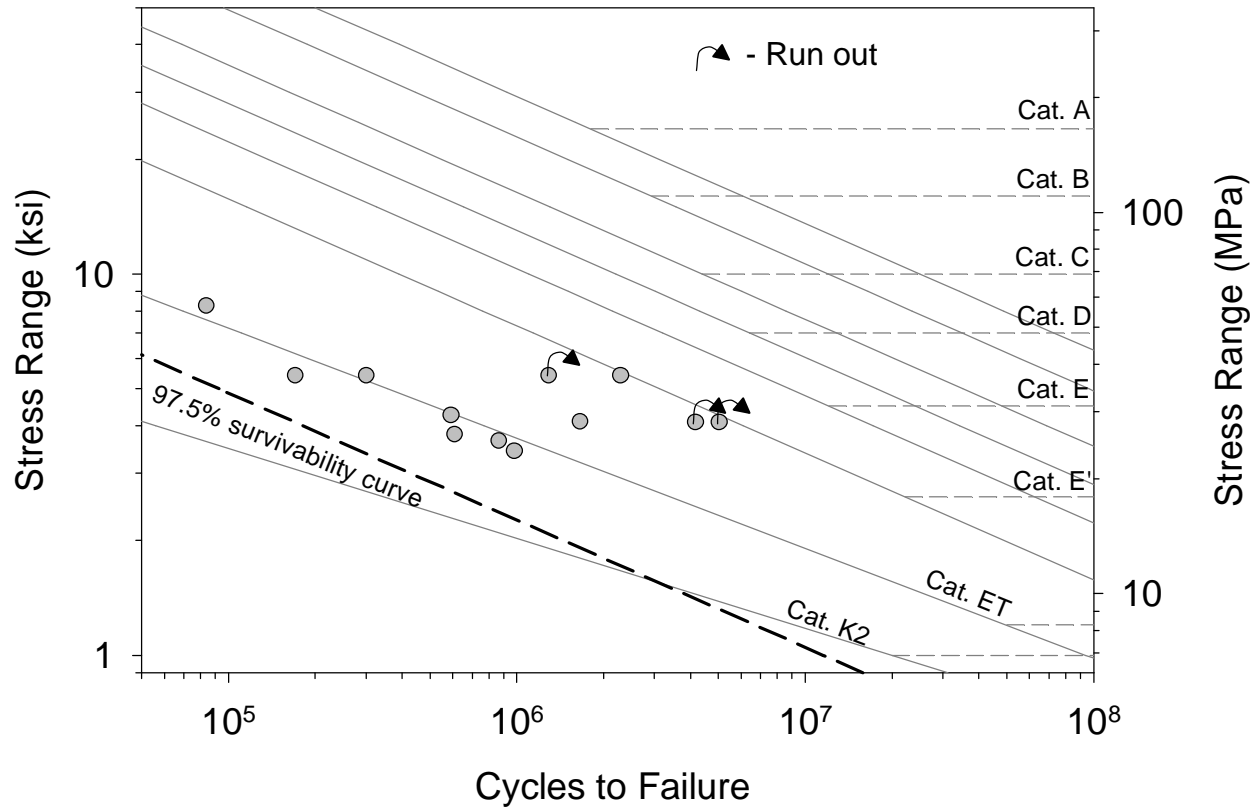


Figure 7.6 S-N plot of untreated socket connections with 31.8 mm (1.25 inch) thick base plates.

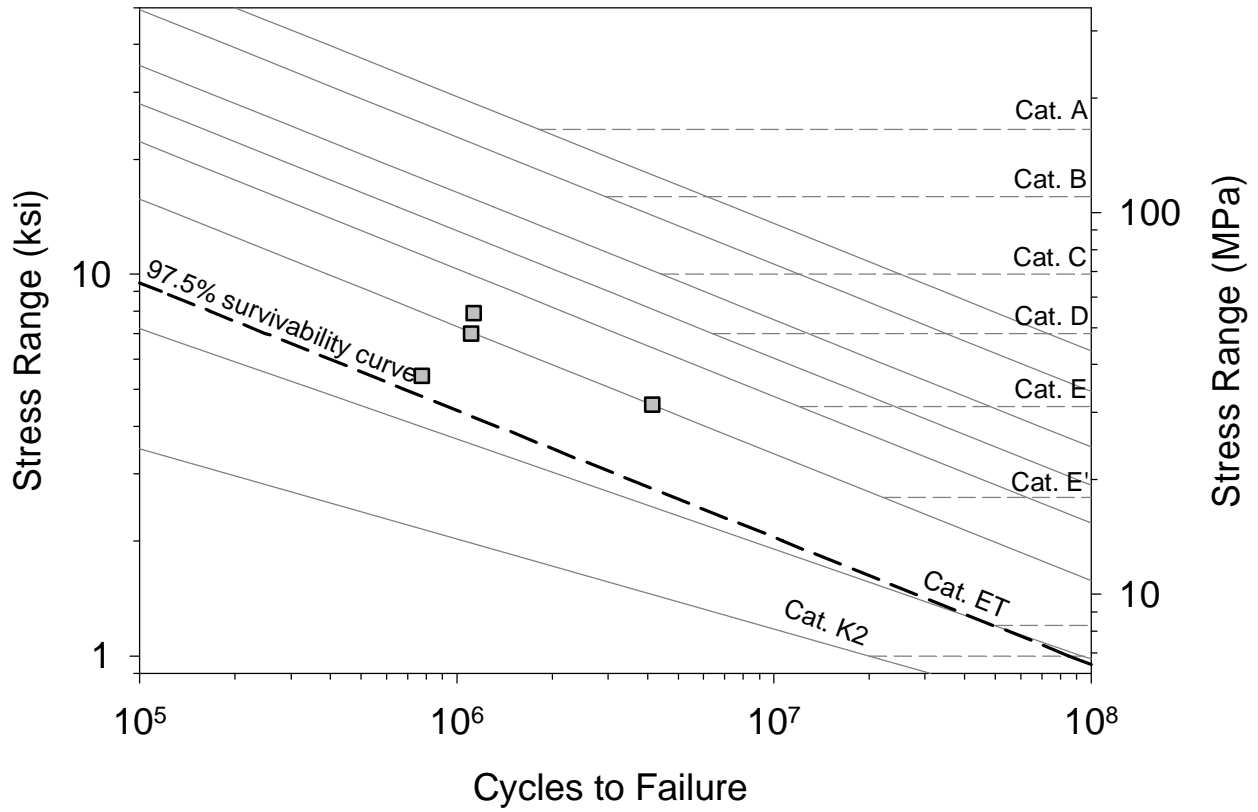


Figure 7.7 S-N plot of hammer-peened repaired socket connections with 31.75 mm (1.25 inch) thick base plates.

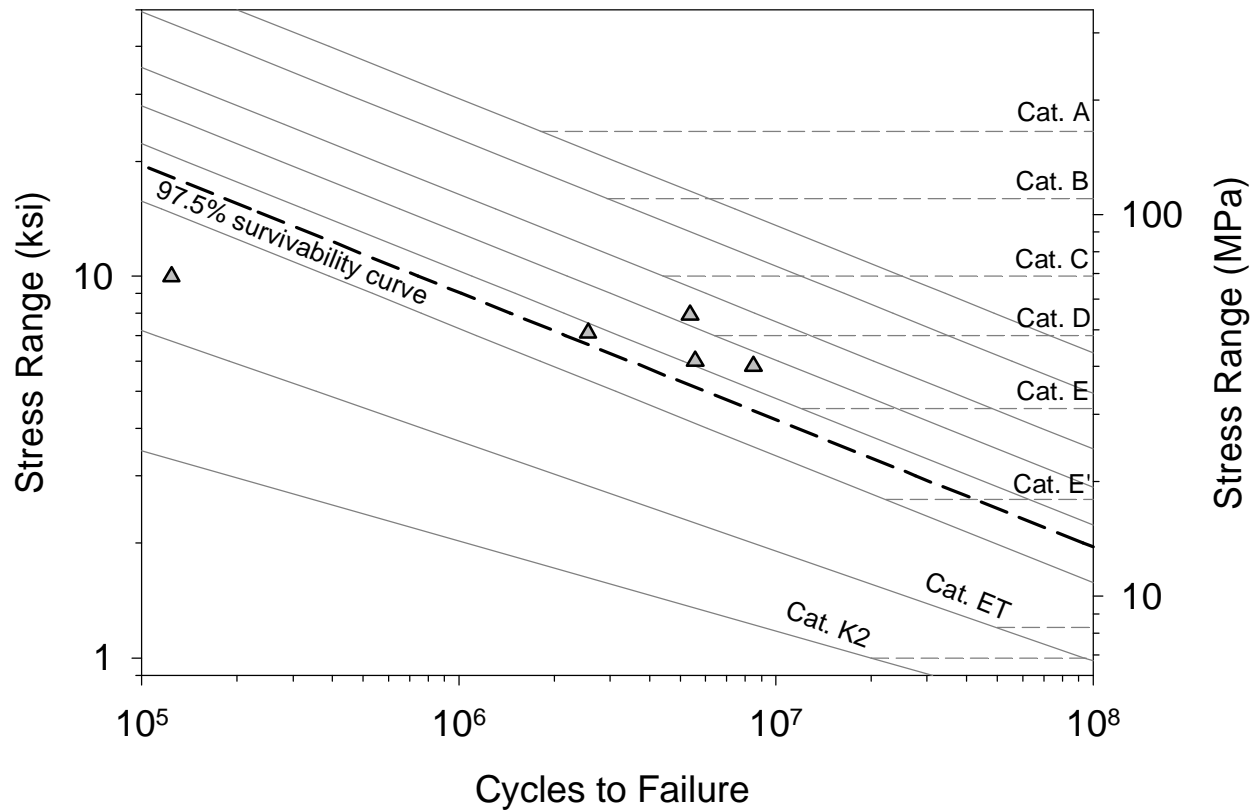


Figure 7.8 S-N plot of hammer-peen retrofitted socket connections with 31.75 mm (1.25 inch) thick base plates.

Table 7.3 Fatigue Results of Thick Base plate Pole Specimens

Pole # [wall thickness]	Actuator Min/Max Loads, kN (kip)	Moment Arm Distance, mm (inch)	Failure Location (see Figure 5.6)	Stress Range, MPa (ksi)	Cycles to Failure
1, 1 st side [7.94 mm (5/16 inch)]	-26.47 / -10.45 (-5.95 / -2.35) for 4112106 cycles -29.36 / -7.56 (-6.60 / -1.70) for 110887 cycles	3359.2 (132.25)	P_68 ^c	77.01 (11.17) ^a	4222993
1, 2 nd side	-29.36 / -7.56 (-6.60 / -1.70)	3359.2 (132.25)	P_248 and P_292	102.73 (14.90)	81924
1, 2 nd side hammer peened weld toe	-29.36 / -7.56 (-6.60 / -1.70)	3359.2 (132.25)	P_292 ^c	102.73 (14.90)	978382
2, 1 st side [7.94 mm (5/16 inch)]	-28.25 / -8.67 (-6.35 / -1.95)	3714.8 (146.25)	P_68 and P_112	102.73 (14.90)	566119
2, 2 nd side	-28.25 / -8.67 (-6.35 / -1.95)	3714.8 (146.25)	P_248 and P_292	102.73 (14.90)	101916
3, 1 st side [4.76 mm (3/16 inch)]	-17.44 / -5.25 (-3.92 / -1.18)	3714.8 (146.25)	P_68 and P_112	103.42 (15.00)	330137
3, 2 nd side	-17.44 / -5.25 (-3.92 / -1.18)	3714.8 (146.25)	P_248 and P_292	103.42 (15.00)	140545
4, 1 st side [4.76 mm (3/16 inch)]	-17.44 / -5.25 (-3.92 / -1.18)	3714.8 (146.25)	P_68 and P_112	103.42 (15.00)	183638
4, 2 nd side	-17.44 / -5.25 (-3.92 / -1.18)	3714.8 (146.25)	P_248 and P_292	103.42 (15.00)	86888
^a – increasing load ranges were used and an equivalent stress range calculated using Miner’s rule is reported (Miner, 1945) ^b – because the pole was rotated to test both side of the socket connection, the positive moment direction shown in Figure 5.6 is actually reversed for first side testing. This clarification is needed to show the tube flat between P_68 and P_112 was the extreme tension bending fiber for first side testing and the tube flat between P_248 and P_292 was the extreme tension bending fiber for second side testing ^c – weld root crack					

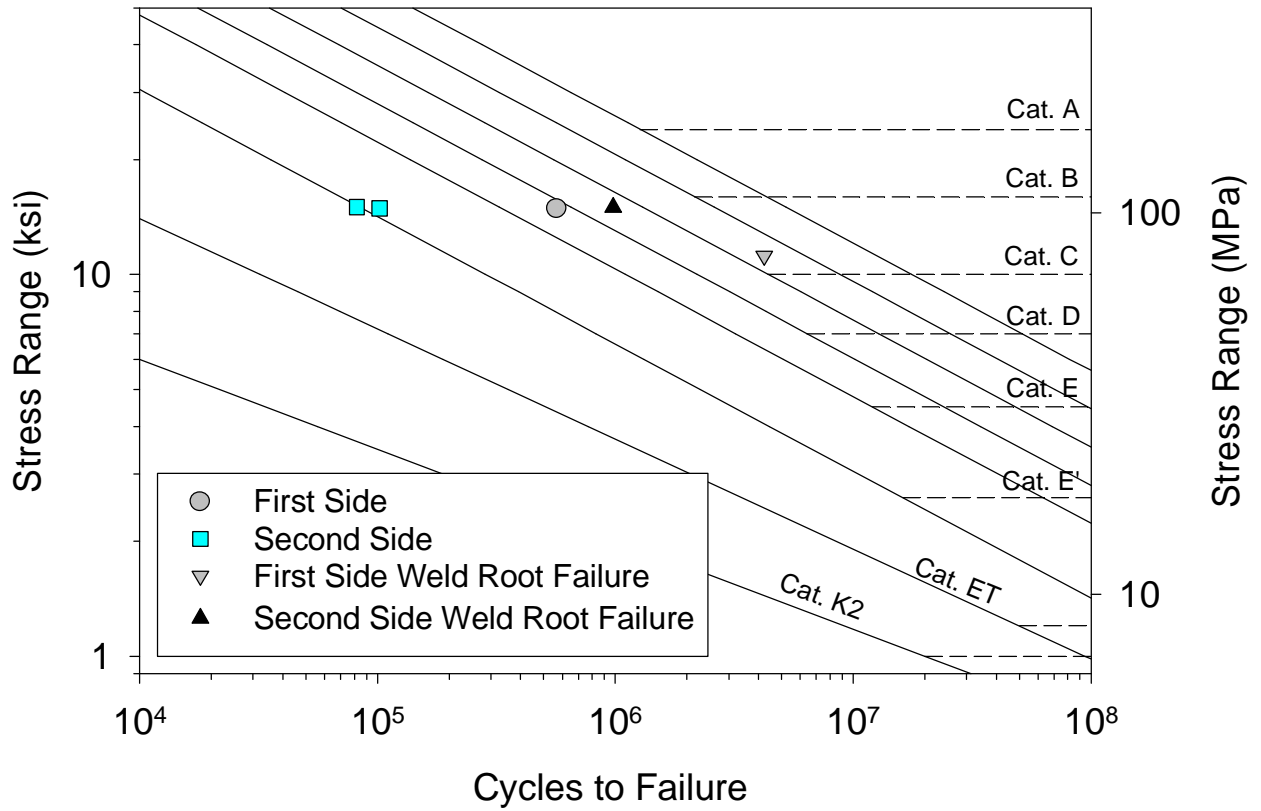


Figure 7.9 S-N plot of thick base plate socket connection with 7.94 mm (5/16 inch) pole wall thickness.

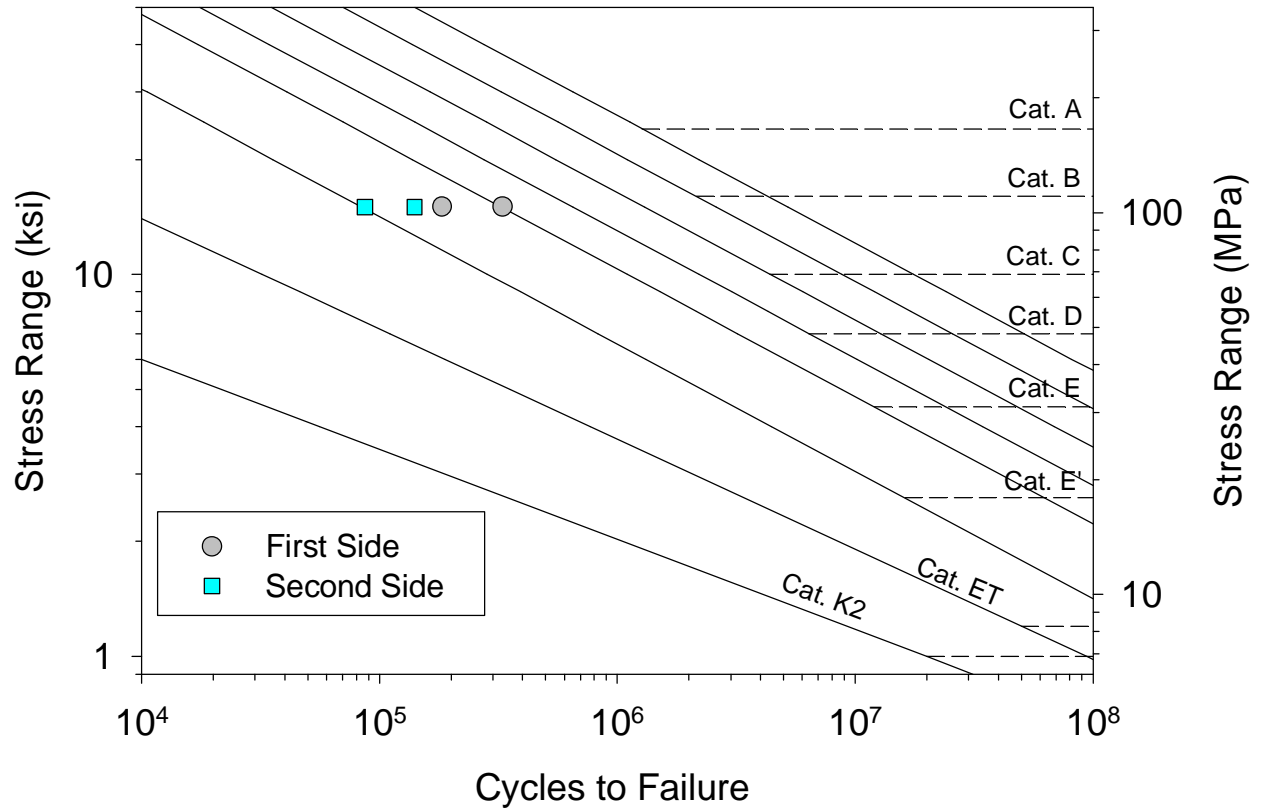


Figure 7.10 S-N plot of thick base plate socket connection with 4.76 mm (3/16 inch) pole wall thickness.

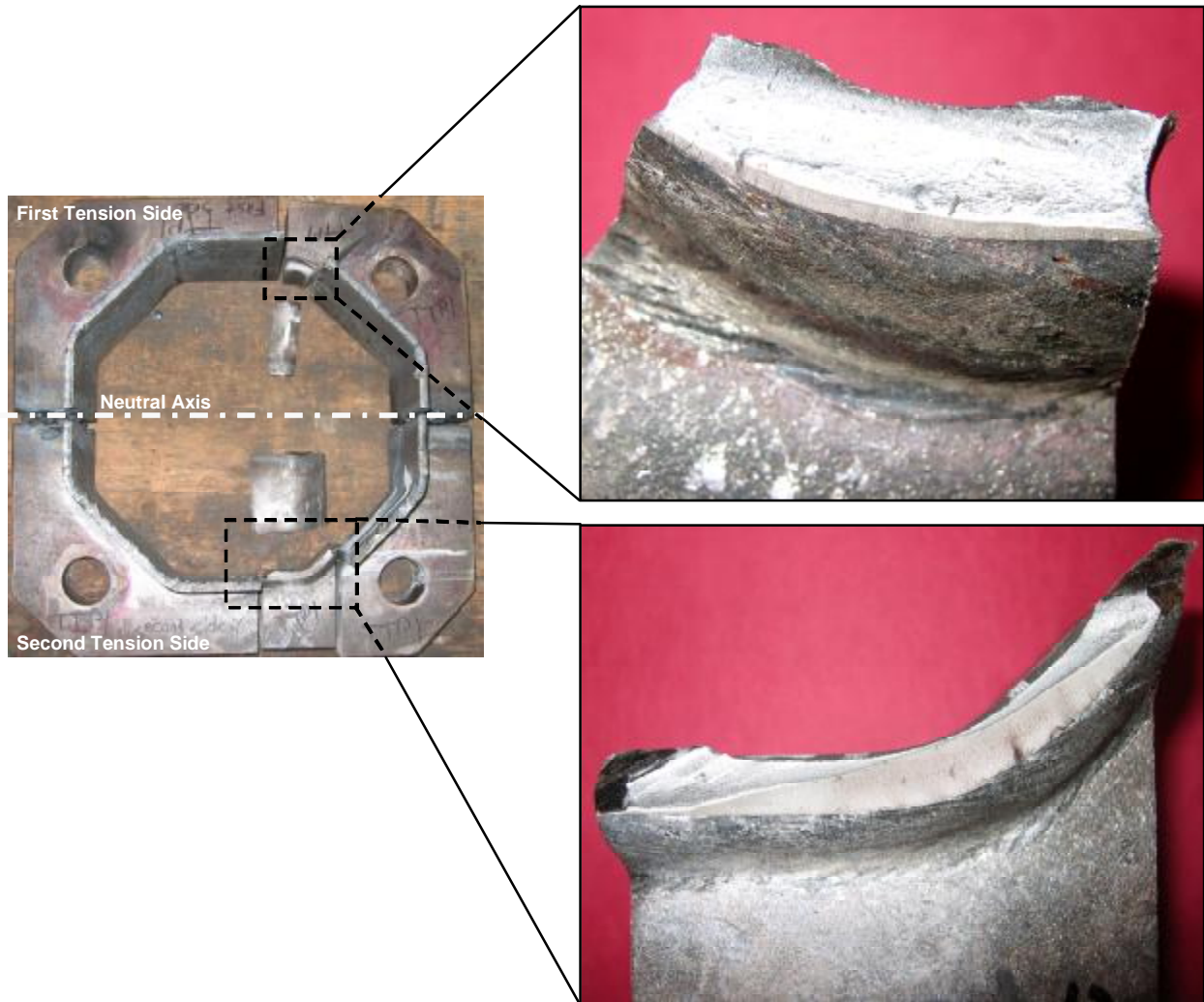


Figure 7.11 Crack surfaces of excavated Pole 2 socket.

7.2 Type I Box Connections

The box connections could only be cracked in Frame 1 for out-of-plane and 45 degree loading. For in-plane loading, the pole socket connection cracked prior to the box connection, and in-plane cycling had to be continued in Frame 3.

The original testing matrix was only going to fatigue three box connections in out-of-plane loading. For out-of-plane loading, cracks were expected to form in one of the two top corners of the box where the side plate intersected the pole tube because the side plate was under tension in this region from the presence of the dead load moment. The first two out-of-plane box connections did crack in a top corner, however the third box cracked in one of the bottom corners. Therefore it was decided to forgo one of the 45 degree box tests and conduct a fourth out-of-plane box fatigue test. The fourth out-of-plane box cracked in the bottom corner,

therefore it was concluded there was no bias for out-of-plane cracking in the box connection between the top and bottom corners where the side plate intersected the pole. In the one 45 degree specimen, the crack formed the same fashion, but formed on a top corner of a side plate/pole intersection. A typical crack in the box connection from out-of-plane loading is shown in Figure 7.12. Also shown in this figure is a cross-section of the crack surface, attained by excavating out the crack with a bandsaw. All the cracks from the out-of-plane and 45 degree loading cases were opened up and all demonstrate similar cracking patterns, where the crack grew elliptically into the thickness of the pole tube, but never grew through-thickness.

For in-plane loading, only a small number of cycles were accumulated in Frame 1 because the pole socket connection cracked and cycling had to cease on the box connection. Cracks were expected to form at the corners of the side plates where they intersect the pole, as was found in the Wyoming fatigue tests described in Chapter 3. Cycling continued in Frame 3 which was exclusively constructed to load the box connection by minimizing the load transfer through the pole's socket connection. The first specimen tested in Frame 3 was T1P2 and shown in Figure 7.13 are the cracks that formed at the bottom intersection between the side plate and the flange plate. The cracks originated at the weld root and grew outwards. Observation of the next specimen, T1P1, showed the side plates were buckling out-of-plane at the bottom of the side plate where the side plate was transferring compression. This deformation mode is shown in Figure 7.14 showing that as the side plate buckles away from the pole, the weld root is opened up between the side plate and flange plate, indicating this crack is primarily a mode I crack. For fabrication reasons, the flange plate is first welded to the pole, then the side plates are welded to the pole and flange plate. Unfortunately, this welding sequence leaves an exposed weld root with no opportunity to place a reinforcing fillet weld, and the unevenness of the weld root spawns fatigue initiation sites. The second in-plane box connection, T1P1, initiated cracks within 100,000 cycles at the bottom corner of the side plates where it intersected the flange plate. However, the crack could only be observed by looking from the back of the pole, upward into the inside of the box connection, not a likely position for an inspector to find cracks. The failure criterion for this project was a 25.4mm (1 inch) long observable crack, but this was modified to include a crack observable from the outside of the specimen. These cracks did eventually come to the surface, but never propagated longer than 25.4 mm (1 inch). Inspection was conducted at the other welded details as the crack growth seemed to cease at the bottom corner of the side plate/flange plate intersection. This inspection found four other cracks to be growing, and all the cracks are shown in Figure 7.15. The third specimen, T1P3 was the last specimen, and like T1P1, it also immediately initiated cracks at the bottom corner of the side plate/flange plate intersection within 100,000 cycles. However, this crack did not reach failure criterion prior to two cracks forming in the top corners of the flange plate/pole intersection, as shown in Figure 7.16.

The 2001 Specifications require four fatigue design checks for box connections, and these checks are outlined in Figure 7.17. First the weld adjoining the side plate to the flange plate is a Category E' detail because it is a transversely loaded fillet weld. Two, the stresses in the pole below the box should be compared to Category E. The last two checks are for the intersection between the side plate and pole. The code requires the stress range in the side plate be checked against Category ET and then the side plate stress range can be transformed into a punching shear stress range in the pole wall which can be compared to Category K₂. The punching shear stress range multiplies the side plate stress range by the ratio of the side plate-to-pole thickness and an

ovalizing parameter dependant upon the loading direction. The ET and K_2 fatigue designations are derived from fillet-welded tube-to-tube connections where a smaller diameter brace member intersects with a larger diameter chord member. In the case of the box connection, the side plate is considered the brace member, while the pole can be interpreted as the chord member. The stress ranges to be presented will follow the methodology of the 2001 Specifications to gain insight if Minnesota's box connections are being conservatively or unconservatively designed. Nominal stress ranges can be easily calculated at the intersection plane between the flange plate and the pole using the moment of inertia of the weld group adjoining the flange plate to the pole. However, it should be noted this calculation produces stresses normal to the flange plate and cannot be interpreted as the stresses in the side plates because they incline towards the pole. The stress ranges normal to the flange plate are presented for all eight specimens in Table 7.4. A second set of stress ranges are presenting in bold face for the specimens cycled in out-of-plane and 45 degree loading. In these two loading cases, cracks occurred at the corners of the side plate, in the pole wall, indicative of a punching shear failure according to the 2001 Specifications. Therefore, the boldface stress ranges represent the transformed stress range normal to the flange plate into the membrane stress range in the side plate, and finally turned into the punching shear stress range in the pole wall. For in-plane loading, the majority of cracks occurred near the intersecting region between the pole and flange plate, which is supposedly a Category E detail, and the stress ranges normal to the flange plate are sufficient for the fatigue analysis. The fatigue data is plotted against the AASHTO S-N curves in Figure 7.18. For in-plane loading, the stresses normal to the flange plate are plotted, and for out-of-plane and 45 degree loading, the punching shear stress range is plotted. Since cracking occurred in the pole for out-of-plane and 45 degree loading, the 2001 Specifications would predict K_2 resistance. The 97.5% survivability curve plots just above the K_2 curve indicating the box connection meets code requirements for out-of-plane and 45 degree loading. For in-plane loading, most cracks formed in the welds between the flange plate and side plates, which according to current specifications should be a Category E' detail. However, the lower bound resistance from the three in-plane specimens plot between Category ET and E', meaning in this direction of loading, the box connection demonstrates resistance about half a category below assumed resistance.

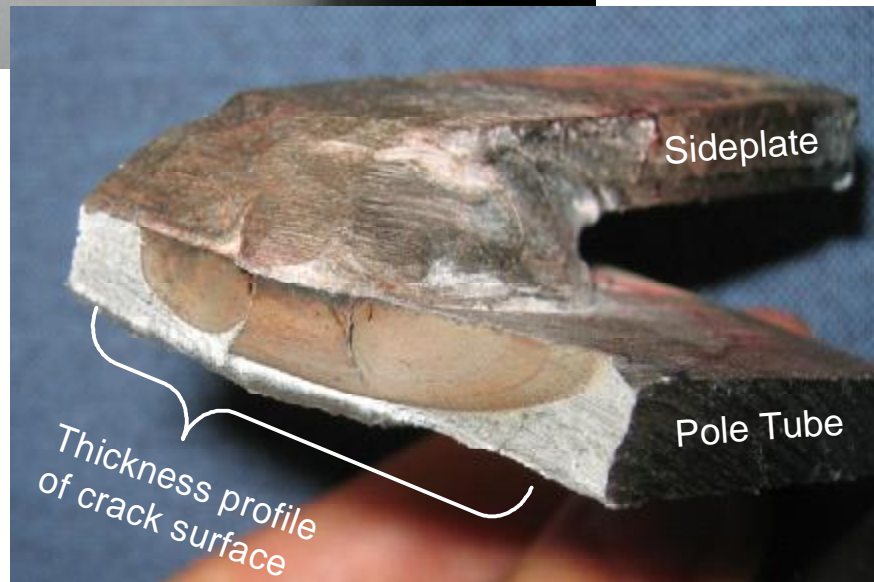
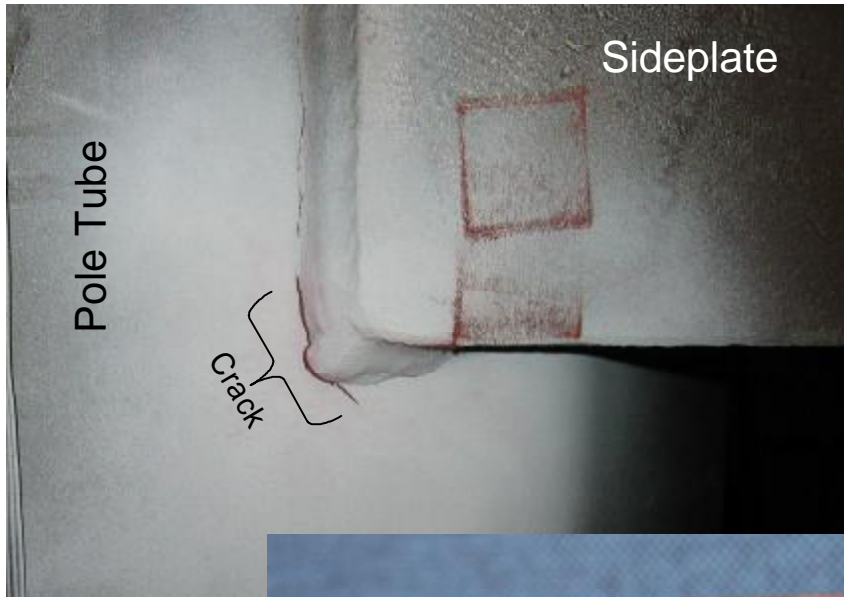


Figure 7.12 Crack in box connection from out-of-plane loading (Pole #6).

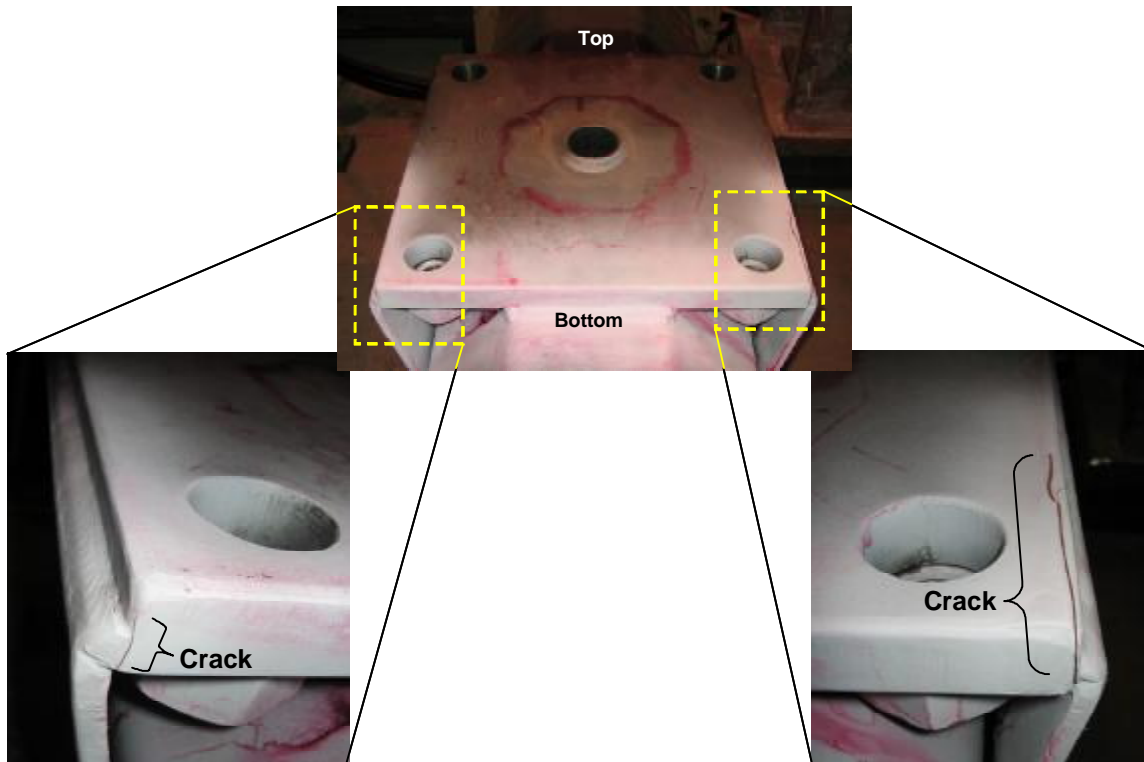


Figure 7.13 Type I box connection cracking from in-plane loading (T1P2)

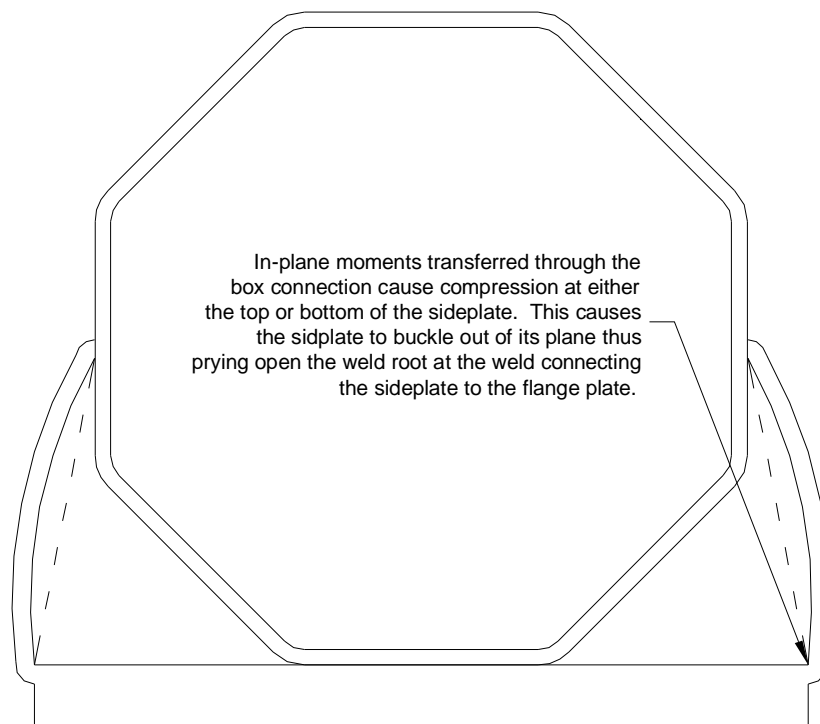


Figure 7.14 Cross-section of box connection depicting side plate deformation under in-plane loading.

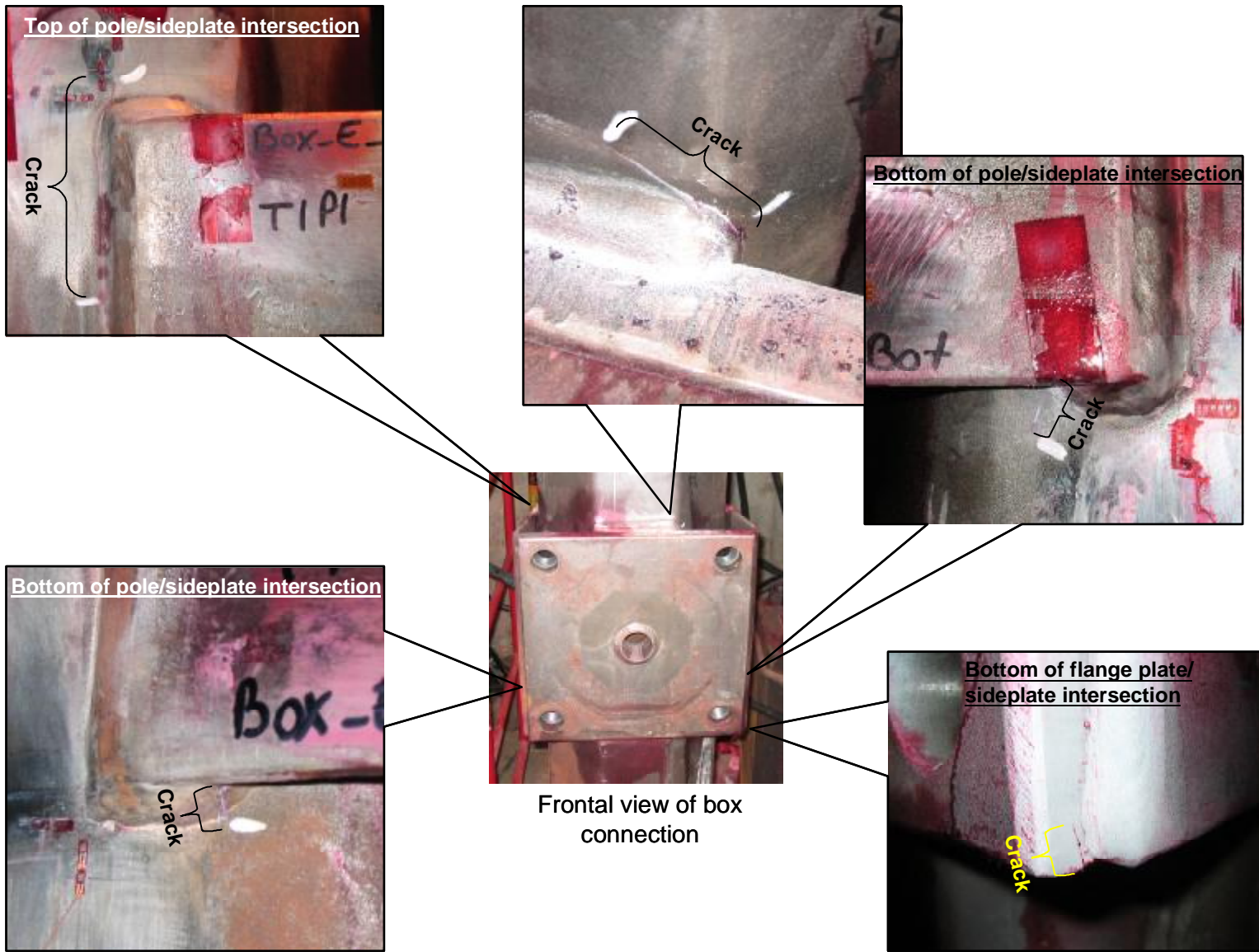
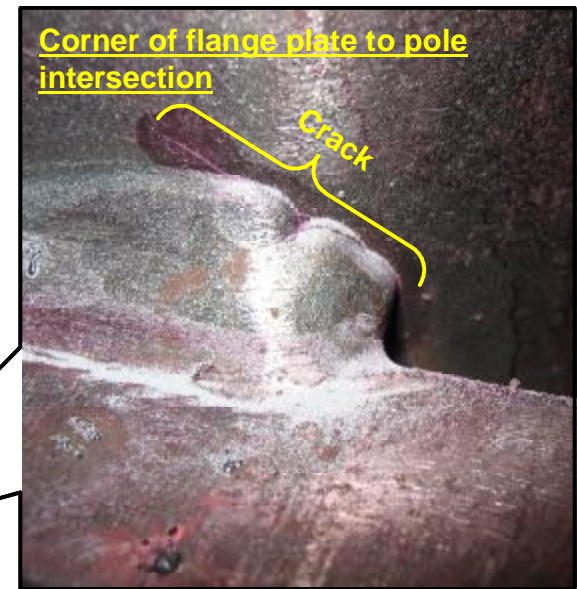
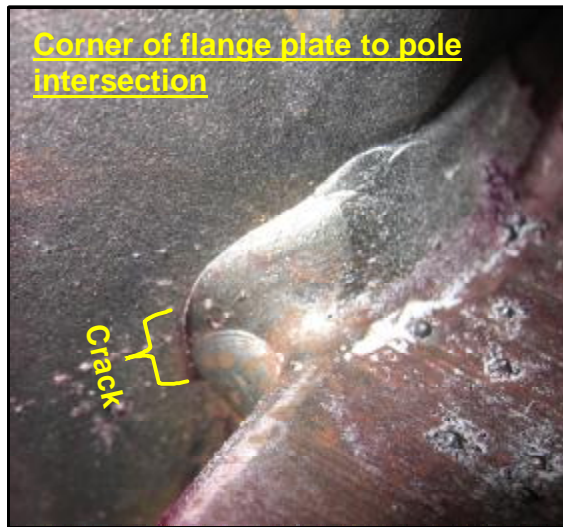


Figure 7.15 Box connection cracks in Type I Pole 1 (T1P1)



Frontal view of box connection

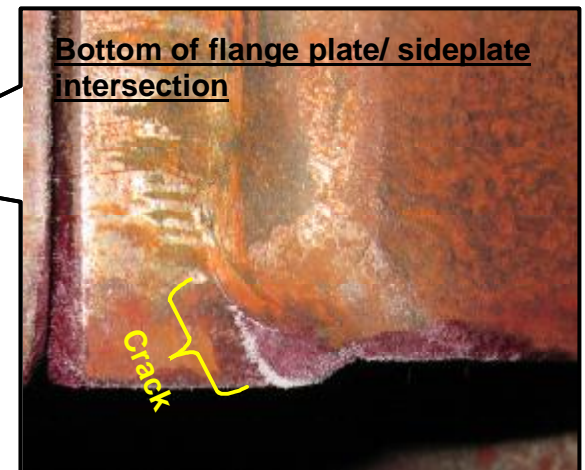


Figure 7.16 Box connection cracks in T1P3

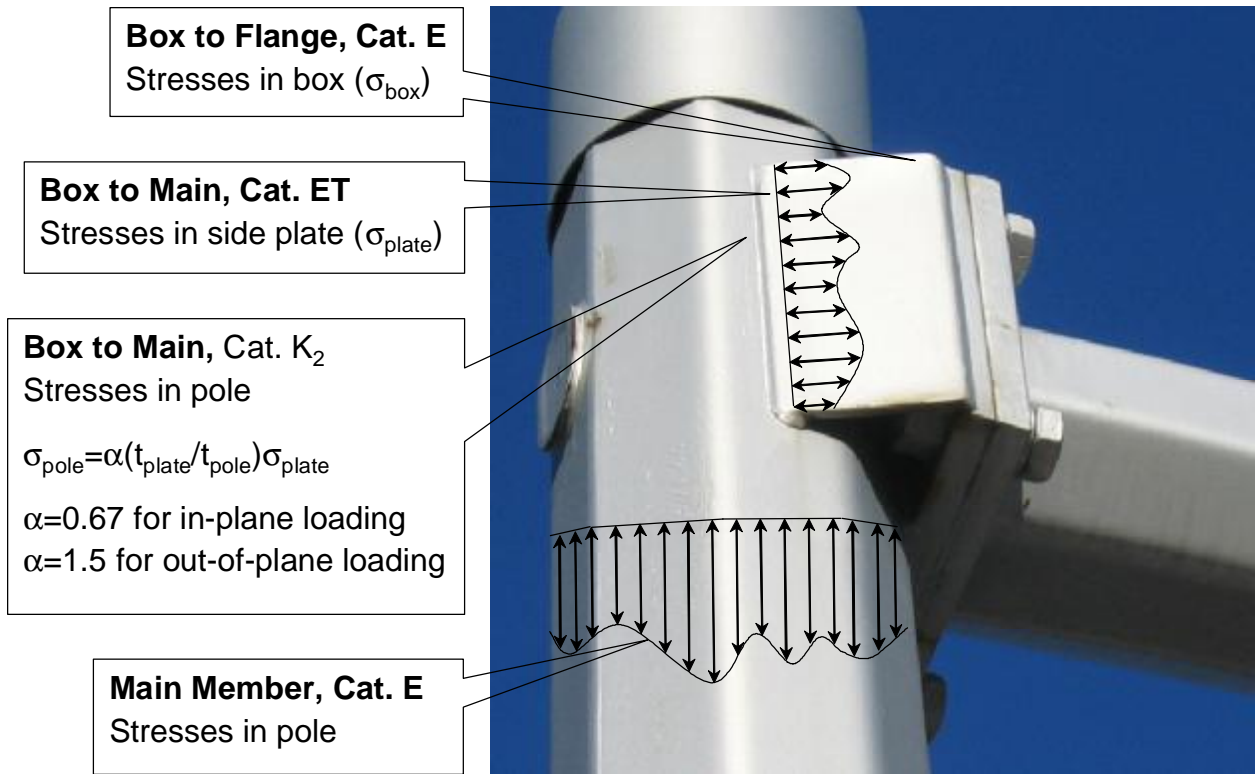


Figure 7.17 2001 Specifications fatigue checks on box connections.

Table 7.4 Fatigue Results for Type I Box Connections

Specimen ^a	Load Frame	Applied Load Range, kN (kip)	Stress Range ^b , MPa (ksi)	Cycles to Failure
T1P1 (IP)	1 and 3	191793 cycles in Frame 1, 26.69 / 53.38 (6.00 / 12.00) 3815885 cycles in Frame 3 -62.28 / -22.24 (-14.00 / -5.00)	31.44 (4.56) ^c	4007678
T1P2 (IP)	1 and 3	1004174 cycles in Frame 1, 34.83 / 46.12 (7.83 / 10.38) 3696203 cycles in Frame 3 -51.15 / -33.36 (-11.50 / -7.50) 9096639 cycles in Frame 3, -53.38 / -31.14 (-12.00 / -7.00) 764707 cycles in Frame 3, -62.28 / -22.24 (-14.00 / -5.00)	18.06 (2.62) ^c	14561723
T1P3 (IP)	1 and 3	3110494 cycles in Frame 1, 34.25 / 46.71 (7.70 / 10.50) 1798020 cycle in Frame 1, 32.47 / 48.49 (7.30 / 10.90) 1647138 cycles in Frame 3, -62.28 / -22.24 (-14.00 / -5.00)	20.96 (3.04) ^c	6555652
T1P4 (OP)	1	-6.67 / 6.67 (-1.50 / 1.50)	10.34 (1.50) 14.96 (2.17)	4002065
T1P5 (OP)	1	-8.90 / 8.90 (-2.00 / 2.00)	13.79 (2.00) 19.92 (2.89)	800000
T1P6 (OP)	1	-8.90 / 8.90 (-2.00 / 2.00)	13.79 (2.00) 19.92 (2.89)	1292565
T1P7 (OP)	1	-8.90 / 8.90 (-2.00 / 2.00)	13.79 (2.00) 19.92 (2.89)	2293739
T1P8 (45)	1	22.24 / 35.56 (5.00 / 8.00)	15.10 (2.12) 15.86 (2.30)	4175643

^a (IP) – in-plane loading, (OP) – out-of-plane, (45) – 45 degree loading

^b Stress ranges were calculated using the moment at the face of the flange plate on the box connection, which correlates to a moment arm distance of 1327.2 mm (52.25 inch) for Frame 1 and 1276.4 mm (50.25 inch) for Frame 3. Stress ranges presented are at the intersection plane between the flange plate and the pole. Stress range were calculated using simple bending equations and the gross moment of inertia of the weld group attaching the flange plate to the pole and side plates; $I_{in-plane} = 31646.1 \text{ cm}^4$ (760.3 in⁴), $I_{out-of-plane} = 34518.1 \text{ cm}^4$ (829.3 in⁴). **For out-of-plane and the 45 degree loading case, these stress ranges were transformed into a membrane stress range in the side plates and multiplied by the out-of-plane ovalizing parameter (1.5) to attain the values in boldface.**

^c Stress ranges presented are equivalent found using Miner's Summation Rule.

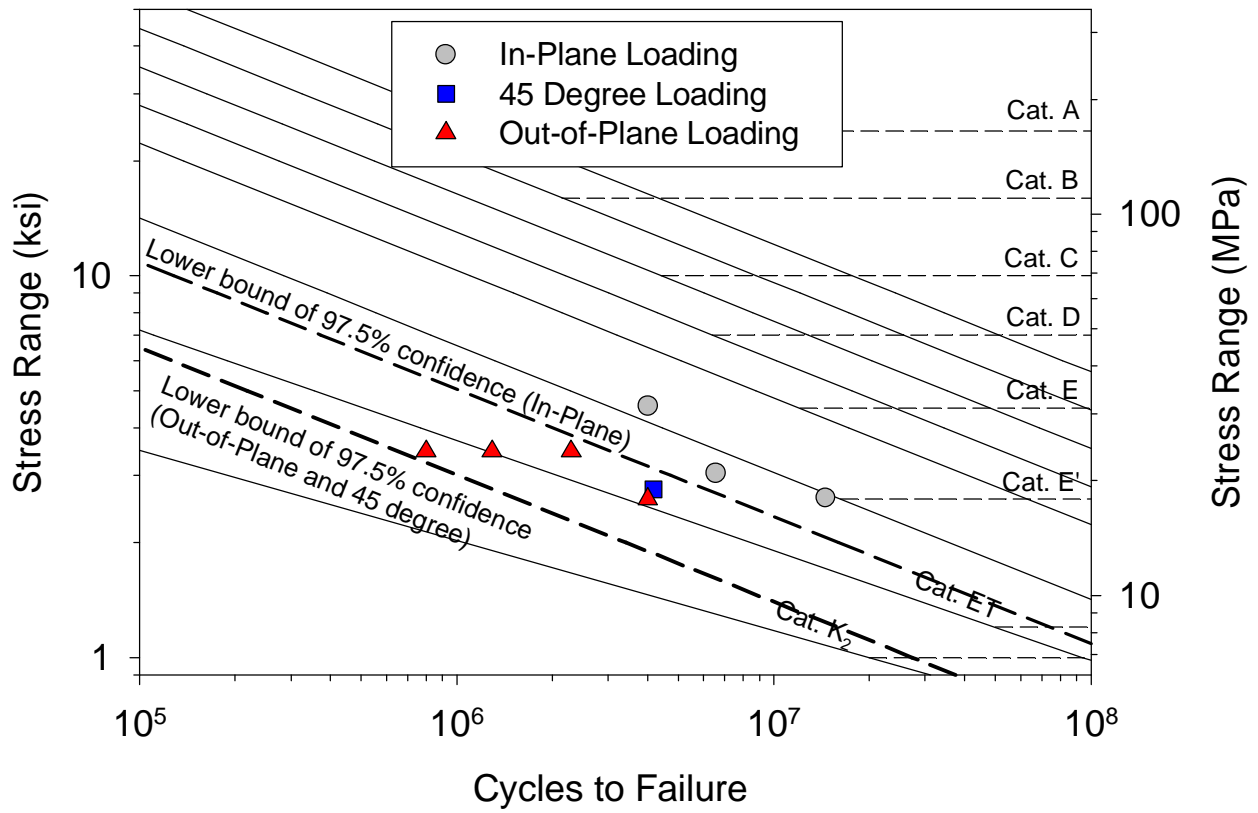


Figure 7.18 S-N plot of Type I box connection fatigue data.

7.3 Type I Mast Arms with Full-penetration Welds

The mast arms with full-penetration welds were exclusively tested in Frame 3. The distance from the centerline of the actuator to the base plate of the mast arm was 1251.0 mm (49.25 inch) in Frame 3. Cracks originated at the two bent corners in extreme tension from bending, though in some cases the failure criterion was only met at one corner. Cracks exposed with magnetic particles can be seen in Figure 7.19. Also shown in this figure is the cross-section of a crack exposed after saw cutting open one specimen. The fatigue striations clearly show how the crack originates at the outside surface of the tube and grows inward, elliptically through the tube thickness.

Like the Type I poles, the connection was cracked, then cycling ceased and the mast arm was unbolted and rotated 180 degrees so the first side cycling in compression was then cycled in tension. No bias was found in the data between the fatigue strength on the first and second side of the same mast arm, therefore, compression cycles have no effect on fatigue life. The fatigue results are presented in Table 7.5 and plotted against the AASHTO S-N curves in Figure 7.20. As seen in Figure 7.20, the 97.5% survivability regression line plotted in-between Category E and E'. However, this regression has a wide scatter band because of the one specimen cycled at a lower stress range having a much longer life. If this one point is neglected, the 97.5% survivability curve plots in-between Category E and Category E', thus the full-penetration mast arm detail should be classified as an AASHTO Category E' detail. In the 2001 Specifications, full penetration welds where the backing ring is continuously welded to base plate, or a two-sided weld after the backing bar is back gouged is classified as a Category E detail. If the backing ring is left in place and not welded to the base plate, the strength is decreased to Category E' because of the unfused notch created by the backing bar. The backing bar on the tested specimens was left in place and neither welded to the base plate, nor the mast arm tube, therefore was only a one-sided weld. The current AASHTO designation seems to be appropriate for the tested geometry.



Figure 7.19 Typical cracks on Type I full-penetration weld mast arm.

Table 7.5 Fatigue Failure Results for Type I Full-Penetration Weld Mast Arms

Mast Arm #	Actuator Min/Max Loads, kN (kip)	Failure Location (see Fig. 5)	Stress Range, MPa (ksi)	Cycles Failure to
1, 1 st side	-31.1 / -53.4 (-7.0 / -12.0)	MA_68 and MA_112	58.88 (8.54)	6997582
2, 1 st side	-22.2 / -62.3 (-5.0 / -14.0)	MA_68 and MA_112	105.97 (15.37)	420785
3, 1 st side	-22.2 / -62.3 (-5.0 / -14.0)	MA_68 and MA_112	105.97 (15.37)	434329
4, 1 st side	-22.2 / -62.3 (-5.0 / -14.0)	MA_68 and MA_112	105.97 (15.37)	242060
1, 2 nd side	-22.2 / -62.3 (-5.0 / -14.0)	MA_68 and MA_112	105.97 (15.37)	420662
2, 2 nd side	-22.2 / -62.3 (-5.0 / -14.0)	MA_68 and MA_112	105.97 (15.37)	372056
3, 2 nd side	-22.2 / -62.3 (-5.0 / -14.0)	MA_68	105.97 (15.37)	298023
4, 2 nd side	-22.2 / -62.3 (-5.0 / -14.0)	MA_68	105.97 (15.37)	267922
* All Type 1 full-penetration welded mast arms were tested in Frame 3. The distance from the centerline of the actuator to the base plate was 1244.6 mm (49 inches). *				

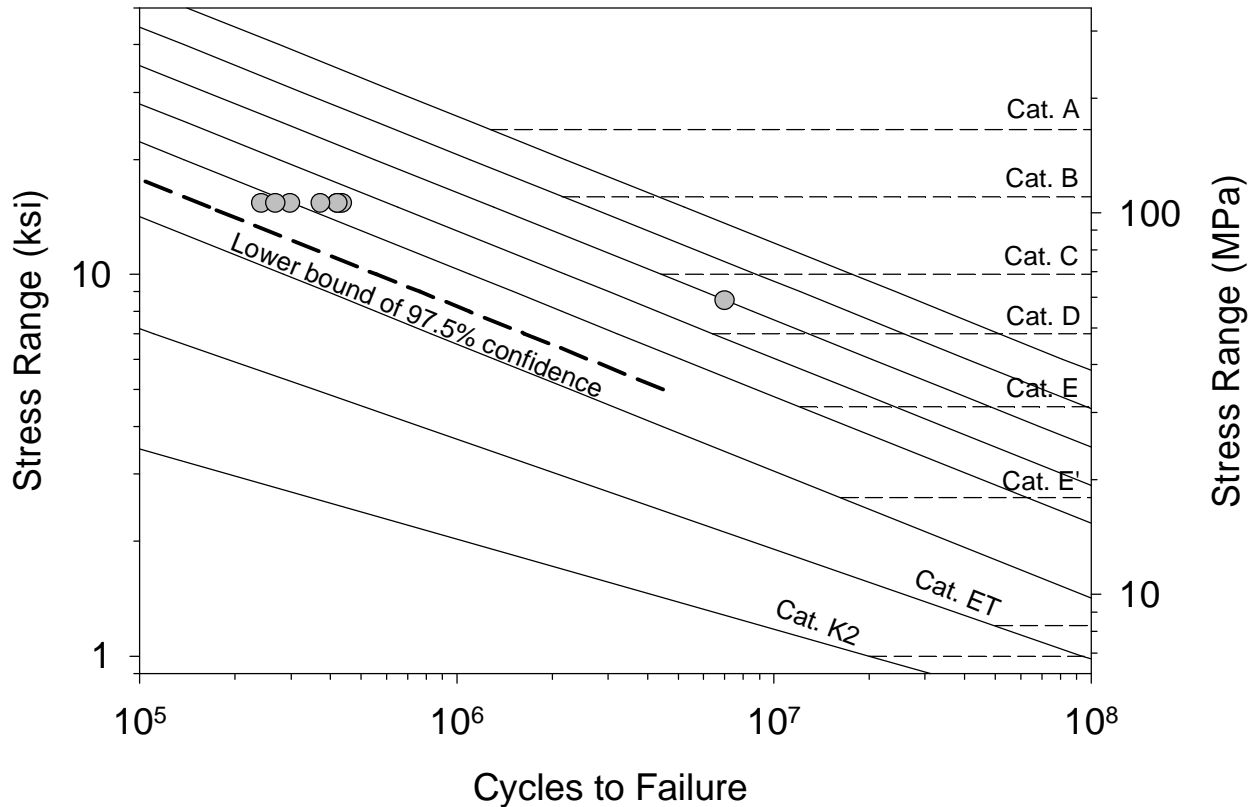


Figure 7.20 Fatigue results of Type I, full-penetration weld mast arm plotted against S-N curves.

7.4 Type I Mast Arm with Gusset Plate Stiffeners

Like the other Type I specimens, each gusset-stiffened specimen was tested twice by cracking one side and then rotating the specimen 180 degrees to crack the opposite side. The gusset-stiffened mast arm specimens were mainly tested in Frame 3, however the fourth specimen had to be tested in Frame 2 because all the in-plane box connections cracked in Frame 3. The distance from the centerline of the actuator to the base plate of the mast arm was 1251.0 mm (49.25 inch) in Frame 3, and the weld toe of the gusset tip was 222.3 mm (8.75 inch) away from the base plate. The moment arm distance of the fourth specimen tested in Frame 2 was increased to 1625.6 mm (64.0 inch) because the loading system changed. All the fatigue results for the gusset-stiffened specimens are tabulated in Table 7.6.

The intent of the gusset plates is to improve the fatigue resistance of an unstiffened socket connection. The gussets increase the section modulus (i.e., lower the stress range) at the socket weld, and move the critical fatigue location to the tip of the gusset. In the 2001 Specifications, AASHTO categorizes the tips of gusset plates as Category E when subjected to specific recommendations that stiffeners should not be detailed less than 101.6 mm (4 inch) long. In all four specimens, the gusset plates never prevented cracking in the corners of the tube, at the toe of the socket weld. When cracks were observed in the socket weld, cycling was ceased and the cracked weld toes were hammer peened with the dead load present. Hammer peening introduces

beneficial compressive residual stresses that aid to stop crack growth. Hammer peening the cracked weld toes allowed cycling to continue until the gusset plates cracked. Figure 7.21 shows a macro-etch of a cross-section cut right through a cracked gusset plate, showing how the crack grows into the tube wall, originating at the weld toe at the tip of the gusset plate. Most of the gussets cracked in this manner. Two specimens simultaneously cracked at the gusset tip and at the base of the gusset where it is welded to the base plate. These two types of cracks are shown in Figure 7.22. There was one anomalous crack that formed on the first side of third specimen, at one of the bent corners, and grew in the longitudinal seam weld. This crack is shown in Figure 7.23 and shows the fatigue striations pointing to the seam weld toe on the inside of the tube.

All the fatigue data is plotted against AASHTO S-N curves in Figure 7.24. The 97.5% survivability line for the socket weld plots between Categories ET and E'. But recall that the pole socket connections demonstrated K_2 resistance, therefore since the gusset-stiffened socket welds came in one category higher, the gusset plates are being activated. However, the gussets should have prevented the socket weld from cracking, so it can be presumed the gussets are not 100% activated since cracking did occur in the socket weld. Provided the socket weld has adequate fatigue resistance, the tips of the gusset show a lower bound resistance just below Category D. However, the true resistance would have to be reported as the next lowest category, or Category E as currently predicted by the 2001 Specifications.

Table 7.6 Fatigue Results for Gusset-stiffened Mast Arms.

Mast Arm #	Actuator Min/Max Loads, kN (kip)	Failure Location	Stress Range, MPa (ksi)	Cycles to Failure
1, 1 st side ^a	191793 cycles in Frame 1 ^b 26.69 / 53.38 (6.00 / 12.00)	MA_68 and MA_112 ^d	28.61 (4.15) ^c	1642305
	1004174 cycles in Frame 1 ^b 34.70 / 46.26 (7.80 / 10.40)			
	446338 cycles in Frame 1 ^b 34.25 / 46.35 (7.70 / 10.42)			
2, 1 st side	620057 cycles at -57.83 / -26.69 (-13.00 / -6.00)	Tip of gusset plate ^d	77.91 (11.30) ^c	1300949
	680892 cycles at -62.28 / -22.24 (-14.00 / -5.00)			
3, 1 st side	-62.28 / -22.24 (-14.00 / -5.00)	MA_68 and MA_112 ^d	71.57 (10.38)	171695
		Seam weld crack at MA_68	71.57 (10.38)	1311495
		Base of gusset plate	95.84 (13.90)	1311495
4, 1 st side ^e	-47.68 / -17.04 (-10.72 / -3.83)	MA_68 and MA_112 ^d	71.22 (10.33)	186036
		Tip of gusset plate ^d	89.63 (13.00)	1230085
2, 2 nd side	-62.28 / -22.24 (-14.00 / -5.00)	MA_68 and MA_112 ^d	71.57 (10.38)	223987
		Tip of gusset plate	85.84 (12.45)	1236189
3, 2 nd side	Cycling was not performed on second side because cracking was too severe from the first side.			
4, 2 nd side ^e	-47.68 / -17.04 (-10.72 / -3.83)	MA_68 and MA_112 ^d	71.22 (10.33)	157123
		Tip of gusset plate	89.63 (13.00)	1201278
		Base of gusset plate	95.35 (13.83)	1201278
^a -This mast arm was used to cycle eight Type I poles in Frame 1 and one box connection in Frame 3, therefore the stress range calculation would be too convoluted to calculate for the second side cracking as this mast arm was cycled in three different directions. Therefore only the first crack experienced will be reported. ^b -The distance from the actuator centerline to base plate in Frame 1 is 1301.8 mm (51.25 inch). ^c -Reported stress range is an equivalent range calculated using Miner's Summation Rule. ^d -Socket weld toe was hammer peened under dead load prior to continued cycling. ^e -4th mast arm was tested in Frame 2 and moment arm increased to 1625.6 mm (64.0 inch).				

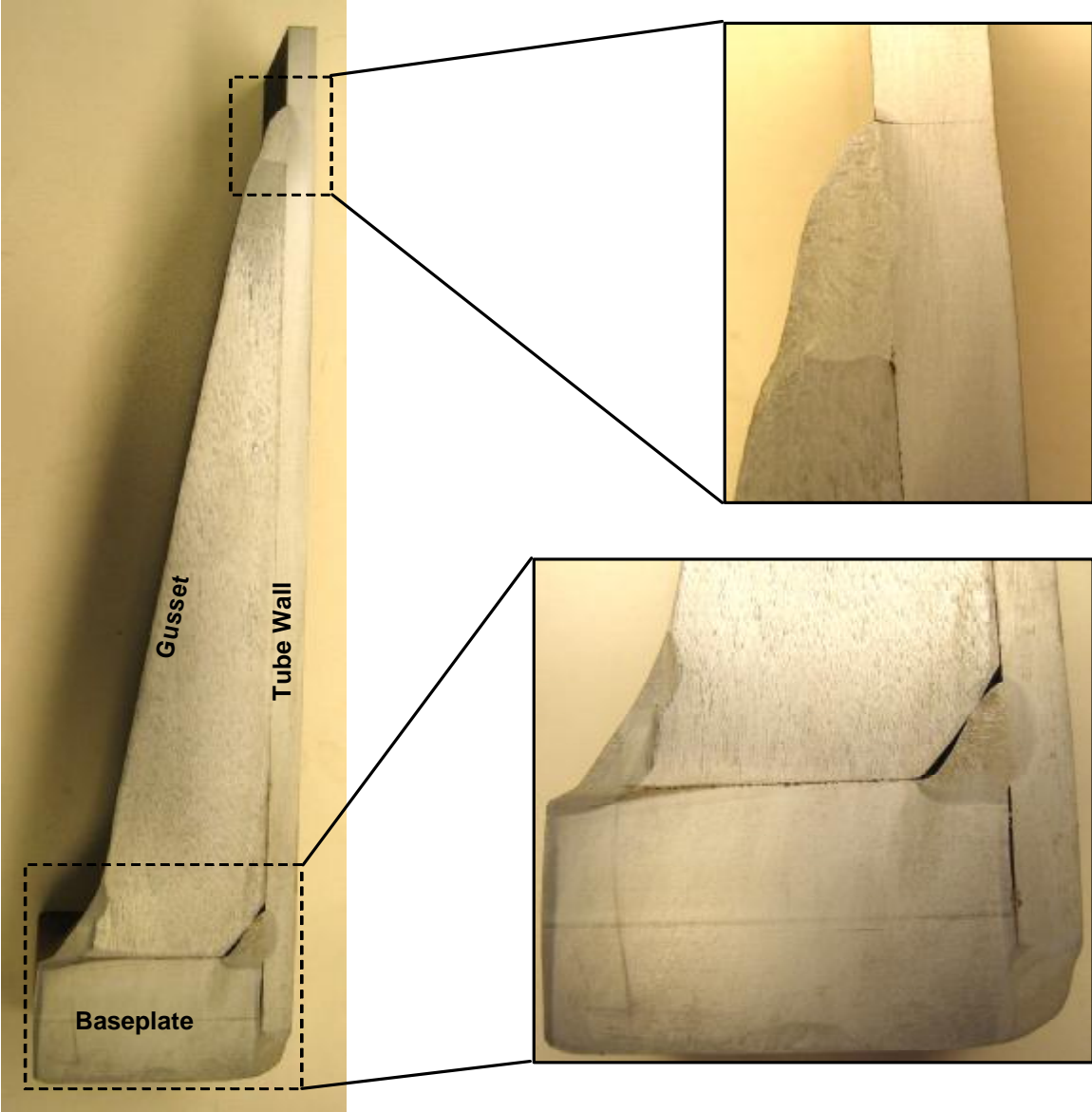


Figure 7.21 Macro etch of gusset stiffener cross-section.

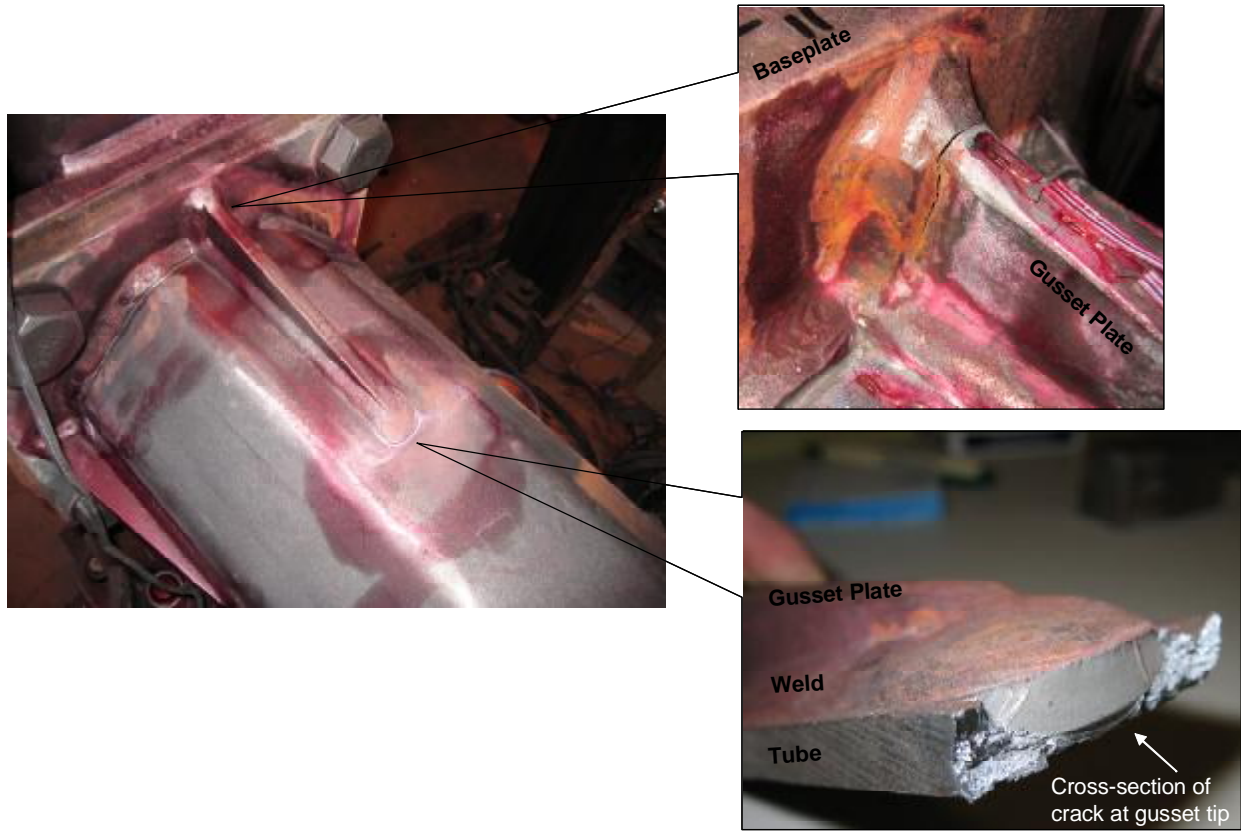


Figure 7.22 Typical cracks found in gusset plates.

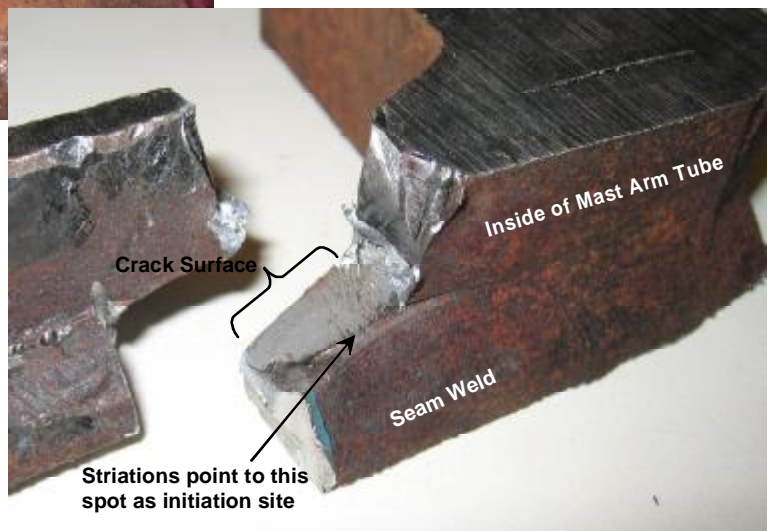
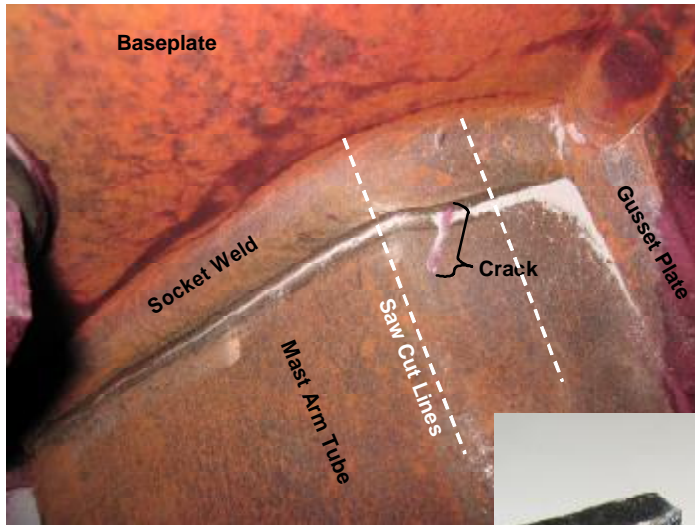


Figure 7.23 Seam weld crack in gusset-stiffened specimen.

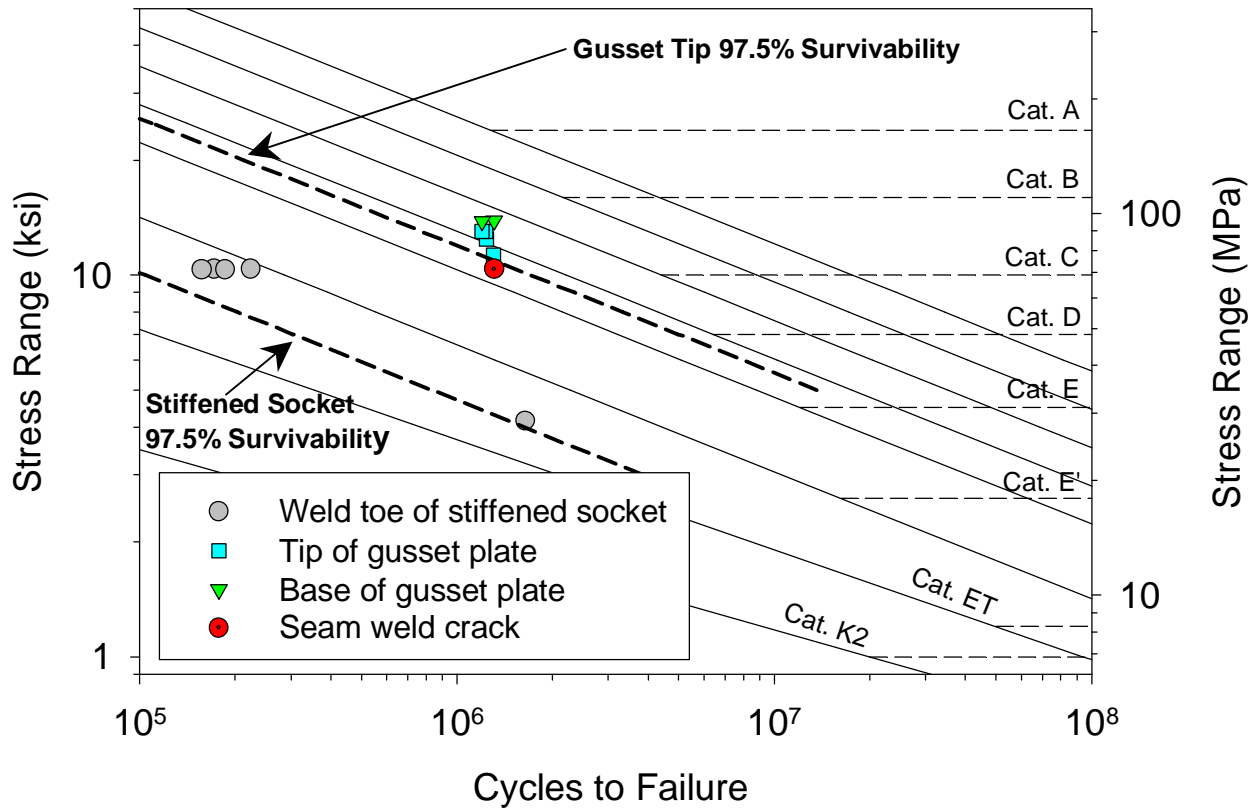


Figure 7.24 S-N plot of gusset-stiffened mast arm specimens.

7.5 Type I Transformer Base Cracking

Transformer bases were used in testing to represent true boundary conditions in the pole socket connections, and the bases were never instrumented during any testing. In the testing of the Type I specimens, two transformer bases cracked and the results of these two bases are presented herein.

The first transformer base to crack was from cycling in Frame 1. The access hole in the transformer base was orientated such that the access hole was on the neutral bending axis from the in-plane dead load moment. During the testing of the fourth Type I pole/mast arm specimen, a crack formed in a top corner of the access hole. The previous in-plane cycling from the first three specimens was probably inconsequential since the access hole was located near the neutral bending axis. However, the out-of-plane loading on the fourth pole induced a torque on the transformer base, thus causing large shearing deformations of the access hole. Since the crack emanated from the corner of the access hole at a 45 degree angle shown in Figure 7.25, indicates there was diagonal tension at the corner of the door, which is primarily caused from the twisting moment.

Table 7.7 shows the complete load history imposed upon the first transformer base until the crack formed. Three moments are also presented and were calculated at the level the crack formed. Since this crack most likely formed from the twisting moment, there is no good way to convert this loading history into a nominal stress range to compare against the AASHTO fatigue curves. Therefore, just the load history is presented. A plate was fillet welded into the opening of the access hole and the crack tip was drilled out so cycling could continue. No more cracking was experienced from the retrofit.

The second transformer base was devoted to Frame 2 and experienced cracking in the shell of the transformer base at the weld toe adjoining the lower base plate to the shell of the transformer base. A picture of this crack can be seen in Figure 7.26. The base was orientated such that the access hole was placed on the extreme compression bending fiber. The base was subjected to variable amplitude loading which is summarized in Table 7.8. In bold at the bottom of this table are the total number of accumulated cycles, as well as an equivalent stress range calculated using Miner's summation rule. However, in the stress range calculations, the moment of inertia of the shell at the level of the crack, DID NOT account for the presence of the access hole. This is important for future comparisons using this one data point. Though not shown, plotting this one data point against the AASHTO fatigue curves demonstrates strength just below Category E' resistance.

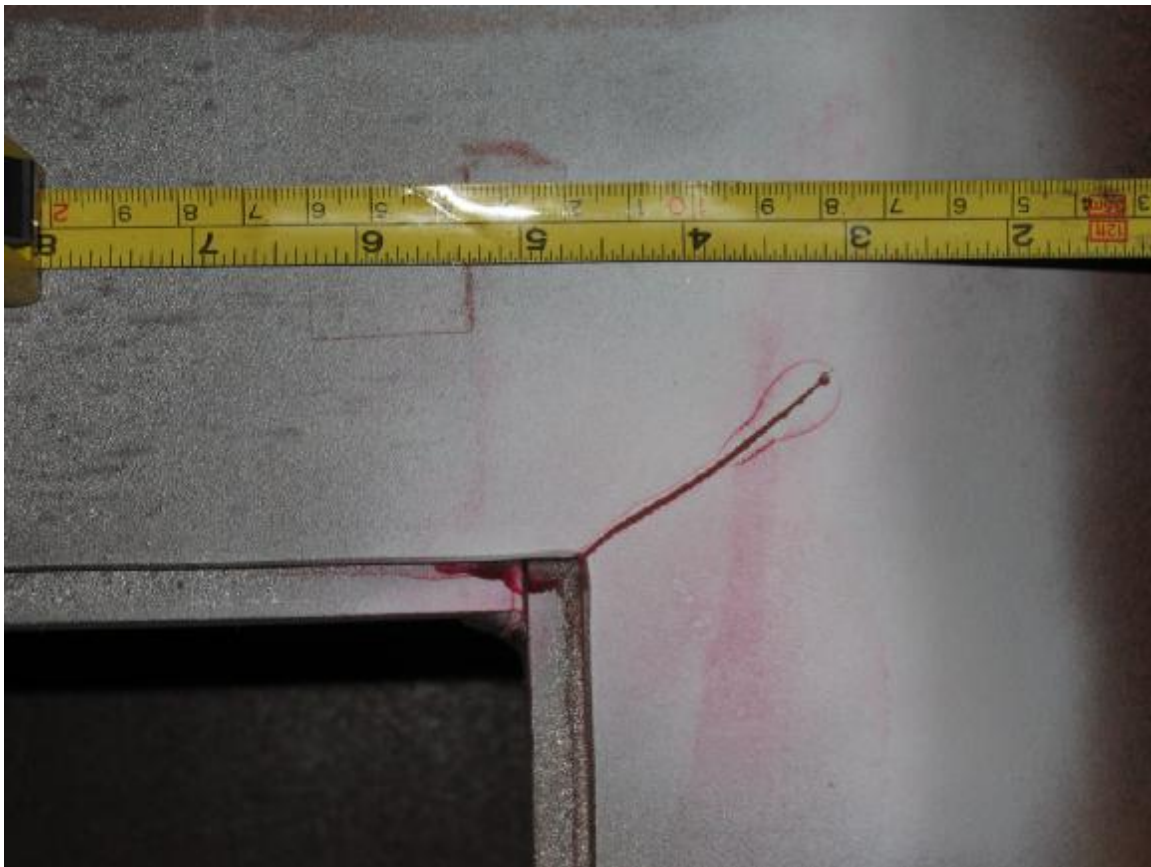


Figure 7.25 Crack in first transformer base originating from access hole.

Table 7.7 Loading History on First Transformer Base

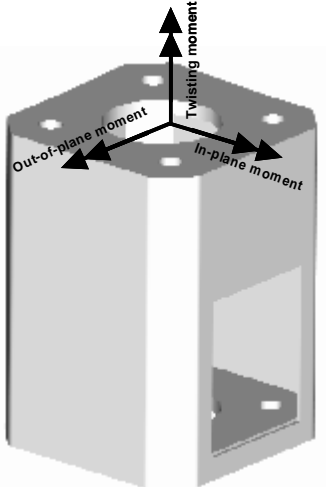
	Cycles	Actuator Loads, kN (kips)	In-plane Moment Range, kN-m (kip-in)	Out-of-plane Moment Range, kN-m (kip-in)	Twisting Moment Range, kN-m (kip-in)
	191793	26.69 / 53.38 (6.00 / 12.00)	40.7 / 31.3 (360.0 / 720.0)	Not Applicable	Not Applicable
	1004174	34.70 / 46.26 (7.80 / 10.40)	52.9 / 70.5 (468.0 / 624.0)	Not Applicable	Not Applicable
	2921100	34.25 / 46.71 (7.70 / 10.50)	52.2 / 71.2 (462.0 / 630.0)	Not Applicable	Not Applicable
	1987414	32.00 / 48.49 (7.20 / 10.90)	48.8 / 73.9 (432.0 / 654.0)	Not Applicable	Not Applicable
	5038549	-6.67 / 6.67 (-1.50 / 1.50)	Not Applicable	-12.3 / 12.3 (-109.1 / 109.1)	-10.2 / 10.2 (-90.0 / 90.0)



Figure 7.26 Crack in second transformer base.

Table 7.8 Load History of Second Transformer Base to Crack

Cycles	Loads, kN (kips)	Stress Range MPa (ksi)
591696	-48.0 / -33.8 (-10.8 / -7.6)	13.17 (1.91)
1106830	-52.5 / -29.4 (-11.8 / -6.6)	21.44 (3.11)
3494630	-47.2 / -35.1 (-10.6 / -7.9)	11.17 (1.62)
4352730	-47.6 / -33.4 (-10.7 / -7.5)	13.17 (1.91)
2120331	-50.7 / -31.1 (-11.4 / -7.0)	18.13 (2.63)
2028816	-53.4 / -28.5 (-12.0 / -6.4)	23.10 (3.35)
124147	-57.4 / -24.5 (-12.9 / -5.5)	30.54 (4.43)

4324934	-50.7 / -31.1 (-11.4 / -7.0)	18.13 (2.63)
1246362	-52.5 / -29.4 (-11.8 / -6.6)	21.44 (3.11)
1658906	-47.6 / -34.3 (-10.7 / -7.7)	12.34 (1.79)
1131798	-53.8 / -28.0 (-12.1 / -6.3)	23.92 (3.47)
2558528	-52.5 / -29.4 (-11.8 / -6.6)	21.44 (3.11)
952442	-53.8 / -28.0 (-12.1 / -6.3)	23.92 (3.47)
Total 25692150		Equivalent 18.55 (2.69)

7.6 Type II Mast arms

In the 2001 Specifications, the nearest detail categorization for the mast can detail is a mast arm fillet welded directly to a pole (i.e., a tube-to-tube connection). The Minnesota design varies slightly in that it utilizes a full-penetration weld, hence it would be thought to have a higher fatigue resistance, though the code does not address this. Assuming the tube-to-tube categorization can be used for the mast can detail, it is considered an ET detail with respect to stress in the mast arm, and K_2 with respect to the punching shear stress range in the mast can. The 2001 Specifications guide designers as how to calculate the punching shear stress range. The punching shear stress range is a function of the stress range in the mast arm and an ovalization parameter that is dependant in the direction of loading (i.e., in- or out-of-plane). Despite the loading condition, cracks always formed at the weld toe, on the mast can side of the full-penetration weld. For in-plane loading, the cracks formed at the MC_68 and MC_112 positions of the mast arm, which correlates to the two bent corner of the tube in extreme tension from bending, though one specimen did form a crack along the entire tube flat as shown in Figure 7.27. For out-of-plane loading all four cracks formed in the same place, MC_158. This location is a bent corner of the mast arm in extreme bending for out-of-plane loading and in the tensile bending zone from the in-plane dead load moment. A picture of an out-plane crack is seen in Figure 7.28. The 45 degree loading crack formed at MC_22 which is a bent corner of the mast arm in the tensile bending zone for both in- and out-of-plane loading.

The fatigue results for the eight, Type II mast arms is presented in Table 7.9. Since the cracking occurred on the mast can side of the weld, this is indicative of a punching shear failure. Table 7.9 presents the stress range in the mast arm, and the punching shear stress range in the mast can using the ovalization parameters from the 2001 Specifications. Since all the mast arms failed via punching shear, Figure 7.29 plots the punching shear stress ranges for all the mast arm specimens against the AASHTO S-N curves. The lower bound of the fatigue data falls in-between the Category ET and K_2 S-N curves, indicating considering this connection as a fillet-welded tube-to-tube connection would be sufficient, with a bit of conservatism.

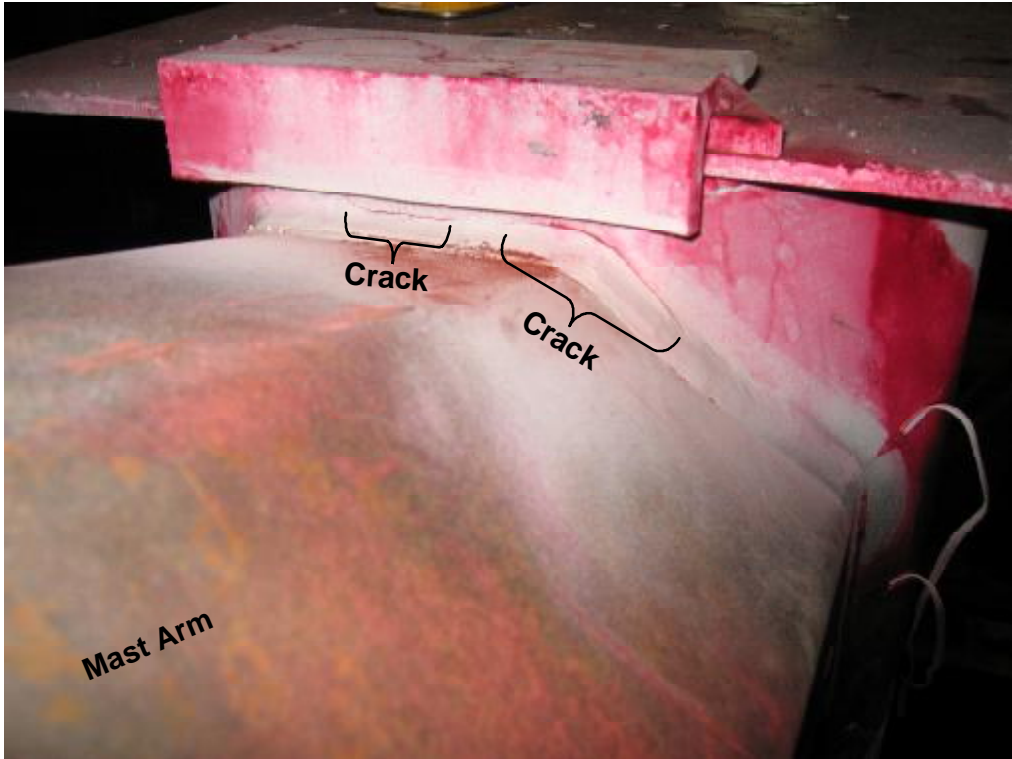


Figure 7.27 In-plane crack for Type II specimen.

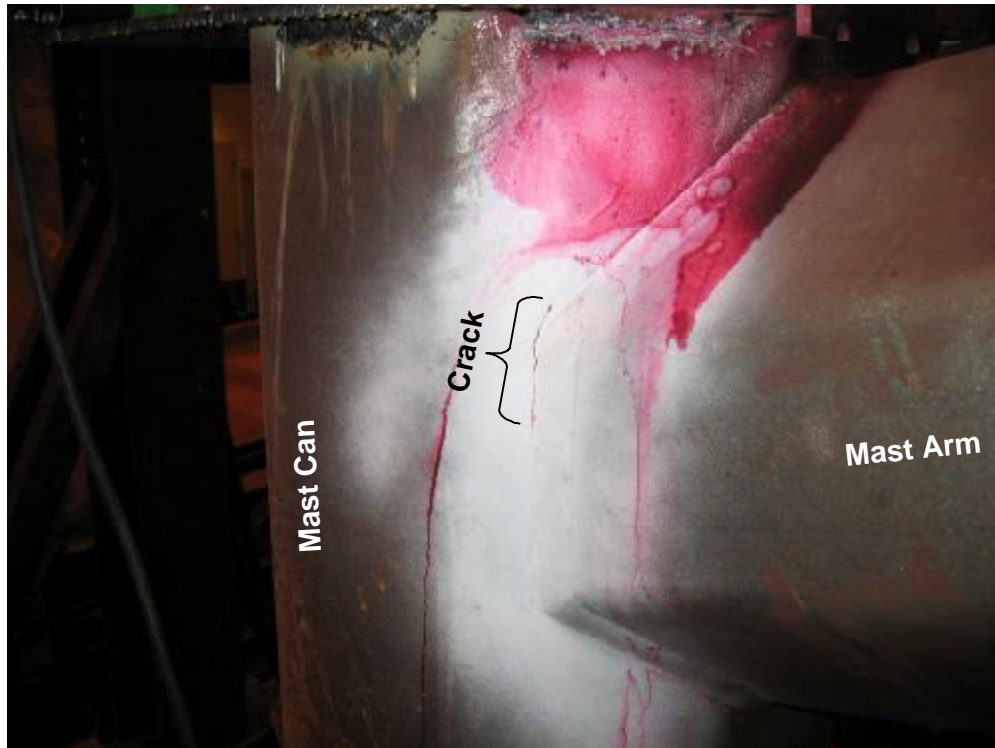


Figure 7.28 Out-of-plane cracks for Type II specimen.

Table 7.9 Fatigue Results of Type II Mast Arms

Pole # and condition	Load Direction ^a	Actuator Min/Max Loads kN (kip)	Failure Location ^c	Mast Arm Stress Range MPa (ksi)	Mast can Stress Range MPa (ksi) ^d	Cycles to Failure
1	IP	32.47 / 45.82 (7.3 / 10.3)	MC_68	37.30 (5.41)	24.99 (3.62)	2399939
2	IP	30.25 / 48.04 (6.8 / 10.8)	MC_68 and MC_112	49.78 (7.22)	33.35 (4.84)	925771
3	IP	30.25 / 48.04 (6.8 / 10.8)	MC_112	49.78 (7.22)	33.35 (4.84)	1224032
4	OP	-6.67 / 6.67 (-1.5 / 1.5)	MC_158	37.79 (5.48)	56.69 (8.22)	120426
5	OP	-5.56 / 5.56 (-1.25 / 1.25)	MC_158	31.49 (4.56)	47.24 (6.84)	497056
6	OP	^b	MC_158	28.34 (4.11)	42.51 (6.17)	1997251
7	OP	-5.56 / 5.56 (-1.25 / 1.25)	MC_158	31.49 (4.56)	47.24 (6.84)	170999
8	45	17.79 / 28.91 (4.0 / 6.5)	MC_22	31.49 (4.56)	47.24 (6.84) ^e	178641

^a - IP (in-plane), OP (out-of-plane), 45 (45 degree loading)
^b - increasing load ranges were used and an equivalent stress range calculated using Miner's rule is reported (Miner, 1945)
^c - see Figure 5.7 for labeling convention
^d - mast arm stress ranges were multiplied by 0.67 to get mast can stress range for in-plane loads and 1.5 for out-of-plane loads as per note b) of Table 11-2 in 2001 Specifications
^e - crack locations were identical for out-of-plane loading and 45 degree loading, therefore the out-of-plane ovalizing parameter was used

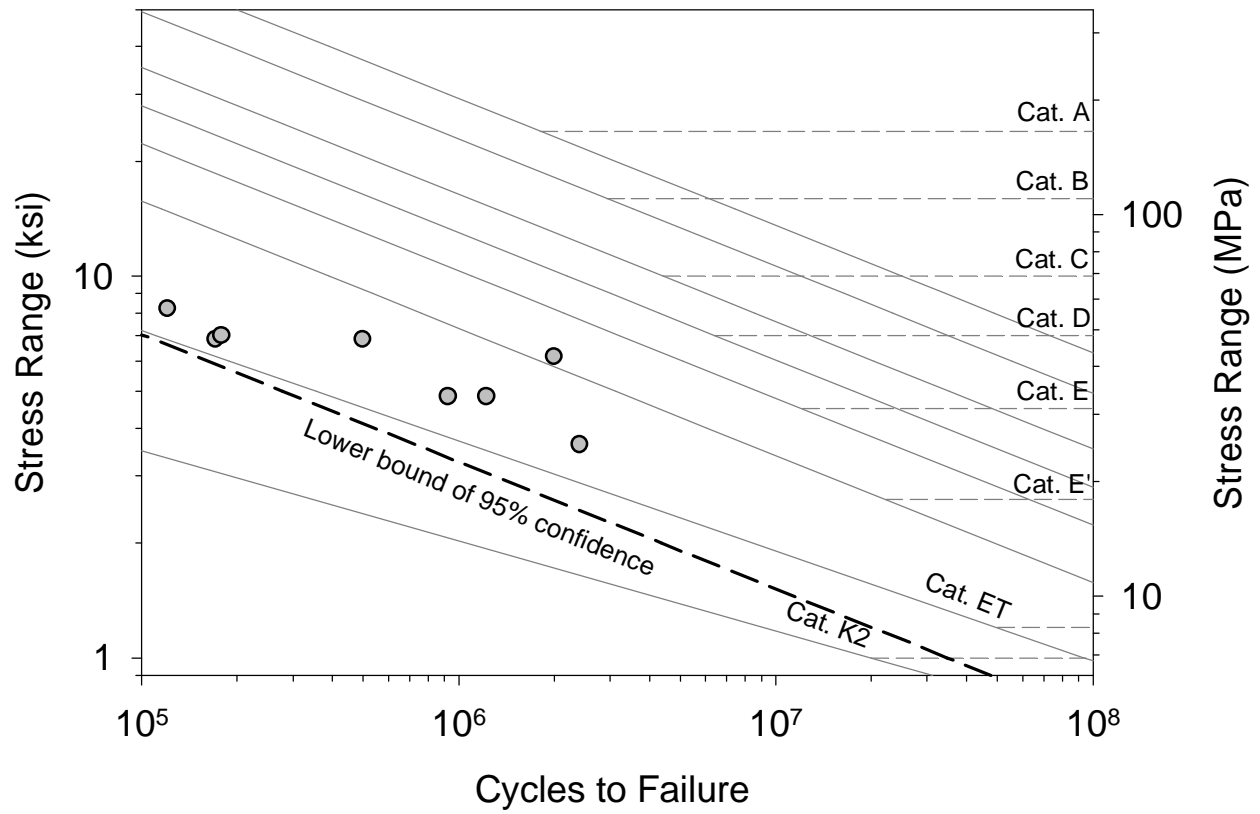


Figure 7.29 S-N plot of Type II mast arm fatigue results.

7.7 Type II Poles

The Type II poles utilized a 4-bolt anchor rod pattern in the base allowing for four different orientations of the of the access hole in the pole base. Two of these orientations had the access hole of the compression side from bending and the other two had it on the tension side. Seven of the poles tested the orientation with the access hole on the tension side and one specimen cycled the access hole on the compression side. These orientations are pictorially shown in Figure 7.30. The poles had two welded details that could potentially crack, the full-penetration weld between the pole and the integrated tapered base and the access hole detail. The full-penetration weld was not expected to crack as it is a Category C detail and would require large load ranges to form cracks. The cracks that did form in all eight specimens formed in one or both of the corners at the bottom of the access hole detail. There were two different ways the cracks propagated in the shell of base once initiated and both are shown in Figure 7.31. The first type of crack initiated at the flame cut corner of the access hole, and grew away from the door into the base shell, this crack is shown on the left side of Figure 7.31. The second type of crack is shown on the right side of Figure 7.31. This type of crack originated at the fillet weld attaching the access hole stiffening ring to the lower base plate of the tapered base. The fillet weld cracked and severed the stiffening ring from the base plate, but because of continuity from welding, this crack was able to keep propagating into the shell of the base. Figure 7.32 shows a cross-section of this second type of cracking, as well as a picture showing how the crack propagated through the cross-section.

When the access door was orientated on the tension side of the pole, the fillet weld adjoining the stiffening ring to the base plate cracked within 50,000 cycles and it was just a matter of time for it to propagate into the shell. The corner of the access door was a reentrant corner, which is a very poor detail for fatigue and it is not surprising cracks developed there, especially after the stiffening ring became severed from the base plate. However, when the access door was cycled in compression, cracks never formed, and the test was terminated after the fifth set of anchor rods cracked. At that point, the pole was unbolted from the foundation plate and rotated placing the access hole in tension. The fatigue results from all the access hole details of the Type II pole specimens are summarized in Table 7.10. This data is further plotted against the AASHTO S-N curves in Figure 7.33. Since the cracks occurred at the bottom of the access door, the stress ranges were calculated using the net section properties of the transformer shell at the level where cracks formed. The two corners of the access door were at different distances from the cross-section centroid, hence the large variation in the stress range calculations which attributes to the large amount of scatter in the data. Three cracks from different specimens were excavated to examine the crack surfaces to see if there was an explainable reason for such different fatigue lives, yet no anomalies were found on the crack surfaces (i.e., inclusions, hydrogen cracks, etc.). The two data points for Pole 4 were neglected in the regression analysis because it is not proper to include runouts and when the specimen finally cracked, it was after the pole was rotated indicating there may have been an effect from the previous compression cycling. The regression performed on only seven of the specimens showed a 97.5% survival curve that intersects but is predominately below the K_2 line, therefore it would be prudent to classify the access door detail as Category K_2 .

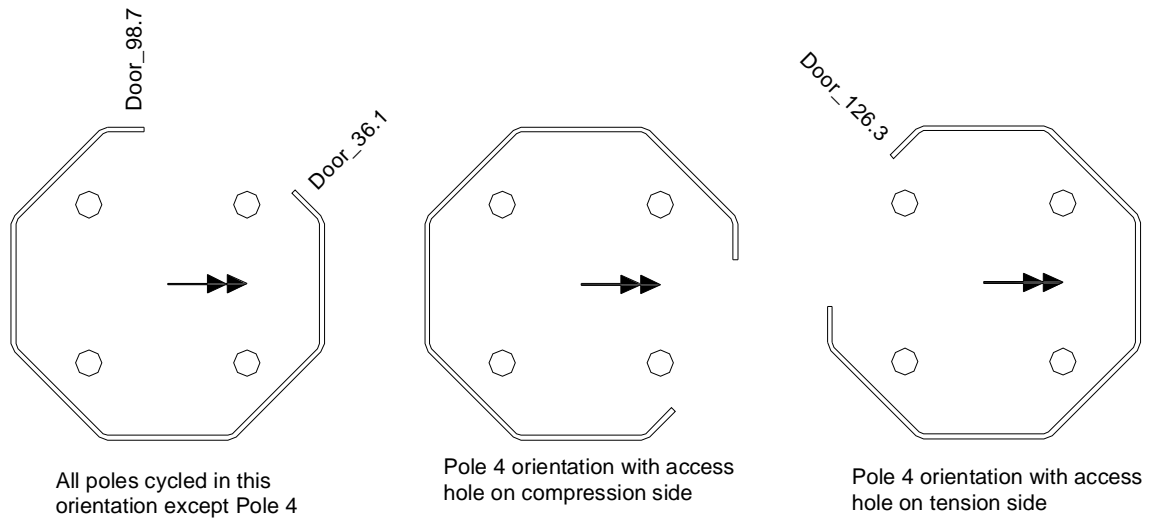


Figure 7.30 Orientations of Type II pole specimens

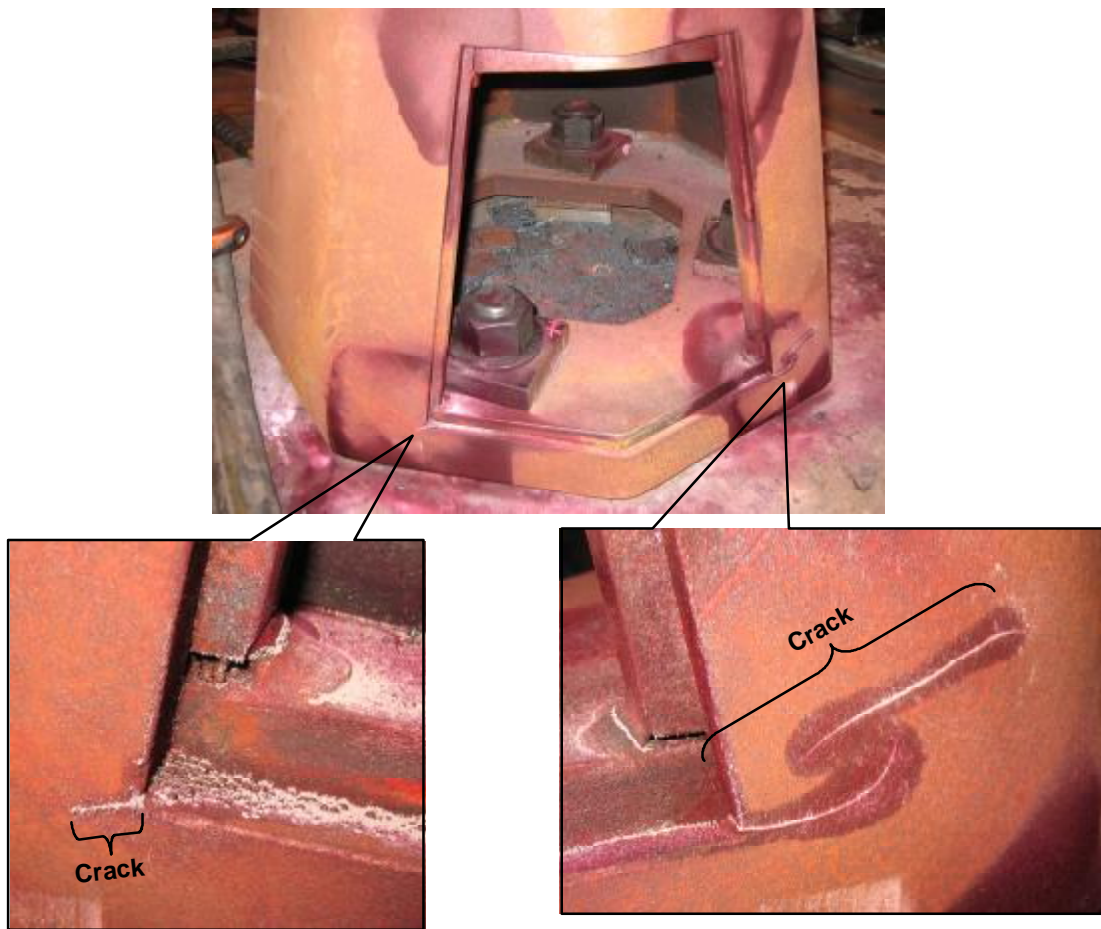


Figure 7.31 Access hole cracks in Type II poles.

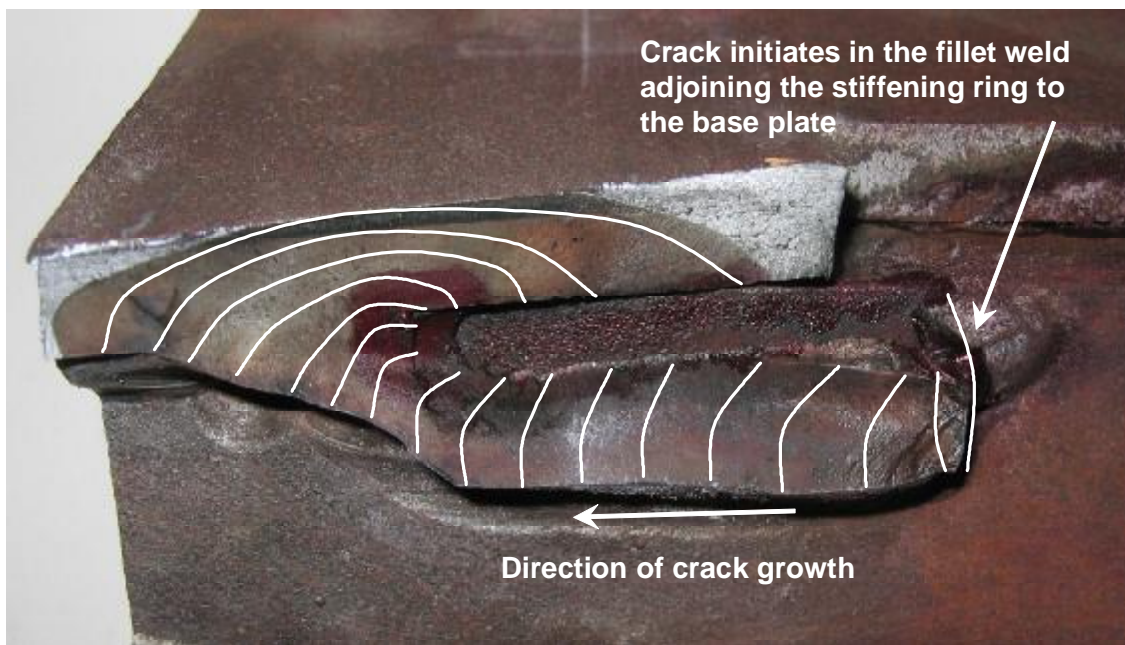
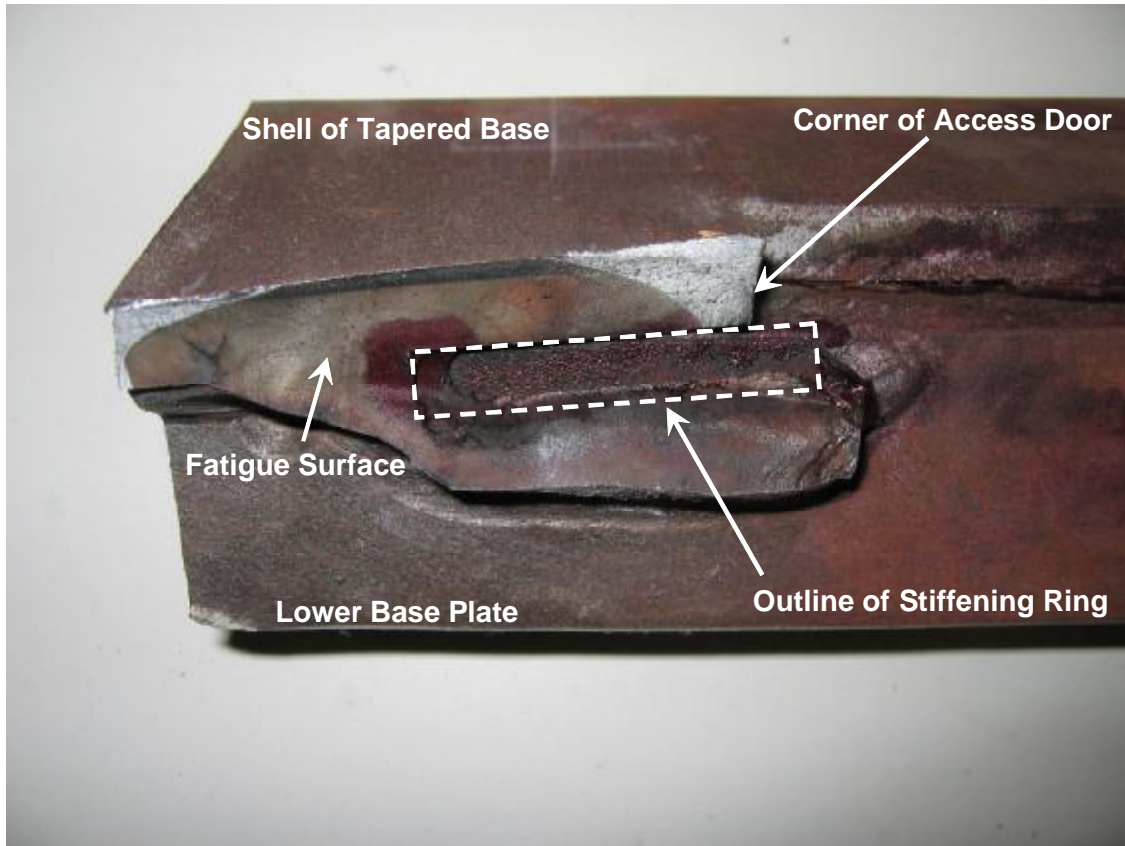


Figure 7.32 Cracking in tapered base shell originating from stiffening ring.

Table 7.10 Fatigue Results for Type II Pole Specimens

Pole # and condition	Actuator Min/Max Loads kN (kip)	Failure Location ^b	Stress Range MPa (ksi)	Cycles to Failure
1 ^a	16.46 / 43.15 (3.70 / 9.70)	Door_36.1	21.44 (3.11)	1006066
2	16.46 / 43.15 (3.70 / 9.70)	Door_36.1	21.44 (3.11)	797137
3	16.46 / 43.15 (3.70 / 9.70)	Door_98.7	32.54 (4.72)	1478924
4 (access hole on compression side)	2929999 cycles at 16.46 / 43.15 (3.70 / 9.70) 2393563 cycles at 14.23 / 45.37 (3.20 / 10.20)	No crack	19.37 (2.81)	5323562
4 ^c	14.23 / 45.37 (3.20 / 10.20)	Door_126.3	21.03 (3.05)	288236
5	14.23 / 45.37 (3.20 / 10.20)	Door_36.1	25.03 (3.63)	333876
6	14.23 / 45.37 (3.20 / 10.20)	Door_98.7	38.00 (5.51)	2935383
7	14.23 / 45.37 (3.20 / 10.20)	Door_36.1	25.03 (3.63)	737712
8	14.23 / 45.37 (3.20 / 10.20)	Door_98.7	38.00 (5.51)	703611
^a – the cycles reported in this table are only from the pole cycling by itself, neglecting all loading from the cycling the eight Type II mast arm specimens. ^b – see Figure 7.30 for failure locations. ^c – the cycles with the access hole on the compression side were neglected when the crack formed on the tension side				

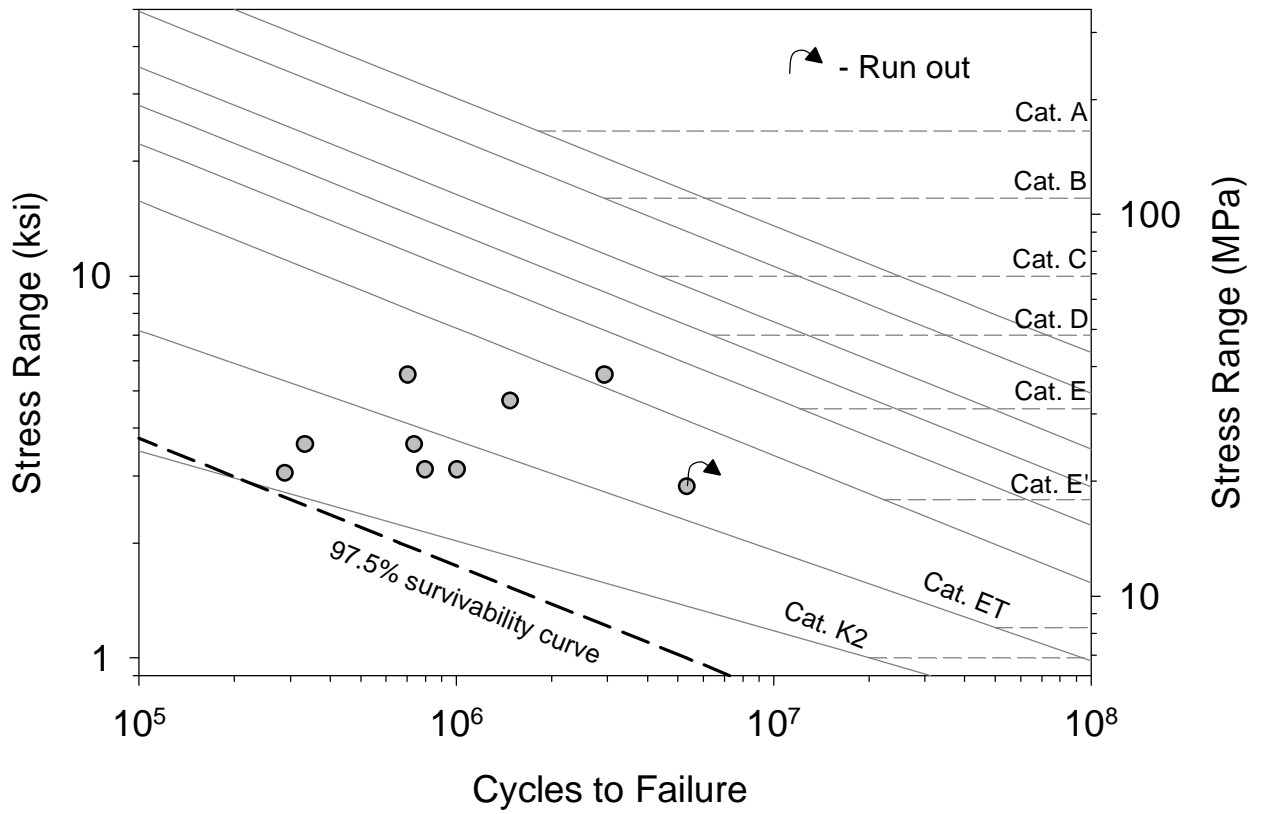


Figure 7.33 S-N plot of Type II pole specimens.

Chapter 8

Conclusions and Recommendations

In the complete testing program for this research project, there were 36 individual specimens tested encompassing eight different welded details used in Minnesota's traffic signal structures. This chapter summarizes those fatigue results and provides recommendations to enhance the strength of these connections.

8.1 Multi-sided Tube-to-Transverse Plate Connections

In total, five different tube-to-transverse plate details were tested. All these connections used 8-sided polygonal tubes with 4-bolt patterns, but two different tube diameters and thicknesses were tested. The tested pole tubes had corner-to-corner dimensions of 355.6 mm (14.00 inch), a pole wall thickness of 7.94 mm (0.3125 inch), and 31.75 mm (1.25 inch) thick base plates in a fillet-welded socket connection. These connections demonstrated Category K_2 resistance. However once cracked, they showed a one category fatigue life improvement after being hammer peened. If hammer peening was conducted prior to cycling, the socket connection was shown to have Category E' resistance. This same geometry was tested with double thickness base plates (i.e., 63.5 mm thick), and two different tube wall thicknesses of 4.7 mm (0.1875 inch) and 7.9 mm (0.3125 inch). The thickened base plate detail with 7.94 mm (0.3125 inch) pole wall thickness demonstrated roughly Category E resistance, a three category fatigue life improvement over its 31.75 mm (1.25 inch) thick base plate counter part. However, the thick base plate socket connection with a 4.7 mm (0.1875 inch) thick pole wall only achieved Category E' resistance. The two types of mast arm specimens used a smaller 294.6 mm (11.6 inch) diameter tube with either a full-penetration weld detail, or a stiffened socket, tube-to-transverse plate connection. The full-penetration weld details were expected to be Category E' details according to the 2001 Specifications. However, they achieved a resistance between Category E and E', therefore met the current classification in the 2001 Specifications. The stiffened socket connections had two likely locations to crack, either at the tip of the gusset plate, or in the socket weld itself. The fatigue resistance at the tips of the gusset plates was Category E, which agrees with the Interim provisions of the 2001 Specifications. Also, the socket weld of the stiffened specimens achieved Category ET resistance, though it cannot be determined whether this increase in resistance is from the smaller diameter tube, or because the connection was stiffened.

As a result of this data, it may be concluded that the published fatigue resistance in the 2001 Specifications is incorrect for significant varieties of socket connection details. This research has definitively shown that some multi-sided socket connections have a lower fatigue resistance than currently published in the 2001 Specifications mainly because of the large stress concentration factor present at the bent corner of the tube and the thickness of the base plate. Potentially, other multi-sided tube geometries may also have better or worse fatigue resistance than currently predicted by the 2001 Specifications. Though not enough specimens were tested to provide a statistically significant sample, doubling the base plate thickness of socket connections is seen to have the potential to provide a two to three category fatigue life improvement. There was also a tube wall thickness effect on the fatigue resistance, with thinner tubes exhibiting lower fatigue

resistance. The stiffened socket connections attained a higher fatigue resistance than the pole socket connections with the main difference being the diameter of the tubes and the bolt circles. Therefore, while it remains to be verified with a wider range of tests, tube and bolt circle diameters also appear to have an effect on fatigue life.

8.2 Tube-to-Tube Connections

The mast can detail tested represents a tube-to-tube connection detail, though in Minnesota this connection is used as a mast arm-to-pole connection. In comparison to other tube-to-tube connections from other industries (i.e., offshore oil industry) the boundary conditions on the mast can detail are obscure, as it uses a slip fit connection where loads are transferred through bearing and friction. This detail is unclassified in the 2001 Specifications, but the closest detail in the 2001 Specifications is a fillet-welded tube-to-tube connection in a T-, Y-, or K-configuration. However, the mast can detail uses a one-sided full-penetration weld with a back-up bar, which would lead one to think it would have slightly better fatigue resistance than fillet welded connections. The current tube-to-tube connection fatigue design dates back to early offshore oil platform research of tube-to-tube connections. Initially, the industry used the classification approach for tube-to-tube connections but soon found with a huge variety of possible connections, the classification method for fatigue design was unwieldy. The ET and K_2 classifications were the byproduct of using the nominal stress approach for tube-to-tube connections, but represent the lower bound from a variety of tested connections, and therefore in many situations may be overly conservative. According to the 2001 Specifications, there are two fatigue design checks required for fillet-welded tube-to-tube connections. The first requires the designer to check the stress in the branching member (mast arm tube in this case) against stress Category ET. This stress range check was meant to provide thick enough tubes to avoid cracking at the weld in the branching member. A punching shear stress range check must then be performed on the chord member (mast can in this case) and checked against K_2 resistance. The code provides the designer with ovalizing parameters to multiply the branching member stress range with to simply calculate the punching shear stress range in the chord (mast can). There are two different ovalizing parameters for in- and out-of-plane loading. For in-plane loading it is recommended the punching shear stress range is 0.67 times the stress range in the branching member, and 1.5 times for out-of-plane loading. This means that the fatigue strength for in-plane loading should be higher than that for out-of-plane loading. For the designer, the thickness of the mast can may be thickened if punching shear becomes a problem, and should be to avoid cracking at the weld, in the mast can. All tested Type II mast arms exhibited cracking in the weld toes on the mast can side of the weld, indicating that all cracking, despite loading direction, was from excessive punching shear stress. The data presented in Figure 7.29 used the punching shear stress range calculated in the mast can. The data show the tube-to-tube categorization is slightly conservative as the 97.5% survivability curve plots slightly above the K_2 S-N curve. However, this is not surprising since the K_2 curve was derived as a lower bound resistance of many tube-to-tube connections tested in the late 1960's.

8.3 Box Connections on Multi-sided Tubes

The Type I box connections tested in this research project were like no other previously tested because the tubes were multi-sided, not round. With round tubes, the box connection is made from five plates welded to the tube; a top, bottom, left, right, and a frontal flange plate. This type

of box connection is very susceptible to ovalization and punching shear in the pole from the side plates. With a multi-sided tube, the top and bottom plate are not needed as the flange plate can bear directly on a tube flat. With the flange plate bearing directly upon the tube flat of the pole, the load path becomes ambiguous because a designer does not know the distribution factor for load directly into the pole, and that carried by the side plates. This too makes the stress range calculations ambiguous. For out-of-plane loading and the one 45 degree loading case, the tested geometry always cracked in the pole wall, at the corner of the side plate. This cracking would indicate a punching shear problem and agrees with the findings from box connection tests on round tubes. The cracks that formed from the three in-plane loaded specimens were wildly different, yet mainly occurred at the intersection between the pole and flange plate. All three specimens suffered from a problem with the side plates buckling outwards under load, opening the weld root and cracking. Potentially this problem could be mitigated by adding a reinforcing fillet weld to the inside of the box connection where the side plate intersects the flange plate, at least in the bottom few inches as shown in Figure 8.1. The method chosen to calculate the stress range used the moment of inertia of the weld group attaching the flange plate to the pole and side plates. In essence, this method is calculating the stress range in the weld at the intersecting plane between the pole and flange plate. Since the majority of in-plane loading cracks occurred on this plane, these stress range were used to categorize the detail. However, for the out-of-plane and 45 degree loading cases, this stress was transformed into a membrane stress range in the side plates, then a punching shear stress range in the pole wall. The punching shear stress ranges were used to categorize this detail for out-of-plane and 45 degree loading directions. For in-plane loading, the 2001 Specifications currently predict Category E' resistance, yet the detail achieved resistance just below ET. For out-of-plane and 45 degree loading, K_2 resistance was expected and slightly better than K_2 resistance was achieved. Based on these results, for the multi-sided box connection tested, the punching shear classification is sufficient for the welds between the side plates and the pole, but the current Category E' resistance between the flange and side plates should be reduced down to Category ET as well.

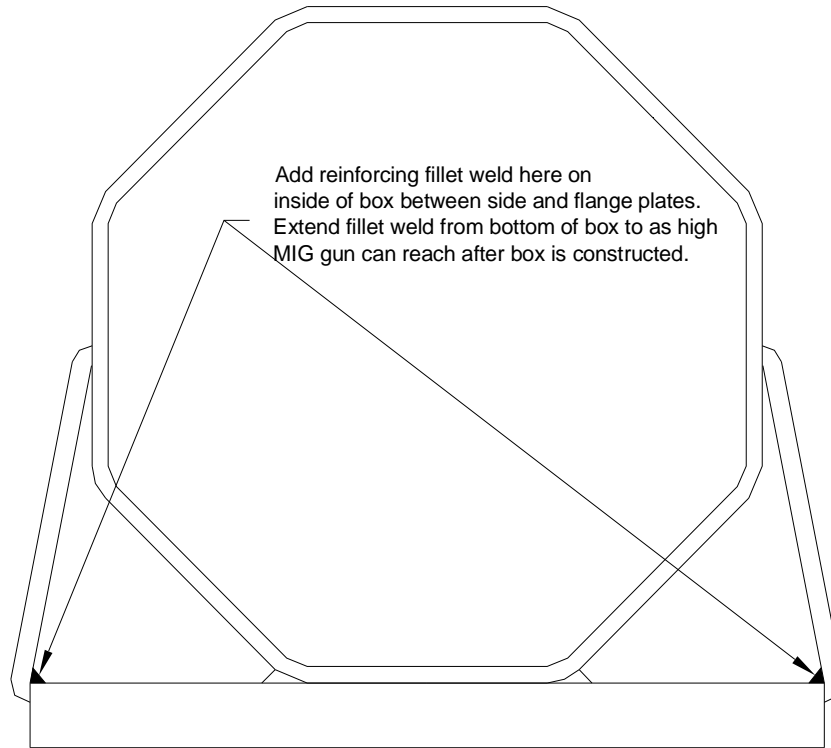


Figure 8.1 Detail recommendations for Type I box connection.

8.4 Access Holes

The Type II poles use a tapered tube with an integrated transformer base that itself uses a much larger taper than the pole. To allow access to wiring and anchor nuts, an access hole is provided in the integrated transformer base of this detail. The 2001 Specifications do not explicitly outline the detail of the particular access hole detail tested. However, it assigns holes and cutouts to be Category D details on the net section, and assigns access hole reinforcement to be Category E details because the height of the hole is greater than 102 mm (4 inch). The access holes cracked at the bottom of the hole where the moment was a maximum. However, there is a reentrant corner in the door at this location which drastically increases the stress concentration factor over the assumed round hole by the code. To exacerbate the problem, the stiffening ring was poorly welded to the base plate and once cracked just allowed more stress to flow to the reentrant corner. Using the net section stress ranges, the access door detail achieved less than Category K_2 behavior when the hole was orientated on the tension side of the pole from the dead load moment. When the access hole was orientated on the compression side of the pole from the dead load moment, cracks were not observed. This leaves two courses of action. Either it should be mandatory that poles should be orientated so the access hole is located directly beneath the mast arm (i.e., where compression stress is a maximum from dead loads). However, the true resistance of doing this is unknown since cracks never formed in this orientation. Alternatively, the best plan of action would be to detail these holes differently, by elevating the access hole

away from the base plate and using radiused corners. This way the stiffening ring can be fillet-welded completely to the shell, avoiding the fillet weld in the direct tension when the stiffening ring is welded to the base plate. The radiused corners also prevent the severe stress concentration associated with a reentrant corner. These detailing recommendations are outlined in Figure 8.2.

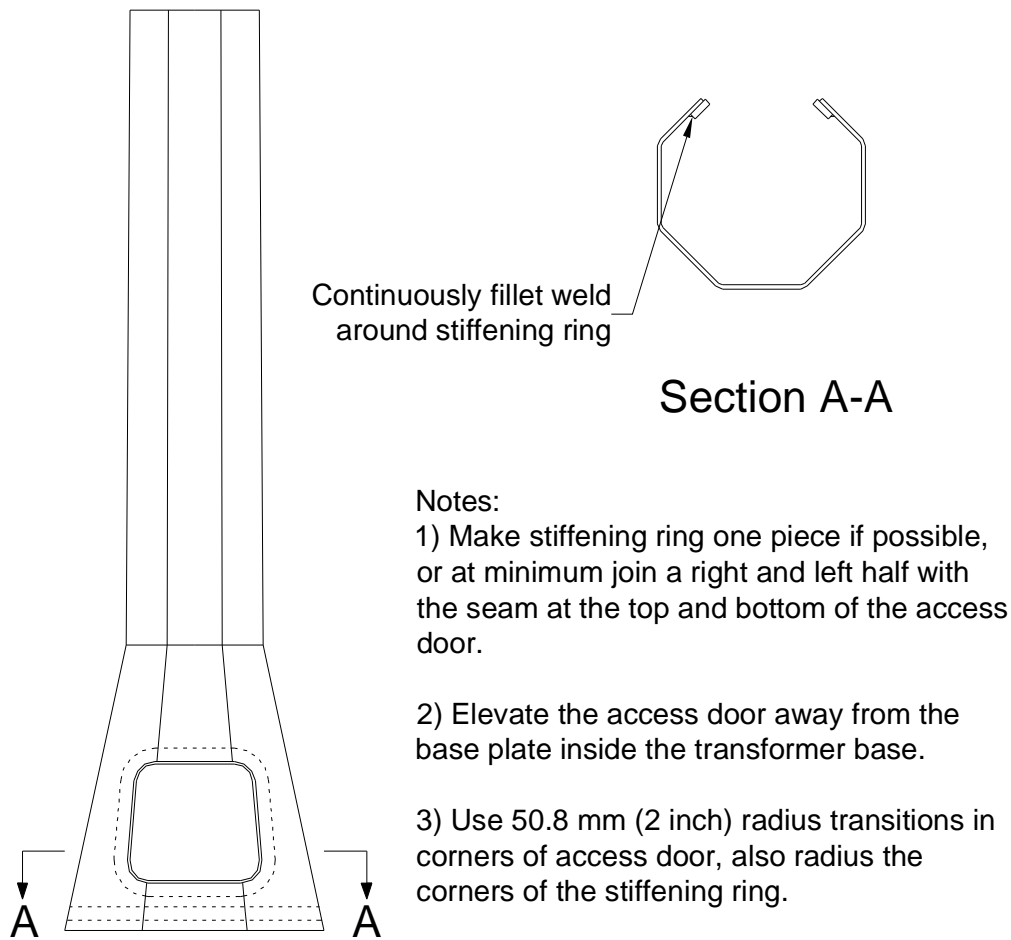


Figure 8.2 Access hole detail recommendations.

8.5 Suggestions for Future Research

This research showed that for some multi-sided, tube-to-transverse connections, the fatigue resistance was less than expected. Therefore, the important conclusion from the data presented is; there is not one, all encompassing fatigue strength classification that works for all tube-to-transverse plate connections, whether they use fillet-welded socket connection detailing, or full-penetration welds. The classification is highly dependant upon the geometry of the tube and base plate. Thus, the findings dictate a need for more experimental and analytical research into fatigue strength of tube-to-transverse plate connections with a variety of geometries, focusing on tube diameter, tube thickness, number of anchor rods, positioning of anchor rods, base plate

thickness, and tube shape. The synthesis of this additional work would be more uniform fatigue design provisions to account for various fatigue strengths as the tube-to-transverse plate connection geometry changes.

In Chapter 3, scant data was presented for the fatigue resistance of mast arm-to-pole connections using common box connection detailing. To date, there has only been one experimental and two analytical studies performed regarding the fatigue resistance of these details. To exacerbate the issue, these studies only investigated connections with round tubes. This research slightly expanded that knowledge base by including multi-sided tube box connections. Some of the failure modes were similar between the multi-sided tube box connections and the previously tested round tubes, but some failure modes were different. This indicates a need for more experimental and analytical research into the geometric parameters that can affect the fatigue resistance of box connection details for both round and multi-sided tubes.

Historically, Minnesota has only experienced two fatigue failures of traffic signal structure details. However, this research showed that the common details have lower resistance than what the 2001 Specifications predict. It may thus be questioned why Minnesota has not experienced more failures in the past. This research only focused on the resistance of details, but clearly there remains a need to understand the loading phenomena on Minnesota's traffic signal structures that causes fatigue. Perhaps the equivalent fatigue limit state loads outlined in the 2001 Specifications are too simplified to represent real loading behavior on Minnesota detailed structures. Field monitoring should be performed to better grasp the real loads imposed upon these structures and what particular aeroelastic and aerodynamic wind phenomena affect them.

References

- 1 AASHTO, *Standard Specifications for Structural Supports for Highway Signs, Luminaries, and Traffic Signals, 4th Edition*, (Washington D.C.:American Association of State and Highway Transportation Officials, 2001).
- 2 AASHTO, *Standard Specification for Highway Bridges, 12th edition*, (Washington D.C.:American Association of State and Highway Transportation Officials, 1977).
- 3 Culp, J., *Action Plan for Cantilever Sign Problem, Report to Management* (Lansing, MI: Michigan Department of Transportation, April 1990).
- 4 Kaczinski, M., Dexter, R., and Van Dien, J., *Fatigue-resistant Design of Cantilevered Signal, Sign, and Light Supports, National Cooperative Highway Research Program (NCHRP) Report 412* (Washington D.C.: Transportation Research Board, 1998).
- 5 Dexter, R., and Ricker, M., *Fatigue-resistant Design of Cantilever Signal, Sign, and Light Supports, National Cooperative Highway Research Program (NCHRP) Report 469* (Washington D.C.: Transportation Research Board, 2002).
- 6 Fischer, F. L., and Frank, K. H., *Axial Tension Fatigue Strength of Anchor Bolts, Research Report 172-1* (Austin, Tx.: Center for Highway Research, University of Texas at Austin,1977).
- 7 Fisher, J., Albrecht, P., Yen, B., Klingerman, D., and McNamee, B., *Fatigue Strength of Steel Beams with Welded Stiffeners and Attachments, National Cooperative Highway Research Program (NCHRP) Report 147* (Washington D.C.: Transportation Research Board, 1974).
- 8 Fisher, J., Frank, K., Hirt, M., and McNamee, B., *Effect of Weldments on the Fatigue Strength of Steel Beams, National Cooperative Highway Research Program (NCHRP) Report 102* (Washington, D.C.: Transportation Research Board, 1970).
- 9 Maddox, S., *Fatigue Strength of Welded Structures, Second Edition* (Cambridge, UK: Abington Publishing, 1991).
- 10 Petershagen, H., and Zwick, W., *Fatigue Strength of Butt Welds Made by Different Welding Processes* (Cambridge, UK: International Institute of Welding document XIII-1048-82, Abington Publishing, 1982).
- 11 Fisher, J. W., Nussbaumer, A., Keating, P. B., and Yen, B. T., *Resistance of Welded Details Under Variable Long-Life Fatigue Loading, National Cooperative Highway Research Program (NCHRP) Report 354* (Washington, D.C.: Transportation Research Board, 1993).
- 12 Miner, M., "Cumulative Damage in Fatigue," *Transactions of the American Society of Mechanical Engineers*, vol. 67, (1945).

- 13 Zhao, X. et al, *Design Guide for Circular and Rectangular Hollow Section Welded Joints Under Fatigue Loading* (ed. by Comite International pour le Developpement et l'Etude de la Construction Tubulaire, 1999).
- 14 Dexter, R., Tarquinio, J., and Fisher, J., "Application of Hot-spot Stress Fatigue Analysis to Attachments on Flexible Plate," *Proceedings of the 13th International Conference on Offshore Mechanics and Arctic Engineering Conference (OMAE)*, ed. by Salama et al, American Society of Mechanical Engineers, Vol. III, Materials Engineering, (27 February - 3 March 1994), pp. 85-92.
- 15 BS 7608, *Specification of Practice for Fatigue Design and Assessment of Steel Structures* (London, UK: British Standards Institute, 1994).
- 16 AASHTO, *AASHTO LRFD Bridge Design Specifications, Second Edition* (Washington D.C.: American Association of State Highway and Transportation Officials (AASHTO), 1998).
- 17 Dong, P. et. al., *WRC Bulletin 474: Master S-N Curve Method for Fatigue Evaluation of Welded Components* (New York, NY: Welding Research Council (WRC), 2002).
- 18 Ferreira, J., Pereira, A., and Branco, C., "A Fracture Mechanics Based Fatigue Life Prediction for Welded Joints of Square Tubes," *Thin-walled Structures*, vol. 21, (1995), 107-120.
- 19 Archer, G., and Gurney, M., "Fatigue Strength of Mild Steel Fillet Welded Tube to Plate Joints," *Metal Construction*, vol. 2, no. 5 (1970), 207-210.
- 20 Miki, C., Fisher, J., and Slutter, R., *Fatigue Behavior of Steel Light Poles* (Lehigh, PA.: Fritz Engineering Laboratory Report No. 200.81.714.1, 1981).
- 21 South, J., *Fatigue Analysis of Overhead Sign and Signal Structures, Physical Research Report No. 115* (Springfield, IL.: Illinois Department of Transportation, Bureau of Materials and Physical Research, 1994).
- 22 South, J., *Fatigue of Tube-to-Plate Fillet Welds and Methods for Their Improvement, Physical Research Report No. 118* (Springfield, IL.: Illinois Department of Transportation, Bureau of Materials and Physical Research, 1997).
- 23 Hartnagel, B., and Barker, M., "Strain Measurements on Traffic Signal Mast Arms," *Proceedings of the 1999 Structures Congress*, (1999), 1111-1114.
- 24 Alderson, J., *Fatigue Study of Cantilevered Traffic Signal Mast Arms*, (Rolla, MI.: Master's Thesis – University of Missouri-Rolla, 1999).
- 25 Heeden, A., *Fatigue Evaluation of the Mast-Arm-to-Pole Connection in Traffic Signal Structures using Finite Element Analysis* (Lawrence, KS.: Master's Thesis- Department of Civil Engineering, University of Kansas, 1999).

- 26 Kashar, L., Nester, M., Jones, J., Hariri, M., and Friezner, S., "Analysis of the Catastrophic Failure of the Support Structure of a Changeable Message Sign," *Proceedings of the 1999 Structures Congress*, (1999), 1115-1118.
- 27 Gilani, A., and Whittaker, A., "Fatigue-life Evaluation of Steel Post Structures. I: Background and Analysis," *Journal of Structural Engineering*, vol. 126, no. 3 (March 2000), 322-330.
- 28 Deschamp, B., *Fatigue Testing of Traffic Signal Structures* (Laramie, WY: Master's Thesis - Department of Civil and Architectural Engineering, University of Wyoming, 2002).
- 29 Hamilton, H.R., Puckett, J.A., and Deschamp, B., "Fatigue Damage Characteristics of Cantilever Traffic Signal Structures," *TRB 2003 Annual Meeting Compendium CD*, January 12-16 (Washington D.C.: Transportation Research Board, 2003).
- 30 Gilani, A., and Whittaker, A.; "Fatigue-life Evaluation of Steel Post Structures. II: Experimentation," *Journal of Structural Engineering*, vol. 126, no. 3, (March 2000), 331-340.
- 31 Koenigs, M. T., *Fatigue Resistance of Traffic Signal Mast-arm Connection Details* (Austin, TX.: Master's Thesis presented to Graduate School of The University of Texas at Austin, May 2003).
- 32 Marshall, P., "Welded Tubular Connections – CHS Trusses," *Structural Engineering Handbook* (Boca Raton, FL: ed. by W. F. Chen, CRC Press LLC, 1999).
- 33 Van Wingerde, A., Packer, J., and Wardenier, J., "Criteria for the Fatigue Assessment of Hollow Structural Section Connections," *Journal of Construction Steel Research*, vol. 35 (1995), pp.71-115.
- 34 Van Wingerde, A., Packer, J., and Wardenier, J., "New Guidelines for Fatigue Design of HSS Connections," *Journal of Structural Engineering*, vol. 122, no. 2 (February 1996), pp. 125-132.
- 35 Zhao, X., and Packer, J., *Fatigue Design Procedure for Welded Hollow Section Joints* (Cambridge, UK: International Institute of Welding documents XIII-1804-99 and IIW document XV-1035-99, Abington Publishing, 2000).
- 36 AWS, *AWS D1.1:2000, Structural Welding Code – Steel* (Miami, FL.: American Welding Society (AWS), 2000).
- 37 Dexter, R. J., "Investigation of Cracking of High-Mast Lighting Structures," Final report to Iowa Department of Transportation, July 22, 2004.
- 38 Fisher, J. W., Hausammann, H., Sullivan, M. D., and Pense, A., *Detection and Repair of Fatigue Damage in Welded Highway Bridges, National Cooperative Highway Research Program (NCHRP) Report 206* (Washington, D.C.: Transportation Research Board, 1979).

Appendix A

Appendix A

Results of T-12 Questionnaire on Usage of 4th Edition Standard Specifications for Structural Supports for Highway Signs, Luminaires, and Traffic Signals

T-12 Technical Committee for Structural Supports for Signs, Luminaires, and Traffic Signals developed a questionnaire to collect information on the 4th Edition. 29 responses from the states were received. The responses were re-written due to the size of the questionnaire. T-12 thanks all respondents for the time required to complete this effort.

Number of responses = 30 (x) - Indicates number of same responses

Part I, Use of 4th Edition

1) Is your organization using the 4th Edition?

Yes 22 (73%)

No 8 (27%)

2) Are you using it in its entirety?

Yes 9 (41%)

No 13 (59%)

3) If you answered No to Question 2), which provisions are you using or not using?

All provisions not used, except for high mast lighting.

All provisions not used, except for major overhead signs, especially VMS.

Deflection criteria, increased from 8" to 12" on signal arms.

Fatigue provisions on cantilever signs and signals.

Fatigue provisions on short signal mast arms (less than 50').

Fatigue provisions on some structures.

Galloping on traffic signals.

Traffic signal mast arms.

Truck induced gusts, limited to 55 mph.

Vibration Mitigation Devices.

Wind maps.

Wind provisions in Appendix C.

4) Has your organization started developing new Standard Drawings or evaluating your current standards in accordance with the 4th Edition?

Yes 21 (84%)

No 4 (16%)

5) If you answered Yes to Question 4), approximately how far along are you with their development?

% Complete	Number
0% to 25%	3
26% to 50%	7
51% to 75%	3
76% to 100%	8

Part II, Design

6) Have you experienced any increase in time to design structures under the 4th Edition compared to older designs?

Yes 10 (42%)
 No 2 (8%)
 No Data 12 (50%)

7) If you answered Yes to Question 6), approximately how much of an increase in time have you experienced?

% Increase in Design Time	Number
0%	2
20%	2
25%	1
30%	1
100%	2
> 100%	2

8) If you answered Yes to Question 6), what areas are contributing to the increased time? (Check all that apply)

Learning curve associated with new specification 11
 Fatigue provisions. 11
 Complexity. 4
 Questions raised in Commentary. 3

More design provisions.

7

Other (Please Specify):

Checking procedures; developing new ones and redeveloping them when the code changes.

Complex connections; increased detailing time.

Industry; reviewing and answering questions and comments.

Interpreting 4th Edition.

Standard design tables; preparation.

Identify better load paths and details.

9) Are longitudinal stiffeners (gusset plates) used to meet fatigue requirements?

Yes 9 (41%)

No 13 (59%)

10) If you answered Yes to Question 9), on what elements are longitudinal stiffeners used? List the element and explain the use of the longitudinal stiffener.

Cantilever sign post to base plate connections.

Post to Truss connections.

Traffic signal mast arm to end plate connections.

11) The 4th Edition provided several options for galloping. For cantilever sign and signal structures, approved vibration mitigation devices can be used in lieu of designing for galloping. Traffic signal structures can also be designed without galloping and erected without mitigation devices provided they do not exhibit galloping once in service. Lastly, the owner may choose to exclude galloping from the design of four chord horizontal truss cantilever sign support structures. Which options do you use? (Check all that apply)

Design all cantilever sign and signal structures for galloping

10

Install mitigation devices up front on all cantilever sign and signal structures

0

Install mitigation devices up front on selected cantilever sign and signal structures

3

Install mitigation devices on traffic signals only if they exhibit in service galloping 12

Exclude galloping in the design of four chord cantilever sign support structures

8

12) If you use vibration mitigation devices, what types are used on each structure type?

“Stockbridge” damper installed at center of all overhead truss sign structures.

“Stockbridge” dampers used on lighter aluminum trusses.

“Stockbridge” damping device used on all new and some existing span and cantilever sign structures.

Eccentric weight on aluminum Luminaires.
 Sign blank (aerodynamic damper) used as retrofit for some traffic mast arms if they exhibit galloping and on some new mast arms greater than 40' in length.
 Signal head back plate removed from mast arms showing galloping.

Part III, Construction Cost

13) Have you experienced an increase in construction cost for structures designed under the 4th Edition compared to older designs?

Yes 11 (46%)
 No 2 (9%)
 No Data 11 (46%)

14) If you answered Yes to Question 13), which Group Loads contribute to the increased costs? (Check all that apply)

Group Load I (DL) 0
 Group Load II (DL + W) 4
 Group Load III (DL + Ice + 1/2 W) 0
 Group Load IV (Fatigue) 14

15) If Group Loads I, II, or III contribute to the increased cost, explain.

25 year design life used for all luminaire and high mast lighting.
 4th Edition requires higher wind speeds.
 Adopted an 80 mph fastest wind speed or 100 mph 3 second wind gust to design sign structures.

16) If you have an increased cost due to Group Loads I, II, or III, what is the percent increase in cost?

% Increase in Cost	Number
10%	1
12%	1
30%	1
150%	1

17) If Group Load IV (Fatigue) contributes to the increased cost, which fatigue loads are controlling the design? (Check all that apply and indicate importance factor used in the design)

Galloping: 10

Cantilever sign and signal structures.
 Vortex shedding: 1
 Non-tapered lighting structures.
 Natural wind gust. List structure types controlled by this loading: 10
 Aluminum box truss span sign structures.
 Butterfly sign structures.
 Cantilever overhead signs.
 High mast lighting and luminaires.
 Traffic signals.
 Truck-induced gust. List structure types controlled by this loading: 5
 Aluminum box span sign structures.
 Cantilever overhead sign and traffic signal structures.
 Struts of two tube sign structures.
 Variable Message Sign structures.

18) List specific details or structure elements that contribute most to the increased construction cost.

Cantilever sign structures, all elements.
 Fabrication costs; NDT requirements, full penetration butt welds, break-press forming requirements, procedures to prevent warping.
 Gusset plates added to poles and mast arms.
 Traffic signal mast arms, all elements.
 Tubular member sizes increase, more costly connections, increased size of foundations.

Part IV, Research & Testing

19) Provide a description of the research and testing relating to the 4th Edition that you are currently sponsoring. (number in parentheses indicates multiple recommendations)

AASHTO fatigue design loadings; actual load conditions compared 4th Edition.
 Fatigue testing signal pole connections including acoustic emissions.
 Aluminum overhead sign structure; field and lab testing to measure performance and durability.
 Finite element analysis with static verification testing.
 Vibration mitigation.
 Aluminum overhead sign structure; retrofit of cracked diagonals using FRP for strength and fatigue.
 Mast arm to post connection field test.
 Socket joints treated with ultrasonic impact treatment (UIT).
 Truss chord circular tube buckling strength.
 Traffic signal pole in-service field monitoring.
 Fillet weld detailing for stiffeners; evaluate fatigue performance of mast arm to pole connection and the role of stiffeners.

20) Provide a list of research and testing you believe is important to enhance the 4th Edition.

Anchor bolts, diameters over 2".
 CAFL on welded joint details.
 Concentric ring plate; alternative to gusseted post to base plate connection.
 Calibration of fatigue loads for span type structures. (2)
 Connections details, full scale testing. (3)
 Design fatigue loads are correct.
 Field monitoring of various structures to verify natural wind gust loads.
 Fluted poles.
 Gusset plates; end transitions.
 Mast arm connections, less conservative details. (2)
 Economical fatigue resistant connection details. (3)
 Fatigue loading for existing welds and connections.
 Do stiffeners work on thin walled material?

Part V, Inspection & Maintenance

21) Have you implemented an inspection program for sign, luminaire, and signal structures?

Sign structures: Yes 19 (70%)
 No 8 (30%)

Frequency	Number
2 years	1
2.5 years	1
4 years	3
4.5 years	1
5 years	6
6 years	2
Not Established	5

Luminaires: Yes 5 (19%)
 No 21 (81%)

Frequency	Number
3 years	1
4 years	1
4.5 years	1
5 years	1
Not Established	1

Traffic Signals: Yes 6 (22%)

No 21 (78%)

Frequency	Number
1 year	1
4 years	1
4.5 years	1
5 years	1
Not Established	2

22) If you inspect these structures, what methods are being used?

D-meter
Dye-penetrant (3)
Hammer sounding of anchor bolts
Lead paint testing
Magnetic Particle
NDT of pole to base plate connection on VMS
Thickness gauge
UT of anchor bolts (5)
Visual (17)

23) Indicate typical problems found during these inspections.

Aluminum structures; fatigue cracks in base metal (2)
Aluminum structures; weld cracks (6)
Anchor bolts; loose and/or broken (5)
Bi-metal corrosion
Bolts; loose and/or missing at connection (8)
Concrete foundation deterioration (2)
Deteriorated poles; section loss (2)
Weathering steel excessive corrosion
Original construction problems (3)
Weld cracks (6)

Part VI, Comments on 4th Edition

24) Have you identified provisions within the 4th Edition that are unclear or difficult to interpret?

4th Edition does not cover our typical overhead sign structures.
Chapter 11 (Fatigue); examples are confusing when trying to select the appropriate case.
Chapter 11 (Fatigue); fatigue category descriptions make it difficult to apply anything but Category I to all structures. (3)
Chapter 11 (Fatigue); some suggested details are nearly impossible to achieve (e.g., welding backing ring to plate instead of tube).
Chapter 11 (Fatigue); section is difficult to follow.
Chapter 11 (Fatigue); need better explanation application of fatigue analysis to gusseted connections.
Section 11.4 (Applicable Structure Types) Commentary; states fatigue provisions do not apply to “common lighting structures”. What is the height limitation for “common lighting structures”?
Section 13.7.1 (Geotechnical Design) Commentary; unclear if this applies to uniaxial bending, Section 3.9.3 on uniaxial bending is not for substructures.
Section 3.9.3 (Design Loads for Vertical Supports); does this section apply to fatigue?
Section 5.12.1 (Vertical Cantilever Pole Type Supports); does equation 5-16 apply to Group Load I (DL) and Group Load IV (Fatigue)?

25) Have you identified provisions within the 4th Edition that appear to need modification or where additional information in the specification or commentary appears warranted?

Anchor bolt pre-tensioning; guidance would be valuable.
Design examples would be helpful.
Design life should be consistent with other codes. 4th Edition defines design life as the wind event and not how long a structure will last.

Equation 4-1 in Section 4.8.1 (Simplified Method); valid only when $kl/r < (2\pi^2E/F_y)^{0.5}$. What procedure should be followed when this condition is not met?

Figure 11-1 (b) (Illustrative Examples); Example 6 lacks guidance for the fillet weld of the gusset plate to the tubular chord/arm.

Galloping fatigue provisions seem too restrictive.

Industry testing does not support the fatigue categories. Too much emphasis towards gusset details compared to the socket detail which have no history of problems.

Ring plate mast arm connection; note (g) of Table II advises to use the section properties of the mast arm in calculating connection stress. This leads to double the material in the connection compared to a detailed (finite?) analysis.

Saddle supports for large diameter thin walled pipe chords; recommend adding provisions based on Tubular Steel Structures Theory and Design by M.S. Troitsky.

Section 11 (Fatigue); provisions look too conservative for cantilever signs and traffic signals. (2)

Section 11.4 (Applicable Structure Types); Is fatigue loading (gust and truck induced) applicable to 2 post planar truss structures? These structures are subject to wind and truck forces.

Section 13.6 (Drilled Shafts); need to define “tolerable” settlements and lateral displacements.

Section 3 (Loads); no provisions for snow or thermal loads.

Section 3.9.4 (Unsymmetrical Wind Loading); guidance is lacking for single arm cantilever overhead sign structures when the un-symmetry is about the horizontal axis.

Section 5.14.1 (Minimum Thickness of Material); could provide a better definition of what are primary and secondary members.

Section 5.15.2 (Longitudinal Seam Welds); should require 100% of full-penetration welds be inspected by both NDT and visual methods. Currently, fabricator could use visual inspection only since it is an acceptable method described in AWS.

Section 5.15.3 (Base Connection Welds); requires 25% of full-penetration base welds be inspected by radiography or ultrasonics. This is not practical, radiography cannot be performed on the “T” joint configuration and ultrasonic testing is not practical for thin material (thickness less than approximately 0.188”).

Table 11-2 (Fatigue Details of Cantilevered Support Structures); Detail 19 should cite Example 6.

Table 5-2 (Width-Thickness Ratios of Nontubular Sections); recommend adding provisions for stems of structural tees, AISC code.

Thin walled tubes at bearing supports; recommend adding provisions based on AISC Hollow Structural Sections Connection Manual.

Vibration Mitigation Devices; should provide a listing of all approved devices. (2)

26) Any other Comments?

Fabricators; concerns on use of new specification. (2)
4th Edition; code revisions should be developed working more closely with industry.
4th Edition; overall it is comprehensive and more refined than the previous 1994 Specification.
Implementation; waiting for other states to implement.
NCHRP Report 469; seems to say that even quadri-chord sign bridge trusses should be designed for fatigue. Is any code change anticipated?
Section 11 (Fatigue); much higher costs for structures that historically have performed well. May be due to concept of infinite fatigue life, fatigue loads too high, and/or CAFL of connections not accurate.
Section 11 (Fatigue); applying the 4th Edition to traffic signals leads to much larger and more expensive supports.
Section 11 (Fatigue); consider retracting Section 11.
Section 11 (Fatigue); need to look at fatigue categories. (3)
4th Edition forces you to use Category 1 for all designs.
Section 11 (Fatigue); some fatigue categories details such as post to base plate socket welds, seem quite severe considering the lack of a major service problem.
Section 11 (Fatigue); the jump in cantilever structure stiffness may not be warranted in the 4th Edition.
Section 11 (Fatigue); this specification only shows connections with poor fatigue resistance.
Section 13.4 (Determination of Soil Properties); requires a geotechnical study shall be performed for all structures. 4th Edition should provide conservative suggestions suitable for most installations.
Section 5 (Steel Design); 4th Edition should require AISC certification (simple bridges) for fabrication of steel structures, except roadside signs.
Section 5.15.2 (Longitudinal Seam Welds); is there a limit to the number of longitudinal seam welds that can be used in pole and arm members?
Section 5.15.3 (Base Connection Welds); other than the last two sentences of this Section, are these specifications applicable to multi-ply (2 to 5 tubes) members?
Section 5.15.3 (Base Welds); should laminated posts be used considering torsion? Even if butt welds are adequate, skin friction is required to transfer tensional shear to the inner shell(s).
Section 5.15.3 (Base Welds); UT and RT cannot be used on laminated sections butt welded to base plates.
Section 5.16 (Bolted Connections); do “clamp connections” meet the definition of slip-critical in the Standard Specifications for Highway Bridges?
Section 11 (Fatigue Design) only addresses built-up mast arm to post pass-through bolted connections.
Section 5.16 (Bolted Connections); do connections such as mast arm to pole connections have to meet the sealing requirements in the Standard Specifications for Highway Bridge for high strength bolted connections?

Section 5.16 (Bolted Connections); do drilled and tapped high strength bolts meet the requirements of the Standard Specification for Highway Bridges?

Section 5.4 (Material - Structural Steel); 4th Edition should provide Charpy requirements.

Table 5-3 (Allowable Bending Stress, F_b , for Tubular Members); can other multisided shapes be used such as 18 sided? One fabricator calculates a roundness ratio for multi-sided sections and if within certain limits, they consider it round. (References to multi-sided sections are also shown in Table 3-6, Table 5-1, and Table B-1)